

GEOLOGY MINERALOGY AND ORIGIN OF KAOLIN DEPOSITS
OCCURRING AROUND AHIRÖZÜ (MİHALIÇCIK-ESKİŞEHİR)

A THESIS SUBMITTED TO
THE GRADUATE SCHOOL OF NATURAL AND APPLIED SCIENCES
OF
MIDDLE EAST TECHNICAL UNIVERSITY

BY

IŞIL ÖMEROĞLU SAYIT

IN PARTIAL FULFILLMENT OF THE REQUIREMENTS
FOR
THE DEGREE OF DOCTOR OF PHILOSOPHY
IN
GEOLOGICAL ENGINEERING

SEPTEMBER 2018

Approval of the thesis:

**GEOLOGY MINERALOGY AND ORIGIN OF KAOLIN DEPOSITS
OCCURRING AROUND AHIRÖZÜ (MİHALIÇÇIK-ESKİŞEHİR)**

submitted by **İŞİL ÖMEROĞLU SAYIT** in partial fulfillment of the requirements for the degree of **Doctor of Philosophy in Geological Engineering Department, Middle East Technical University** by,

Prof. Dr. Halil Kalıpçılar
Dean, Graduate School of **Natural and Applied Sciences**

Prof. Dr. Erdin Bozkurt
Head of Department, **Geological Engineering**

Prof. Dr. Asuman Günel Türkmenoğlu
Supervisor, **Geological Engineering Dept., METU**

Examining Committee Members:

Prof. Dr. Nilgün Güleç
Geological Engineering Dept., METU

Prof. Dr. Asuman Günel Türkmenoğlu
Geological Engineering Dept., METU

Assoc. Prof. Dr. Zehra Karakaş
Geological Engineering Dept., Ankara University

Assoc. Prof. Dr. Kaan Sayıt
Geological Engineering Dept., METU

Assist. Prof. Dr. Ceren Küçükuysal
Geological Engineering Dept., Muğla Sıtkı Koçman University

Date: 06.09.2018

I hereby declare that all information in this document has been obtained and presented in accordance with academic rules and ethical conduct. I also declare that, as required by these rules and conduct, I have fully cited and referenced all material and results that are not original to this work.

Name, Last name: Işıl, Ömerođlu Sayıt

Signature:

ABSTRACT

GEOLOGY MINERALOGY AND ORIGIN OF KAOLIN DEPOSITS OCCURRING AROUND AHİRÖZÜ (MİHALIÇÇIK-ESKİŞEHİR)

Ömerođlu Sayıt, Işıl
PhD., Department of Geological Engineering
Supervisor: Prof. Dr. Asuman Gnal Trkmenođlu

September 2018, 197 pages

Hydrothermally originated Ahırz kaolin deposits were developed within the contact of granite-serpentinite rocks in Ahırz-Hamidiye villages, Mihaliççık, Eskişehir-Turkey. The purpose of this research is to investigate the mineralogy, geology and genesis of Ahırz kaolin deposits by using petrographical analyses, chemical analyses (ICP-MS and ICP-ES), X-ray powder diffraction (XRD) method, scanning electron microscopy with an energy dispersive X-ray spectroscopy (SEM-EDX) analyses, stable isotope analyses (oxyhen/hydrogen) and fluid inclusion analyses. Experimental studies of CO₂-H₂O-serpentine based reactions were performed to understand the formation mechanism of listwanites occurred in the study area. Experiments were conducted at 25 °C and 80 °C with P (CO₂) = 110 to 130 bar.

The argillic alteration zone (Zone A) includes kaolinite, halloysite, natroalunite and accessory pyrite. The presence of K-Feldspar and graphic texture in the Zone A indicates that the protolith rock has a granitic origin. The propylitic alteration zone (Zone B) is mainly characterized by chlorite-smectite-illite and epidote. Zone C represents silica sinter formation. According to the fluid inclusion analyses, it has been obtained that the homogenization temperature (Th°C) varies between 126°C

and 365⁰C and wt. % NaCl values change between 3.9- 6.2. Thus, it is indicated that these kaolin deposits have an epithermal hydrothermal origin. The rocks in the kaolin deposit are depleted in Rb and Pb while being enriched in Cs and U elements. Regarding to the stable isotope analyses, δD varies between -80.86 and -88.81 whereas $\delta^{18}O$ values ranges from 5.03 to 8.73 which indicating the contribution of magmatic waters in the hydrothermal system.

Keywords: hydrothermal alteration, kaolin deposits, epithermal deposits, Ahırözü, Mihaliççık

ÖZ

AHIRÖZÜ (MIHALIÇÇIK-ESKİŞEKİR) DOLAYLARINDAKİ KAOLEN YATAKLARININ JEOLJİSİ MİNERALJİSİ VE OLUŞUMU

Ömeroğlu Sayıt, Işıl
Doktora, Jeoloji Mühendisliği Bölümü
Tez Yöneticisi: Prof. Dr. Asuman Günal Türkmenoğlu

Eylül 2018, 197 sayfa

Hidrotermal kökenli Ahırözü kaolen yatakları, granit-serpantinit kontağında gelişim göstermiş olup, Ahırözü-Hamidiye, Mihaliççik-Eskişehir, Türkiye’de yer almaktadır. Bu çalışmanın amacı, Ahırözü kaolen yataklarını; mineralojik, jeolojik, ve kökensele bakımdan; petrografik analizler, kimyasal (ICP-MS ve ICP-ES) analizler, X-ışınları toz difraksiyon (XRD) yöntemi, taramalı elektron mikroskopisi (SEM-EDX), duraylı izotop analizleri (oksijen/hidrojen) ve sıvı kapanım analizleri yardımı ile incelemektir. CO₂-H₂O-serpantin reaksiyonlarına dayalı deneysel çalışmalar, sahada gözlenen listvenitlerin oluşum mekanizmalarını anlamak maksadıyla gerçekleştirilmiştir. Deneyle, 25 °C ve 80 °C’lik sıcaklıklar altında; 110 bar ile 130 bar arasında değişim gösteren basınç aralığında uygulanmıştır.

Arjilik alterasyon zonu (Zon A), kaolinit, haloysit, natroalünit ve düşük miktarda pirit minerallerini içermektedir. Zon A içerisinde, K-Feldispat ve grafik dokunun varlığı ana kayacın granitik kökenli bir kayaç olduğuna işaret etmektedir. Propilitik alterasyon zonu (Zon B), klorit-simektit-illit ve epidot gibi mineraller ile karakterize edilmektedir. Zon C ise silika sinter oluşumunu temsil etmektedir. Sıvı kapanım analizlerine göre, homojenleşme sıcaklığı (Th°C) 126°C ile 365°C aralığında değişmekte olup, tuzluluk yüzdesi (wt % NaCl) 3.9- 6.2 değerleri arasındadır. Buna

baęlı olarak; kaolen yataklarının, epitermal hidrotermal kökene sahip oldukları anlaşılmaktadır. Kaolen yatakları içerisindeki kayaçlar, Rb ve Pb element miktarı açısından düşüş gösterirken; Cs ve U elementleri açısından zenginleşmektedir. Duraylı izotop analizlerine göre; δD -80.86 ile -88.81 arasında değişirken, $\delta^{18}O$ 5.03 ile 8.73 değerleri arasındadır. Bu durum, magmatik kökenli suların hidrotermal sisteme karıştığını göstermektedir.

Anahtar kelimeler: hidrotermal alterasyon, kaolen yatakları, epitermal yataklar, Ahırözü, Mihalıççık

To my dear family;

and

my dear husband

for supporting me all through this study with their precious love

ACKNOWLEDGEMENT

I am deeply grateful to my supervisor Prof. Dr. Asuman Günel Türkmenođlu for her precious guidance, support and encouragement throughout this study. This thesis would not be accomplished without her advices. It was an honor for me to have the chance to work with her.

I would like to thank to TÜBİTAK “The Scientific and Technological Research Council of Turkey” for financially funding me during my research at the University of Illinois at Chicago, USA under the scope of the 2214-A International Research Fellowship Programme in 2014. Hereby, I wish to express my special thanks to my supervisor at University of Illinois at Chicago, USA, Prof. Dr. Steve Guggenheim, for his valuable suggestions and broadening my perspective. Also, I would like to thank August F. Koster van Groos who helped me a lot at each step of my experiments at the Clay and XRD Laboratories with Prof. Dr. Steve Guggenheim.

I wish to thank my examining committee members, Prof. Dr. Nilgün Güleç, Assoc. Prof. Dr. Zehra Karakaş, Assoc. Prof. Dr. Kaan Sayıt and Assistant Prof. Dr. Ceren Küçükuysal for sharing their valuable recommendations and critics with me.

I am also grateful to Prof. Dr. M. Cemal Göncüođlu for his scientific help and guidance on petrographical analyses during this thesis. He reserved his precious time for my thin-section examinations and gave suggestions to improve the perspective of this study.

Especially, I would like to express my deepest gratitude to my dear parents, my sister and my husband who supported me all throughout this study with their endless love and patience. The preparation of this thesis would not be possible without the courage and support they have given to me all through my life.

Last but definitely not least, my greatest thanks go to my grandparents who encouraged me to pursue an academic career and taught me the importance of the education. They were the ones who supported me all through my life with their everlasting love and compassion. I wish they were here with me today.

This study was financed by METU-BAP-07-02-2012-101, METU-BAP-03-09-2013-001 and METU-BAP-03-09-2017-006.

TABLE OF CONTENTS

ABSTRACT	v
ÖZ	vii
ACKNOWLEDGEMENTS	x
TABLE OF CONTENTS	xii
LIST OF TABLES	xvi
LIST OF FIGURES	xvii
CHAPTERS	
1. INTRODUCTION	1
1.1. Overview.....	1
1.2. Purpose and Scope.....	4
1.3. Study Area.....	5
1.4. Previous Studies.....	8
1.5. Method of Study.....	15
2. REGIONAL GEOLOGY	19
2.1. Tectonic Setting of the Region.....	19
2.2. Geologic Setting and Stratigraphy of Study Area.....	23
3. EPITHERMAL DEPOSITS	27
3.1. High Sulfidation Deposits.....	27
3.2. Low Sulfidation Deposits.....	32
4. RESULTS: FIELD STUDIES	37
4.1. Local Geology and Field Sampling.....	44
4.1.1. Kaolin Deposits.....	44
4.1.2. Gossan Zone.....	51
4.1.3. Listwanite Occurrences.....	52
4.1.4. Metamorphic and Ultramafic/Mafic Rock Units.....	55

5. RESULTS: MINERALOGICAL AND PETROGRAPHICAL ANALYSES.....	59
5.1. Thin-section Analyses.....	59
5.1.1. Argillic Alteration.....	59
5.1.1.1. L-1 to L-11 Series - Ayın Tepe Kaolin Pit.....	60
5.1.1.2. Hmd Series - Hamidiye Kaolins.....	60
5.1.2. Gossan Zone.....	71
5.1.3. Propylitic Alteration.....	72
5.1.3.1. L12/L13 Series and L1A and L1B Series.....	73
5.1.3.2. H-Series.....	77
5.1.4. Silicified Rocks.....	80
5.2. XRD Analyses.....	81
5.2.1. Argillic Alteration.....	83
5.2.2. Propylitic Alteration.....	89
5.3. Morphological Features.....	94
6. RESULTS: CHEMICAL ANALYSES.....	97
6.1. Mineralogical Fingerprinting of Geochemical Variations.....	97
6.2. Geochemical Signatures of Alteration and Tectonic Setting.....	99
6.3. Intensity of Hydrothermal Alteration as revealed by Alteration Index	105
6.4. Fluid Inclusion Analyses.....	109
6.5. Stable Isotope Geochemistry.....	112
7. CO ₂ -ROCK-WATER INTERACTION: LISTWANITES	
AN EXPERIMENTAL STUDY ON SERPENTINE-BASED REACTIONS IN THE STUDY AREA.....	115
7.1. Introduction to the Experimental Procedure.....	115
7.2. Starting Material.....	117
7.3. Preparation of the Original Sample for the CO ₂ -Rock-Water Reactions Experiment.....	118

7.4. Experimental Procedure.....	121
7.5. Experimental Data.....	122
7.5.1. Experiments Conducted for 80°C.....	123
7.5.1.1. Run 2-2.....	123
7.5.1.2. Run 2-3.....	124
7.5.1.3. Run 2-4.....	125
7.5.1.4. Run 2-5.....	126
7.5.1.5. Run 2-8.....	127
7.5.1.6. Run 2-9.....	127
7.5.1.7. Run 2-10.....	128
7.5.1.8. Run 2-13.....	129
7.5.2. Experiments Conducted for 25°C.....	130
7.5.2.1. Run 3-4.....	130
7.5.2.2. Run 3-5.....	131
7.5.2.3. Run 3-6.....	131
7.5.2.4. Run 3-8.....	132
7.6. Research Results.....	133
8. DISCUSSIONS.....	139
8.1. Studies on Hydrothermal Alteration and Zoning.....	139
8.2. Textural and Mineralogical Aspects in the Interpretation of the Style of Epithermal Systems.....	141
8.3. Wall Rock Alteration and Listwanite Occurences.....	143
8.4. Origin of the Hydrothermal Fluids.....	144
9. CONCLUSIONS AND RECOMMENDATIONS.....	147
REFERENCES.....	151
APPENDICES.....	163
A. CHEMICAL COMPOSITIONS OF ROCK SAMPLES.....	163

B. DIAGRAMS BASED ON LISTWANITE-CO ₂ -H ₂ O REACTIONS USING SERPENTINE FOR 80°C.....	171
C. DIAGRAMS BASED ON LISTWANITE-CO ₂ -H ₂ O REACTIONS USING SERPENTINE FOR 25°C.....	185
CURRICULUM VITAE.....	193

LIST OF TABLES

Table 3.1: Characteristics of acid-sulphate (high sulphidation) and adularia-sericite (low sulphidation) type deposits (compiled from White & Hedenquist, 1995; Hedenquist et al., 1996; Sillitoe & Hedenquist, 2003).....	28
Table 4.1. Coordinates of sampling locations regarding to Universal Transverse Mercator (UTM) projection system.....	39
Table 5.1. Table of X-ray diffraction data for clays and non-clay minerals (Chen, 1977).....	82
Table 6.1. The major element analyses of selected samples from the Ahırözü kaolin deposits (Ömeroğlu-Sayıt et al. 2018).....	100
Table 6.2. The trace element analyses of selected samples from the Ahırözü kaolin deposits (Ömeroğlu-Sayıt et al. 2018).....	102
Table 6.3. AI and CCPI data generated by using representing rock-specimens acquired from the study area.....	106
Table 6.4. Homogenization temperature (Th °C) and wt% NaCl (salinity) ranges given for the samples L 12-11,L12-2, Hmd 1-4 and Hmd 1-2 (Ömeroğlu-Sayıt et al. 2018).....	111
Table 6.5. The data derived by Oxygen/Hydrogen stable isotope analyses for 9 kaolin samples acquired from the study area.....	113
Table 7.1. The table showing the data derived at 80 ⁰ C.....	134
Table 7.2. The table showing the data derived at 25 ⁰ C.....	135
Table A-1. Geochemical compositions of 57 rock samples acquired from the study area.....	163

LIST OF FIGURES

Figure 1.1. Location map of Ahırözü kaolin deposits. The circular area represents the main study area investigated in this study-Global Mapper SRTM and Google Earth Data (Ömeroğlu-Sayıt et al. 2018).....	7
Figure 2.1. Tectonic map of Turkey comprising the major sutures and continental blocks (Okay & Tüysüz 1999; Okay, 2008).....	20
Figure 2.2. Tectonic map showing different basement types and complexes of Turkey (Okay et al., 2006; Okay, 2008).....	22
Figure 2.3. Geologic map of the study area (after Gözler, 1987).....	24
Figure 2.4. Generalized stratigraphic section of the study area (after Gözler, 1987).....	25
Figure 3.1. Cross-sections of alteration zones characteristic for high sulphidation deposits (Stoffregen, 1987; Arribas, 1995).....	29
Figure 3.2. Models showing two main stages of evolution of HS systems (White, 1991; Rye, 1993; Hedenquist et al., 1994; Arribas, 1995).....	31
Figure 3.3. Thermally induced hydrothermal minerals in the epithermal ore zone (Henley & Ellis, 1983; Reyes, 1990; White and Hedenquist, 1995).....	34
Figure 3.4. Distribution of hydrothermal alteration associated with high and low sulphidation deposits (White and Hedenquist, 1995).....	35
Figure 4.1. Location map of Ayının Tepe (Ahırözü kaolin deposits) and Yarıklı kaolin pits (Fuji et al., 1995).....	37
Figure 4.2. Field photographs of rock samples from L7 to L11 given on geology map of study area with close-up image of locations.....	46
Figure 4.3. Close-up location map of Hmd series including the photographs taken from the field.....	47
Figure 4.4. Hematite (red) and goethite (black) overprints observed in the field.....	48

Figure 4.5. Limonite veins occurred as stockwork structures in carbonated serpentized wall-rocks.....	48
Figure 4.6. Cross-section of topography from L-2 to L-6 (386366E 4409680N).....	49
Figure 4.7. General view of Ahrözü kaolin deposits.....	50
Figure 4.8. Kaolinized white colored rocks resulted from hydrothermal alteration of granitic rock.....	50
Figure 4.9. Cross-section drawn at the main deposit itself from northwest to northeast direction (386517E 4409334N).....	51
Figure 4.10. The contact between argillic alteration zone and gossan in the field. Rusty colored lithology refers to the gossan zone due the enrichment of iron in the rock component.....	52
Figure 4.11. Listwanite rock located at stop L-1 (386473E 4406690N).....	53
Figure 4.12. Cross-section drawn from southeast to northwest direction at 386061E 4412002N.....	54
Figure 4.13. Field photographs of rock samples from L-12/L-13 and H-series given on geology map of study area with close-up image of locations.....	56
Figure 4.14. Serpentized rock sample acquired from the H-8 location.....	57
Figure 5.1. Thin-section photos of L-1 showing the entity of carbonate alteration dominantly. A) “Dol” indicates dolomite B) “Opq” represents opaque minerals C) Veins are implied with circular marks and arrows D) “Hem” states the entity of hematite in brownish red colours.....	61

Figure 5.2. Thin-section micro-photographs taken from L-3 to L-6 rock samples. A. Photograph of the thin-section of L-3 rock sample in general indicating the abundance of kaolin “Kao” in the sample itself B. The micro-photograph of L-4A implies the silicification “Si” occurred after the argillic alteration “Arg” C. The veins consisting of secondary quartz crystals represented by “Qtz” at L-4B D. Hematite formation as a result of the oxidation of possible goethite minerals indicated by “Hem” at the rock sample L-4B.....	62
Figure 5.3. A. Entities of opaque minerals in the rock sample L-7 in spherical-circular shapes B. Argillic alteration in the rock sample L-7 followed by silicification C. “C” represents the the entity of “Crustification” in the rock throughout the external wall of the vein D. Relict foliated texture interstafified by opaque minerals resulted from the flow of chemical fluids throughout them E. Primary quartz “Qtz” crystals cut by argillic alteration F. Intense silicification “Si” dominated throughout the veins in the rock sample L-11.....	65
Figure 5.4. A. Primary large quartz crystals represented by “Qtz” in the sample of Hmd 1-1 B. Hmd 1-2 conserving its primary quartz minerals (Qtz) in addition to the secondary quartz crystals (Q2) C. Primary large quartz crystals (Qtz) in addition to clay material and silicification in Hmd 1-3 D. “Qtz” stands for primary quartz crystals conserved in fractured appearance filled by argillic material and subjected to silicification (Q2) in the rock-specimen of Hmd 1-4 E. Hmd 1-5 was subjected to silicification (Q2) and argillic alteration whereas it conserves its primary quartz crystals (Qtz) smaller in size comparing to the samples coded from 1 to 4 in Hmd 1 series F. Photograph of hematite (Hem) bearing veins and silicification (Q2) are given as an example in the rock sample of Hmd 1-6 G. Large and fractured quartz crystals (Qtz) detected in the rock-specimen Hmd 1-7 H. “Bio” stands for oxidized relict biotite minerals of Hmd 1-7.....	68

Figure 5.5.A. Primary quartz crystals “Qtz” cut by hematitic veins “Hem” in Hmd 1a	
B. Oxidized biotite mineral conserving partly its mottled extinction represented by “Bio” in the rock-specimen Hmd 1a	
C. Retained plagioclase minerals indicated by “Plg” in Hmd 1a	
D. Relict graphic texture (Grp) in the rock-sample Hmd 2a marked with a circular arrow.....	70
Figure 5.6.A. Silica matrix represented by “Si” examined in Hmd 3	
B. Rhombohedral shaped opaque minerals identified as goethite crystals (Goe) in Hmd 3	
C. “Hem” stands for hematite veins cutting silica (Si) matrix resulted as post event in Hmd 3	
D. Hematite (Hem) bearing carbonate (Ca) veins overlying the silica matrix in Hmd 3-1.....	71
Figure 5.7. A. Carbonate alteration is represented by “Ca” whereas “Hem” stands for hematite bearing veins in the rock-sample Hmd 1-7a	
B. Hmd 1-8 was enriched by wide veins coated by iron-oxide bearing fluids.....	72
Figure 5.8. Micro-photographs of thin-section examinations taken from rock-specimens L1A and L1B. A. Relict muscovite minerals represented by letter “Mus” in L1A rock specimen	
B. relict foliated texture represented by “Fol” in the figure with an arrow	
C. Quartz vein represented by “Qtz” whereas “Ca” stands for carbonate veins in rock sample L1A	
D. The letter “Opq” stands for opaque minerals resulted from the flow of chemical fluids through the carbonate vein represented by “Ca” in rock-specimen L1B.....	74
Figure 5.9. A. Comb textured carbonate vein are shown by the arrows in the sample L12-4	
B. Veins including amorphous silicate material “Si” crosscut by carbonate material filled vein in the rock-specimen L12-4. “Sme” in this figure stands for smectite mineral	
C. Veins fullfilled by hematite bearing carbonate material in rock-specimen L12-4.....	75
Figure 5.10. A. Stockwork structure coated rock-specimen L12-5a in which iron-bearing and carbonate material are observable. “Opq” represents cubic opaque minerals.	
B. Pseudomorph olivine crystal “Oli” in the sample L12-5a.	76

Figure 5.11. A. Relict plagioclase microlites “Plg” were observed in the thin-section examination of L12-5b B. “Act” stands for actinolite crystals marked with circular arrow in the photograph of the rock-sepcimen L12-5b C. Vesicles implying the entity of volcanic source rock represented by “Ves” filled by partially secondary carbonate material “Ca”.....	76
Figure 5.12. Crustification is shown in the rock sample L12-8. “Si” stands for amorphous silicate composing the crustified material whereas “Ca” representing carbonate recrystallized material.....	77
Figure 5.13. Micro-photograph of the rock sample H-2 A. Foliation texture represented by “Fo” whereas opaque minerals are shown by “Opq” B. Plagioclase minerals “Plg” are recognized with typical polysynthetic twinning C. Epidote “Epi” minerals are very well known key mineral while identifying propylitic alteration zones. Flakey muscovite mineral is shown by “Mus” in the figure.....	78
Figure 5.14. Micro-photograph of the rock sample H-3 A. Relict aphanitic texture of the rock-specimen represents the entity of volcanic source rock in the study area B. Plagioclase “Plg” and pyroxene “Pyx” crystals were identified in the thin section analyses C. Chlorite mineral was observed as a result of the propylitic alteration that the rock had been subjected to.....	79
Figure 5.15. Micro-photograph of H-5. “Mi” stands for mica minerals, whereas “Pyr” represents pyrite crystals.....	80
Figure 5.16. Micro-photograph of the rock sample H-6. The sample introduces silicified “Qtz” rock specimen representing siliceous sinter formation in the study area.....	81
Figure 5.17. A. XRD diagram showing the entity of chlorite (Chl), plagioclase (Plg), dolomite (Dol), magnetite (Mag) and Lime (syn) in the random extraction of the rock-specimen L-1 B. Clay fraction of the specimen L-1 including kaolin group minerals (Kao) treated by ethylene glycol C. L-1 clay fractionated mount heated at 300 °C including kaolin group minerals (Kao)....	84

Figure 5.18. A. The whole rock XRD diffractogram of rock-specimen L-5 showing the entity of pyrite “Pyr”, goethite “Goe” and magnetite “Mag”. In the figure, “Kao” symbolizes kaolin group minerals, K-Feldspar minerals and feldspar group minerals are shown by “K-Feld” and “Feld”, respectively. “Sulp” stands for sulphur whereas “Qtz” is short for quartz. B. The whole rock XRD diagram of rock-specimen L-7 in which hematite “Hem”, goethite “Goe” and magnetite “Mag” minerals are found. In the figure, “Ca” represents calcite detected different from the rock-sample L-5.....	86
Figure 5.19. Whole rock XRD diagram of the rock-specimen L-6 including dawsonite (Daw) mineral. In the diagram, smectite is represented by “Sme”, kaolin minerals by “Kao”, natroalunite indicated by “N” whereas “Qtz” and “K-feld” stand for quartz and K-Feldspar minerals.....	87
Figure 5.20. XRD diagram of L-3 comprising whole rock and clay fraction analyses (Ömeroğlu-Sayit et al. 2018).....	88
Figure 5.21. XRD analyses of L-12-1 including whole rock and clay fractions (Ömeroğlu-Sayit et al. 2018).....	90
Figure 5.22. XRD diffractometer of the rock-sample L-12-4 showing the entity of chlorite “Chl, talc “Tlc”, illite and mica minerals “I+Mca”, quartz “Qtz”, dolomite “Dol”, plagioclase “Plg”, magnetite “Mag”, psilomelane “Psi” and pyrolusite “Pyr”, respectively.....	91
Figure 5.23. XRD analyses of L-12-5b including whole rock and clay fractions.....	93
Figure 5.24. SEM-EDX analysis of sample L-6 from argillic zone revealing natroalunite (N) and halloysite (H) association (Ömeroğlu-Sayit et al. 2018)..	94
Figure 5.25. SEM-EDX analyses of the sample L-3 from argillic zone verifying the entity of kaolinite crystals both in morphological and chemical data. “Kao” stands for kaolinite stacks in this figure.....	95

Figure 5.26. SEM micro-photograph of Sample L12-1 showing chlorite morphology and the EDX analysis of chlorite (Chl) (Ömeroğlu-Sayıt et al. 2018).....	96
Figure 6.1. Trace element spider diagram of selected samples from the kaolin deposit (Ömeroğlu-Sayıt et al. 2018).....	103
Figure 6.2. Tectonic setting of granite in the study area (Pearce et al. 1984).Syn COLG, syn-collision granites; WPG, within-plate granites; VAG, volcanic arc granites; ORG, ocean ridge granites. Symbols are same as in Figure 6.1 (Ömeroğlu-Sayıt et al. 2018).....	104
Figure 6.3. CCPI vs AI diagram generated for representing samples to show the intensity of the alterations (modified from Large et al. 2001).....	109
Figure 6.4. Average Th °C and wt. % NaCl values of L 12-11 and Hmd 1-2 are plotted on the homogenizing temperature-salinity diagram (from Wilkinson, 2001) indicating epithermal type of hydrothermal deposits in the study area.....	112
Figure 6.5. Data derived by hydrogen and oxygen stable isotope analyses minerals (after Taylor, 1974).....	114
Figure 7.1. XRD pattern of BM 2-1A (starting material) acquired by using both backfill and smear method generated by using JADE software.....	119
Figure 7.2. A. Samples are crushed and powdered by using hammer B. Samples ground to pass 325 to 200 mesh sieves.....	120
Figure 7.3. A. Powdered sample was grinded B. Front side of the sample flattened by using backfill method to x-ray.....	120
Figure 7.4. Titanium made vessel used in the experiments.....	121
Figure 7.5. Pressure vs. time diagram show the changes observed at 80 ⁰ C. The minerals showed in red colour are the ones formed after the reaction.....	135
Figure 7.6. Pressure vs. time diagram used to plot each run for 25 ⁰ C by showing the components of final products. The minerals showed in red colour are the ones formed after the reaction.....	136

Figure 7.7. Comparison diagrams showing the existence of nesquehonite only in Run 2-3 in the solid phases of reaction products.....	137
Figure 7.8. Nesquehonite formation took place in Run 3-4 and Run 3-5 is given by comparing each final product with each other at 25 ⁰ C.....	138
Figure 8.1. Zone map of study area (after Gözler, 1987).....	140
Figure B-1. The final product obtained at the end of Run 2-2.....	171
Figure B-2. X-ray reaction pattern of Run 2-3.....	172
Figure B-3. Aqueous liquid of the final reaction product including nesquehonite in Run 2-3.....	173
Figure B-4. XRD pattern obtained from the reaction product at the end of Run 2-4.....	174
Figure B-5. Aqueous liquid of final reaction product obtained from Run 2-4 consisting of nesquehonite.....	175
Figure B-6. XRD pattern of reaction product of Run 2-5.....	176
Figure B-7. Aqueous liquid acquired from Run 2-5 including nesquehonite...	177
Figure B-8. X-ray pattern of the reaction product of Run 2-8.....	178
Figure B-9. Nesquehonite observed in the aqueous liquid of Run 2-8.....	179
Figure B-10. XRD results acquired from final reaction product at the end of Run 2-9.....	180
Figure B-11. XRD results acquired from the reaction material of Run 2-10...	181
Figure B-12. Nesquehonite produced in the co-existing aqueous liquid.....	182
Figure B-13. XRD pattern of final/reaction product of BM 2-1A at the end of Run 2-13.....	183
Figure C-1. XRD results obtained from reaction product of Run 3-4.....	185
Figure C-2. Nesquehonite obtained from aqueous liquid upon evaporation.....	186
Figure C-3. XRD pattern of reaction product of Run 3-5.....	187
Figure C-4. In the co-existing aqueous liquid product of Run 3-5, nesquehonite was described as newly formed mineral.....	188
Figure C-5. XRD results of Run 3-6.....	189

Figure C-6. XRD pattern showing the entity of nesquehonite and silicon oxide peaks in the co-existing aqueous liquid (Red lines represent silicon oxide whereas green lines indicate nesquehonite).....	190
Figure C-7. XRD patters for Run 3-8.....	191
Figure C-8. The co-existing aqueous liquid consisted of silicon oxide and nesquehonite.....	192

CHAPTER 1

INTRODUCTION

1.1. Overview:

Epithermal systems are known as near-surface systems related to gold, silver and base metal mineralizations. Epithermal systems are categorized into two main deposits which are high sulphidation (HS) and low sulphidation (LS). The term HS describes an initially S-rich hydrothermal systems in a relatively oxidized (SO₂) state (Hedenquist, 1987). High sulphidation (HS) deposits associated with continental type magma related hydrothermal systems are pertinent to andesitic volcanoes having high temperature fumaroles and acid-sulphate-chloride hot springs and crater lakes (Henley & Ellis, 1983; Arribas, 1995). On the other hand, low sulphidation (LS) systems form due to the interaction of near neutral pH and reduced H₂S rich hydrothermal fluids (Henley & Ellis, 1983; White & Hedenquist, 1995). Comparably, both LS and HS deposits arise in hydrothermal systems comprising silica sinter depositing hot springs and steam heated acid sulphate alterations (Henley & Ellis, 1983). It is known that general textural features of the LS systems contain cavity-filling veins with sharp boundaries, or stockworks of small veins (White & Hedenquist, 1995). Banded, crustiform with quartz, chalcedony-lined and druse-lined cavities, and vein breccias are determined as other textural aspects of LS deposits, as well (White & Hedenquist, 1995). As a common property, both LS and HS deposits are typically structurally controlled systems (White & Hedenquist, 1995). According to White & Hedenquist (1995), it has been stated that chalcedony, calcite and adularia are detected in LS deposits, whereas kaolinite, pyrophyllite-diaspore, alunite and barite observed more widespread in HS deposits. It is important

to determine alteration mineral assemblages and their zonations within epithermal deposits in order to provide useful information on economic mineralization related to hydrothermal systems (White & Hedenquist, 1995; Henley & Ellis, 1983; Reyes, 1990; Izawa et al., 1990; Meyer & Hemley, 1967).

In terms of clay minerals, under the neutral pH conditions (e.g. LS geochemical environment) smectite is stable at <160° C and transforms to interstratified illite-smectite and with increasing temperature, to illite, which is generally stable at >220°C (Reyes, 1990). On the other hand, comparing to the LS deposits, in HS deposits it more common to identify kaolinite, dickite, pyrophyllite, diaspore and alunite within alteration zones since these secondary mineralization products are stable under acidic conditions (Reyes, 1990).

It is determined that most of the Turkish kaolin deposits were resulted from hydrothermal processes influencing andesitic, dacitic rocks and their associated tuffs, granitic intrusions and less commonly metamorphic rocks (Seyhan, 1978; Sayın, 1984; Sayın, 2007; Sayın 2016; Ünal-Ercan et al. 2016). One of the most important Turkish kaolin deposits is hydrothermal originated Düvertepe kaolin deposits in the province of Balıkesir. Ece et al. (2013), studied these deposits and detected that these deposits were formed due to fault controlled hydrothermal alteration of Miocene rhyolites-rhyodacites and tuffs. In this study, kaolin type and alunite type paragenetic groups were also identified. Within this fault controlled deposit, throughout the Simav graben situated along Düvertepe and Şaphane district, high sulphidation system was determined. In addition to kaolinite and alunite type minerals, halloysite rich deposits were also detected in the Turplu area located to the northwest of Balıkesir on the Biga peninsula. These alteration resulted in mineral associates occurred related to the influences of sulfate rich hydrothermal and meteoric waters on the volcanic rocks across the fault zones (Ece & Schroeder, 2007; Ece et al. 2008). On the other hand, the kaolin occurrences in the Küre kaolin pit situated in the Bilecik region, Söğüt area, were formed as a result of shear faulted controlled hydrothermal alteration of granodioritic rocks. In the Çanakkale region, Çan district,

Kırıklar halloysite deposit which is the purest halloysite deposit of Turkey was found (Sayın, 1984). Kırıklar halloysite deposit was formed due to the hydrothermal alteration of dacitic crystal tuffs (Sayın, 1984). Sarıbeyli-Sığırlı and Bodurlar kaolin-alunite deposits were found to be located in the province of Çanakkale region resulting from the interaction of magmatic waters with the Late Eocene-Miocene calc-alkaline volcanic rocks in the region (Ünal-Ercan et al. 2016). According to Ünal-Ercan et al. 2016, mineral paragenesis observed in the study area in addition to the isotopic studies of $\delta^{18}\text{O}$ depletion and δD enrichment in the Sarıbeyli-Sığırlı and Bodurlar kaolin-alunite deposits represent both supergene and hypogene processes.

The genesis of the Hisarcık (Emet-Kütahya) kaolin deposits occurred due to the hydrothermal alteration of Miocene dacite and dacitic tuffs resulting in strong kaolinization in which mineral associations as kaolinite-alunite-natroalunite-hematite was detected in the vicinity of Kızılçukur, Ulaşlar and Kurtdere (Sayın, 2007).

Karaçayır kaolin deposits located in the Uşak-Güre basin were proved to be formed due to the epithermal hydrothermal alteration of both Miocene rhyolite-andesite and Paleozoic schists depending on mineralogical, chemical and isotopic data derived (Kadir & Erkoyun, 2013).

In the province of Eskişehir, around Mihaliççık district, Fuji et al. (1995) studied the kaolin deposits near Yarıkkı pit which was formed as a result of the hydrothermal alteration of fine grained tuff situated along the southern margin of the ophiolitic complex. Moreover, the Ayının Tepe pit kaolin deposits, which is one of the most significant kaolin resources of Turkey, distributed around Ahırözü-Üçbaşı-Hamidiye villages in the Mihaliççık district was investigated by Seyhan (1978) and Sincan (1978). The reason that makes these studies as the main concern in our research is that these sources comprise our present study area. In the Ayının Tepe pit location, granite and serpentinite rocks have fault contact resulting in hydrothermal alteration (Ömeroğlu-Sayıt et al. 2018).

Consequently, there was no detailed research associated with the occurrence, genesis and geology of kaolin deposits in the study area, located in Ahırözü, Mihaliççık district, Eskişehir-Turkey during the literature survey. Then, it was aimed to explore the hydrothermal alteration products and detect effective hydrothermal system type using mineralogical, textural and geochemical features within the Ahırözü kaolin deposits situated in Mihaliççık district, Eskişehir-Turkey. In order to study the genesis and geology of the Ahırözü kaolin deposits in relation to the epithermal system dominated in the study area, except from mineralogical and petrographical studies; fluid inclusion, isotope analyses, major oxides and trace element analyses were also conducted to reveal the hydrothermal alteration zones, mode of occurrence and tectonic setting of the kaolin deposits.

1.2. Purpose and Scope:

The purpose of this study is to investigate the mineralogy, geology and origin of hydrothermally occurred Ahırözü kaolin deposits distributed around Ahırözü-Hamidiye villages located to the southeast of Mihaliççık-Eskişehir province. Therefore, the research has intended to focus on the influences of hydrothermal fluids on the mineralogy, texture and composition of the rocks associated with the kaolin deposits exposed in the study area by using mineralogical, petrographical and geochemical methods. Moreover, it is also aimed to study other alteration products in relation to kaolin deposits in order to detect alteration zones dominated in the study area.

Accordingly, the context of the study, is limited by a set of questions given below:

1. What is the parent rock of kaolinized rock units, known as Ahırözü kaolin deposits, in the study area, both located at the Aydın Tepe pit and Hamidiye villages?

2. Which alteration products, except for kaolin, were observed in the study area?
3. How could we determine the original rocks of altered wall rocks distributed in the study area different from kaolinized rocks?
4. How can we explain the formation of listwanite in a hydrothermal area and the change in mineralogy of serpentinized ultramafic rocks while altering to listwanites?
5. Which alteration zones can be identified in the study area in relation to alteration products?
6. Regarding to the original rock of kaolinized rocks located in the study area, what is the tectonic setting of the protolith rock and how should we evaluate the geochemical imprints on these kaolinized rocks?
7. What is the origin/nature of fluids interacted with the original/ parent rock of kaolinized rocks in the study area?
8. Is Ahırözü kaolin deposit estimated as a part of an epithermal system? If it is, is it low-sulphidation system or high sulphidation system? Thus, in general, is the system influenced by meteoric waters or magmatic waters? Related to this, is the alteration occurred as a result of hypogene or supergene processes?

1.3. Study Area:

The study area is included within 1/25000 topographic map of İ-27. The kaolin deposits distributed around Ahırözü, Hamidiye and Üçbaşı villages are located to the southeast of Eskişehir-Mihalıççık district (Figure 1.1). The kaolin deposits are

distributed throughout a granitic intrusion which is represented by mainly yellow and green colours in Figure 1.1 due to increasing elevation values in the region.

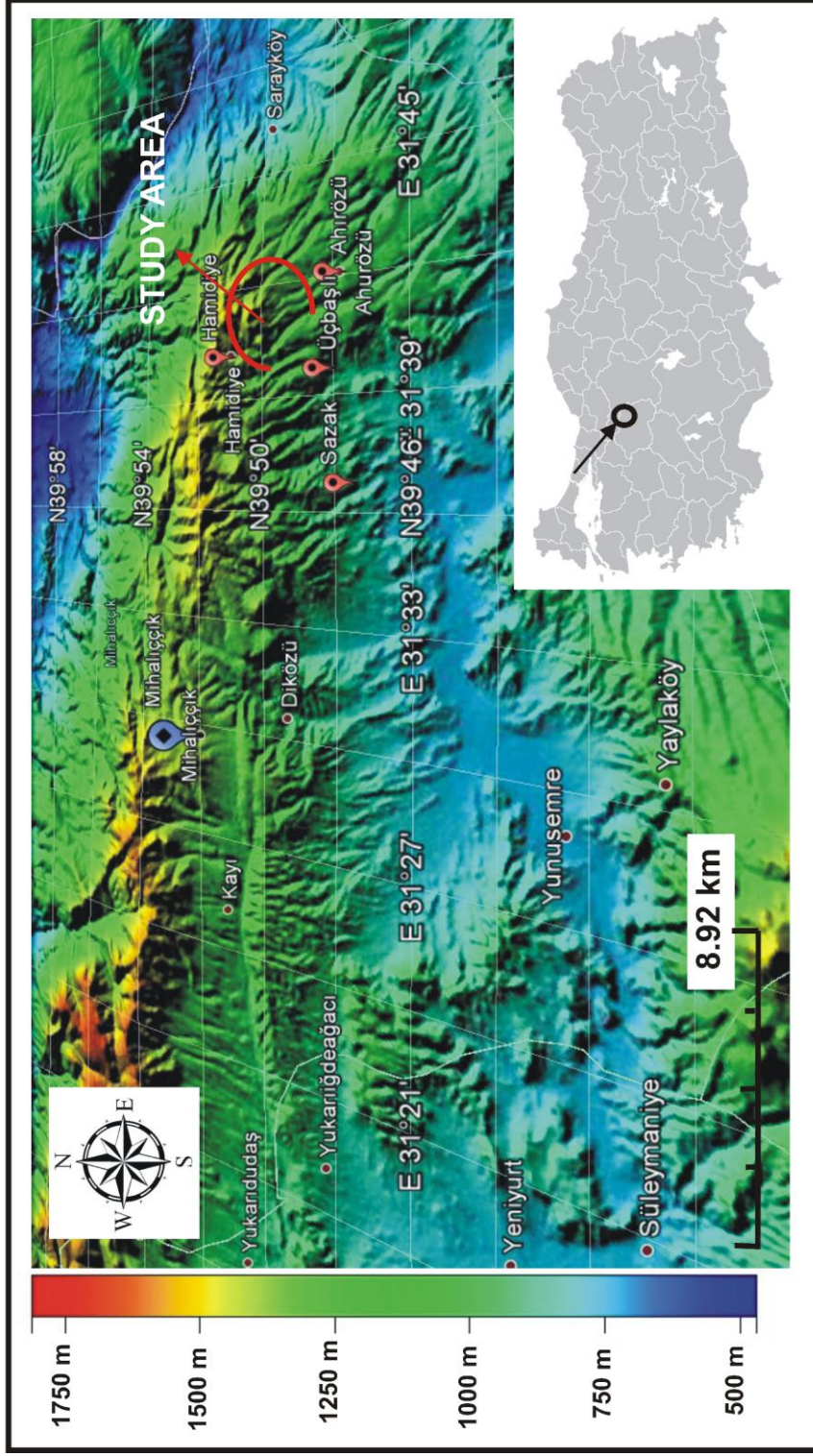


Figure 1.1. Location map of Ahırözü kaolin deposits. The circular area represents the main study area investigated in this study-Global Mapper SRTM and Google Earth Data (Ömeroğlu-Sayıt et al. 2018)

1.4. Previous Studies:

The literature survey has been focused on the sources comprising the kaolin deposits and their features occurred around and within the study area which is Mihaliççık province of Eskişehir and the studies performed related to the origin, geology and mineralogy of hydrothermally originated clay minerals, dominantly kaolin minerals, distributed in different regions of Turkey and some locations on the world. However, in addition to the sources related to the origin, geology and mineralogy of kaolin deposits, sources based on CO₂-H₂O-rock interaction reactions associated with the listwanite occurrence in the area of interest have been also discussed to form a basis to understand the alteration mineralogy occurred as a result of the hydrothermal processes in the study area. Moreover, it may be also stated that there are other sources mentioned below, briefly, compose a data-set related to the features of kaolin minerals, and related hydrothermal alteration mineralogy (e.g. carbonates, chlorites and etc.) by means of factors influencing their formation in epithermal deposits in order to define alteration zones (e.g. argillic alteration, propylitic alteration and etc.) and mineralization.

Seyhan (1978) revealed that many kaolin deposits in Turkey are hydrothermally originated. Additionally, in this study, the relevance between these kaolin deposits and hydrothermally originated mineralizations has been reviewed in detail. According to Seyhan (1978), it was revealed that intensive silicification and limonitization and the related ore minerals given as mercury, antimony, fluorite and sulphur are more like an indicator while defining the hydrothermal origin and the thickness of these hydrothermal kaolin deposits which are basically controlled by volcanic processes. Turkish kaolin deposits which were occurred due to hydrothermal processes are generally considered as uneconomic deposits since there is widespread alunization, pyrite mineralization and sulphur formations (Seyhan, 1978). The chemical processes occurred due to kaolinization result in the formation of high concentrated metallic ores (Seyhan, 1978). These chemical changes have an

influence on pH condition directly and increase the amount of illite and montmorillonite content within kaolin deposits (Seyhan, 1978).

Chen et al. (1997) focused on the kaolin deposits of the Kauling and Dazhou areas, Kiangsi, China. An investigation both on type locality and adjacent abandoned mining sites was performed in the scope of this study. The kaolinized muscovite-granitoid from the Dazhou mining area was delved by optical microscopy, XRD, TEM, SEM, EDS and isotopic analysis. The data introduced that the alteration of the granitic rocks was occurred as a result of two stages which were sericitic alteration of feldspar, probably triggered by hydrothermal fluids, and weathering of these granitic originated rocks.

Cravero et al. (1997) studied the geology and genesis of three kaolin deposits (Las Mellizas, Chita and Misud), located in the Neuquen basin (Argentina). In this research, kaolin mineralogy and oxygen isotopic data stated that kaolinite was formed in the lower to middle Jurassic times; then in which was transported into a fluvial environment.

Ekosse (2000) investigated, petrographically and mineralogically, the kaolin samples from the Makoro kaolin deposit in southeastern Botswana in order to reveal the genesis of this deposit. Mineral identification and characterization studies were conducted by using powder X-ray diffraction (XRD), differential thermal analyses/thermogravimetric analyses (DTA-TGA), and scanning electron microscopy with an energy dispersive X-ray spectrum (SEM-EDX) technique. According to the analyses performed in this study, it was determined that kaolinite was the major phyllosilicate in the deposit, while the smectite crystals were detected in minor values. On the other hand, hematite, goethite, quartz and K-feldspar were identified as accessory occurrences in the deposit, itself. Thus, the mineral associations and kaolinite morphology studied by SEM/ EDX method revealed that these kaolin deposits were originated from the alteration of feldspathic arenites-arkose.

Hansen et al. (2005) did a research on carbonated serpentinite (listwanite) at Atlin, British Columbia. According to the study, it was stated that listwanite was a carbonate-altered serpentinite mainly related to the gold and mercury mineralization. It represents a natural analogue to CO₂ sequestration. The reaction path was studied to be Serpentine + olivine + brucite reacted with CO₂ to form serpentine + magnesite, then magnesite + talc, and finally magnesite + quartz. In the study, it was implied that this mineralogical transformation could be tracked experimentally except for the volatile species; such as CO₂ and H₂O. These carbonation reactions resulting in a change of mineral chemistry were basically controlled by the CO₂ in the fluid phase.

According to Mutlu et al. (2005), the ore body included by Rhyolitic-Rhyodacitic Civanadağ Tuff Member located to Şaphane region in Western Anatolia consists of alunite, kaolin and more or less pyrite crystals. In this research, alunite formation was identified resulted from alteration of K-feldspars and volcanic glass found in the rhyolitic-rhyodacitic parent rocks.

Sei et al (2006) introduced a research associated with mineralogical, crystallographic and morphological characteristics of natural kaolins from the Ivory Coast (West Africa). Thirteen clay samples from four deposits in the Ivory Coast were studied using X-ray diffraction, thermogravimetric analysis and chemical analysis in which kaolinite was detected as a principal mineral. In the research, it was suggested that the kaolinite was the main mineral, whereas others were defined in minor values. The minor minerals detected in this study were illite, quartz, anatase and iron oxides. The entity of iron dioxide in relation to the deposit was determined that it was resulted from reduced structural ordering and thermal stability of kaolinite, as well.

dos Santos Jr. et al (2007) suggested a study connected with the origin of the Rio Capim kaolinites (northern Brazil) by using $\delta^{18}\text{O}$ and δD analyses. In the scope of the research, deuterium (δD) and oxygen ($\delta^{18}\text{O}$) isotope data from the Rio Capim kaolin, were combined with optical studies in order to determine the genesis of the kaolinites. The results showed that $\delta^{18}\text{O}$ values from a lower soft kaolin unit range

from 6.0‰ to 19.2‰ for Ka (size ranging from 1 to 3 μm) and Kb (size ranging from 10 to 30 μm) kaolinites, and from 15.4‰ to 24.9‰ for Kc (size <200 nm) kaolinites. The δD values range from -63.1‰ to 79.5‰ for the Ka+Kb kaolinites, and from -68.8‰ to -244.35‰ for the Kc kaolinites. An upper semi flint kaolin unit, dominated by Kc kaolinites, displays $\delta^{18}\text{O}$ and δD values ranging from 15.1‰ to 21.8‰, and -71.3‰ to -87.4‰ , respectively. Based on these data, and the $\delta^{18}\text{O}$ and δD values obtained for the surface meteoric water and groundwater, it has been concluded that the kaolinites are not in equilibrium with the modern weathering environment, but they reflect isotopic compositions of the formation time.

Sayın (2007) focused on the kaolin deposits, situated approximately 20 km south of Hisarcık-Kütahya, has been formed by the alteration of dacite and dacitic tuffs related to the Miocene volcanism associated with extensional tectonics. Kaolinite is the only clay mineral associated with alpha-quartz, K-feldspar, plagioclase, alunite, natroalunite and hematite in some kaolins, whereas, other kaolinite accompanies smectite, which represents a moderate kaolinization.

dos Santos Jr. and Rossetti (2008) discovered the origin of the Rio Capim Kaolin based on optical (petrographic and SEM) data. The Ipixuna Formation (Late Cretaceous?-Early Tertiary) exposed in the Rio Capim area, northern Brazil, is subdivided recently into three stratigraphic units, informally known as the lower soft kaolin, the intermediate kaolin, and the upper, endured, semi-flint kaolin. These units had their primary texture and composition strongly modified after deposition. Petrographic and scanning electronic microscopic (SEM) investigation revealed many remaining features that led to relate the soft and the semi-flint kaolin to two depositional sequences.

Dill et al. (2008) carried out a study related to the supergene and hypogene alteration in the dual-use kaolin-bearing coal deposit in Angren, SE Uzbekistan. The major coal seam, attaining a thickness between 4 and 24 m, is encased by kaolin-bearing bed-sets which were derived from supergene pre- and hypogene post coal kaolinization. Post-coal kaolinization affecting trachyandesites and trachytes is of

low-temperature origin and low-sulphidation-type. The temperature of formation was below 200 °C, deduced from the absence of dickite in the clay mineral assemblage.

Siddiqui and Ahmed (2008) studied the geochemistry of the kaolin deposits of Swat (Pakistan). Kaolin deposits of the Swat District in Pakistan were indicated to have been derived by hydrothermal alteration of felsic intrusives including high amount of feldspars in the component. Therefore, the raw kaolin containing unaltered plagioclase was characterized by a rather low silica (46.54–50.93%) and potash (0.1%), and high alumina (23.54–26.77%), Fe₂O₃ (1.73–5.45%) and lime (8.13–16.93%) content. Kaolinization has been proceeded with a decrease in SiO₂ and increase in Al₂O₃.

Fernandez-Caliani et al. (2010) conveyed a research investigating the origin and geochemical evolution of the Nuevo Montecastelo kaolin deposit (Galicia, NW Spain). The context of study provided an insight into large-scale kaolinization of Variscan granitoids in the Iberian massif. In the research, it has been detected that mineral composition of the kaolinized granite is dominated by well-ordered kaolinite with minor amounts of quartz, K-feldspar, mica (illite/ muscovite), locally emplaced gibbsite in addition to accessory minerals; such as rutile, ilmenite, zircon and monazite. According to the isotope composition of the kaolin, it has been observed that δ¹⁸O values vary around +20.5‰, whereas δD values diversify around –60‰ which are consistent with a supergene origin. Hence, it has been concluded that kaolinite distributed in the study area, was formed by extensive hydrolysis of feldspars, in equilibrium with meteoric waters at about 21 °C.

Ünal (2010), focused on two different epithermal gold deposits (Kartaldağ and Madendağ) in Çanakkale, Turkey. The study includes isotopic, geochemical, mineralogical-petrographical and fluid inclusion analyses. The purpose of the research was to reveal the genetic formation of these deposits. According to the study, Kartaldağ deposit was composed of four main alteration types which were propylitic, quartz-kaolin, quartz-alunite-pyrophyllite and silicification. On the other

hand, Madendağ deposit includes two alteration types; such as argillization and silicification. Illite and kaolin were detected as the most abundant clay minerals in the argillic zone. Oxygen and sulphur isotope analyses were conducted on quartz minerals. In Kartaldağ deposit, regarding to oxygen and sulphur isotope analyses, carried on quartz ($\delta^{18}\text{O}$: 7.93- 8.95 ‰) and pyrite ($\delta^{34}\text{S}$: -4.8 ‰) minerals, it was suggested that there was a magmatic source for the fluid. On the contrary, isotopic data performed on quartz ($\delta^{18}\text{O}$: 9.55-18.19 ‰) mineral in Madendağ deposit, it was detected that there was a contribution of metamorphic fluid.

Baioumy (2013) studied the origin and geochemistry of the Cretaceous sedimentary kaolin deposits in Red Sea, Egypt. Mineralogical and geochemical analyses of both bulk deposits in addition to the sand and clay fractions acquired from these deposits indicated that they are composed of kaolinite (average of 75 wt.%) and quartz (average of 22 wt.%) . The results derived from clay fractions of the samples showed that they are composed of relatively high contents of TiO_2 (average of 2.1%), Ni (average of 103 ppm), Nb (average of 98 ppm), Y (average of 67 ppm), and Zr (average of 630 ppm).

Abdioğlu et al. (2015) introduced a study on alteration mineralogy, lithochemistry and stable isotope geochemistry of the Murgul (Artvin, NE Turkey) volcanic hosted massive sulfide deposit. Mineralogical results derived from the studies were like; illite, illite/smectite + chlorite \pm kaolinite and chlorite in the footwall rocks, whereas illite \pm smectite \pm kaolinite and chlorite \pm illite in the hangingwall rocks. On the other hand, the alteration pattern was given as silica, sericite, chlorite and chlorite–carbonate–epidote–sericite (propylitic alteration zone) and quartz/albite zones.

Dill et al. (2015) focused on mineralogical, chemical and micromorphological studies of the argillic alteration zone of the epithermal gold deposit Ovacik, Western Turkey. In the scope of the study, it was determined that the outward side of the argillic alteration zones formed a transition between the ore zone and the subvolcanic, volcanic and volcanoclastic host rocks. By using XRD and SEM-EDX

methods, it was also detected that these zones include zircon, pyrite and barite minerals as accessory minerals.

Akaryalı (2016) introduced that the area situated in Altınpınar district, Torul-Gümüşhane to the south of Eastern Pontides is considered to be one of the most important metallogenic provinces in the Alpine-Himalayan belt which was intruded by the Late Carboniferous granitic rocks, known as Gümüşhane granitoid. Pb, Zn and +/- Au mineralizations within the study area was found to be related to the silica veins varying from few millimeters to 40 cm in thickness. Alteration mineralogy includes sulfidic, hematitic, silicic, argillic, intense chloritic and carbonate minerals in the study area. Sphalerite, galena, pyrite, chalcopyrite, tennantite and quartz were observed as mineral associations. Fluid inclusion analyses were also conducted to identify the origin of this deposit, whether it was epithermal or not. The homogenization temperatures were detected between 170 °C and 380 °C. On the other hand, the wt.% NaCl eqv. salinity of ore-forming fluids varied from 2.4 to 7.3 by verifying the epithermal system's entity. Moreover, according to the oxygen and hydrogen isotope analyses, varying between 8.5‰-10.2‰ and -91‰--73‰, respectively, it has been revealed that the fluids including the mineralization were derived from the mixture of magmatic and meteoric water in the deposit.

Boskabadi et al (2016) studied carbonate alteration of ophiolitic rocks in Egypt and the implications of the formation Au deposits, as well. They investigated ultramafic rocks, the member of ophiolite in the Arabian-Nubian Shield (ANS) introducing a wide carbonate alteration by forming carbonated serpentinites, and thus, listwanites. Carbonation of rocks takes place when rocks interact with CO₂ enriched fluids by causing alteration and precipitation of carbonate minerals. Mafic and ultramafic rocks tend to be exposed to carbonation due to the entity of olivine ((Mg,Fe)₂SiO₄) and pyroxene ((Ca,Mg,Fe)₂Si₂O₆) since when these minerals react with H₂O and CO₂, the reaction ends up with hydrous silicates as serpentine, Fe-oxides (e.g. magnetite) and carbonate minerals (Kelemen & Matter, 2009). As a result of the study, it was suggested that carbonation of ANS ultramafic units associate with the

influx of mantle originated CO₂-bearing fluids resulting in break down of Au-bearing minerals by releasing Au and S to the hydrothermal system in order to form the Au-deposits itself.

1.5. Method of Study:

Geological field investigations and laboratory research constituted the two major steps for the methodology applied during the study. A total of 59 rock samples were collected from the kaolin deposits and the outcrops of granitic, mafic/ultramafic and metamorphic rock units.

Polarizing microscope was used while investigating the mineralogical properties of the rock samples acquired from the study area. Moreover, the scanning electron microscope equipped with energy dispersive X-ray spectrometer (SEM-EDX) and X-ray powder diffractometer (XRD) were also used while studying mineralogical and petrographical properties of the rock samples. SEM-EDX analyses were performed in the Central Laboratory of Middle East Technical University whereas thin-section analyses and XRD analyses were conducted in the laboratories of the Department of Geological Engineering, Middle East Technical University.

Chemical analysis of the samples was carried out by inductively coupled plasma mass spectrometry (ICP-MS) and inductively coupled plasma emission spectrometry (ICP-ES) by ACME Analytical Laboratories Ltd. (Vancouver, Canada).

Fluid inclusion studies were performed at the General Directorate of the Mineral Research and Exploration, Ankara. In the meanwhile, stable isotope analyses were conducted by Cornell Isotope Laboratory in Ithaca, New York, USA. CO₂-H₂O-rock interaction experiments based on serpentine reactions to listwanite were carried out in the University of Illinois at Chicago, USA, as well.

The whole rock and clay mineralogy of the samples were preferred to be studied by using XRD, a Rigaku Miniflex II diffractometer with Ni filtered CuK α radiation, and a graphite monochromator in the Department of Geological Engineering, METU as it was indicated previously. The X-ray tube of the machine was always operated at 35kV and 15 mA with a scanning speed of $2^\circ 2\theta$ /min. Clay fractions were separated with the grain size of $<2\mu\text{m}$. Afterwards, the whole rock sample was first treated by buffer solution (NaOAc) in order to eliminate the carbonate cement might have been included (Jackson, 1975). In general, sedimentation and centrifugation were carried out after the acid treatment to obtain clay paste. XRD mounts were prepared by using smear method by applying clay paste on glass slides. XRD diffractograms were generated for air-dried (AD), ethylene glycolated (EG), heated at 350° and 550°C (Jackson, 1975).

SEM-EDX studies were performed by means of Quanta 400F field emission instrument in order to identify crystal morphologies and textural characteristics. Operating conditions were adjusted as 32 s counting time and 20kV accelerating voltage. Additionally, chemical data were obtained by EDX.

Fluid inclusions were studied in transparent gangue mineral quartz collected from kaolinized samples. A total of four (4) kaolinized samples (L12-11, L12-2, Hmd 1-4 and Hmd 1-2) were analyzed in order to estimate the homogenization temperatures (Th°C) and salinity (NaCl %) values. The analysis was performed by using Leica DM 2500P microscope LINCAMMDS 600TS 1500. Fluid inclusion analysis system available at General Directorate of Mineral Research and Exploration (MTA) Mineralogy Petrography Laboratories.

Experimental studies carried out on “CO₂ Sequestration of ultramafic rocks in hydrothermal fields” using by “Environmental Chamber”, based on pressure and temperature rates, were performed in University of Illinois at Chicago under the supervision of Prof. Dr. Steve Guggenheim in 2014. The aim of the experiments were to study rock-water-CO₂ interactions of listwanites (carbonate-altered serpentinites) since the listwanites were observed very widely within the granite and

serpentinite contact zone where hydrothermal kaolin deposits occurred in the study area.

Stable isotope analyses (Oxygen and Hydrogen analyses) were performed on a Thermo Delta V ratio mass spectrometer (IRMS) in Cornell Stable Isotope Laboratories interfaced to a Temperature Conversion Elemental Analyzer (TC/EA). The columns in summarized run worksheets were labelled as follows:

Sample/ Standard ID: This is the name of the sample and the name of the in-house standards.

Weight (mg): Weight of sample/ standard in mg

H₂ and CO Amp: The amplitude of the sample peak in mV

%H or %O: The percent element results

$\delta^2\text{H}$ or $\delta^{18}\text{O}$ vs VSMOW: This is the corrected isotope delta value for ^2H and ^{18}O measured against a primary reference scale. The primary reference scale for these isotopes is Vienna Standard Mean Ocean Water.

Note: Delta values are measured in units of per mil (‰)

In these analyses it was also verified that in-house and chemical standards were routinely calibrated against international reference materials provided by the International Atomic Energy Association (IAEA). To ensure the accuracy and precision of the instrument an in-house standard was analyzed after every 12 samples. The standard deviation for the internal standard Internal Benzoic Acid for $\delta^2\text{H}$ was 1.63 ‰ and for $\delta^{18}\text{O}$ was 0.31 ‰. Corrections were performed using a two point normalization (regression) based on a standards IAEA CO-1 and IAEA CO-8 for $\delta^{18}\text{O}$ IAEA CH7 and EMA -P1 for $\delta^2\text{H}$.

CHAPTER 2

REGIONAL GEOLOGY

This chapter is a review of the geology of the study area and its environment based on the published data in the literature. The chapter is divided into two sections. The first section describes evolution of the tectonic setting in which the study area, Ahırözü kaolin deposit, is located. In the second section, the stratigraphy and local geology of the area will be explained based on the geological maps prepared by the General Directorate of Mineral Research and Exploration of Turkey (Gözler, 1987).

2.1. Tectonic Setting of the Region:

Okay, (2008) suggested that Turkey is composed of several continental sectors combined together into a single landmass in the Late Tertiary. Continental sectors were separated by oceans resulted in ophiolitic sequences distributed across the Anatolia by forming terranes. There are three terranes occurred in northern Turkey which are Strandja, İstanbul and Sakarya, known as the Pontides. Pontides are terranes derived from Variscan and Cimmeride orogenies. Pontides were formed resulting from merging of pontic terranes in a single terrane during the Mid-Cretaceous times. The Pontides were occurred as a large region consisting of northern fragment of İzmir-Ankara-Erzincan suture. Three terranes of Pontides, called as Strandja, İstanbul and Sakarya, were evolved totally different geologically. The Sakarya terrane, *in which our study area is situated*, extends from the Aegean region of Turkey from the west to the Eastern Pontides (Figure 2.1).

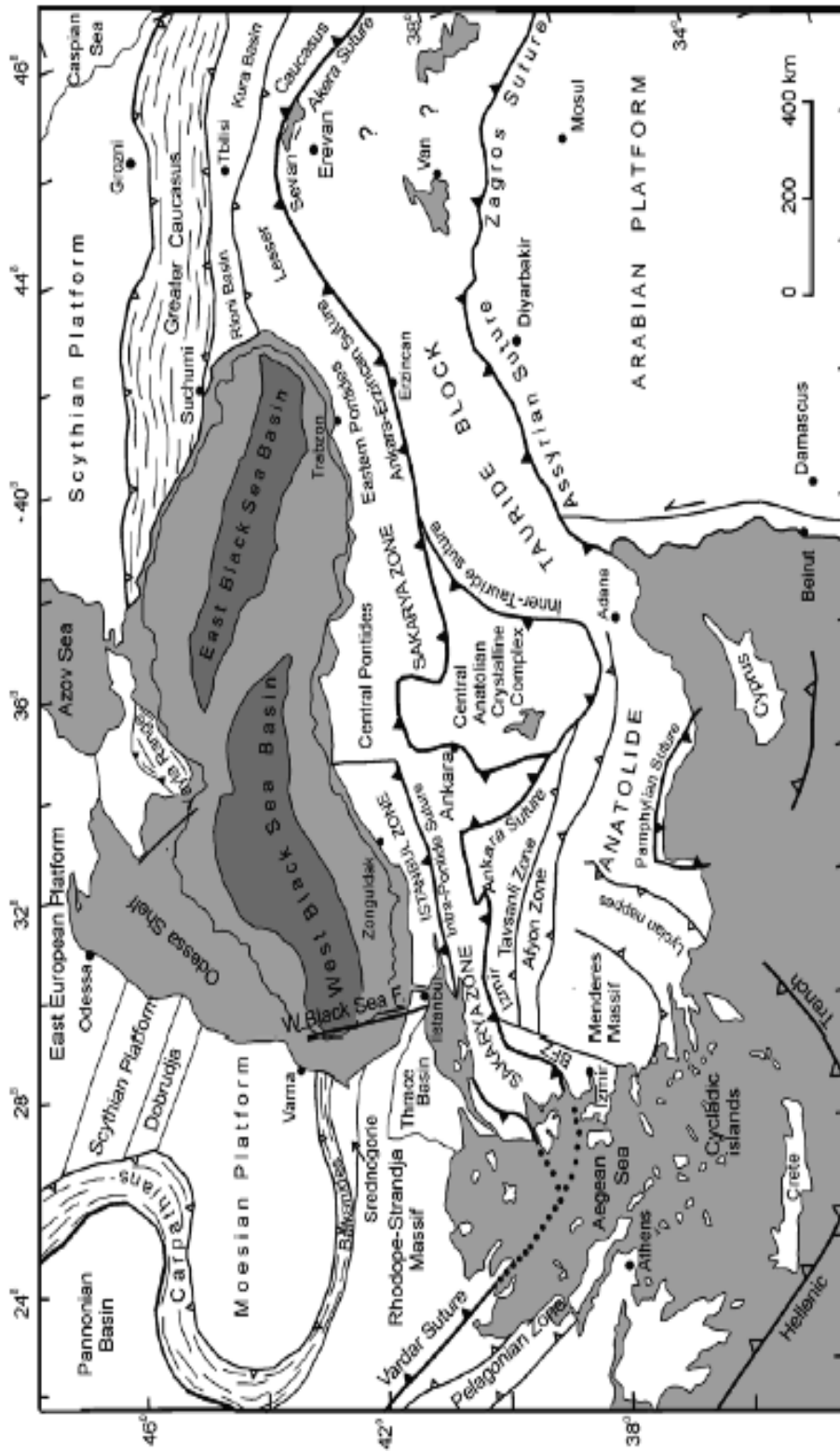


Figure 2.1. Tectonic map of Turkey comprising the major sutures and continental blocks (Okay & Tüysüz 1999; Okay, 2008)

The Sakarya terrane includes Variscan metamorphic sequence composed of gneiss, amphibolites, marble and metaperidotite (Okay, 2008). The age of the metamorphic sequence has been determined as Carboniferous (Topuz et al., 2004; Topuz et al., 2007 and Okay et al., 2006). Granitoids formed in the crystalline basement of Sakarya terrane have been dated to Devonian, Carboniferous or Permian ages (Delaloye & Bingöl, 2000; Okay et al., 2002; Okay et al., 2006; Okay, 2008; Topuz et al., 2007).

The Lower Karakaya Complex which is a low grade metamorphic complex, as a member of Sakarya terrane, consists of Permo-Triassic metabasite in addition to Late Triassic blue-schists and eclogites (Okay & Monie, 1997; Okay et al., 2002; Okay, 2008) (Figure 2.2).

The Lower Karakaya Complex is overlain by clastic and volcanic rocks with Carboniferous and Permian limestone and radiolarian chert blocks (Okay, 2008). The Karakaya Complex is unconformably overlain by the Early Jurassic sedimentary and volcanic succession (Okay, 2008). Early Jurassic lithology is represented by fluvial to shallow marine sandstone, shale and conglomerate units whereas volcanic succession is differentiated by volcanoclastic rocks to the east (Okay, 2008). The Central Pontides are identified with granitic rocks which was intruded in early to Mid Jurassic times (Yılmaz & Boztuğ, 1986; Okay, 2008).

Altner et al. (1991) suggested that the Lower Jurassic clastics of Karakaya Complex are overlain by Upper Jurassic-Lower Cretaceous limestone units. These limestones are, then, overlain by deep sea sandstones and shales as a result of the Alpidic orogeny (Okay, 2008).

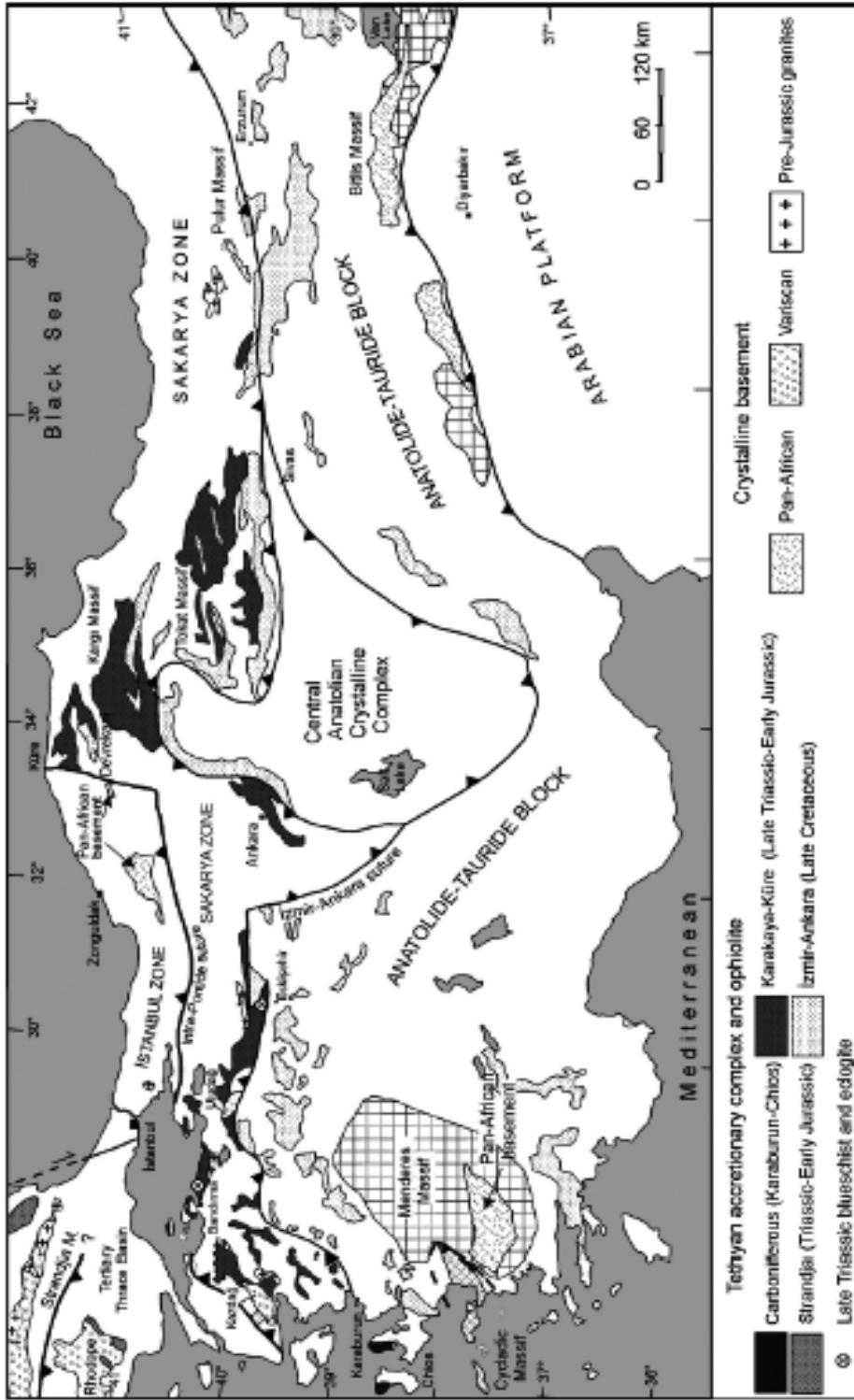


Figure 2.2. Tectonic map showing different basement types and complexes of Turkey (Okay et al., 2006; Okay, 2008)

2.2. Geologic Setting and Stratigraphy of Study Area:

The basement rocks in the study area comprise Early to Middle Triassic blue-green schists, and marbles, and serpentinite rocks (Gözler, 1987). Early Eocene to Late Miocene sedimentary rocks which are conglomerate, sandstone, marl, dolomitic claystone and limestone overlay the basement formations; Early to Middle Triassic metamorphic units and ultramafic rocks, unconformably (Gözler, 1987; Karakaş, 2006). The recent alluvial deposits, observed as partially terrace deposits, in the study area lie unconformably over these older units and resulted in the formation of the topmost lithology in the generalized stratigraphic section of the region (Figure 2.3 & Figure 2.4). In the study area, Late Triassic aged granitic rock units are situated to the south of Hamidiye village, whereas Early-Mid Triassic blue-green schists and marble as metamorphic units are located to the north of Hamidiye village (Figure 2.3) (Gözler, 1987).

In the studied area, faulted boundaries between the granites, serpentinites and schists by forming the channel-ways for hydrothermal solutions may cause the alteration of wall rocks giving rise to the kaolin occurrences in granite and carbonate-silica enrichment (so called listwanite) in serpentinite (Sincan,1978).

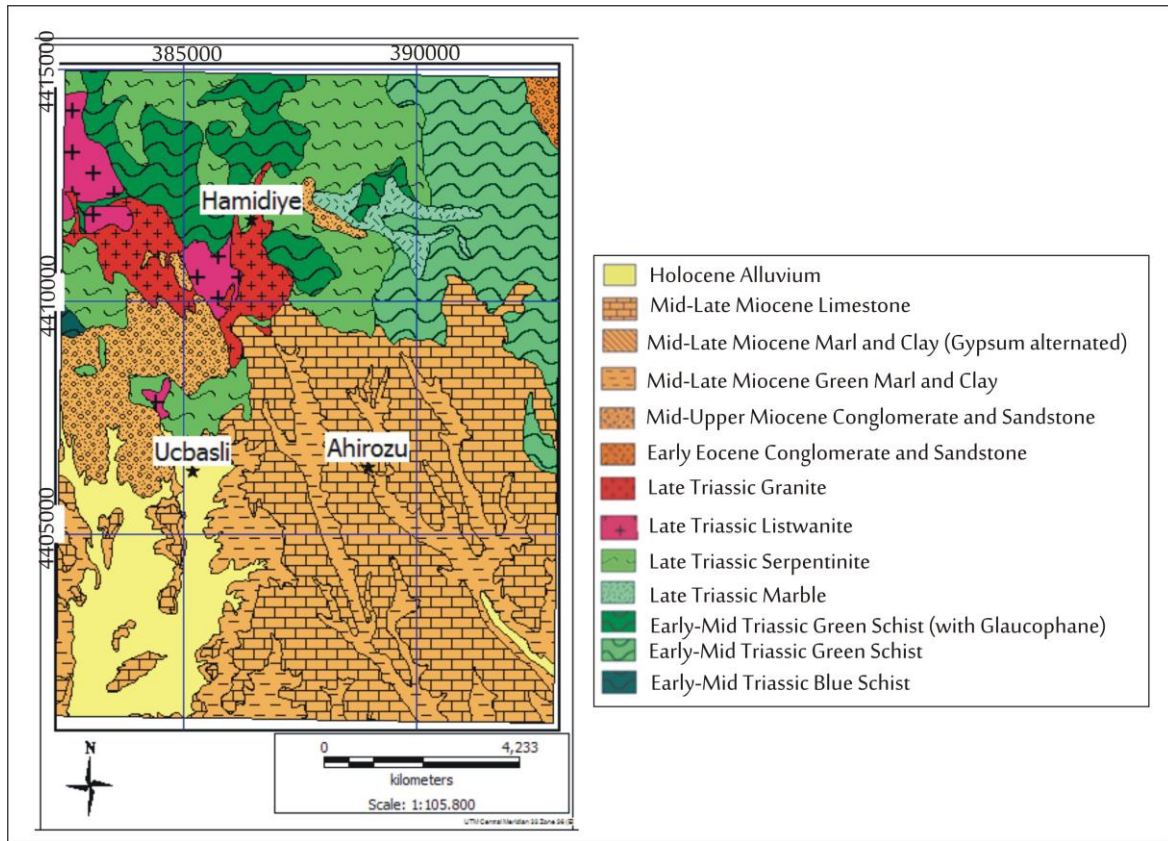


Figure 2.3. Geologic map of the study area (after Gözler, 1987)

Period	Epoch	Lithology	Description
Quaternary	Holocene		Alluvium
Neogene	Mid-Late Miocene		Limestone
			Gypsum alternated marl and clay
			Green marl and clay
			Conglomerate and sandstone
Paleogene	Early Eocene		Conglomerate and sandstone
Triassic	Late		Granite
			Listwanite
			Serpentinite
	Early- Mid		Marble
			Glaucophanitic green schist
			Green Schist

Figure 2.4. Generalized stratigraphic section of the study area (after Gözler, 1987)

CHAPTER 3

EPITHERMAL DEPOSITS

In this chapter, the features of epithermal deposits will be stated to understand the emplacement of Ahırözü kaolin deposits in the model of a dynamic system. The main study area in this research is composed of different alteration products introducing different alteration zones with the entity of mineralizations which arises a question whether this system, in general, is influenced by meteoric or magmatic water sources meaning if the alteration occurred as a result of hypogene or supergene processes.

Two main classes of epithermal deposits can be determined as “Low Sulphidation” and “High Sulphidation”. However, the main properties differentiating the sub-types of epithermal deposits have been recently listed in Table 3.1 in order to compare them, briefly.

3.1. High Sulfidation Deposits:

High sulfidation deposits (HS) generate from oxidized magmatic source arising to the near-surface with water-rock interaction at depth (White & Hedenquist, 1995). Thus, in HS systems, the HCl- and SO₂-rich vapor can be absorbed by groundwater by resulting in a hot (200-300°C), and highly acidic (pH 0-2) fluid (Rye, 1993; White & Hedenquist, 1995).

Table 3.1. Characteristics of acid-sulphate (high sulphidation) and adularia-sericite (low sulphidation) type deposits (compiled from White & Hedenquist, 1995; Hedenquist et al., 1996; Sillitoe & Hedenquist, 2003)

	Acid-Sulphate	Adularia-Sericite
Structural setting	Intrusive centres	Structurally complex volcanic environments, commonly in calderas
Size: length / width ratio	Relatively small equidimensional	Variable; some very large, usually 3:1 or greater
Host rocks	Rhyodacite typical	Silicic to intermediate volcanics
Timing of ore and host	Similar ages of host and ore (<0.5 Ma.)	Ages of host and ore distinct (>1 Ma.)
Mineralogy	Enargite, pyrite, native gold, electrum, and base-metal sulphides. Chlorite rare. No selenides. Mn-minerals rare. Sometimes bismuthinite.	Argentite, tetrahedrite, tennantite, native silver and gold, and base-metal sulphides. Chlorite common. Selenides present. Mn gangue present. No bismuthinite.
Production data	Both gold- and silver- rich deposits, noteworthy Cu production	Both gold- and silver-rich deposits, variable base-metal
Alteration	Advanced argillic to argillic (\pm - sericitic)	Sericitic to argillic ¹
Key Alteration Mineralogy	Extensive hypogene alunite. Major hypogene kaolinite. No adularia Pyrophyllite is very common Dickite at depth	Supergene alunite. Occasional kaolinite. Abundant adularia
Source of fluids	Dominantly meteoric, possibly significant magmatic component	Dominantly meteoric
Silica Gangue	Massive and fine grained silicification, vuggy residual quartz	Vein filling crustiform and comb quartz/ chalcedony, carbonate replacement texture
Source of sulphide sulphur	Deep-seated, probably magmatic	Deep-seated, probably derived by leaching wallrocks deep in system
Source of lead	Volcanic rocks or magmatic fluids	Precambrian or Phanerozoic rocks under volcanics
¹ Could be supergene in some districts.		

HS deposits dominantly consist of quartz with subordinate barite in their shallower parts in addition to enargite-luzonite (more rarely stibio-luzonite and famatinite) and tennantite-tetrahedrite (Arribas, 1995). FeS_2 included minerals; such as pyrite, marcasite and melnikovite are widely observed in these deposits, as well (Sillitoe & Hedenquist, 2003). Covellite, chalcocite and bismuthinite can be identified, occasionally (Arribas, 1995).

Regarding to the detailed research of the Summitville Au-Cu-Ag deposit, Stoffregen (1987) showed that a fracture controlled vuggy silica rock which is composed of intense leached volcanic rock including quartz in its content is a common distinguishing property for HS deposits (Figure 3.1) (Arribas, 1995).

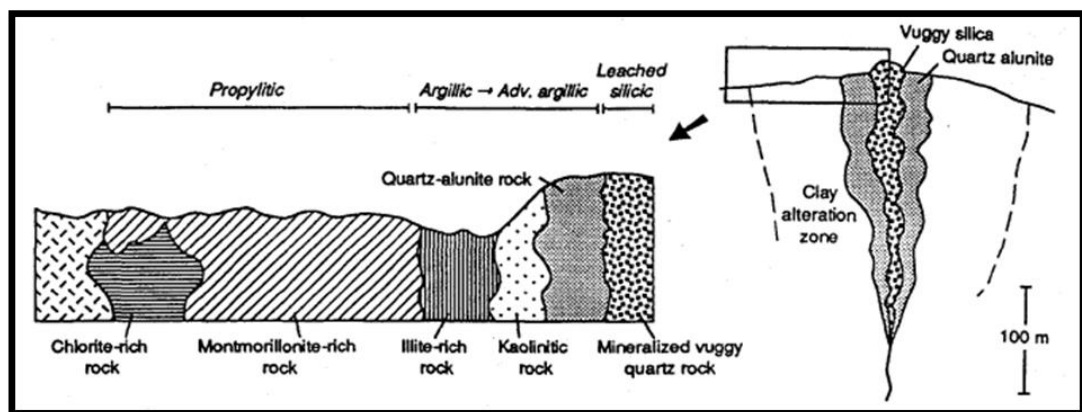


Figure 3.1. Cross-sections of alteration zones characteristic for high sulphidation deposits (Stoffregen, 1987; Arribas, 1995)

The phantoms in high sulphidation can be derived by different mechanisms in principal geological environments (Bethke, 1984; Rye et al., 1992; Arribas, 1995):

1. *By the disproportionation of magmatic SO_2 to H_2SO_4 and H_2S (magmatic hydrothermal)*

2. *As a result of atmospheric oxidation of H₂S in the vadose zone over the water table, connected with fumarolic discharge of vapor unleashed by deeper boiling fluids (steam-heated)*

3. *Due to atmospheric oxidation of sulfides resulted from weathering*

Magmatic hydrothermal alunite is associated with minerals which are diaspore, pyrophyllite, kaolinite, dickite, and zunyiteas resulted from hypogene ($T = 200\text{-}350\text{ }^{\circ}\text{C}$) acidic conditions (Meyer & Hemley, 1967). This kind of alunite is formed characteristically in HS deposits, however it may also be determined in such areas dominated by advanced argillic alteration void of ore mineralization (Iwao, 1962; Hall, 1978). Alunite, in steam-heated environments, forms together with kaolinite except from interlayered illite smectite transpires approximately at the temperatures changing from 100 to 160 °C where fumarolic vapor condenses above the boiling zone of neutral-pH, H₂S-rich fluid which is known as a typical occurrence of the systems leading to low-sulfidation deposits (Arribas, 1995).

As a result of magma degassing, different styles of magmatic-hydrothermal systems with or without associated mineralization may occur (Giggenbach, 1992). To form the styles of alteration and alteration zones in HS deposits, degassing must serve an important function with oxidized high temperature magmatic vapor reaching shallow depths with little reaction with rock or dilution by groundwaters at greater depths (Figure 3.2.A) (Arribas, 1995).

In high sulphidation deposits, when high temperature magmatic vapor reaches shallow depths (less than a kilometer), it can be absorbed by groundwater. As a result of this interaction, the liquid starts to cool, first at temperatures below ~400 °C by disproportionate of SO₂ to form H₂SO₄ and H₂S (Arribas 1995), then by progressive dissociation of H₂SO₄ and HCl at lower temperatures (<300 °C). Hence, due to the reaction of increasing acidic liquid with wallrock results an upward alteration sequence of sericite, alunite, kaolinite and vuggy silica, respectively (Figure 3.2.A) (Arribas, 1995). The vuggy silica rock results from leaching of rock

contents by hydrothermal solution with a pH <2 and temperatures probably <250 °C (Stoffregen 1987). Based on the volatile transport hypotheses (Figure 3.2.B₁), the magmatic hypersaline liquid may revolve at depth throughout the evolution of the hydrothermal system resulting in mineralization (Arribas, 1995). In the hypersaline liquid transport hypothesis (Figure 3.2.B₂), the magmatic vapor plume responsible for early alteration, whereas the lithostatic-pressured system fractures and the metal-bearing hypersaline liquid may tend to move into the porous leached zone (Hedenquist et al. 1994).

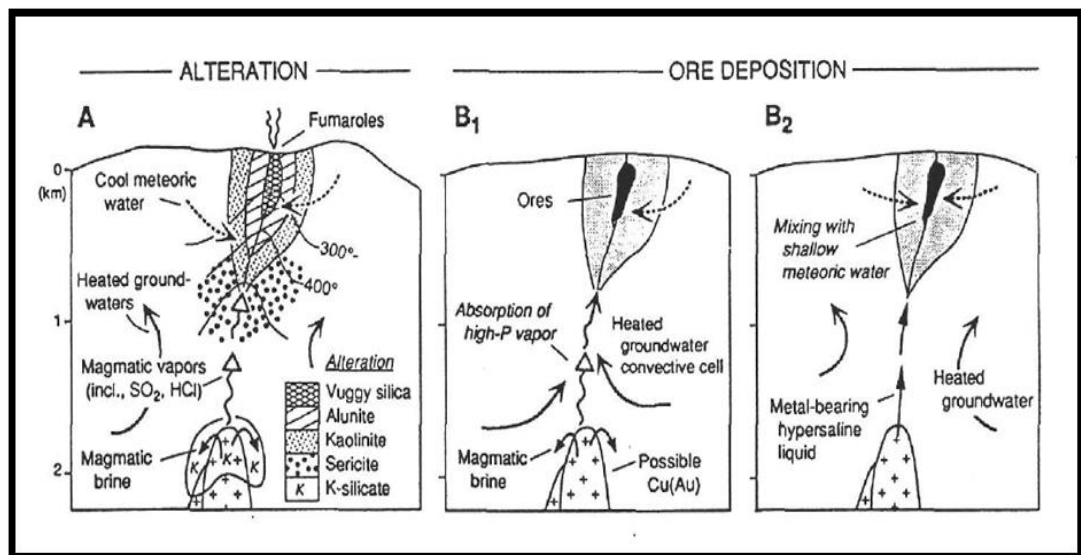


Figure 3.2. Models showing two main stages of evolution of HS systems (White, 1991; Rye, 1993; Hedenquist et al., 1994; Arribas, 1995)

3.2. Low Sulfidation Deposits:

When we compare the low and high sulfidation deposits we should take into consideration that there is considerable overlap in characteristics, but there are also many distinctive aspects in the features of determining the type of the epithermal deposit.

Generally, it is determined that low-sulfidation (LS) deposits consist of **cavity-filling veins** with sharp boundaries, or **stockworks** of small veins (White & Hedenquist 1995). Veins may be also important in high-sulfidation deposits, however the majority consist of dispersed ores replacing a leached country rock (White & Hedenquist, 1995). Both type of sulphidation deposits are typically structurally controlled.

LS-Deposits show wide variety of textures which are described as *banded, crustiform quartz and chalcedony veins, druse-lined cavities, and spectacular, multiple-episode vein breccias* (White & Hedenquist, 1995).

The ore-associated alteration in low-sulfidation deposits is produced as a result of near-neutral pH thermal waters, in addition to temperature decreasing with decreasing depth and increasing distance due to fluid flow (White & Hedenquist, 1995).

With increasing temperature, smectite (stable at <160°C), transforms to interstratified illite-smectite in which illite is generally stable at >220°C (Reyes, 1990). This type of progression commonly results in upward and outward zonation of minerals from low-sulfidation ore bodies, as well (White & Hedenquist, 1995). The ore zones contain minerals stating the highest pH (adularia and calcite), where it causes CO₂ loss and increase in pH (White & Hedenquist, 1995). Other temperature-sensitive minerals can be Ca-silicates such as epidote (stable above 200-240°C); and/or hydrothermal biotite and amphiboles occurred about 280°C (White & Hedenquist, 1995).

In contrast to neutral-pH alteration, minerals such as kaolinite, dickite, pyrophyllite, diaspore and alunite are stable under acidic conditions (Reyes, 1990) (Figure 3.3). Pyrophyllite may form at a temperature which is less than 160°C. At the condition in which pyrophyllite occurs, silica molecules concentrate at high amounts by forming chalcedony or amorphous silica; however it is also determined that as a result of this progression, pyrophyllite may associate with dickite or illite where the temperature is less than 200°C (White & Hedenquist, 1995).

In LS-systems it is stated that the host rock most is mainly composed of leached silicic alteration in addition to advanced argillic alteration (White & Hedenquist, 1995).

Some of the lower temperature, acid-stable minerals, such as kaolinite and alunite, are also formed resulting from the reaction of near-surface steam-heated waters with the host rock (Figure 3.4) (White and Hedenquist, 1995). In these systems acid-sulfate waters form at near 100°C (Reyes, 1990). Where hydrothermal kaolinite and alunite occur in these deposits, they are either overlying or overprinting alteration zones (White and Hedenquist, 1995).

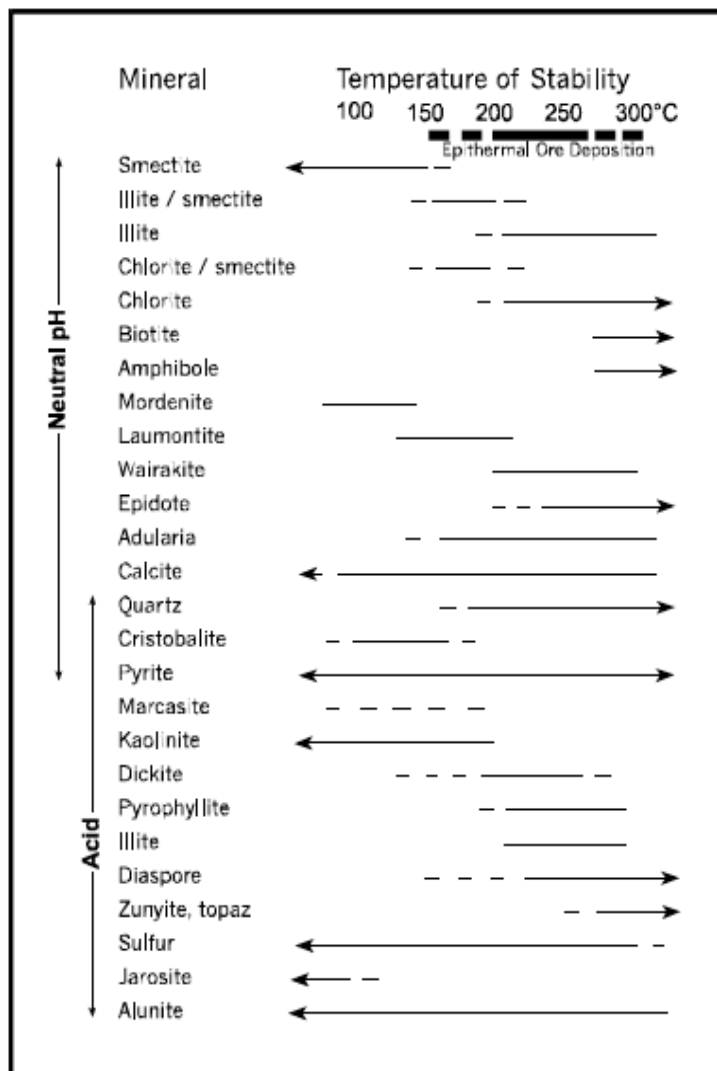


Figure 3.3. Thermally induced hydrothermal minerals in the epithermal ore zone (Henley & Ellis, 1983; Reyes, 1990; White and Hedenquist, 1995)

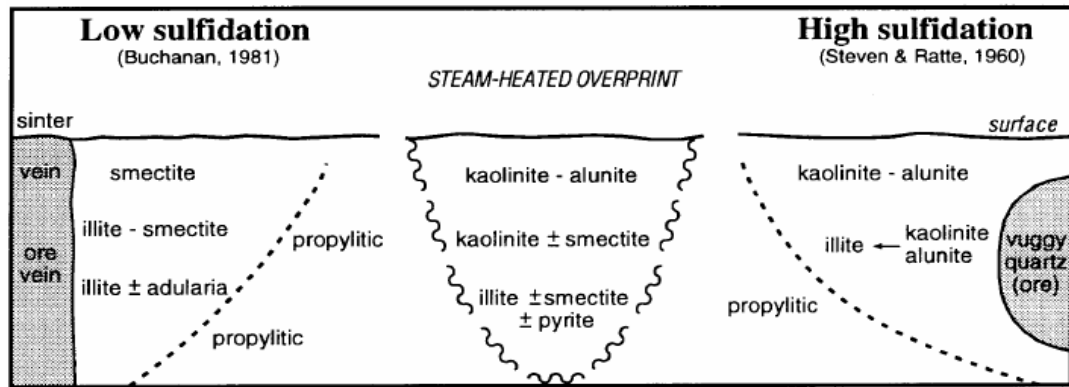


Figure 3.4. Distribution of hydrothermal alteration associated with high and low sulphidation deposits (White and Hedenquist, 1995)

CHAPTER 4

RESULTS: FIELD STUDIES

In Mihalıççık district, mainly there were two kaolin pits in the past which were Yarıkkçı pit and Ayının Tepe pit (Fuji et al., 1995). The locations of these pits are given in Figure 4.1. However, in this study, our main area of interest is determined as Ayının Tepe pit and Hamidiye kaolins which is located to the northwest side of Ayının Tepe kaolin pit.

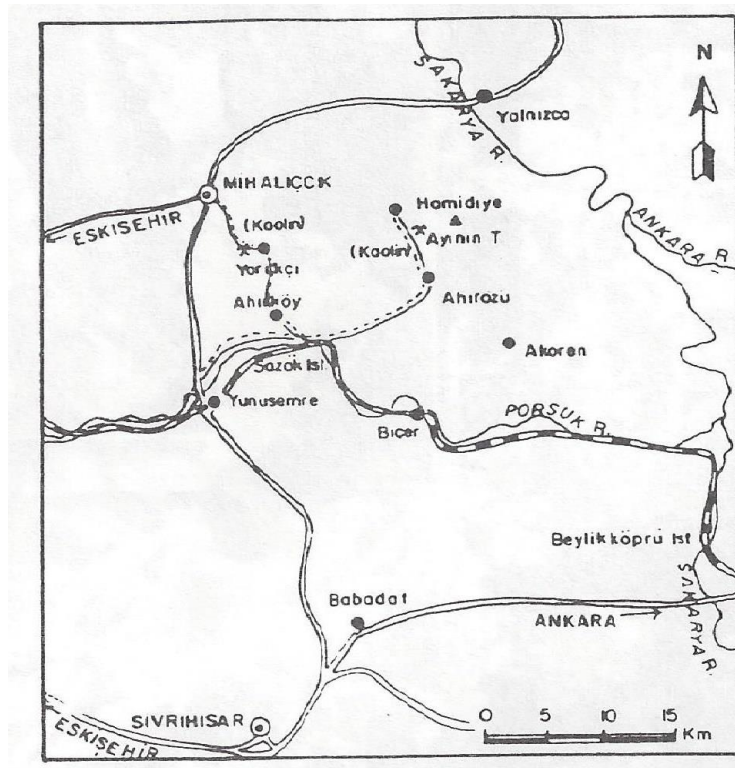


Figure 4.1. Location map of Ayının Tepe (Ahırözü kaolin deposits) and Yarıkkçı kaolin pits (Fuji et al., 1995)

The study area was highly vegetated and the bedrocks were totally covered by thick soil layers. Hence, exposures along the fault zones and kaolin quarries were the most suitable sites for sampling areas. However, road and valley cuts also provided good exposures for sampling different alteration zones.

These zones were formed when the hydrothermal fluids and wall rocks reacted around N30W oriented structural conduits in the study area (Ömeroğlu et al., 2016; Ömeroğlu-Sayıt et al., 2018). The argillic (composed of mainly kaolinite, natroalunite paragenesis with minor pyrite) and overprinting propylitic alterations in country rocks around the fault zones is very narrow (Ömeroğlu et al., 2016; Ömeroğlu-Sayıt et al., 2018).

There were four excursion studies carried out in 2012, 2013, 2014 and 2015 in which different sampling processes were performed, systematically. L1-L11 series, L12/L-13 series, Hmd series and H series are the codes of rock samples generated with respect to the field study periods. The field studies performed in 2012 was mainly planned as reconnaissance, whereas the field performance in 2013 was dominantly based on acquiring the samples systematically to examine them to reveal the secondary mineralization products and determine the source rocks in association with them. In 2014, the field studies were directed to a different route since it was aimed to study on listwanized rocks in the field. Listwanites are mainly described as unusual rocks which are formed from carbonate alteration in ultramafic rocks (Hansen et al., 2005). These carbonate alteration might be seen through thin or thick veins, therefore it is not obligatory to observe the whole ultramafic rock altered into totally carbonate. Experimental studies were planned to carry on listwanites to understand their formation mechanism in the field. Therefore, the field study was performed in Kavak Chromite Mine situated in the province of Mihalıççık to obtain the drilling core samples of serpentinites and dunites which were possible source rocks of listwanites. In 2015, the field studies were conducted to compare the laboratory results to the geology of the study area to verify the formation mechanism and generate cross-sections systematically.

In the study area, there were 59 samples collected, systematically, along the outcrops of granitic, ultramafic (serpentinite) and metamorphic units to reveal the mineralogy of rock units in order to identify the origin of them. The coordinates of these sampling locations in UTM projection system were given in Table 4.1.

Table 4.1. Coordinates of sampling locations regarding to Universal Transverse Mercator (UTM) projection system

Sample Code	Lithology	Possible Parent Rock	Alteration Product/ Process	Location		Easting (X)	Northing (Y)
L-1*	Ultramafic rocks subjected to intense carbonate alteration	Ultramafic /Mafic	carbonate dominated (listwanite)	Ayın Tepe Pit	Ahrözü Kaolin Deposits	386366	4409680
L-2	ARGILLIC ZONE	Granitic	kaolin				
L-3							
L-4A & L-4B							
L-5							
L-6							
L-7							
L-8A & L-8B							
L-9**							
L-10							
L-11							
						386600	4409862
						386570	4409950
						386560	4409870
						387066	4410045

Sample Code	Lithology	Possible Parent Rock	Alteration Product/ Process	Location		Easting (X)	Northing (Y)		
Hmd 1a	ARGILLIC ZONE	Granitic	kaolin	Hamidiye kaolins		386517	4409334		
Hmd 2a									
Hmd 1-1									
Hmd 1-2									
Hmd 1-3									
Hmd 1-4									
Hmd 1-5									
Hmd 1-6									
Hmd 1-7									
Hmd 1-7a	GOSSAN ZONE	original parent rock can not be detected	intense iron-oxidation through veins + chlorite + kaolin ? + smectite + illite						
Hmd 1-7b									
Hmd 1-8									
Hmd 2*	Ultramafic rocks subjected to intense carbonate alteration	Ultramafic	chlorite + carbonate +clay? (listwanite)					386647	4409408
Hmd 3, Hmd 3-1, Hmd 3-2	ARGILLIC ZONE	Granitic	kaolin + carbonate (veins) + amorphous silicate					386676	4409468
Hmd 4		Granitic	silicification + kaolin			386734	4409505		
Hmd 5		Granitic	silicification + kaolin			386744	4409513		

Sample Code	Lithology	Possible Parent Rock	Alteration Product/ Process	Location		Easting (X)	Northing (Y)
L1A	Metamorphic/ Ultramafic rocks subjected to intense carbonate alteration	Metamorphic	carbonate + silicate	Wall Rocks		386528	4409356
L1B		Metamorphic	carbonate				
L12-1		Ultramafic/Mafic	smectite + illite + carbonate + silicate (listwanite)				
L12-2	Granitic	amorphous silicate + kaolin					
L12-3		kaolin					
L12-4	PROPYLITIC ALTERATION	Ultramafic/Mafic	carbonate (veins) + silicate + smectite+ chlorite				
L12-5a &L12-5b		Ultramafic/ Mafic	carbonate + smectite + chlorite				
L12-6		Ultramafic/ Mafic	silicate + smectite + illite + chlorite				
L12-7		Ultramafic/ Mafic	silicate + smectite + illite + chlorite				
L12-8		Ultramafic/ Mafic	silicate + carbonate + smectite + illite + chlorite ?				
L12-9		Granitic	kaolin + silicate				
L12-10			kaolin				

Sample Code	Lithology	Possible Parent Rock	Alteration Product/ Process	Location		Easting (X)	Northing (Y)
L12-11		Granitic	kaolin				
L13		Ultramafic/ Mafic	carbonate + smectite + illite + chlorite				
H-1		Caliche	carbonate				
H-2	PROPYLITIC ALTERATION	Metamorphic	chlorite + smectite + illite			386301	4406610
H-3		Mafic/Basaltic	chlorite + smectite			386439	4410890
H-4		Metamorphic	Silicate + illite + chlorite				
H-5		Metamorphic	Silicate + illite + chlorite			386407	4411186
H-6		SILICA SINTER FORMATION	Not detected	Recryst. quartz			386399
H-7	PROPYLITIC ALTERATION	Metamorphic	silicate + illite + chlorite + carbonate			386422	4411184
H-8 & H-8-1		Ultramafic	Smectite+ illite+silicate+ serpentine + chlorite			386528	4409810
H-9		Felsic igneous rock	illite + kaolin + silicate				
H-10	PROPYLITIC ALTERATION	Ultramafic	clay (illite?) + silicate + serpentine + chlorite			386512	4409804

Sample Code	Lithology	Possible Parent Rock	Alteration Product/ Process	Location		Easting (X)	Northing (Y)
H-11	SILICA VEIN	?	kaolin+ silicate + iron oxidation			386477	4409797
H-12	CARBONATE VEIN	sedimentary	carbonate			386529	4406507
<p>* L-1 and Hmd 2 are listwanized rock samples but considered to be situated in “Argillic Zone” due to the location (Ahrözü kaolin deposits) that it was acquired.</p> <p>** L-9 is metamorphic originated rock but considered to be situated in “Argillic Zone” due to the location (Ahrözü kaolin deposits) that it was acquired.</p>							

In Table 4.1, the samples coded from L-1 to L-11 were acquired from Ayının Tepe kaolin pit, whereas L12/L-13 coded samples were *generally* collected from the ultramafic and metamorphic originated wall rocks exposed to propylitic alteration with some exceptions. L1A and L1B represents metamorphic originated rocks whereas L12-1, L12-4, L12-5a & L12-5b, L12-6, L12-7 and L12-8 stand for ultramafic/ mafic originated rocks. On the other hand, L12-2, L12-3, L12-9, L12-10 and L12-11 were determined as granitic originated rocks due to entity of kaolin as a clay mineral and lack of chlorite. These samples include K-feldspar mineral according to the XRD analyses. Eventhough, the L-1 sample obtained from the Ayının Tepe kaolin pit, this sample represents a typical listwanized ultramafic rock. The samples determined as L-1 to L-11 (except for L-1) representing granitic original rock exposed to argillic alteration. Hmd 1 series (Hmd 1-1, Hmd 1-2, Hmd 1-3, Hmd 1-4, Hmd 1-5, Hmd 1-6 and Hmd 1-7) was also acquired from Hamidiye kaolin deposit itself which is situated to the northwestern of Ayının Tepe kaolin pit. Both Ayının Tepe and Hamidiye kaolin deposits are named as Ahrözü kaolin deposits in this study. Hmd 1-7a, Hmd 1-7b and Hmd 1-8 obtained at the 386517E 4409334N coordinates representing “Gossan Zone” in the study area acquired from the contact along the Hamidiye kaolins. On the other hand, H-series was

systematically collected from both metamorphic rocks and ultramafic/mafic wall rocks exposed to propylitic alteration, mainly, except for the samples H-1, H-6, H-9 and H-12 which were the samples representing caliche, silica sinter formation, possible granitic parent rock and calcite vein wall, respectively.

4.1. Local Geology and Field Sampling:

4.1.1. Kaolin Deposits:

Ahrözü kaolin deposits (Aydın Tepe pit and Hamidiye kaolins) had been extracted by Sümerbank Ceramic Industry in 1976 with the Project no. 6/c, II/02.2.07.01.01 and in 1977 with the Project no. 55a, II/02 (D).2.08.01.01. (Sincan, 1978).

Hereby, there were two groups of rock sample representing the kaolin deposits which were Hmd series and L-1 to L-11 series. The L-1 to L-11 rock samples were acquired from the study area during the field excursion carried out in 2012 Summer. The sampling performed mainly in the kaolin deposit at the Aydın Tepe (near Hamidiye) location except for L-1 coded sample which was identified as listwanized rock afterwards (Figure 4.2). Thus, L-1 coded rock sample will be discussed in detail in this chapter at section 4.1.3. In total 11 rock samples were collected from Aydın Tepe kaolin pit in the context of this study. Moreover, in July 11th 2013, a field excursion was planned to study, basically, argillic alteration and gossan zones, which were characterized by its rusty colour. Eighteen (18) rock samples which are Hmd-1, Hmd-2, Hmd-3, Hmd-4 and Hmd-5 acquired from the study area (Figure 4.3 & Table 4.1). However, gossan zone will be separately discussed in this chapter at the section 4.1.2. The samples representing Hmd 1 series (Table 4.1) were collected from granitic rock altered to kaolin mostly, except for Hmd 2 which was suggested

to have ultramafic originated rock due to intense listwanitization same as the L-1. Hmd series mainly reflects the Hamidiye kaolins.

In the field, feldspar minerals have been observed in conserved habit. The fissures occurred in quartz minerals were emplaced by clay minerals in igneous originated rocks. Silicification was alternated with argillic alteration. In kaolinized zone, dominantly goethite and hematite overprints have been identified, as well (Figure 4.4). Limonite veins are observed throughout the fissures introducing stockwork structures in serpentinized rocks found across the contact of kaolinized rocks (Figure 4.5). An elevated 40 meter length sized topography was studied and investigated from the Ayın Tepe where L-2 to L-6 rock samples were acquired (Figure 4.6).

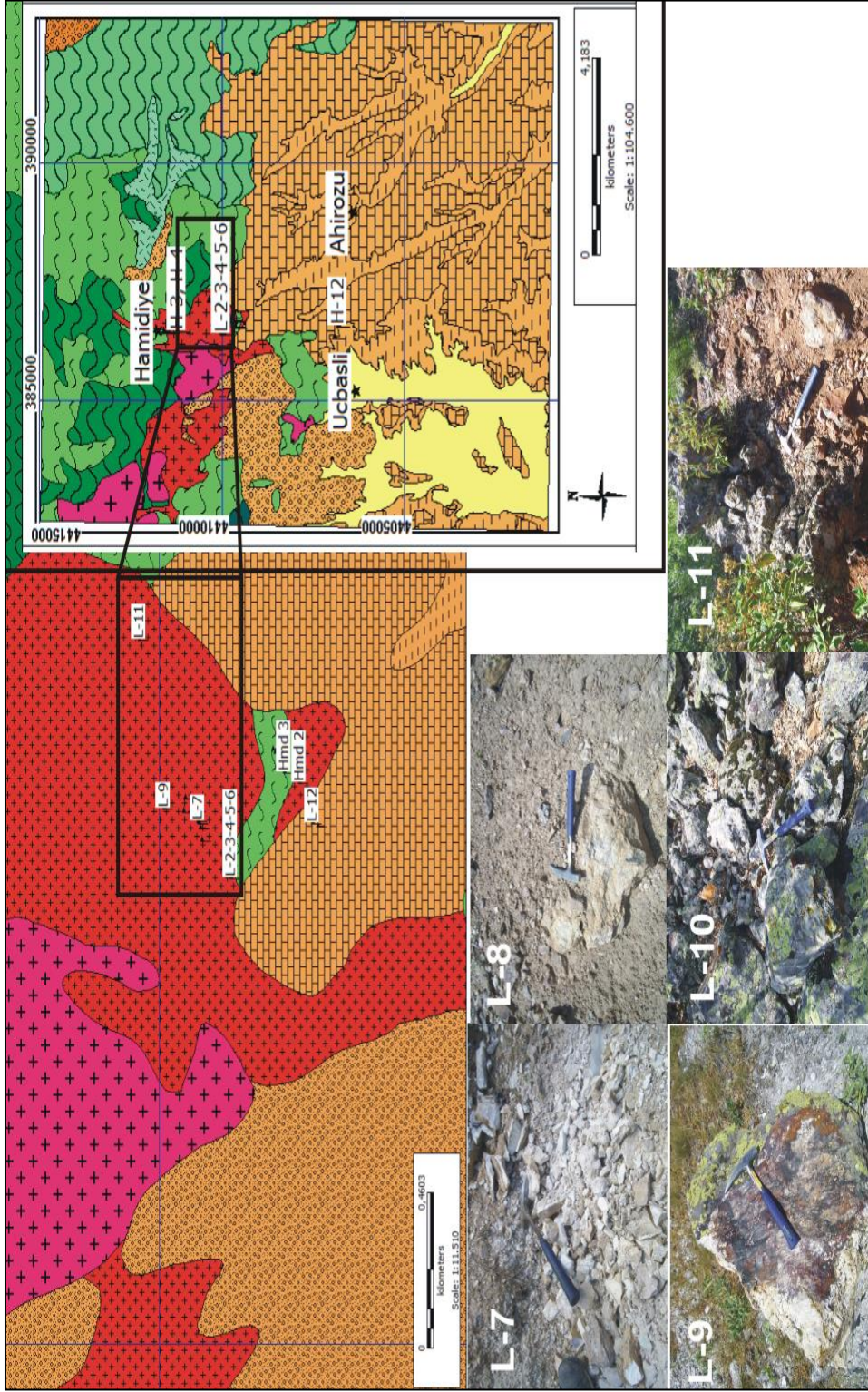


Figure 4.2. Field photographs of rock samples from L7 to L11 given on geology map of study area with close-up image of locations

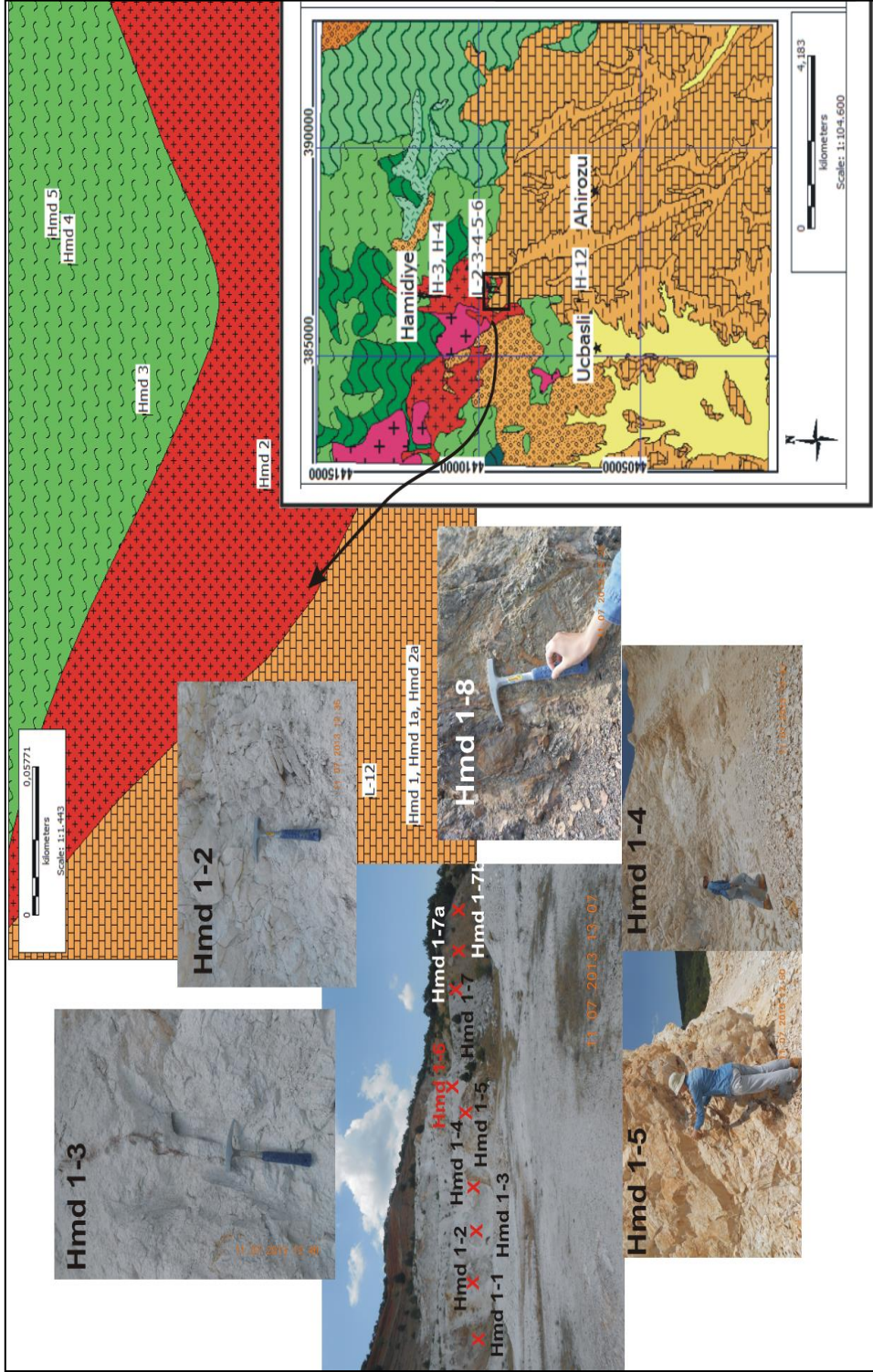


Figure 4.3. Close-up location map of Hmd series including the photographs taken from the field



Figure 4.4. Hematite (red) and goethite (black) overprints observed in the field



Figure 4.5. Limonite veins occurred as stockwork structures in carbonated serpentized wall-rocks

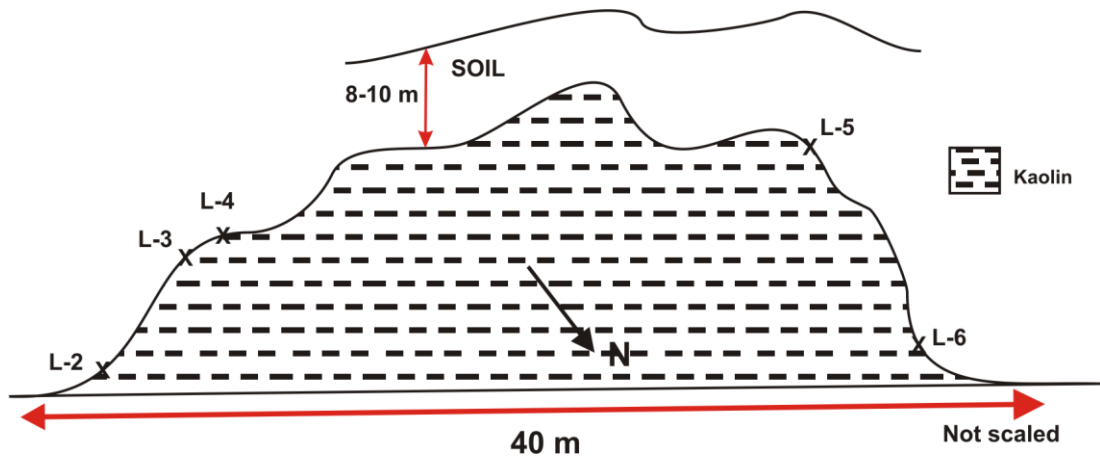


Figure 4.6. Cross-section of topography from L-2 to L-6 (386366E 4409680N)

There were two main open-pit kaolin mine exploration field detected (e.g. L-series, Hmd 1 series) (Figure 4.7). Natroalunite included kaolin outcrops were observed as pink coloured layers. However, the kaolin composed of relict primary quartz crystals were observed as massive white coloured layers (Figure 4.8). In these samples the presence of graphic texture indicated that granitic intrusives were the source rock. Silicification was observed throughout the fractures, occurred due to tectonic activities, carrying hydrothermal fluids which reacted with the original granitic rocks and, resulted in the formation of kaolin deposits. The cross-section drawn at the coordinates with UTM projection system 386636E 4409312N presents differentiated kaolinized rocks in both component and texture (Figure 4.9).



Figure 4.7. General view of Ahırözü kaolin deposits



Figure 4.8. Kaolinized white colored rocks resulted from hydrothermal alteration of granitic rock

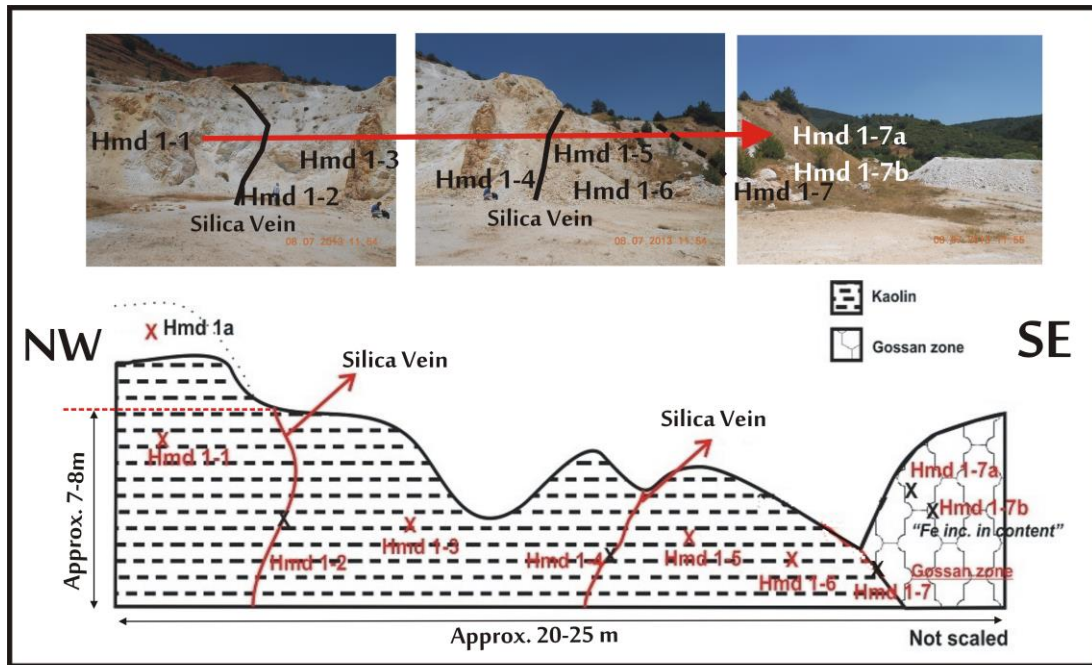


Figure 4.9. Cross-section drawn at the main deposit itself from northwest to northeast direction (386517E 4409334N)

4.1.2. Gossan Zone:

Gossan zone was also shown in the same cross-section given in Figure 4.9. The samples obtained from “Gossan zone” includes high amount of Fe (iron) component (samples coded as Hmd 1-7a, Hmd 1-7b and Hmd 1-8) (Figure 4.3). The samples acquired from the gossan zone consist of stockwork structures. There appears to be a well-defined contact between the kaolinized massive white coloured outcrop and gossan zone (Figure 4.10).



Figure 4.10. The contact between argillic alteration zone and gossan in the field. Rusty colored lithology refers to the gossan zone due the enrichment of iron in the rock component

4.1.3. Listwanite Occurrences:

Carbonated serpentized rocks presenting the silica veins as a result of the precipitation of excess amorphous silica in the hydrothermal system named as listwanite. Listwanites are unusual rocks formed as a result of an ultramafic rock partly or totally carbonated (Hansen et al., 2005). In the field these type of rocks are identified as either silica or micritic carbonate minerals in stockwork textured veins. Listwanites observed in brownish and greenish coloured rocks in the field mainly (Sample L-1) (Figure 4.11). Cross-section drawn from southeast to northwest direction at 386061E 4412001N presents the contact between clayey units

determined as argillic altered zone and listwanites equivalence of carbonated serpentized rocks (Figure 4.12).



Figure 4.11. Listwanite rock located at stop L-1 (386473E 4406690N)

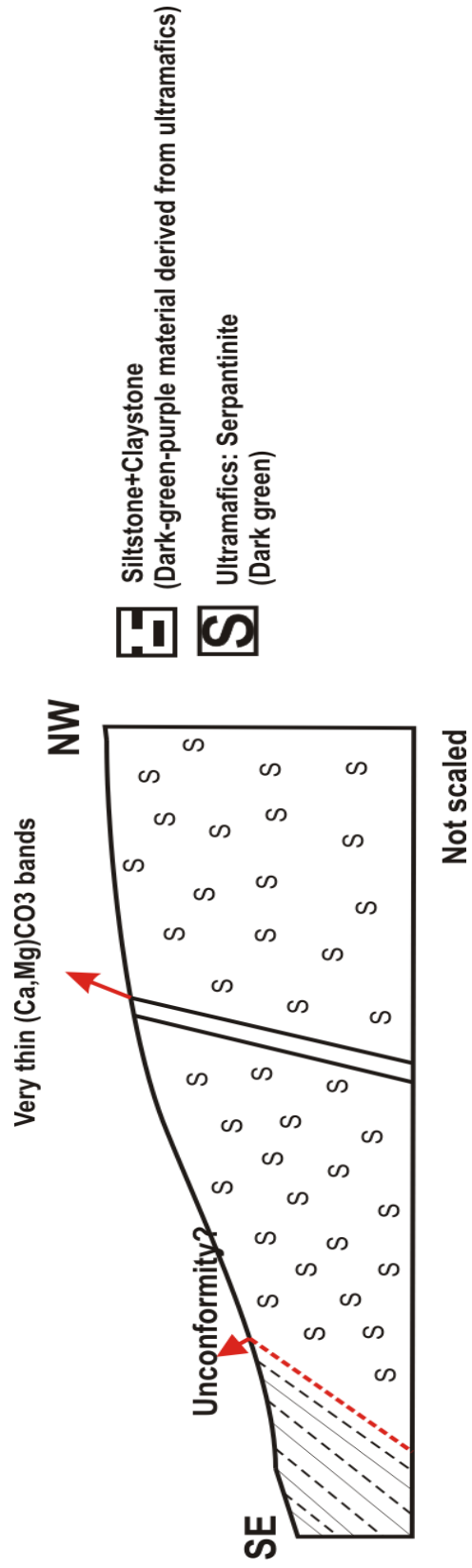


Figure 4.12. Cross-section drawn from southeast to northwest direction at 386061E 4412002N

4.1.4. Metamorphic and Ultramafic/Mafic Rock Units:

Twenty-eight (28) samples were collected from the study area in the summer of 2013, systematically, and coded as L-12/L-13 and H-series (Figure 4.13). The main purpose of this field excursion was to determine the contact of other possible alteration zones with kaolin deposits which will be named as argillic zone in further chapters.

Metamorphic rocks obtained from the study area preserves foliated textural features and relict mica minerals introducing metamorphic features, whereas mafic rock units contain relict microlite plagioclase minerals. These rocks were mainly exposed to intense chloritization and carbonate alteration due to hydrothermal activities dominated in the region, thus it was hard to detect the original parent rock depending on field observations (Figure 4.14). Moreover, intense silicification was also observed by forming both large and minor scaled veins throughout the original rocks.

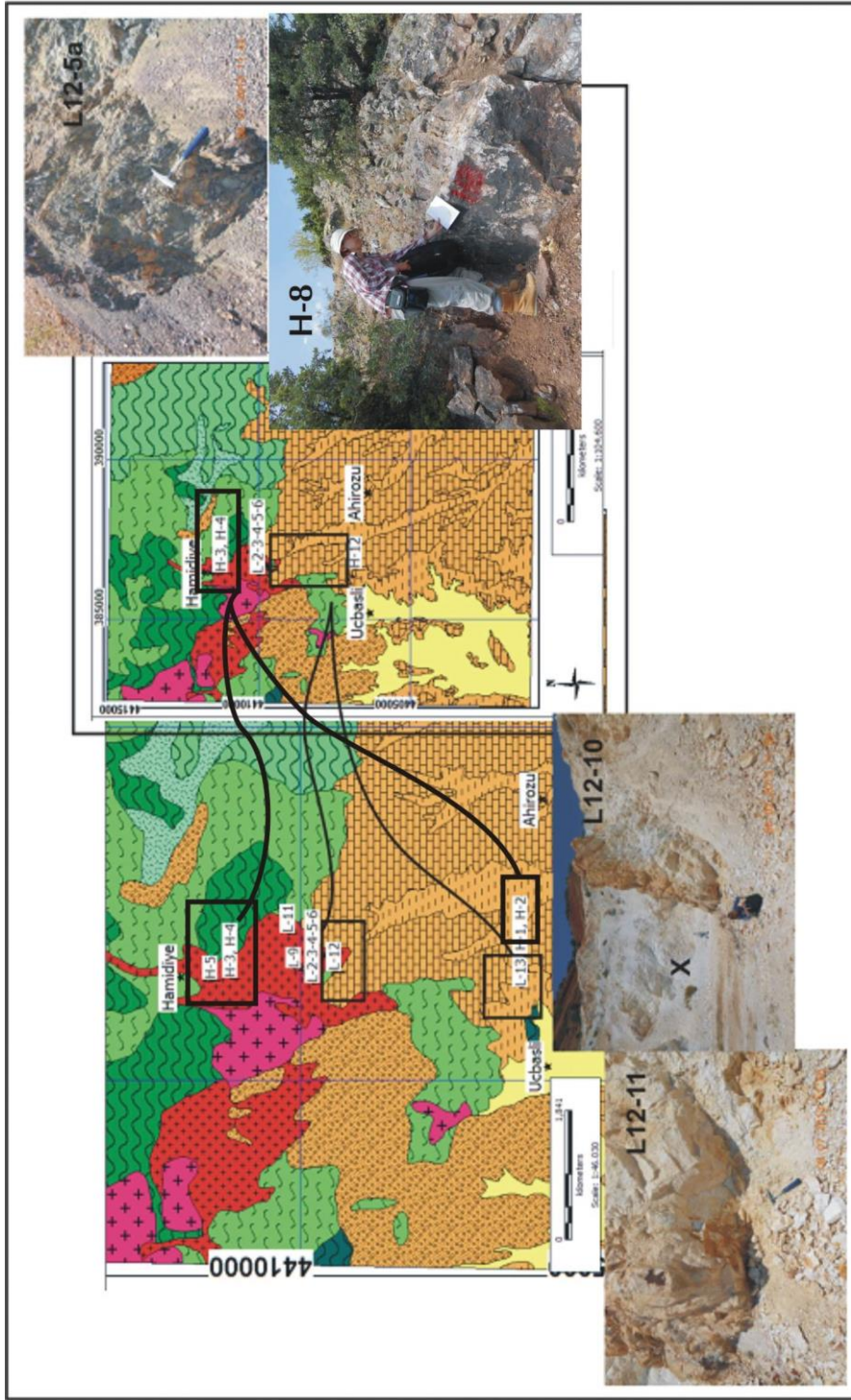


Figure 4.13. Field photographs of rock samples from L-12/L-13 and H-series given on geology map of study area with close-up image of locations



Figure 4.14. Serpentinized rock sample acquired from the H-8 location

CHAPTER 5

RESULTS: MINERALOGICAL AND PETROGRAPHICAL ANALYSES

This chapter includes results of mineralogical and petrographical analysis performed on altered rocks in the study area. To identify the composition of these rocks, thin-section analyses, XRD analyses and SEM-EDX analyses were performed. In this chapter, the rock-samples collected from the field will be discussed considering the alteration type that they are exposed to and the location from which they were systematically collected.

5.1. Thin- Section Analyses:

5.1.1. Argillic Alteration:

Aydın Tepe kaolin pit and Hamidiye kaolins are commonly known as Ahırözü kaolin deposits. These two open pit mines were suggested to occur due to the hydrothermal alteration of granitic rock units. In Aydın Tepe kaolin pit there is a contact zone introducing the border between listwanized rock units and kaolinized rocks. Aydın Tepe kaolins were observed as more fine-grained compared to Hmd coded kaolin samples collected from Hamidiye kaolins situated to the northwestern of Aydın Tepe kaolin pit. These rocks represent the argillic alteration in the study area.

5.1.1.1. L-1 to L-11 Series - Ayının Tepe Kaolin Pit :

The sampling performed mainly in the kaolin deposit at the Ayının Tepe location and Hamidiye kaolins. Except for L-1, these samples were determined to be exposed to intense argillic alteration. Kaolin minerals are the most abundant mineral. Natroalunite was also detected in pink coloured kaolinized samples. Dolomite was determined in the rock-sample L-1 as secondary carbonate mineral resulted from the formation of listwanite from serpentinized ultramafic rocks (Figure 5.1.A). Opaque minerals were also detected in euhedral and subhedral habits (Figure 5.1.B). In thin-section examination, carbonate filled veins were observed as crosscutting the primary carbonate alteration (Figure 5.1.C). Hematite veins which formed at the last phase of hydrothermal processes after carbonate alteration were also observed (Figure 5.1.D).

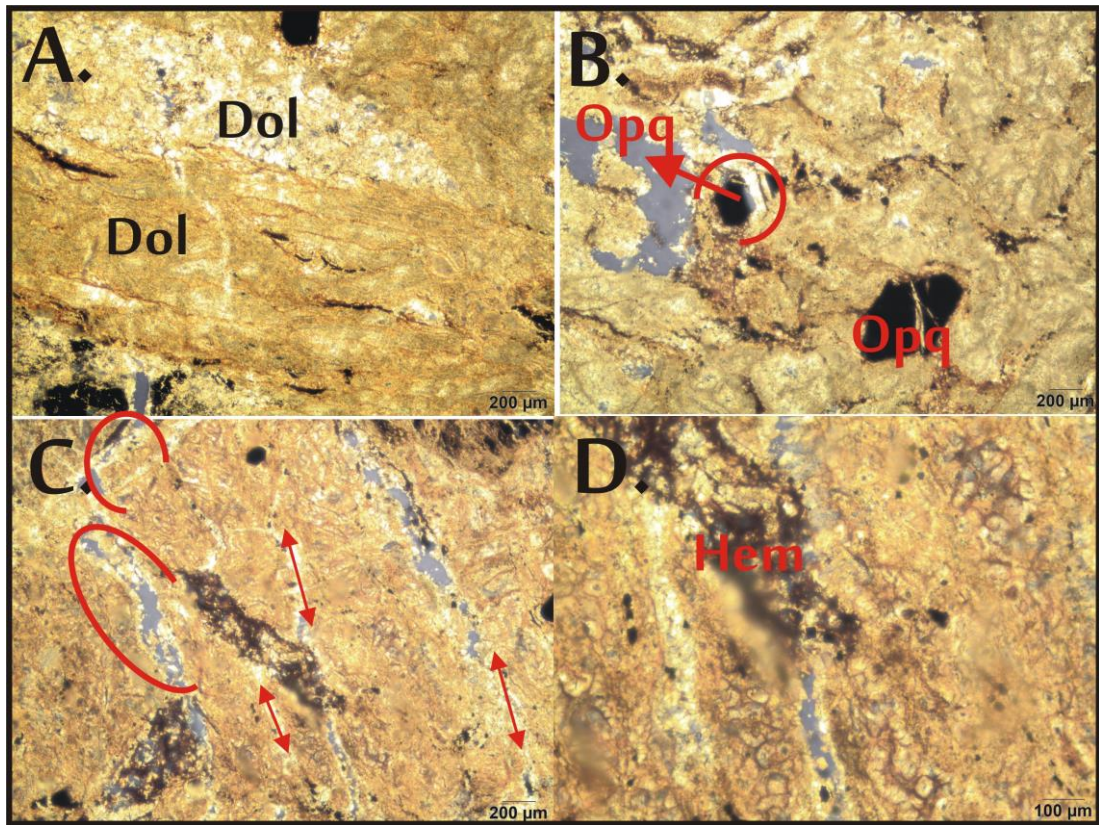


Figure 5.1. Thin-section photos of L-1 showing the entity of carbonate alteration dominantly. A) “Dol” indicates dolomite B) “Opq” represents opaque minerals C) Veins are implied with circular marks and arrows D) “Hem” states the entity of hematite in brownish red colours

Rock samples **L-3 to L-6** are dominantly kaolinized rock samples resulted from argillic alteration introducing different sized clay minerals and change in intensity of opaque minerals in their components under the microscope. Kaolin is the most abundant clay mineral in these samples as it was indicated (Figure 5.2.A) however, silicification which was occurred after the argillic alteration was also identified (Figure 5.2.B). There were veins detected fulfilled with secondary quartz crystals (Figure 5.2.C). Hematite bearing coating was defined implying the last phase in the

hydrothermal alteration probably altered from goethite minerals due to oxidation in the study area (Figure 5.2.D).

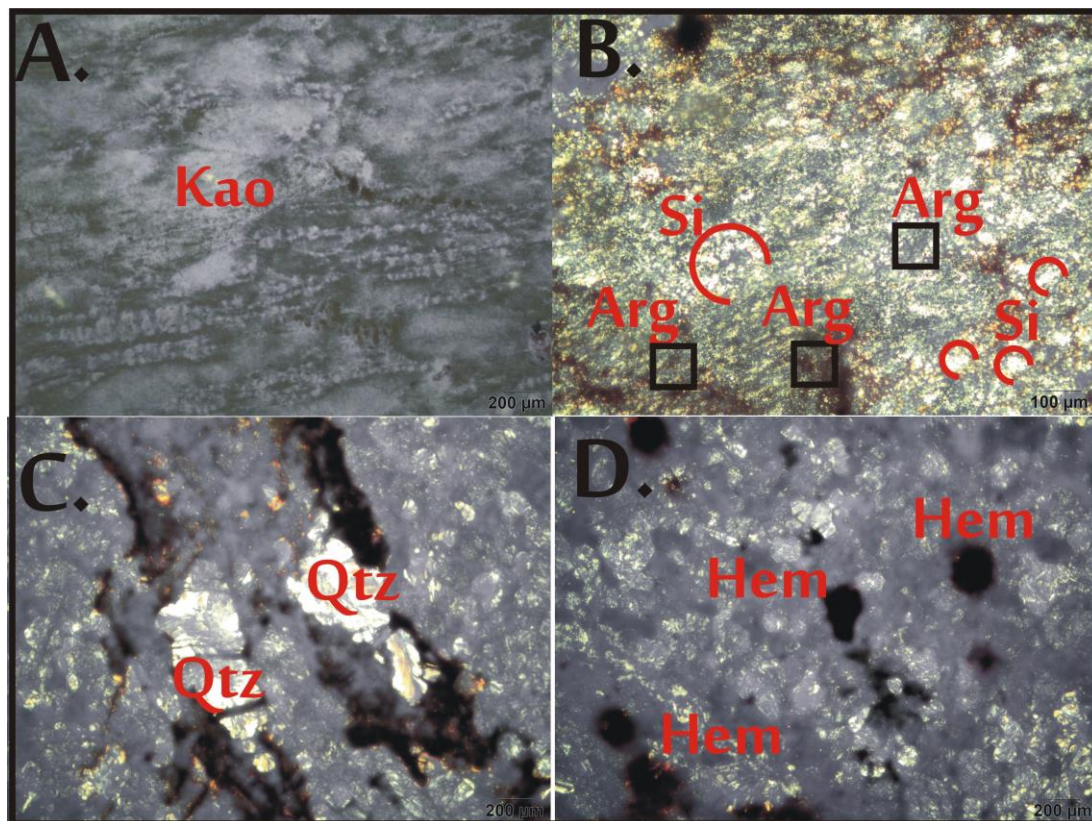


Figure 5.2. Thin-section micro-photographs taken from L-3 to L-6 rock samples. **A.** Photograph of the thin-section of L-3 rock sample in general indicating the abundance of kaolin “Kao” in the sample itself **B.** The micro-photograph of L-4A implies the silicification “Si” occurred after the argillic alteration “Arg” **C.** The veins consisting of secondary quartz crystals represented by “Qtz” at L-4B **D.** Hematite formation as a result of the oxidation of possible goethite minerals indicated by “Hem” at the rock sample L-4B

High amount of opaque minerals were determined while examining the thin-sections, XRD analyses were suggested to perform both for identifying the type of clay minerals and opaque minerals since the samples were nearly totally altered. **L7 to L-11** coded rock samples were obtained from the granitic intrusion in the NE direction away from the main kaolin deposit, systematically. During the sampling, it was planned to locate different alteration zones except from argillic alteration in the field; such as probable propylitic alteration and silicified zone. Rock sample **L-7** consists of hematite in spherical shapes (Figure 5.3.A). This sample comprehends argillic alteration followed by possible carbonate alteration and, then, silicification (Figure 5.3.B). Rock sample **L-8** was subjected to similar alteration processes in appearance, however this rock sample introduces a different texture “crustification” which is used as a key feature while differentiating low and high sulphidation deposits with respect to White and Hedenquist (1995) (Figure 5.3.C). Crustification indicates a decrease in temperature in the system. The sample taken from **L-9** was observed as highly silicified and kaolinized reddish yellowish rock in the study area. In thin-section analyses, silicification was specified as the main alteration product. Linear curved traces implying the entity of foliation was determined, thus, these curved structures estimated as relict foliation were interstratified with opaque minerals by means of flowing hydrothermal fluids throughout them (Figure 5.3.D). Hence, with respect to the relict textural presence of foliation, source rock of this silicified rock was described as metamorphic rock comparing to the previous rocks examined in the context of this rock sample set including the sample codes L3, L4, L5, L6, L-7 and L-8 which source rock was estimated as felsic igneous rock. However, L-1 was characterized totally different since there was carbonification dominated during the hydrothermal processes associated with the occurrence of listwanite by introducing the presence of ultramafic source rock in the field. However, the rock sample **L-10** (386560E 4409950N) states a different condition under the microscope. In this rock sample, primary quartz crystals in large sized grains were cut by argillic alteration across the fissures formed as a result of the dynamism of hydrothermal system but not leached out yet since the temperature decreased due to diverging from the main

fault/fracture which fed the hydrothermal deposits and carried the chemical fluids throughout the rocks by being altered (Figure 5.3.E). The rock sample **L-11** (387066E 4410045N) was examined as reddish very hard silicified rocks in the field. On the contrary, this rock sample is composed of recrystallized silica veins cutting each other associated with intense silicification (Figure 5.3.F). In this rock, the traces of a flow of hematitic fluids were also observed after silicification subjected.

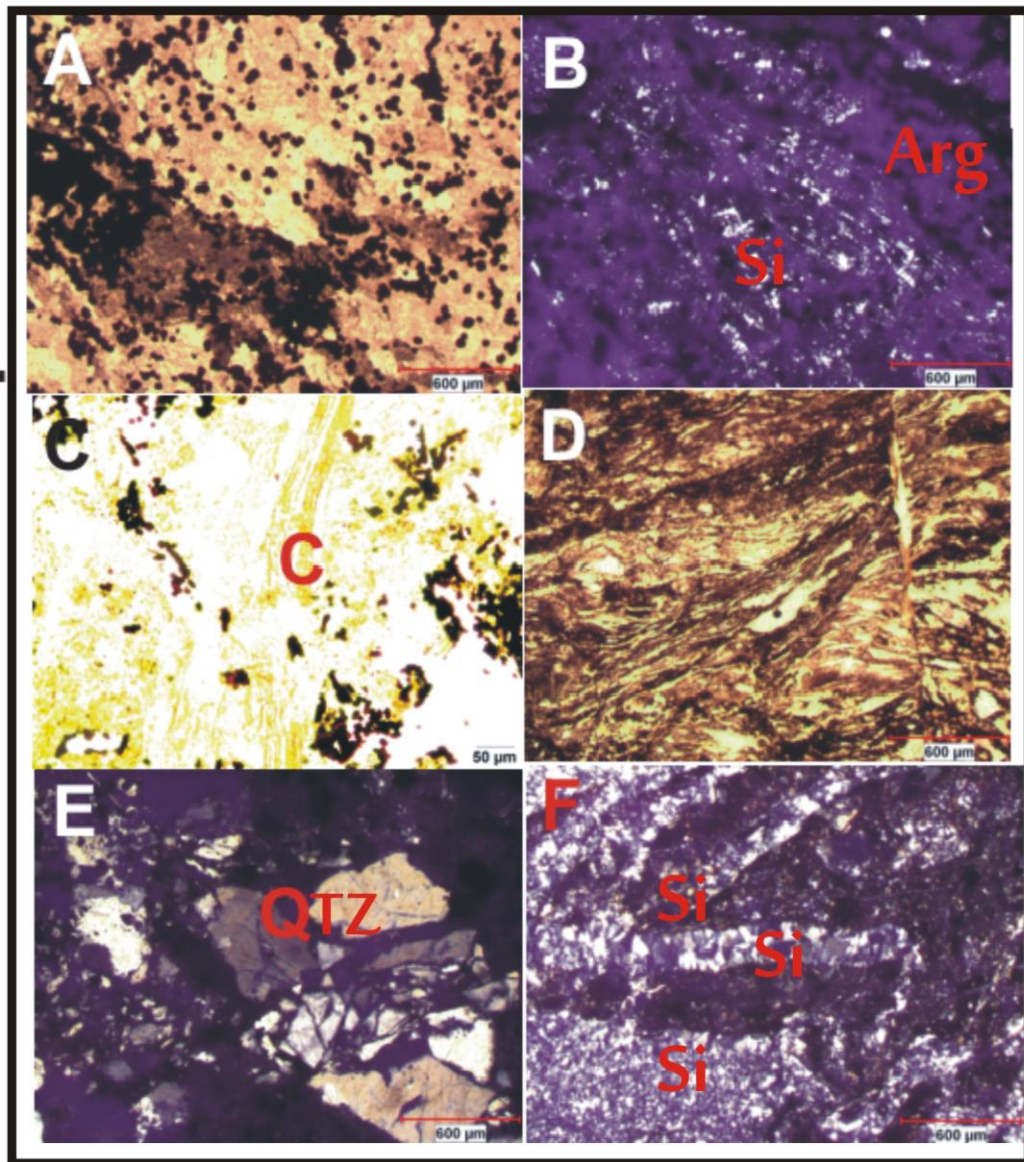


Figure 5.3. **A.** Entities of opaque minerals in the rock sample L-7 in spherical-circular shapes **B.** Argillic alteration in the rock sample L-7 followed by silicification **C.** “C” represents the the entity of “Crustification” in the rock throughout the external wall of the vein **D.** Relict foliated texture interstated by opaque minerals resulted from the flow of chemical fluids throughout them **E.** Primary quartz “Qtz” crystals cut by argillic alteration **F.** Intense silicification “Si” dominated throughout the veins in the rock sample L-11

5.1.1.2. Hmd Series - Hamidiye Kaolins:

Hmd 1 series including Hmd 1a and Hmd 2a rock samples were acquired from the kaolin deposit itself. Among the data series of Hmd 1, Hmd 1-7 serves an important function since it was taken from the contact between argillic alteration zone and gossan zone to examine the transition properties between these two zones. However, Hmd 1-7a and Hmd 1-7b were directly obtained from the “gossan zone” in the field which was observed in rusty colors due to the enrichment of iron in its content.

Hmd 1-1 includes primary large quartz crystals (Figure 5.4.A). However, there were no relict mineral observed except for these since the original granitic rock was subjected to argillic alteration due to the hydrothermal processes. Clay material is dominated in the matrix of the rock- specimen, as well. Hmd 1-2 comprises both primary quartz minerals and secondary recrystallized quartz minerals (Figure 5.4.B). Clay material was detected in the rock resulted from the interaction of chemical fluids and primary rock in the study area. Since it was acquired across the same intrusive rock subjected to the hydrothermal processes resulting in argillic alteration in the particular region, Hmd 1-3 introduces similar mineralogical and textural features; it consists of primary large quartz crystals in addition to clay based material and silicification. Hematite bearing coated relict materials were observed throughout the veins of the rock sample (Figure 5.4.C). The rock represented by Hmd 1-4 sample comprises both secondary quartz minerals smaller in size in addition to primary quartz crystals conserved in fractured appearance filled by argillic material and subjected to silicification (Figure 5.4.D). The entity of opaque minerals was also detected in the sample of Hmd 1-4 in hexagonal shapes. Nevertheless, the abundance of opaque minerals decreased in Hmd 1-5 comparing to the rock-specimen Hmd 1-4. Although similar mineralogical pattern was identified, primary quartz crystals were retained as smaller in size in addition to the clayey material dominated throughout the thin-section (Figure 5.4.E). It was specified that silicification and argillic alteration influenced the granitic rock, basically (Figure 5.4.E). The rock was first

subjected to the argillic alteration since it was detected that the silica veins cut the clayey material in the thin-section. Hematite bearing veins were examined as post event introducing the last phase of hydrothermal alteration occurred in the rock-specimen Hmd 1-6 (Figure 5.4.F). The rock exposed to argillic alteration followed by silicification (Figure 5.4.F). On the contrary, the size of quartz crystals were detected as larger and fractured similar to the rock-samples Hmd 1-1, Hmd 1-2, Hmd 1-3 and Hmd 1-4 in the rock-specimen Hmd 1-7 (Figure 5.4.G). Relict biotite minerals were oxidized, whereas the feldspar minerals altered into kaolin minerals (Figure 5.4.H).

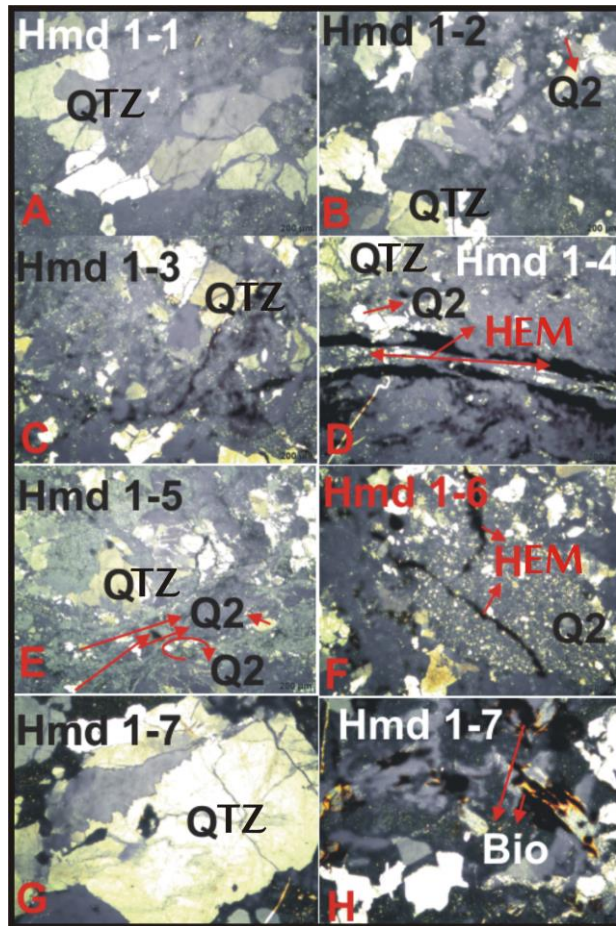


Figure 5.4. **A.** Primary large quartz crystals represented by “Qtz” in the sample of Hmd 1-1 **B.** Hmd 1-2 conserving its primary quartz minerals (Qtz) in addition to the secondary quartz crystals (Q2) **C.** Primary large quartz crystals (Qtz) in addition to clay material and silicification in Hmd 1-3 **D.** “Qtz” stands for primary quartz crystals conserved in fractured appearance filled by argillic material and subjected to silicification (Q2) in the rock-specimen of Hmd 1-4 **E.** Hmd 1-5 was subjected to silicification (Q2) and argillic alteration whereas it conserves its primary quartz crystals (Qtz) smaller in size comparing to the samples coded from 1 to 4 in Hmd 1 series **F.** Photograph of hematite (Hem) bearing veins and silicification (Q2) are given as an example in the rock sample of Hmd 1-6 **G.** Large and fractured quartz crystals (Qtz) detected in the rock-specimen Hmd 1-7 **H.** “Bio” stands for oxidized relict biotite minerals of Hmd 1-7

Hmd 1a comprises primary large quartz crystals with fractures filled by clayey material whereas they were cut by hematite bearing veins, partly (Figure 5.5.A). Separately, relict biotite minerals were detected during the thin-section examination were subjected to oxidation and observed in brownish rusty colors at the analyzer out position with no pleochroism (Figure 5.5.B). However, partially, it was observed that these mica minerals showed mottled extinction (Figure 5.5.B). Furthermore, in the context of the rock, retained plagioclase crystals were also identified stating the decrease of influences of hydrothermal alteration processes exposed on the rock (Figure 5.5.C). Hmd 2a introduces similar mineralogical content comparing to the sample Hmd 1a, nevertheless it conserves relict graphic texture indicating that the source/parent rock was granitic rock which was partially kaolinized by hydrothermal alteration processes (Figure 5.5.D). Opaque minerals were also identified in the context of the sample Hmd 2a.

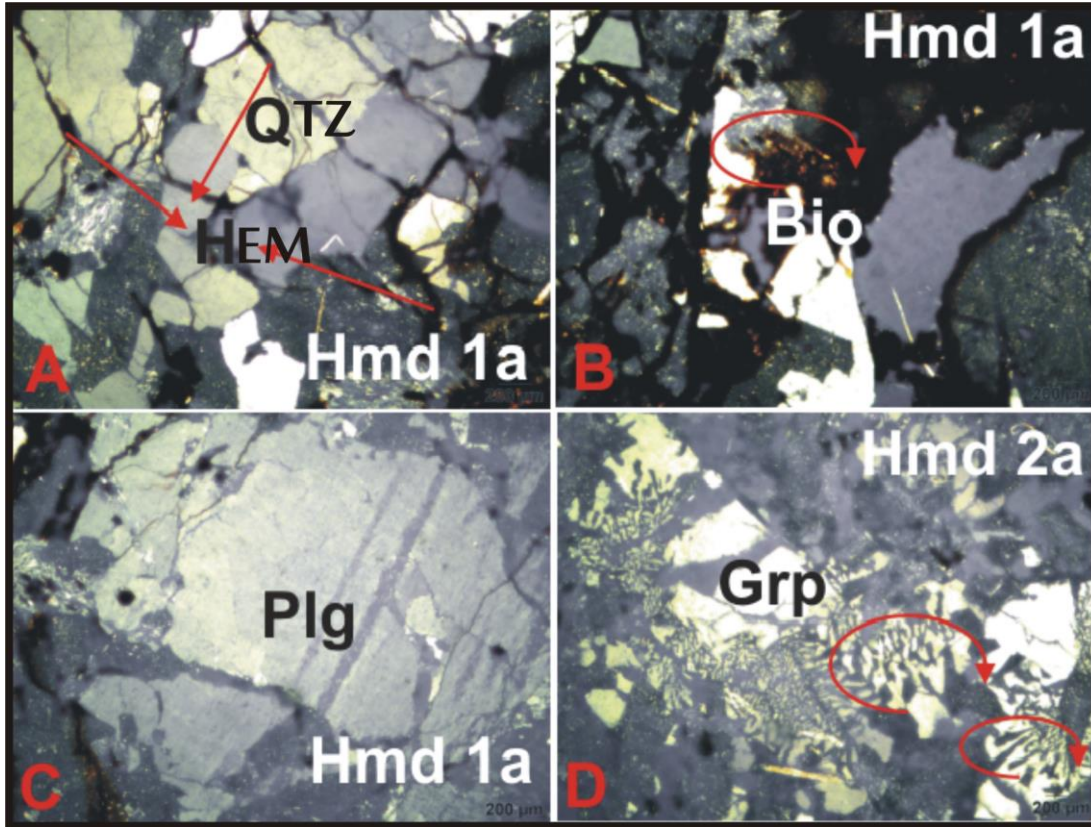


Figure 5.5.A. Primary quartz crystals “Qtz” cut by hematitic veins “Hem” in Hmd 1a **B.** Oxidized biotite mineral conserving partly its mottled extinction represented by “Bio” in the rock-specimen Hmd 1a **C.** Retained plagioclase minerals indicated by “Plg” in Hmd 1a **D.** Relict graphic texture (Grp) in the rock-sample Hmd 2a marked with a circular arrow

Common silicification was determined in the matrix of the rock sample Hmd 3 (Figure 5.6.A). Rhombohedral shaped opaque minerals were suggested as goethite crystals (Figure 5.6.B). Similar to the previous rock samples, hematite veins were also detected by cutting the silicified matrix (Figure 5.6.C). Silicified matrix was identified in Hmd 3-1 cut by hematite bearing carbonate veins in which hematite found as in thin layers throughout the wall of the veins (Figure 5.6.D).

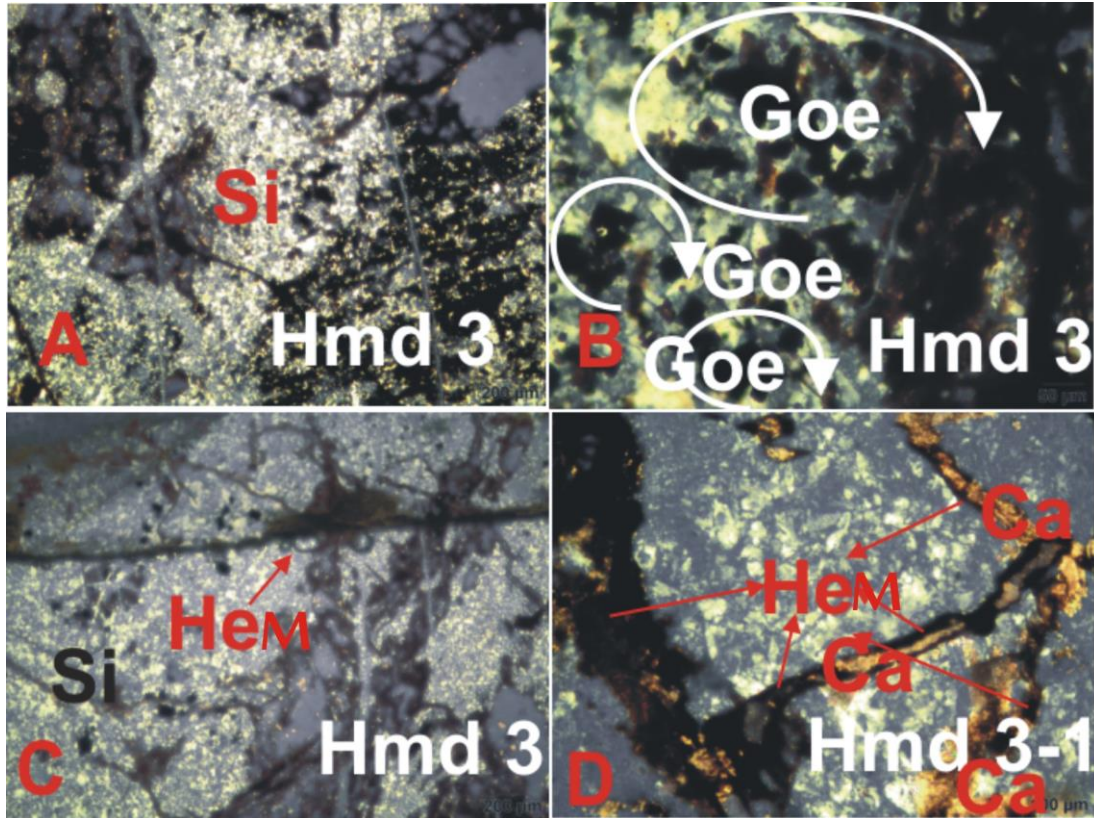


Figure 5.6.A. Silica matrix represented by “Si” examined in Hmd 3 **B.** Rhombohedral shaped opaque minerals identified as goethite crystals (Goe) in Hmd 3 **C.** “Hem” stands for hematite veins cutting silica (Si) matrix resulted as post event in Hmd 3 **D.** Hematite (Hem) bearing carbonate (Ca) veins overlying the silica matrix in Hmd 3-1

5.1.2. Gossan Zone:

The samples coded as Hmd 1-7a, 1-7b and 1-8 acquired from the “gossan zone” in the field were different from the other samples of Hmd series from 1 to 7 with respect to their content and textural features. Hmd 1-7a includes intense carbonate alteration occurred after silicification in the rock and situated at the contact of kaolinized granitic unit known as Hamidiye kaolins in the scope of this study (Figure

5.7.A). Hematite bearing veins were observed as coating material implying that they were occurred as a post-event in the rock, as well. The intensity of oxidation increased with the sample of Hmd 1-8 belonging to “gossan zone”. The sample consisted of dominantly giant veins coated by iron-oxide bearing fluids (Figure 5.7.B).

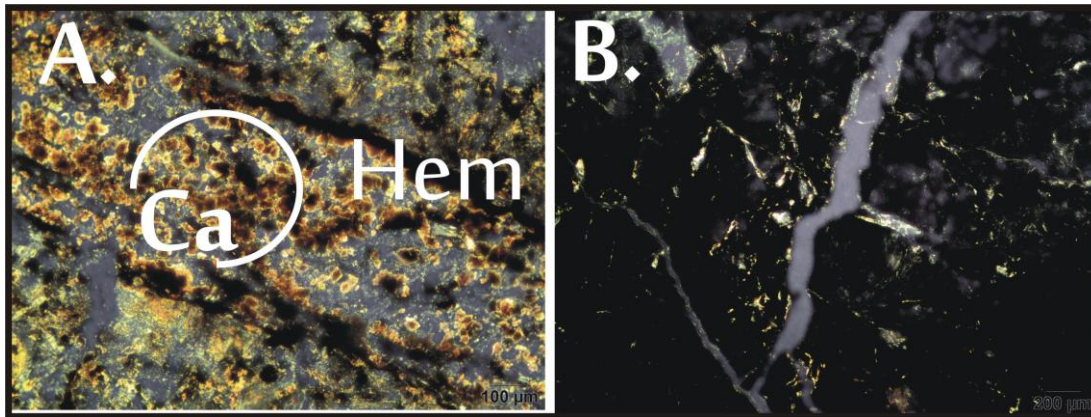


Figure 5.7. A. Carbonate alteration is represented by “Ca” whereas “Hem” stands for hematite bearing veins in the rock-sample Hmd 1-7a **B.** Hmd 1-8 was enriched by wide veins coated by iron-oxide bearing fluids

5.1.3. Propylitic Alteration:

Especially, listwanized and kaolinized rocks were specified during the thin-section examination as the alteration products occurred as a result of hydrothermal processes. Silicification was very common, as well. Metamorphic, and mafic/ultramafic igneous parent rocks coded as L-12/L-13 and H series rock specimens were studied with respect to their relict textural and mineral components. Thus, they were determined to be exposed to propylitic alteration in the study area since these rocks were composed of iron and magnesium rich rock forming minerals

in the first place. In these rocks, chlorite was observed as very common alteration product.

5.1.3.1. L-12/L-13 and L1A and L1B Series:

As an example of a metamorphic original rock types, among L-12/L-13 rock sample series, and L1A and L1B can be shown. Thus, L1A and L1B rock samples consist of relict muscovite minerals and relict foliated textural imprints indicating a schist as an original rock (Figures 5.8.A & 5.8.B). Silicate and carbonate veins are very common, as well in L1A and L1B rock samples (Figures 5.8.C & 5.8.D).

Veins developed in comb textured structures are composed of recrystallized carbonate minerals spread throughout the rock specimen no. L12-4 (Figure 5.9.A). However, silica veins crosscut by carbonate veins were described as very abundant in the rock-specimen L12-4 (Figure 5.9.B). Rhombohedral opaque minerals were detected in addition to the fibrous/flaky low birefringence minerals considered as smectite minerals verified by XRD analyses (Figure 5.9.C). This rock-specimen also introduces iron-bearing network structure coinciding with micritic carbonate minerals throughout the thin- section (Figure 5.9.C).

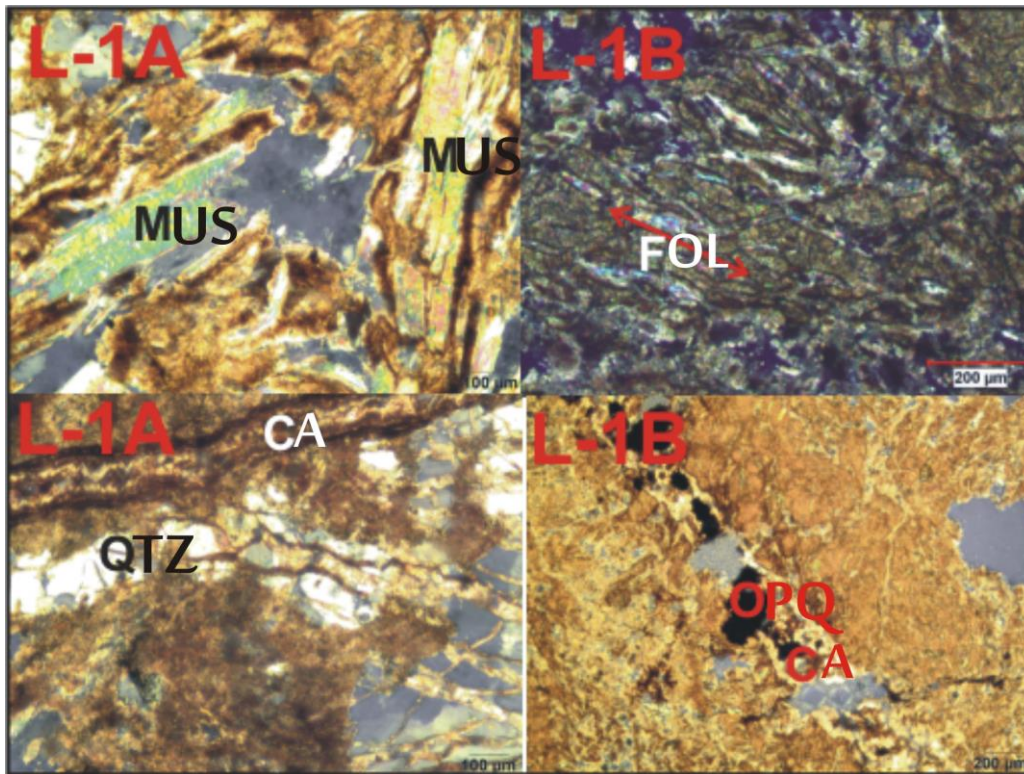


Figure 5.8. Micro-photographs of thin-section examinations taken from rock-specimens L1A and L1B. **A.** Relict muscovite minerals represented by letter “Mus” in L1A rock specimen **B.** relict foliated texture represented by “Fol” in the figure with an arrow **C.** Quartz vein represented by “Qtz” whereas “Ca” stands for carbonate veins in rock sample L1A **D.** The letter “Opq” stands for opaque minerals resulted from the flow of chemical fluids through the carbonate vein represented by “Ca” in rock-specimen L1B

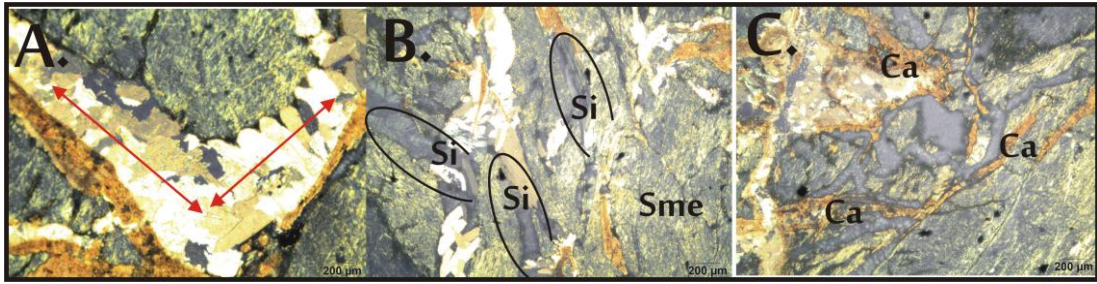


Figure 5.9. **A.** Comb textured carbonate vein are shown by the arrows in the sample L12-4 **B.** Veins including amorphous silicate material “Si” crosscut by carbonate material filled vein in the rock-specimen L12-4. “Sme” in this figure stands for smectite mineral **C.** Veins fullfilled by hematite bearing carbonate material in rock-specimen L12-4

L12-5a and L-12-5b were both considered as very significant rock-specimens since they conserve the most of their primary mineral and textural features. In rock-specimen L12-5a, there were cubic opaque minerals observed (Figure 5.10.A). Stockwork structures were very common in this rock-specimen clearly appeared due to Fe-oxide (hematite) fillings caused by chemical alteration (Figure 5.10.A). Pseudomorph olivine minerals were detected in the thin-section, as well (Figure 5.10.B). Comparing to the L12-5a, L12-5b was detected as more fresh rock sample since it conserves most of the microlite plagioclases implying the entity of basaltic volcanic source rock (Figure 5.11.A). Chloritization is abundant in this rock-specimen by indicating the propylitic alteration. Needle-like green coloured minerals were also suggested as actinolites (Figure 5.11.B). Vesicular texture was also observed under the microscope in which vesicles were partly fulfilled with micritic carbonate material (Figure 5.11.C).

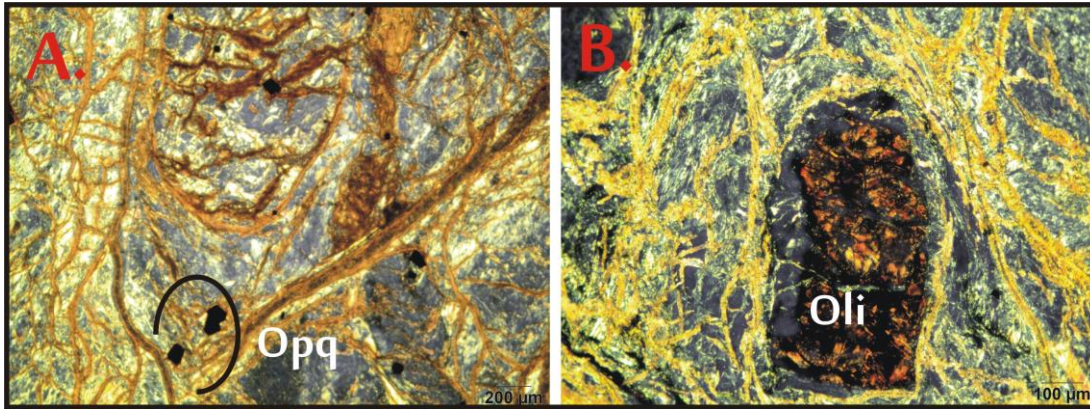


Figure 5.10. A. Stockwork structure coated rock-specimen L12-5a in which iron-bearing and carbonate material are observable. “Opq” represents cubic opaque minerals. **B.** Pseudomorph olivine crystal “Oli” in the sample L12-5a

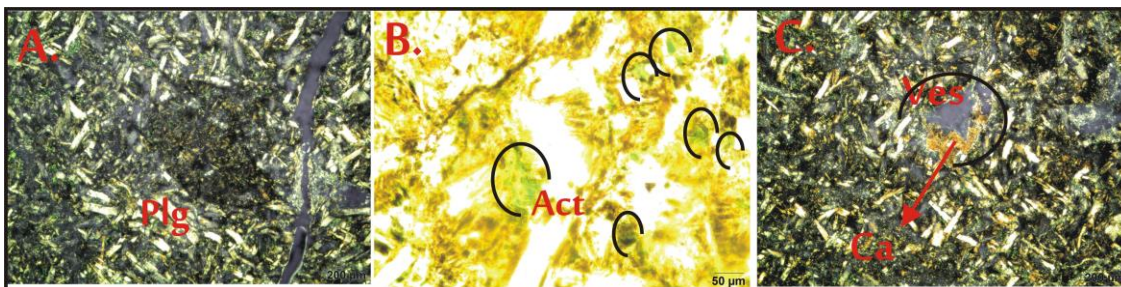


Figure 5.11. A. Relict plagioclase microlites “Plg” were observed in the thin-section examination of L12-5b **B.** “Act” stands for actinolite crystals marked with circular arrow in the photograph of the rock-specimen L12-5b **C.** Vesicles implying the entity of volcanic source rock represented by “Ves” filled by partially secondary carbonate material “Ca”

L12-8 contains “Crustification” composed of amorphous silicate (Figure 5.12). Stockwork structures were also observed fulfilled with hematite bearing carbonate material. These carbonate material was observed to surround the crustified silicate

material (Figure 5.12). Crust forms in successive layers within a cavity or fissure in which silica layers were occurred in banded forms throughout the veins.

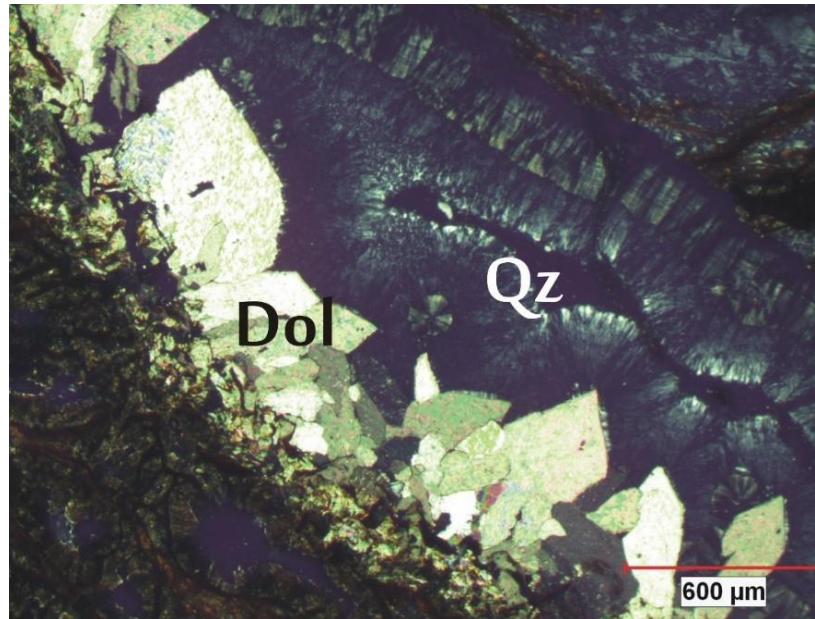


Figure 5.12. Crustification is shown in the rock sample L12-8. “Si” stands for amorphous silicate composing the crustified material whereas “Ca” representing carbonate recrystallized material

5.1.3.2. H-Series:

Rock-sample H-2 consists of chlorite as a result of propylitic alteration. This rock sample was considered to be a metamorphic originated rock since it includes foliated texture (Figure 5.13.A). Opaque mineralization was observed in the direction of foliation (Figure 5.13.A). Plagioclase crystals were detected in addition to epidote and muscovite minerals (Figure 5.13.B). Epidote mineral is important to be observed in thin-section analyses since it is known as a key mineral while identifying propylitic alteration zones (Figure 5.13.C). Carbonate alteration was determined in

the thin-section. Muscovite minerals were observed by showing foliated texture, as well (Figure 5.13.C).

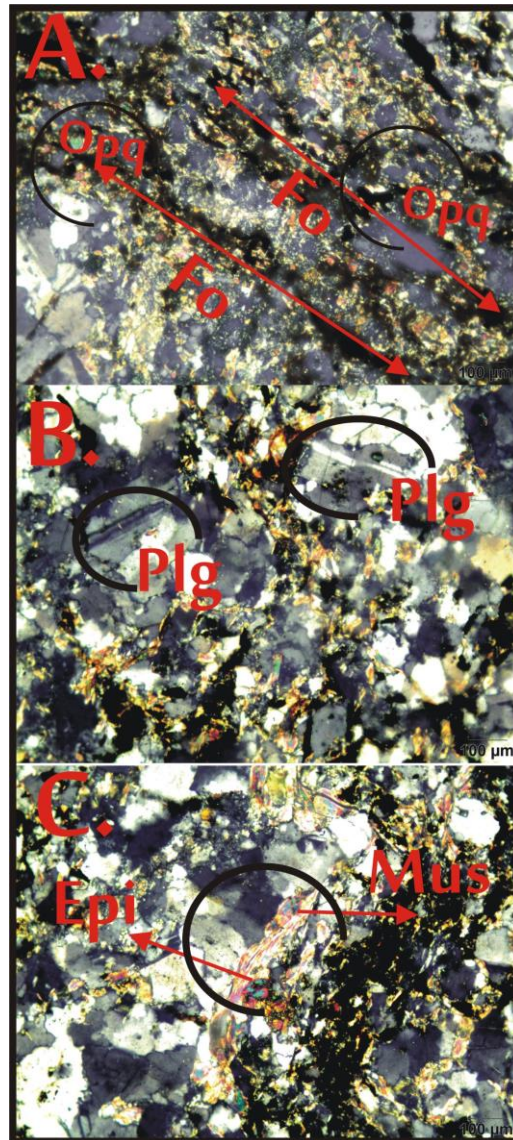


Figure 5.13. Micro-photograph of the rock sample H-2 **A.** Foliation texture represented by “Fo” whereas opaque minerals are shown by “Opq” **B.** Plagioclase minerals “Plg” are recognized with typical polysynthetic twinning **C.** Epidote “Epi” minerals are very well known key mineral while identifying propylitic alteration zones. Flakey muscovite mineral is shown by “Mus” in the figure

Rock-specimen H-3 has aphanitic relict texture (Figure 5.14.A). Plagioclase and pyroxene minerals were detected (Figure 5.14.B). Chlorite is included as a secondary mineral formation resulted from propylitic alteration (Figure 5.14.C). This rock-specimen was considered to be a basaltic volcanic original rock according to the relict textural and mineral content.

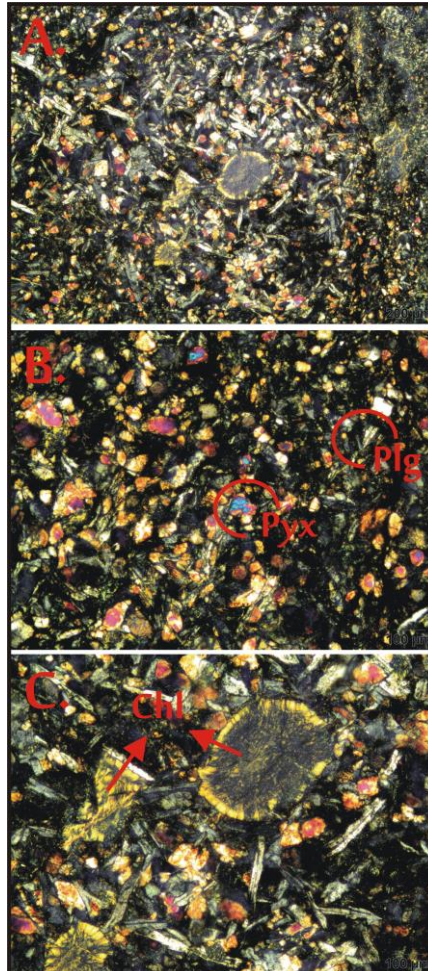


Figure 5.14. Micro-photograph of the rock sample H-3 **A.** Relict aphanitic texture of the rock-specimen represents the entity of volcanic source rock in the study area **B.**

Plagioclase “Plg” and pyroxene “Pyx” crystals were identified in the thin section analyses **C.** Chlorite mineral was observed as a result of the propylitic alteration that the rock had been subjected to

Metamorphic originated rock sample H-5 was subjected to propylitic alteration (Figure 5.15). Besides, pyrite minerals were also determined in giant crystal forms in thin-section analyses of H-5 (Figure 5.15).

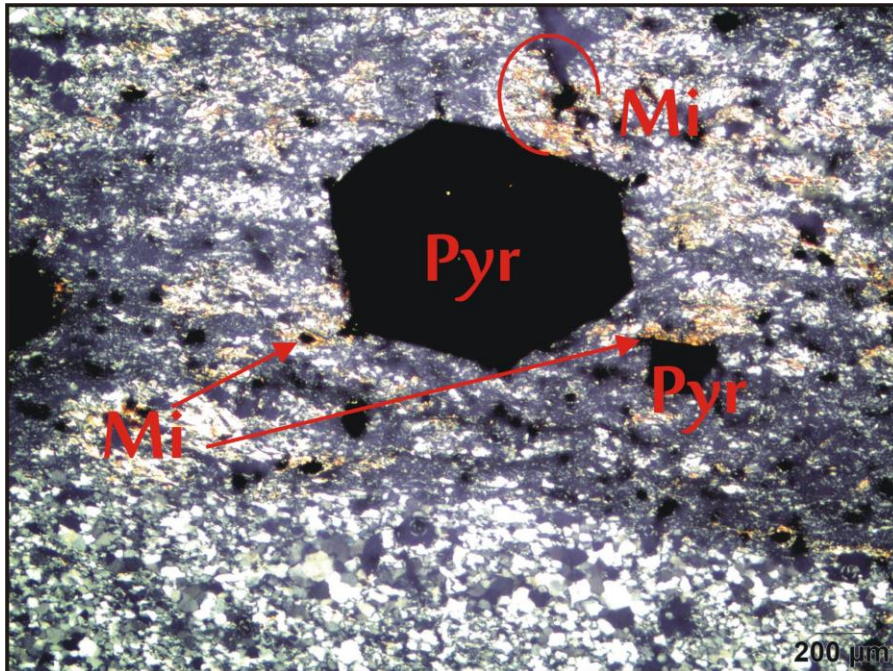


Figure 5.15. Micro-photograph of H-5. “Mi” stands for mica minerals, whereas “Pyr” represents pyrite crystals

5.1.4. Silicified Rocks:

It was detected that rock-specimen H-6 is a rock-sample including >90% secondary quartz crystals in its content representing a vein structure in the study area (Figure 5.16). This rock represents the siliceous sinter formation in the study area.

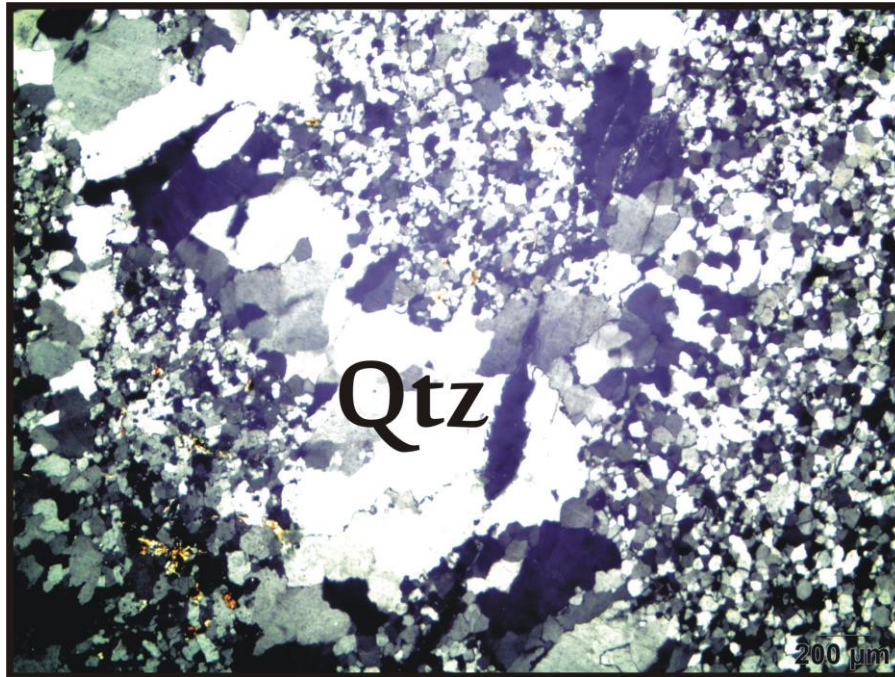


Figure 5.16. Micro-photograph of the rock sample H-6. The sample introduces silicified “Qtz” rock specimen representing siliceous sinter formation in the study area

5.2. XRD Analyses:

XRD analyses were also conducted in relation to the thin-section analyses. Since the secondary minerals could not be detected under the optical microscope, the XRD analyses were performed in order to determine the type of clay minerals, non-clay minerals in fine grained size fractions, and the entity of rock forming primary minerals which may lead us to identify the original type of kaolinized rocks and other altered rock types in the study area regarding to the 2θ (deg) and d-spacing values according to Chen (1977) (Table 5.1).

XRD diffractograms are classified and discussed based on their alteration type below. In total 295 (59*5) XRD diffractograms were generated and particular ones

were selected to represent two main zones dominantly observed in the study area; which are argillic and propylitic alteration zones.

Table 5.1. Table of X-ray diffraction data for clays and non-clay minerals (Chen, 1977)

Mineral	Degrees 2 θ (CuK α)	d-spacing values (Å°)
Chlorite-Swelling Chlorite	3.04-3.12, 6.09, 12(3), 18.10(4), 24.31(8)	30, 14.5, 7.37, 4.9, 3.66
Smectite, Air-Dry	5.73-6.31, 17.7(3), 19.72(6), 29.57(4), 35.92(3)	15.4-14, 5.01, 4.5, 3.02, 2.5
Chlorites	6.18-6.31(7-3), 12.46, 18.80, 25.15, 31.72	14.3-14, 7.10, 4.72, 3.54, 2.82
Illite and Micas	8.75-8.87, 17.73-17.81(4), 19.81-19.95(4), 26.6-26.85	10.01-9.96, 5-4.98, 4.48-4.45, 3.35-3.32
Talc	9.45, 19.38(5), 28.7(5), 34.08(2), 36.22	9.35, 4.58, 3.11, 2.63, 2.48
Amphiboles	10.40-10.53, 27.10-27.35(7-2), 33.17-32.92(3), 28.79-28.42(10-7)	8.5-8.40, 3.29-3.26, 2.7-2.72, 3.1-3.14
Chlorites	12.29-12.55, 6.18-6.49(7-3), 25.15(8), 31.72(3)	7.20-7.05, 14.3-13.6, 3.54, 2.82
<i>Kaolin Group Minerals:</i>		
Nacrite	12.32, 20.36(8), 20.36, 36.99(4), 37.63(4)	7.18, 4.36, 3.59, 2.43, 2.39
Dickite	12.36, 20.80(3), 24.87(8), 35.77(4), 38.81(7)	7.14, 4.27, 3.58, 2.51, 2.32
Kaolinite	12.39, 20.36(6), 24.87, 36.06(6), 38.46(6)	7.14, 4.36, 3.58, 2.49, 2.34
Natroalunite	18.1(7), 15.57(1), 25.52(3), 30.19, 40.63(5)	4.9, 5.69, 3.49, 2.96, 2.22
Al-Serpentine	25.01(8), 12.46-12.29, 36.22(8-4), 31.29(8)	3.56, 7.1-7.2, 2.48, 2.38

Mineral	Degrees 2 θ (CuK α)	d-spacing values (Å°)
Dawsonite	26.36(6), 15.62, 32.19(9), 34.49(7), 35.92(4)	3.38, 5.67, 2.78, 2.6, 2.5
Goethite	26.36(1), 21.25, 33.3(3), 36.67(3), 41.22(2)	3.38, 4.18, 2.69, 2.45, 2.19
Dolomite	30.94, 33.56(1), 41.22(3), 45.1(1), 51.14(2)	2.89, 2.67, 2.19, 2.01, 1.786
Lime (syn)	32.19(4), 37.47, 53.93(5), 64.23(1)	2.78, 2.4, 1.7, 1.45
Pyrite	33.05(8), 28.6(3), 37.15(6), 40.83(5), 56.33	2.71, 3.12, 2.42, 2.21, 1.633
Magnetite	35.48, 18.29(1), 30.08(3), 43.07(2), 62.54(4)	2.53, 4.85, 2.97, 2.1, 1.485
Hematite	35.77(7), 24.25(3), 33.3, 41.02(3), 54.2(4)	2.51, 3.67, 2.69, 2.2, 1.692
Psilomelane	37.31(10-7), 12.73(5), 25.59(6), 31.05(4), 41.22(8)	2.41, 6.95, 3.48, 2.88, 2.19
Pyrolusite	37.31(5), 25.59(1), 28.42, 42.43(2), 56.45(5)	2.41, 3.48, 3.14, 2.13, 1.63

5.2.1. Argillic Alteration:

These samples were obtained throughout the Ayının Tepe location within Ahırözü kaolin deposits. According to the XRD analyses of L-1 to L-11 rock sample set, except for L-1, it was determined that, these samples were dominantly enriched in kaolin minerals. Different from the other samples in the rock-specimen set, L-1 comprises trace quantity of plagioclase and chlorite minerals in the whole rock diffractogram in addition to abundant dolomite (Figure 5.17.A). In the clay fraction, XRD extractions of L-1, it was determined that the rock is deficient in the entity of clay minerals, however major peaks belonging to the kaolin minerals were identified on the diffractograms of the air dried (AD), ethylene glycol (EG) and heated to 300°C treated clay fractions (Figures 5.17.B and 5.17.C). Rock sample L-1 has been interpreted as a listwanite typed rock. Associated with the lack of quartz minerals and K-feldspar crystals in the whole rock XRD analysis of L-1 rock-specimen, it was

concluded that the original rock of the sample should have been a mafic/ultramafic originated igneous rock (Figure 5.17.A).

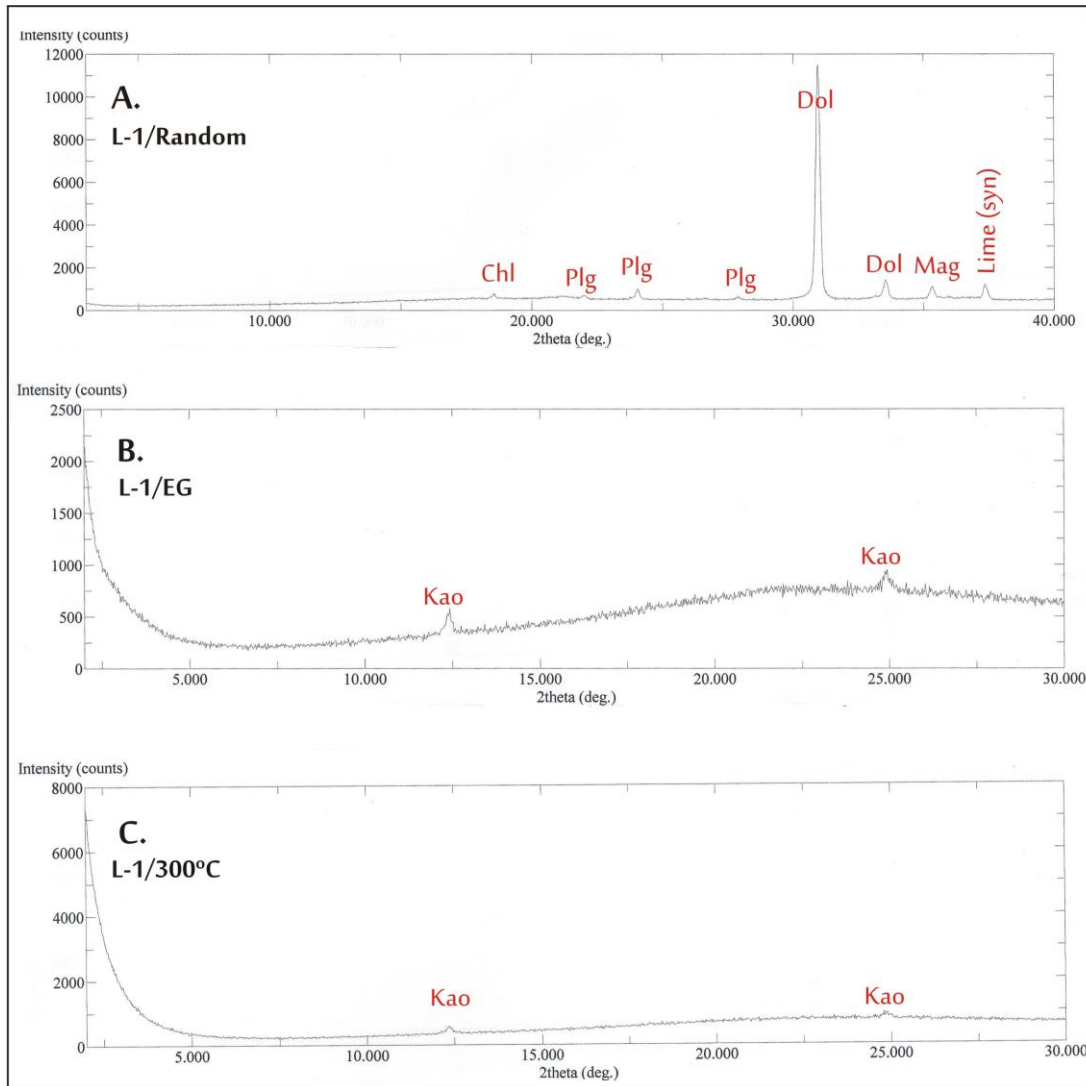


Figure 5.17. A. XRD diagram showing the entity of chlorite (Chl), plagioclase (Plg), dolomite (Dol), magnetite (Mag) and Lime (syn) in the random extraction of the rock-specimen L-1 **B.** Clay fraction of the specimen L-1 including kaolin group minerals (Kao) treated by ethylene glycol **C.** L-1 clay fractionated mount heated at 300 °C including kaolin group minerals (Kao)

Contrary to the rock-specimen L-1, samples ranging from L-3 to L-11 and Hmd series, comprise strong peaks of K-feldspar and quartz crystals in the XRD whole rock diffractogram extractions.

Natroalunite is another important essence detected in this data-set (Figure 5.19). Natroalunite ($\text{NaAl}_3(\text{SO}_4)_2(\text{OH})_6$) is an alunite group mineral formed by solfataric or hydrothermal sulfate-bearing solutions reacting with clays, rarely with sillimanite; may be in laterites and as an authigenic sedimentary mineral (Palache et al. 1951a, Okada et al., 1982, Chitale & Güven 1987, Schoch et al., 1989) . Natroalunite is much more less than alunite in the nature (Palache et al 1951a, Okada et al. 1982, Chitale & Guven, 1987; Schoch et al., 1989).

As opaque minerals observed in thin-section examinations; magnetite, hematite, pyrite and goethite minerals were distinguished in the whole rock analyses of definite samples with particular peaks (Table 5.1) (Figure 5.18). Magnetite (Fe_3O_4) is one of the most widespread iron oxide minerals and occurs in a variety of geologic environments (Palache et al., 1944). It is a common accessory mineral in igneous rocks, but rarely forms crystals large enough to be seen in hand samples. More often, magnetite is dispersed throughout a rock as microscopic crystals that form along the edges of iron-bearing minerals such as biotite, amphiboles and pyroxenes (Palache et al., 1944).

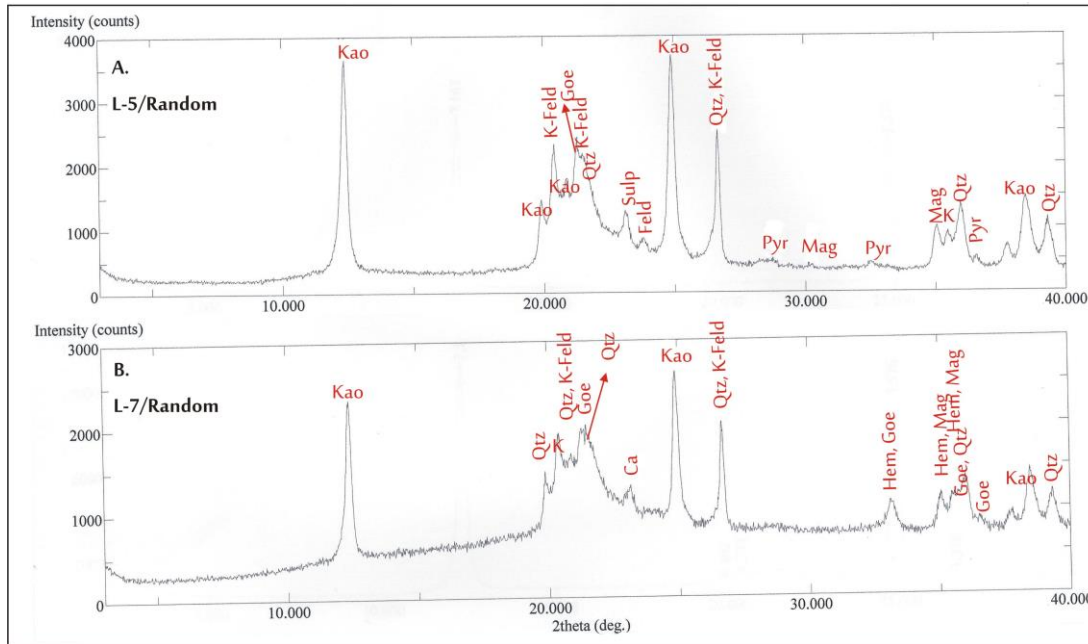


Figure 5.18. A. The whole rock XRD diffractogram of rock-specimen L-5 showing the entity of pyrite “Pyr”, goethite “Goe” and magnetite “Mag”. In the figure, “Kao” symbolizes kaolin group minerals, K-Feldspar minerals and feldspar group minerals are shown by “K-Feld” and “Feld”, respectively. “Sulp” stands for sulphur whereas “Qtz” is short for quartz. **B.** The whole rock XRD diagram of rock-specimen L-7 in which hematite “Hem”, goethite “Goe” and magnetite “Mag” minerals are found. In the figure, “Ca” represents calcite detected different from the rock-sample L-5

Hematite (Fe_2O_3) is found as an accessory mineral in many igneous rocks; commonly as a weathering product of siderite, magnetite, and other iron minerals whereas pyrite (FeS_2) is a very common accessory mineral, found in a wide variety of geological formations from sedimentary deposits to hydrothermal veins and as a constituent of metamorphic rocks (Deer et al., 1962).

Goethite ($\text{FeO}(\text{OH})$) which is a hydroxide mineral serves an important function since it represents vadose zone and found in soil and other low temperature environments (Harrison et al., 1975).

Dawsonite mineral, which is a carbonate mineral formulated as $\text{NaAlCO}_3(\text{OH})_2$, was distinguished in the whole rock analysis of the sample (Figure 5.19). Dawsonite occurs as a coating in vug walls and through fractures in hydrothermally altered feldspathic dikes and hornfels associated with nepheline syenite (Mont Saint-Bruno, Canada); authigenic in alkaline shales and coal-bearing rocks (Green River Formation, USA; Sydney Basin, Australia); in saline soils on nepheline syenite tuffs (Olduvai Gorge, Tanzania) (Palache et al., 1951b; Corazza et al., 1977; Goldbery & Loughnan, 1970; Smith & Milton, 1966; Mandarino & Harris, 1965).

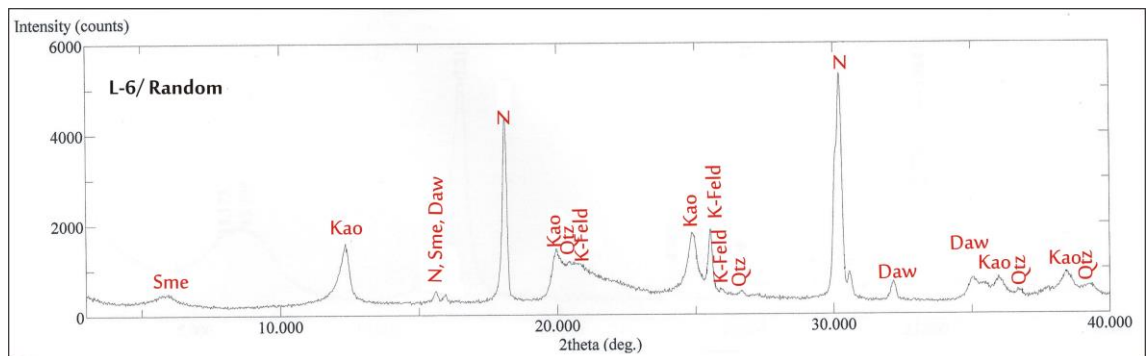


Figure 5.19. Whole rock XRD diagram of the rock-specimen L-6 including dawsonite (Daw) mineral. In the diagram, smectite is represented by “Sme”, kaolin minerals by “Kao”, natroalunite indicated by “N” whereas “Qtz” and “K-feld” stand for quartz and K-Feldspar minerals

Kaolin minerals are the most abundant clay group minerals found in argillic zone (Figure 5.20). The reason of the entity of kaolin minerals in these rock samples acquired from argillic zone is associated with that these minerals are formed resulted from leaching of K-feldspar minerals in felsic/granitic rocks associated with the interaction of hydrothermal fluids and fresh rock, itself.

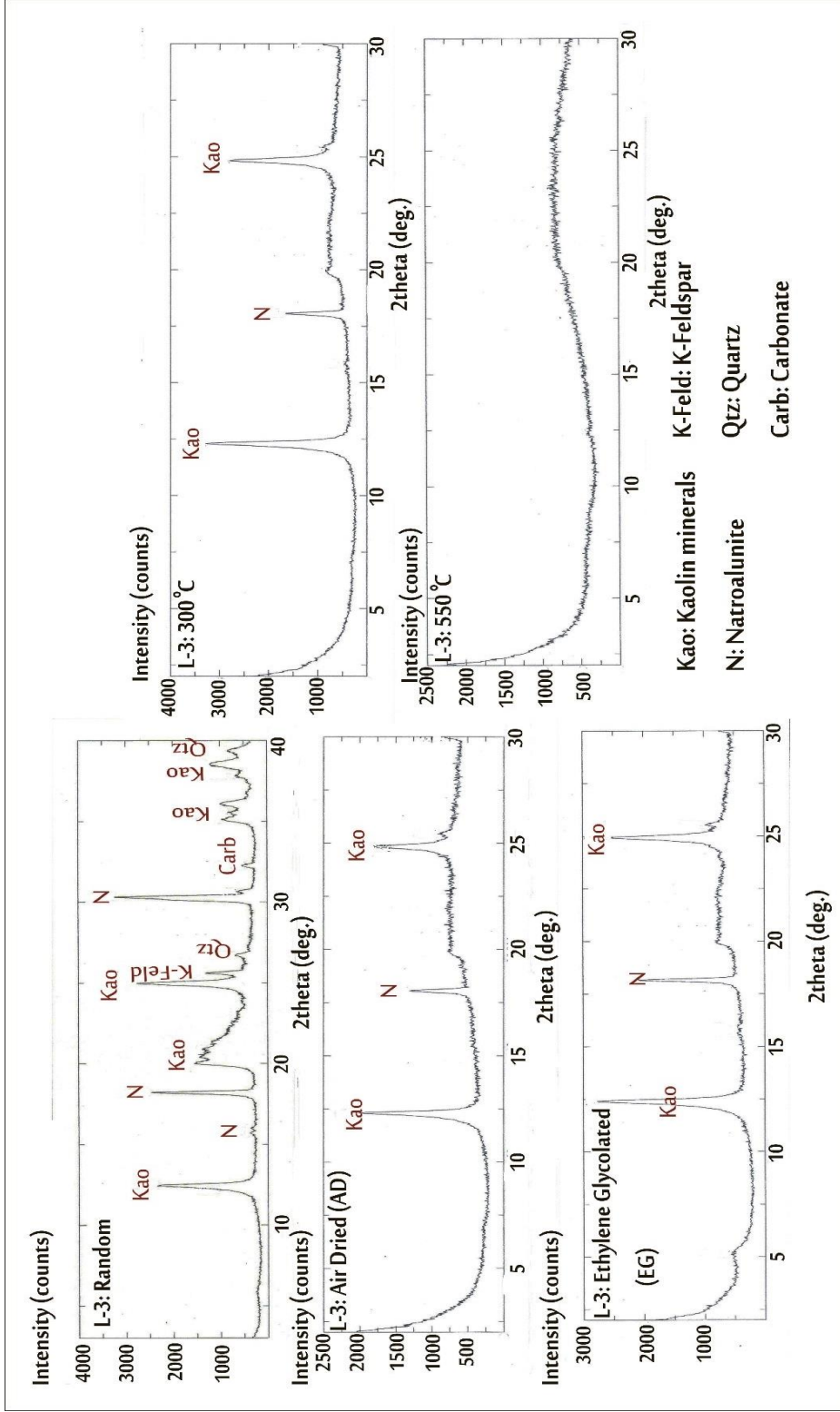


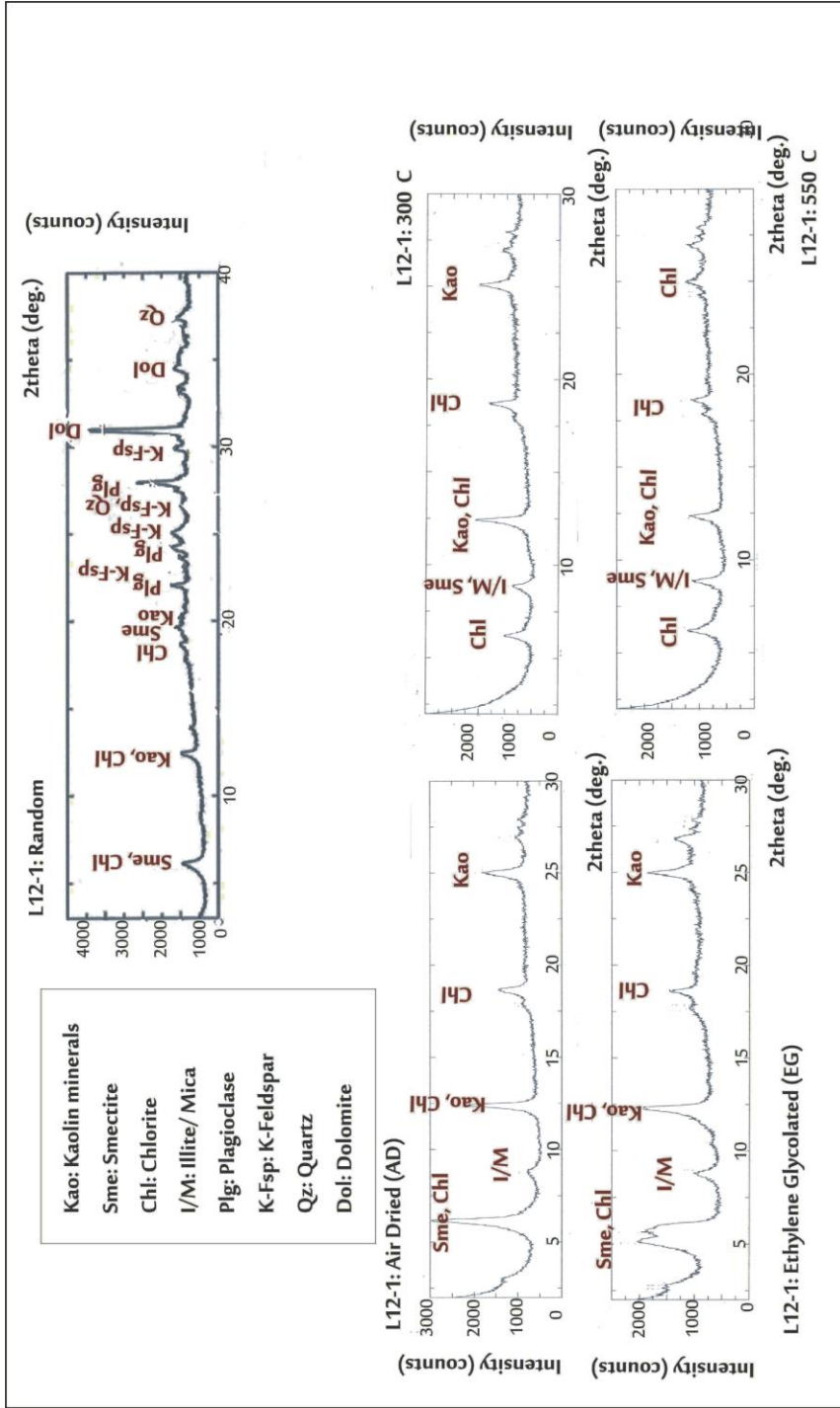
Figure 5.20. XRD diagram of L-3 comprising whole rock and clay fraction analyses (Ömeroğlu-Sayit et al., 2018)

5.2.2. Propylitic Alteration:

These samples were obtained mainly throughout the serpentized wall-rocks. Propylitic and argillic alteration products are very common in this sample set.

The most abundant mineral paragenesis found in L-12/L-13 and H series are chlorite, smectite and illite. Magnetite, goethite and very low amount of ilmenite were detected as accessory minerals.

Illite mineral is more common in the rock-samples enriched by smectite and/or chlorite group minerals comparing to the kaolinized rock samples acquired from argillic zone (Figure 5.21). Dolomite was identified as secondary mineral formation due to carbonitization (Figures 5.21 & 5.22). Talc mineral was also detected in the rock sample which was exposed to dolomitization (Figure 5.22).



Chlorite mineral is a key mineral to the propylitic alteration and very widespread in the samples (Figure 5.21). Moreover, smectite was determined as the most abundant clay group mineral in the rock-samples acquired from the propylitic alteration zone (Figures 5.21 & 5.23).

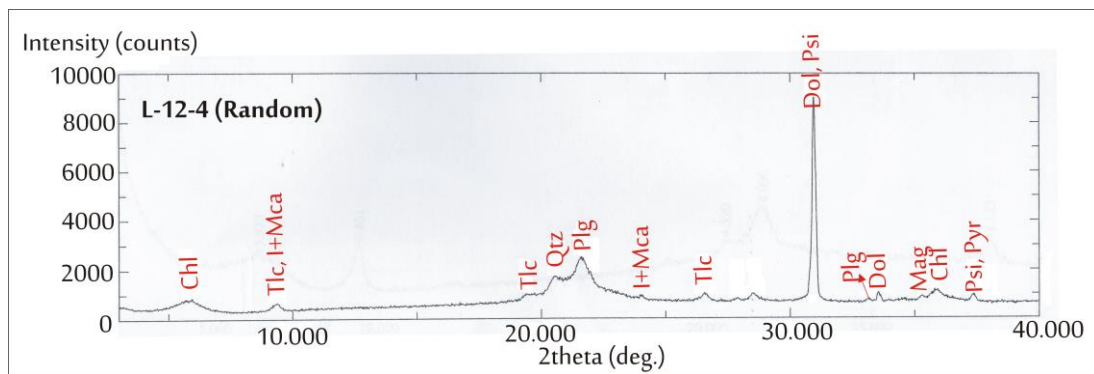


Figure 5.22. XRD diffractometer of the rock-sample L-12-4 showing the entity of chlorite “Chl”, talc “Tlc”, illite and mica minerals “I+Mca”, quartz “Qtz”, dolomite “Dol”, plagioclase “Plg”, magnetite “Mag”, psilomelane “Psi” and pyrolusite “Pyr”, respectively

Psilomelane describes barium manganese hydroxides ($\text{BaMn}^{2+}\text{Mn}^{4+}_8\text{O}_{16}(\text{OH})_4$) (Figure 5.22). Psilomelane is associated with barite, quartz, hematite and pyrolusite minerals. In Figure 5.22, psilomelane was found with pyrolusite.

Amphibole minerals were also identified very abundant in the rock-sample L-12-5b (Figure 5.23). In thin-section analyses these amphibole minerals were suggested as actinolite due to green colour and low birefringence optical properties. Its relief was moderate and observed in prismatic needle-like shaped crystals.

Illite, smectite and chlorite minerals are the most abundant clay group minerals found from metamorphic and ultramafic rock sample set as shown by XRD analyses. The original parent rocks of these altered rocks exposed to propylitic alteration were also detected using thin-section analyses based on relict textural features and relict primary minerals. Hence, the reason of the determination of

certain minerals connected with propylitic alteration in these rocks; such as chlorite is related to these minerals are formed resulted from leaching of iron and magnesium rich minerals as olivine, amphibole and pyroxene minerals in metamorphic (schists) and ultramafic (serpentinite) rocks associated with the interaction of hydrothermal fluids and fresh rock in the study area.

5.3. Morphological Features:

According to the alteration products and zones identified in the study area; mainly argillic and propylitic alteration products were taken into consideration in the morphological analyses similar to the XRD analyses. SEM-EDX analyses were conducted both on representative rock samples acquired throughout the kaolin deposits and wall-rocks. The main purpose to perform SEM/EDX analyses was to study the morphology of clay group minerals and detect the type of kaolin minerals.

Clay and non-clay minerals in addition to accessory minerals were identified by XRD and thin-section analyses, firstly. Also, the presence of K-feldspar, quartz and natroalunite were identified in the Ayının Tepe kaolin deposit and Hamidiye kaolins. The entity of natroalunite suggests high SO_4 content. K-feldspar and its alteration mineralogy suggests that the precursor rock was granitic in character. Natroalunite crystals in sample L-6 displayed rhombohedral morphologies associated with tubular halloysite minerals in this sample (Figure 5.24) (Ömeroğlu-Sayıt et al., 2018). EDX analysis of this sample also showed the existence of Al and Si for halloysite and Na and S for natroalunite (Figure 5.24) (Ömeroğlu-Sayıt et al., 2018).

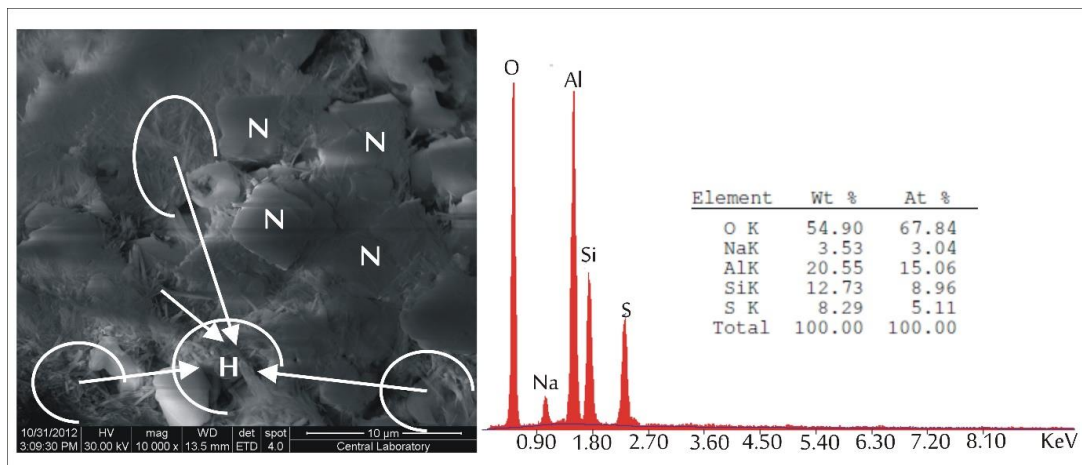


Figure 5.24. SEM-EDX analysis of sample L-6 from argillic zone revealing natroalunite (N) and halloysite (H) association (Ömeroğlu-Sayıt et al., 2018)

Kaolinite minerals were observed in well crystallized pseudo-hexagonal morphology-like platelet which is a typical characteristic appearance for kaolinite crystals (Figure 5.25). In SEM images, these kaolinites may have showed rolled and rough edges (Figure 5.25). Stacks of kaolinites were also studied by EDX to verify its chemical constituent including Al and Si elements, mainly (Figure 5.25).

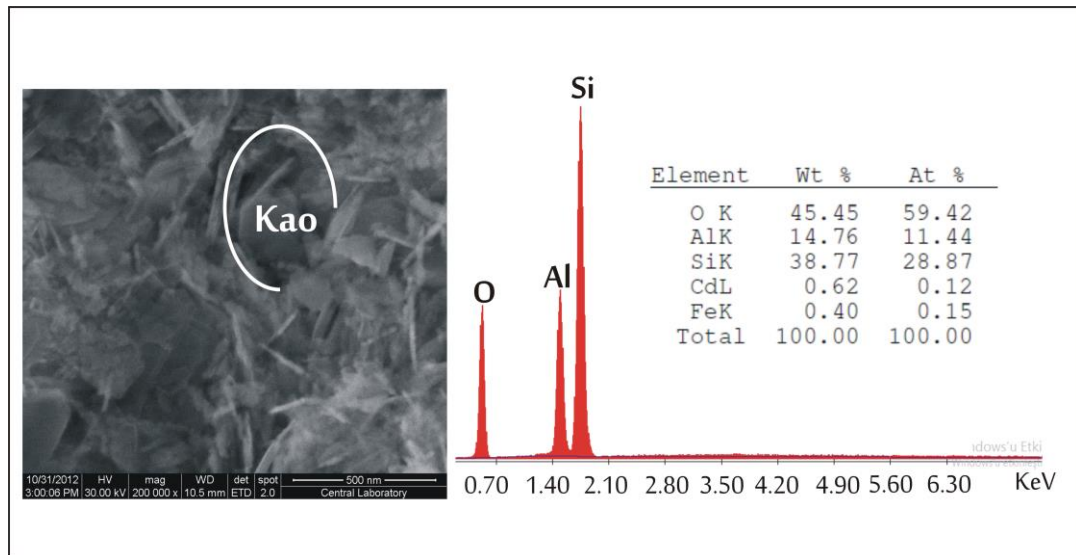


Figure 5.25. SEM-EDX analyses of the sample L-3 from argillic zone verifying the entity of kaolinite crystals both in morphological and chemical data. “Kao” stands for kaolinite stacks in this figure

Rock samples mainly exposed, which is mainly associated with carbonatization in our rock samples were dominantly altered to chlorite-smectite-illite-epidote mineral assemblages (Ömeroğlu-Sayıt et al., 2018). Chlorite is a key mineral while determining the existence of propylitic alteration, therefore, especially the representative samples were selected to be conducted SEM-EDX analyses on them to study morphological features of chlorite minerals and verify the chemical component of them (Figure 5.26).

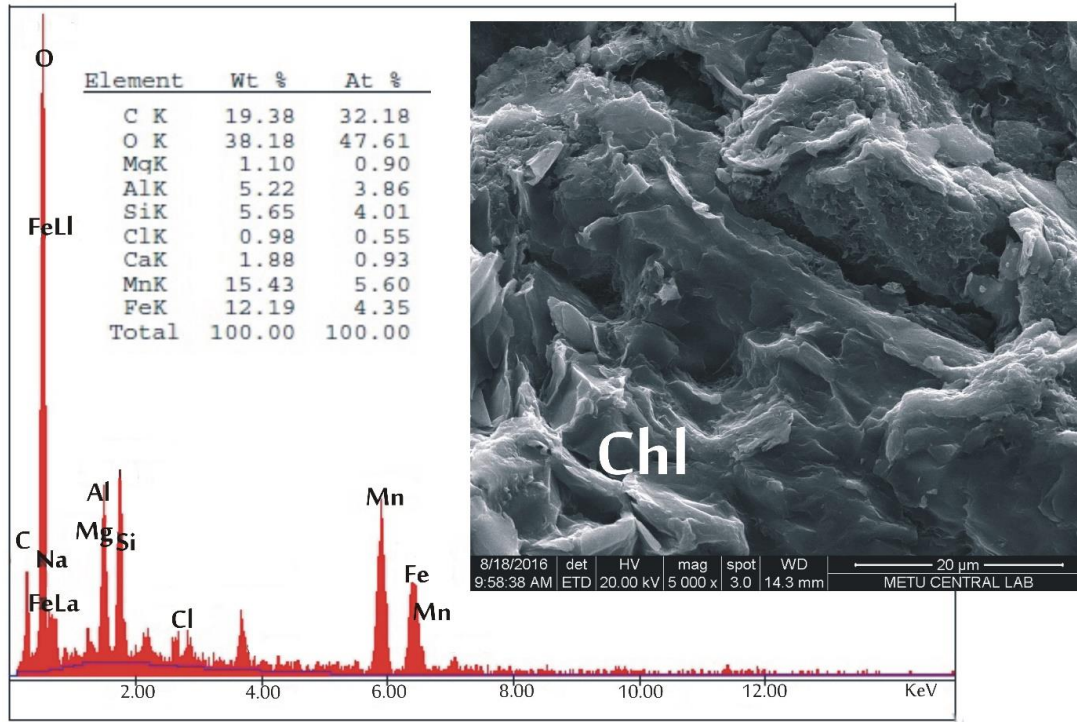


Figure 5.26. SEM micro-photograph of Sample L12-1 showing chlorite morphology and the EDX analysis of chlorite (Chl) (Ömeroğlu-Sayıt et al., 2018)

Therefore, in accordance with the morphological and chemical data given above, it has been determined that mainly there are two kind of kaolin minerals found in argillic zone which are halloysite and kaolinite minerals. On the other hand, chlorite is the most abundant clay group mineral found in propylitic alteration zone.

CHAPTER 6

RESULTS: CHEMICAL ANALYSES

This chapter aims to present the results of geochemical analyses performed on representative kaolin rich rock-specimens from the point of view of (1) comparing the mineralogical and geochemical compositions of the samples which represents the main types of the alteration products, (2) understanding the geochemical signatures of alteration processes and tectonic setting of the protolith granitic rocks, (3) understanding the intensity of alteration giving rise to different alteration types of the exposed rock types in the study area, (4) revealing the nature of mineralizing fluids and the processes by which the mineral deposits were formed, and (5) understanding the age and formation condition of the kaolinite.

6.1. Mineralogical Fingerprinting of Geochemical Variations:

The data derived from major and trace element analyses of 20 selected samples acquired from the Ahırözü kaolin deposits (Aydın Tepe and Hamidiye locations) are given in Table 6.1 and Appendix A, Table A-1. Major element analyses of the samples reflect the presence of the following main minerals in the samples:

High amounts of CaO (26.05%) MgO(17.93%) and LOI (42%) contents show that the sample L-1 was enriched in dolomite as also detected by XRD analysis. This sample exemplifies the carbonate enrichment of the ultramafic rocks outcropping in the study area. Also, since this sample was identified as listwanized rock, it may serve an important function in relation to gold-Au mineralization in further studies that we haven't focused on in the scope of this study (Appendix A, Table A-1). Listwanite-associated gold deposits with serpentinized and carbonate altered

ultramafic rocks are characteristic of tectonically disrupted ophiolite sequences (Ash & Arksey, 1990). The hypothesis for gold deposition in and/or near listwanites/carbonatized ultramafic rock initiates low-salinity hydrothermal fluids rich in carbon dioxide which carry gold in terms of bisulphide complex, $\text{Au}(\text{HS})_2$ (Böhlke, 1989; Kerrich, 1989).

High Al_2O_3 and SiO_2 contents of the samples (L-3, L-4A, L-4B, L-5 and L-6) collected at the Ayının Tepe kaolin deposit location are ranging between 24.44%-36.18% and 21.41% -61.75%, respectively (Ömeroğlu-Sayıt et al., 2018). These samples are dominated by kaolin minerals. Relatively high amounts of Na_2O in the samples L-3 (1.89%), L-4A (4.08%) and L-6 (2.48%) in association with the corresponding TOT/S values (4.23% 8.54%. and 5.65% respectively, are attributed to the mineral natroalunite which is also detected by XRD analysis (Ömeroğlu-Sayıt et al., 2018). Natroalunite is not detected mineralogically, in the sample L-5 having very low concentrations of Na_2O (0.12 %) and TOT/S (<0.02%), respectively.

As can be seen in Table 6.1, the samples (L-7,L-8, L-9, L-10 and L-11) collected along the NE direction away from the Ayının Tepe kaolin deposit, contain relatively higher concentrations of SiO_2 (ranging between 49.15%-93.71%), lower amounts of Al_2O_3 (ranging between 2.53%-25.86%) and Na_2O (ranging between 0.02% - 0.08%) compared with other samples from the Ayının Tepe kaolin deposit. In this group of samples natroalunite is not detected by XRD analysis (Ömeroğlu-Sayıt et al., 2018). The total Fe_2O_3 values of L-4A (9.42%)-L-7 (22.49%), L-8 (29.22%), L-9 (11.85%) and L-11 (2.76%) are mainly related to the presence of iron minerals; such as hematite and goethite (Ömeroğlu-Sayıt et al., 2018).

The rock-samples collected from Hmd 1 series were detected as kaolinized granitic protolith. However, kaolinized Hmd 1 series (Hmd 1-1, Hmd 1-2, Hmd 1-3, Hmd 1-4, Hmd 1-5, Hmd 1-6, Hmd 1-7, Hmd 1a and Hmd 2a) rock-samples were more silicified (Ave SiO_2 : 69.37%) compared to the L-series rock-specimens (Ave SiO_2 : 65.34%) (Table 6.1). Al_2O_3 (Ave: 18.25%) concentration of the Hmd 1 series rock samples is lesser than the L-series (Ave: 18.68%) rock samples (Table 6.1). Hmd 1-7a and Hmd1-7b have high total Fe_2O_3 concentrations comparing to the other selected rock samples collected from Ayının Tepe pit and Hamidiye kaolins.

However, Hmd 1-8 has not been selected to be used in geochemical analyses since it does not include any kaolin peaks in the clay fraction XRD diffractograms. They belong to intensely weathered and oxidized rock which can be defined as “gossan”.

In terms of the trace element concentrations of the analyzed samples geochemical variations exists mainly for the Zr, Sr, Y, Ni and Zn (Table 6.2). The geochemical analysis results of the trace elements are interpreted in the following section.

6.2.Geochemical Signatures of Alteration and Tectonic Setting

A chondrite normalized trace element spider diagram for the selected kaolinized samples from the Ahırözü kaolin deposits is shown in Figure 6.1. Not all of the samples have similar patterns. Some elements such as Cs, Ba, Rb, Th, U, Pb and Nb behave similarly showing parallel positive and negative spikes for all the samples. On the contrary Ce, Sr, Zr, Tb and Y form two groups which corresponds generally with the two different sample locations, namely Aydın Tepe and Hamidiye kaolin deposits. Although the Large Ion Lithophile Elements (LILE) and the High Field Strength Elements (HFSE) behave in an incompatible way during mantle melting, their response to post magmatic processes should differ since the HFSE are usually immobile: that is, they are mostly resistant to metamorphism and hydrothermal alteration so, their contents are likely to be representative of the original rock (White, 2013). On the other hand, the LILE are fluid-mobile and hydrothermal alteration may change their contents in the studied rocks (Ömeroğlu-Sayıt et al., 2018). It can be inferred that similar behavior of at least some of the LILE elements, e.g. Pb, Rb and Ba can be due to the homogenizing effect of the hydrothermal solutions on the original rock composition (Ömeroğlu-Sayıt et al., 2018). On the contrary, immobile HFSE such as Nb, Zr, Y, Ce and Tb concentrations are inherited from the original rock and show high resistance to alteration (Ömeroğlu-Sayıt et al., 2018). Based on these geochemical differences, protolith granitic rocks exposed at Aydın Tepe and Hamidiye locations have some trace element geochemical differences which may indicate the effect of original magmatic processes.

The geochemical signatures of the kaolin samples can be related to hydrothermal alteration processes and can be used while estimating the tectonic setting of the protolith igneous body hosting the kaolin deposits in the study area. A discrimination diagram which was based on trace elements of Rb –Y+Nb (Pearce et al.,1984) (Figure 6.2), was utilized to obtain a preliminary data on the tectonic setting of the granitic protolith of the kaolin deposits in the study area. The samples were plotted in the volcanic arc granites field (VAG) with distinguishable two groupings due to the higher Y+Nb concentration of the samples collected from the Hamidiye kaolin deposit (Ömeroğlu-Sayıt et al. 2018).

Table 6.1. The major element analyses of selected samples from the Ahırözü kaolin deposits (Ömeroğlu-Sayıt et al., 2018)

Sample No.	SiO ₂	Al ₂ O ₃	Fe ₂ O ₃	MgO	CaO	Na ₂ O	K ₂ O	TiO ₂	P ₂ O ₅	MnO	Cr ₂ O ₃	LOI	TOT /S	Sum
L-1	11.80	0.83	0.93	17.93	26.05	0.02	0.02	0.03	<0.01	0.05	0.222	42.0	<0.02	99.92
L-3	35.24	36.18	0.13	0.20	0.13	1.89	<0.01	0.09	0.02	<0.01	0.022	2.2	4.23	99.94
L-4A	21.41	30.20	9.42	0.06	0.11	4.08	0.04	0.25	0.11	<0.01	0.014	34.1	8.54	99.78
L-4B	60.24	25.80	1.18	0.26	0.22	0.16	0.07	0.73	0.02	<0.01	0.008	11.2	<0.02	99.90
L-5	61.75	24.44	0.46	0.14	0.12	0.12	0.04	1.27	<0.01	<0.01	0.011	11.5	<0.02	99.89
L-6	30.14	35.96	0.78	0.42	0.22	2.48	0.08	<0.01	0.04	<0.01	0.019	29.7	5.65	99.83
L-7	49.15	17.60	22.49	0.06	0.11	0.05	0.02	0.49	0.02	0.02	0.086	9.7	0.19	99.84
L-8	57.46	5.25	29.22	0.06	0.11	0.08	0.05	0.78	0.03	0.01	0.024	6.8	0.09	99.85
L-9	81.09	2.53	11.85	0.13	0.11	0.04	0.06	0.07	0.06	0.01	0.565	3.2	0.08	99.86
L-10	60.28	25.86	0.88	0.11	0.18	0.02	0.02	0.14	<0.01	<0.01	0.010	12.4	0.02	99.91
L-11	93.71	0.80	2.76	0.10	0.09	0.02	0.04	<0.01	<0.01	0.03	0.118	2.2	<0.02	99.94

Sample No.	SiO ₂	Al ₂ O ₃	Fe ₂ O ₃	MgO	CaO	Na ₂ O	K ₂ O	TiO ₂	P ₂ O ₅	MnO	Cr ₂ O ₃	LOI	TOT /S	Sum
Hmd1-1	71.03	18.49	0.48	0.28	0.24	<0.01	0.30	0.41	0.04	<0.01	0.006	8.6	<0.02	99.92
Hmd1-2	73.92	17.00	0.39	0.16	0.14	0.02	0.20	0.33	0.02	<0.01	0.002	7.7	<0.02	99.91
Hmd1-3	72.37	17.80	0.93	0.20	0.13	0.01	0.38	0.41	0.04	<0.01	0.003	7.6	<0.02	99.92
Hmd1-4	57.90	27.72	1.64	0.20	0.13	0.01	0.20	0.41	0.03	<0.01	0.003	11.7	<0.02	99.93
Hmd1-5	67.67	19.87	0.50	0.16	0.11	0.25	0.41	0.41	0.07	<0.01	0.012	10.4	0.73	99.91
Hmd1-6	69.48	17.74	2.55	0.07	0.08	0.18	0.28	0.40	0.09	<0.01	0.009	9.0	0.55	99.90
Hmd1-7	77.27	14.34	0.53	0.07	0.07	0.07	0.21	0.30	0.04	<0.01	0.013	7.0	0.21	99.90
Hmd1-7a	46.77	15.86	10.47	6.26	1.70	3.56	0.13	1.62	0.15	0.13	0.021	13.2	<0.02	99.84
Hmd 1-7b	51.61	15.45	18.67	0.61	0.21	0.04	0.02	0.84	0.10	0.02	0.007	12.2	<0.02	99.85

Table 6.2. The trace element analyses of selected samples from the Ahrözü kaolin deposits (Ömeroğlu-Sayıt et al. 2018)

Sample No.	Cs	Ba	Rb	Th	U	Pb	Nb	Ce	Sr	Zr	Tb	Y	Ni	Zn	Ta
L-1	7.0	37	1.3	<0.2	0.6	0.8	0.3	0.6	192.5	2.3	0.03	2.5	358.6	5	<0.1
L-3	1.6	8	1.5	<0.2	<0.1	0.2	0.4	2.0	328.3	4.7	<0.01	<0.1	8.5	3	<0.1
L-4A	1.4	19	4.8	0.5	0.3	2.0	0.6	11.8	329.3	3.3	0.03	0.6	44.8	3	<0.1
L-4B	4.6	17	0.8	<0.2	0.3	0.3	2.4	0.3	19.7	8.3	<0.01	0.2	22.6	2	<0.1
L-5	5.7	12	0.6	<0.2	0.9	0.2	1.2	0.4	14.5	5.8	0.01	0.4	0.3	4	<0.1
L-6	1.5	20	3.6	<0.2	0.7	0.1	0.3	2.0	324.5	1.3	<0.01	0.1	5.0	1	0.1
L-7	1.9	9	<0.1	<0.2	<0.1	0.6	0.5	0.6	19.2	7.0	<0.01	0.2	5.0	11	<0.1
L-8	2.7	15	0.2	<0.2	0.3	0.2	1.0	0.2	21.2	1.3	0.02	0.4	9.1	16	<0.1
L-9	6.2	55	3.9	<0.2	0.1	0.7	1.3	1.2	26.9	3.7	0.02	0.8	1606.7	9	<0.1
L-10	1.6	8	<0.1	<0.2	0.2	0.1	0.6	0.2	10.7	2.3	0.01	<0.1	1.3	2	<0.1
L-11	2.1	35	1.4	<0.2	<0.1	1.8	3.1	0.3	5.5	11.6	0.01	1.1	409.6	15	<0.1
Hmd1-1	7.6	26	3.7	1.1	0.3	0.6	2.8	17.0	32.2	129.8	0.43	23.1	2.7	2	0.2
Hmd1-2	9.0	15	2.9	0.9	0.5	<0.1	3.1	4.9	9.1	192.5	0.50	27.4	5.0	1	0.2
Hmd1-3	8.2	44	4.2	0.8	0.4	0.1	2.5	14.5	37.8	141.4	0.57	21.8	2.4	2	<0.1
Hmd1-4	6.5	24	3.2	0.7	0.3	0.1	2.7	6.0	17.6	116.9	0.41	25.5	3.1	4	0.2
Hmd1-5	4.9	32	3.9	0.8	0.3	0.2	2.7	17.0	67.9	126.6	0.45	21.9	3.5	2	0.2
Hmd1-6	2.6	20	3.1	1.0	1.0	0.5	3.3	21.2	88.1	127.6	0.69	42.4	24.5	4	0.2
Hmd1-7	3.4	23	2.1	0.6	0.5	0.3	2.4	6.3	61.7	290.5	0.30	20.8	2.5	3	0.2
Hmd1-7a	2.6	14	4.1	0.7	0.2	0.4	7.2	13.2	58.5	91.5	0.70	21.2	80.3	83	0.5
Hmd1-7b	5.7	17	0.7	<0.2	0.4	0.4	0.3	1.0	27.6	7.6	0.20	7.1	111.8	153	0.2

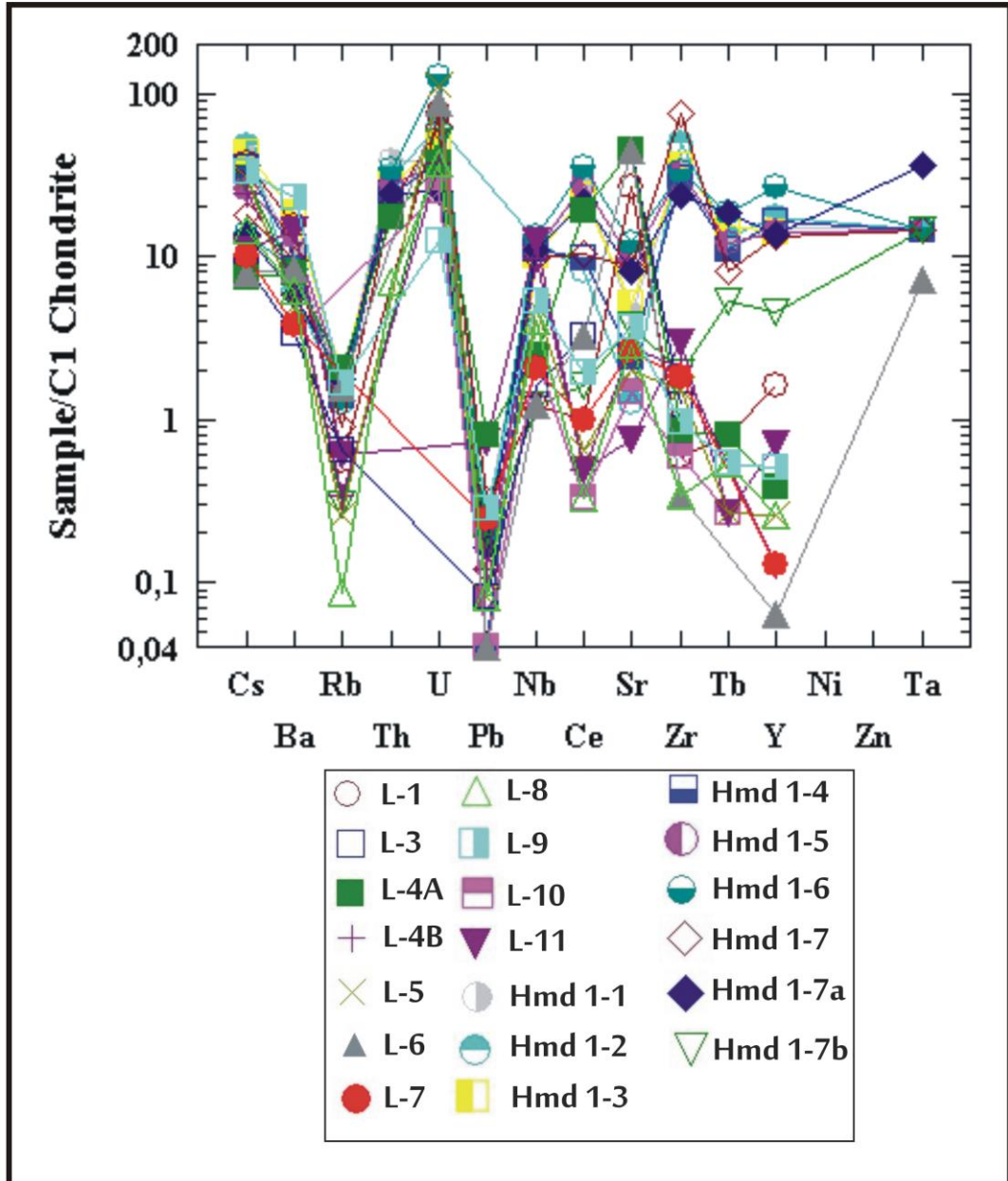


Figure 6.1. Trace element spider diagram of selected samples from the kaolin deposit (Ömeroğlu-Sayıt et al., 2018)

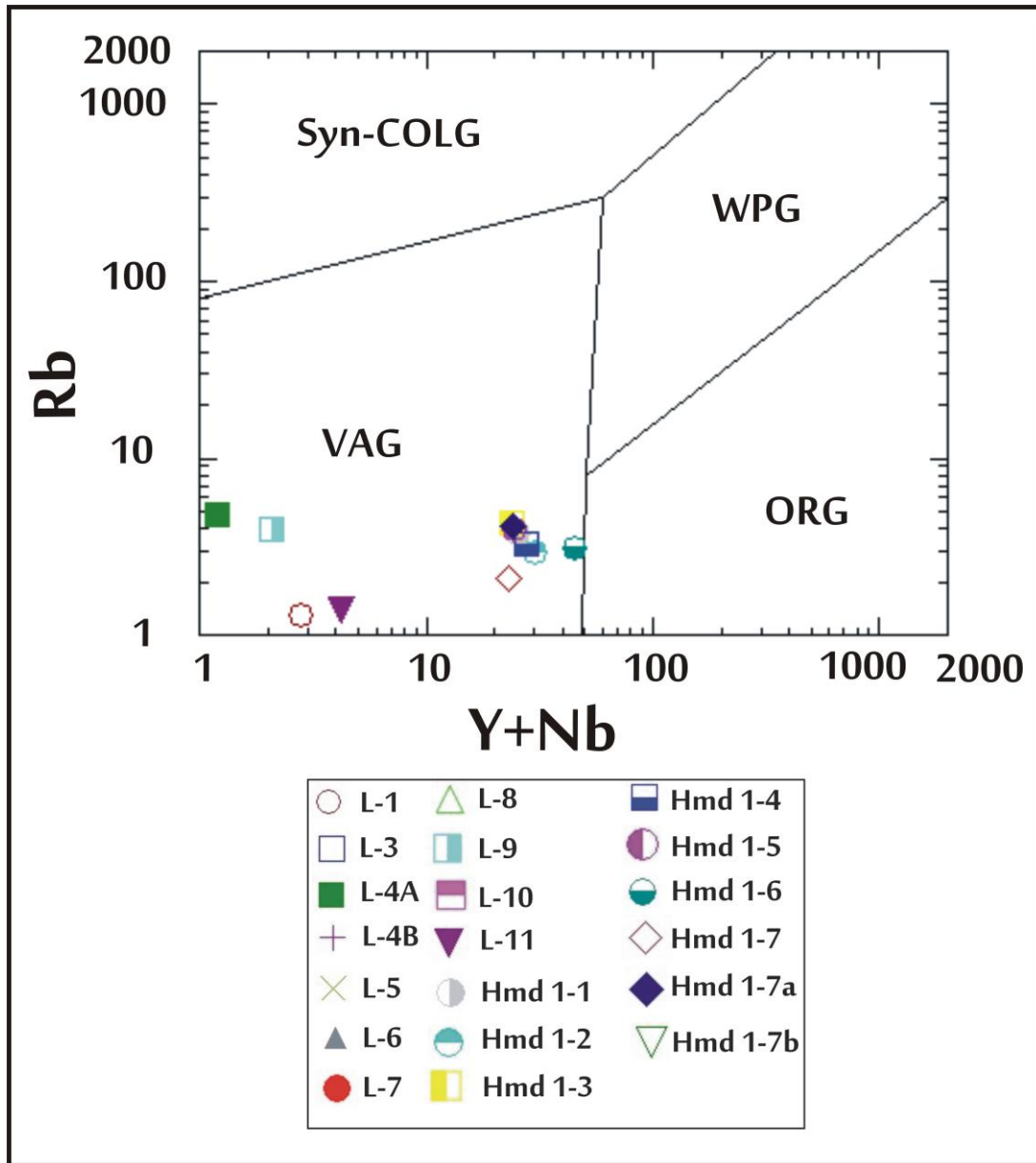


Figure 6.2. Tectonic setting of granite in the study area (Pearce *et al.* 1984).Syn COLG, syn-collision granites; WPG, within-plate granites; VAG, volcanic arc granites; ORG, ocean ridge granites. Symbols are same as in Figure 6.1 (Ömeroğlu-Sayıt *et al.*, 2018)

6.3. Intensity of Hydrothermal Alteration as revealed by Alteration Index:

The Ishikawa alteration index (AI) and the chlorite-carbonate-pyrite index (CCPI) have been used to study the intensity of alteration occurred in the study area. The AI index has been first proposed by Ishikawa et al. (1976) to reveal the effect of sericite and chlorite alteration formed in the footwall volcanics around Kuroko deposits (Large et al., 2001). The main point of this index is the breakdown of sodic plagioclase and volcanic glass by resulting in the replacement of sericite and chlorite (Large et al., 2001). The index introduces values changing from 20 to 60 for unaltered rocks whereas offering values from 50 to 100 (e.g. Hmd 1-1, Hmd 1-2, Hmd 1-3, Hmd 1-4, Hmd 1-5, Hmd 1-6, Hmd 1-7) for hydrothermally altered rocks with an AI=100 including total replacement of feldspars and glass by sericite and/or chlorite (Table 6.3). Chlorite-carbonate-pyrite index (CCPI) has been also developed to calculate the increase in amount of MgO and FeO due to the occurrence of Mg-Fe chlorite in the system when it replaces with albite, K-feldspar or sericite in the igneous rocks by resulted in the loss of Na₂O and K₂O (Large et al., 2001). This index is also connected with carbonate alteration in addition to the enrichment of pyrite, hematite and magnetite assemblages. According to the alteration trends, it has been observed that least altered volcanic samples introduce approximately AI=30 (Table 6.3). With an increased carbonate alteration, CCPI (>90) values of the samples have been increased (e.g. H-10) comparing to the samples dominantly composed of chlorite alteration (Table 6.3).

As it is mentioned above there has been two types of index used to identify the alterations which are Ishikawa alteration index (AI) and chlorite-carbonate-pyrite index (CCPI). Ishikawa alteration index is calculated as below (Large et al., 2001):

$$\text{AI} = 100(\text{K}_2\text{O} + \text{MgO}) / (\text{K}_2\text{O} + \text{MgO} + \text{Na}_2\text{O} + \text{CaO})$$

According to AI, the ranges are as (Large et al., 2001):

AI=20-60 (not altered),

AI=50-100 (hydrothermally altered),

AI=100 (feldspar minerals are replaced by volcanic glass)

On the other hand, chlorite-carbonate-pyrite index is calculated as (Large *et al.* 2001):

$$\text{CCPI} = 100(\text{MgO} + \text{FeO}) / (\text{MgO} + \text{FeO} + \text{Na}_2\text{O} + \text{K}_2\text{O})$$

Table 6.3. AI and CCPI data generated by using representing rock-specimens acquired from the study area

Sample	Na ₂ O	CaO	K ₂ O	MgO	A	F	AI	Fe ₂ O ₃	FeO	CCPI
L-3	1.89	0.13	0.00	0.20	0.20	2.22	9.0	0.13	0.12	14.4
L-4A	4.08	0.11	0.04	0.06	0.10	4.29	2.3	9.42	8.48	67.4
L-4B	0.16	0.22	0.07	0.26	0.33	0.71	46.5	1.18	1.06	85.2
L-5	0.12	0.12	0.04	0.14	0.18	0.42	42.9	0.46	0.41	77.6
L-6	2.48	0.22	0.08	0.42	0.50	3.20	15.6	0.78	0.70	30.5
L-8	0.08	0.11	0.05	0.06	0.11	0.30	36.7	29.22	26.29	99.5
L1A	0.03	14.71	0.27	16.43	16.70	31.44	53.1	6.69	6.02	98.7
L1B	0.03	13.76	0.15	10.11	10.26	24.05	42.7	5.21	4.69	98.8
L12-1	3.87	6.48	2.67	5.57	8.24	18.59	44.3	13.03	11.72	72.6
L12-2	0.11	0.09	0.37	0.14	0.51	0.71	71.8	0.56	0.50	57.3
L12-3	2.38	0.22	0.22	0.29	0.51	3.11	16.4	1.14	1.03	33.6
L12-4	0.12	3.27	0.18	3.65	3.83	7.22	53.0	2.70	2.43	95.3
L12-5a	0.03	11.19	0.04	15.09	15.13	26.35	57.4	8.29	7.46	99.7
L12-5b	5.28	0.96	0.84	7.66	8.50	14.74	57.7	6.66	5.99	69.0

Sample	Na ₂ O	CaO	K ₂ O	MgO	A	F	AI	Fe ₂ O ₃	FeO	CCPI
L12-6	0.06	0.37	0.05	0.55	0.60	1.03	58.3	9.70	8.73	98.8
L12-7	0.17	0.15	0.14	0.15	0.29	0.61	47.5	4.29	3.86	92.8
L12-8	0.09	13.77	0.72	14.06	14.78	28.64	51.6	6.21	5.59	96.0
L12-9	0.41	0.21	0.54	0.13	0.67	1.29	51.9	4.03	3.63	79.8
L12-10	0.09	0.10	0.35	0.12	0.47	0.66	71.2	4.48	4.03	90.4
L12-11	0.00	0.08	0.27	0.09	0.36	0.44	81.8	0.76	0.68	74.1
L13	0.25	20.83	1.11	16.25	17.36	38.44	45.2	5.52	4.97	94.0
Hmd1-1	0.00	0.24	0.30	0.28	0.58	0.82	70.7	0.48	0.43	70.4
Hmd2a	0.02	0.15	0.35	0.15	0.50	0.67	74.6	0.50	0.45	61.9
Hmd1-2	0.02	0.14	0.20	0.16	0.36	0.52	69.2	0.39	0.35	69.9
Hmd1-3	0.01	0.13	0.38	0.20	0.58	0.72	80.6	0.93	0.84	72.7
Hmd1-4	0.01	0.13	0.20	0.20	0.40	0.54	74.1	1.64	1.48	88.9
Hmd1-5	0.25	0.11	0.41	0.16	0.57	0.93	61.3	0.50	0.45	48.0
Hmd1-6	0.18	0.08	0.28	0.07	0.35	0.61	57.4	2.55	2.29	83.7
Hmd1-7	0.07	0.07	0.21	0.07	0.28	0.42	66.7	0.53	0.48	66.1
Hmd1-7a	3.56	1.70	0.13	6.26	6.39	11.65	54.8	10.47	9.42	81.0
Hmd1-8	1.23	8.62	3.57	9.55	13.12	22.97	57.1	10.91	9.82	80.1
H-1	0.64	20.95	0.63	16.63	17.26	38.85	44.4	4.14	3.73	94.1
H-2	4.67	2.00	1.04	3.04	4.08	10.75	38.0	11.43	10.28	70.0
H-3	3.78	7.89	0.02	6.85	6.87	18.54	37.1	12.48	11.23	82.6
H-4	0.03	0.19	0.16	0.16	0.32	0.54	59.3	18.64	16.77	98.9

Sample	Na ₂ O	CaO	K ₂ O	MgO	A	F	AI	Fe ₂ O ₃	FeO	CCPI
H-5	0.00	0.09	0.86	0.35	1.21	1.30	93.1	4.41	3.97	83.4
H-6	0.00	0.06	1.09	0.46	1.55	1.61	96.3	2.77	2.49	73.0
H-7	0.00	0.12	0.34	0.24	0.58	0.70	82.9	2.37	2.13	87.5
H-8	0.05	0.20	0.07	0.08	0.15	0.40	37.5	9.94	8.94	98.7
H8-1	0.04	0.08	0.00	0.03	0.03	0.15	20.0	10.52	9.47	99.6
H-10	0.04	0.25	0.00	0.17	0.17	0.46	37.0	3.50	3.15	98.8
H-11	0.02	0.27	0.04	0.27	0.31	0.60	51.7	13.68	12.31	99.5
H-12	0.00	30.07	0.00	21.17	21.17	51.24	41.3	2.46	2.21	100.0

Studying the samples belonging to different alteration zones, the data were divided into 4 sets (Figure 6.3). Hydrothermally altered rock samples exposed to argillic and propylitic alterations were chosen to illustrate and verify the data associated with the alteration zones based on XRD and thin-section analyses. In Figure 6.3, it is observed that H-series samples were exposed to intense chloritization indicating with the increase in the value of CCPI similar to L12/L13 series. According to Large et al. (2001), with an increased carbonate alteration implied by dolomite as given in Figure 6.3, the samples which consist of chlorite as secondary mineral occurrences introducing high CCPI (>90) values. Hence, these index are commonly more beneficial while identifying the propylitic alteration instead of argillic alteration.

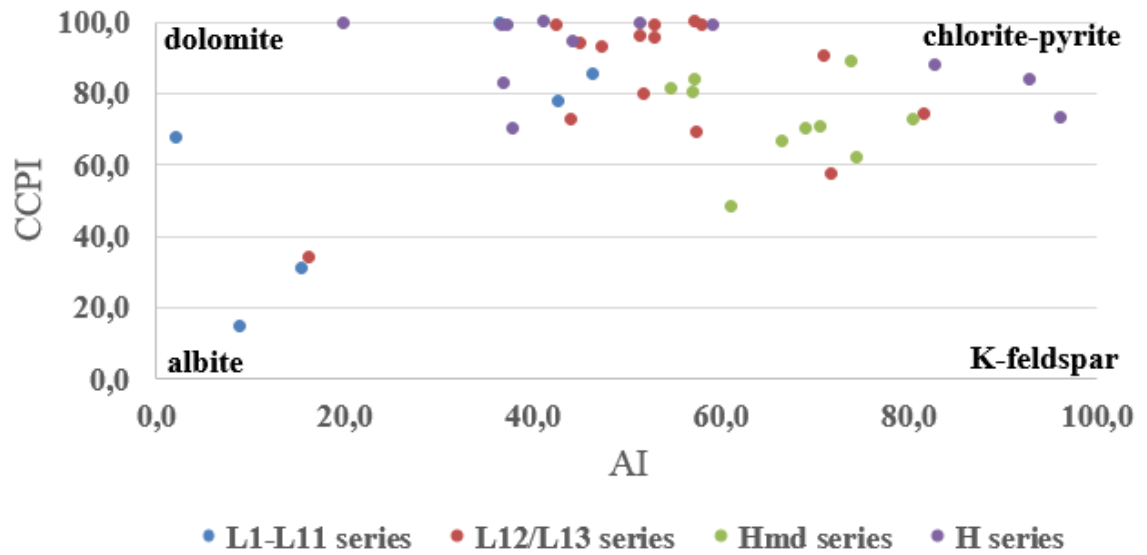


Figure 6.3. CCPI vs AI diagram generated for representing samples to show the intensity of the alterations (modified from Large et al., 2001)

6.4. Fluid Inclusion Analysis:

Fluid inclusions are inclusions in minerals that are filled with fluid (gas and liquid) and sometimes with one or more solid phases. Hydrothermal environments are one of the important areas of the fluid inclusion studies. Fluid inclusions trapped within hydrothermal veins can reveal the nature of mineralizing fluids and the processes by which the mineral deposits were formed (Wilkinson, 2001).

In this study, fluid inclusions were analyzed by using secondary quartz crystals from four different kaolinized rock samples. The fluid inclusions were characterized in terms of three parameters, namely, homogenizing temperature, melting temperature and NaCl equivalent salinity. The studied samples and the obtained results are given below:

Sample L 12-11. Primary and secondary one phase fluid inclusions were observed in translucent crystals. The size of fluid inclusions changes from 2 to 4 μm and they have spherical and ellipsoidal shapes. Two phase (liquid+gas) primary inclusions

were found as trace amounts varying from 4 to 10 μm in size (Ömeroğlu-Sayıt et al., 2018). The homogenization temperatures (T_h °C) of primary two phase (liquid+gas) inclusions vary between 157 and 341° C (Table 6.4) (Ömeroğlu-Sayıt et al., 2018). Moreover, wt. % NaCl values were found by using the mathematical formula used in Bodnar (1993) equilibrium (Table 6.3).

Sample L 12-2. Rarely, translucent quartz crystals were observed. These crystals were found in trace amounts and are being included as primary one phase (gas) inclusions. In very low amounts, one phase (liquid) inclusions were detected. The size of these inclusions varies from 2 to 4 μm (Ömeroğlu-Sayıt et al., 2018). Two phase (liquid+gas) inclusions were identified as trace amounts in the size of 5-6 μm (Ömeroğlu-Sayıt et al. 2018). Homogenization temperatures (T_h °C) acquired from primary two phase (liquid+gas) inclusions are 176°C and 197°C in this sample (Ömeroğlu-Sayıt et al. 2018).

Sample HMD 1-4. Primary and secondary one phase (liquid) inclusions were detected in translucent crystals in the sample Hmd 1-4. Two phase secondary (liquid+gas) inclusions were identified in trace amounts, however, these inclusions were less than 2 μm (Ömeroğlu-Sayıt et al. 2018). Therefore, a result comprising homogenization temperature and salinity measurement could not be reached. In a 3 μm sized one inclusion, it was determined that the homogenization temperature was 351° C (Ömeroğlu-Sayıt et al. 2018).

Sample HMD 1-2. This sample included dull and transparent crystals. There were many one phase (liquid), very rare two phase (liquid+gas) and in trace amounts of one phase (gas) inclusions identified in transparent crystals. The size of two phase (liquid+gas) inclusions were detected as 4-6 μm (Ömeroğlu-Sayıt et al. 2018). Contrarily, one phase (liquid) spherical inclusions were specified as 2-4 μm in size (Ömeroğlu-Sayıt et al. 2018). Additionally, one phase (gas) inclusions were measured as 4 μm in size (Ömeroğlu-Sayıt et al. 2018).

Homogenization temperatures (T_h °C) of primary two phase (liquid+gas) inclusions varied between 126-365°C (Table 6.4) (Ömeroğlu-Sayıt et al. 2018). Mostly, two phase (liquid+gas) primary inclusions were filled with nitrogen to calculate

homogenization temperatures. Thus, wt. % NaCl values were found regarding to the Bodnar (1993) equilibrium (Table 6.4). (Ömeroğlu-Sayıt et al. 2018).

Table 6.4. Homogenization temperature (Th °C) and wt% NaCl (salinity) ranges given for the samples L 12-11,L12-2, Hmd 1-4 and Hmd 1-2 (Ömeroğlu-Sayıt et al. 2018)

Sample No.	Th°C (range)	wt% Salinity
L 12-11	157-341	4.0-6.2
L 12-2	not detected	not detected
Hmd 1-4		
Hmd 1-2	126-365	3.9-6.2

According to Wilkinson (2001), epithermal deposits are primarily occurred resulted from modified, surface-derived fluids identified by low salinity fluids. Thus, homogenization temperatures which varies from <100°C to approximately 300°C implies the epithermal deposits (Wilkinson, 2001). In this study, homogenization temperatures were detected as 126-365°C (Ömeroğlu-Sayıt et al. 2018). The fluid inclusion data obtained during this study was plotted on the temperature –salinity diagram generated by Wilkinson (2001) in which typical ranges for inclusions from different deposit types were illustrated. Thus, the homogenization temperature (Th °C) vs. salinity (wt. % NaCl) values of two kaolinized samples which were L12-11 and Hmd 1-2 matched with the area pointing to the epithermal system in the classification of deposit types (Figure 6.4) (Ömeroğlu-Sayıt et al. 2018).

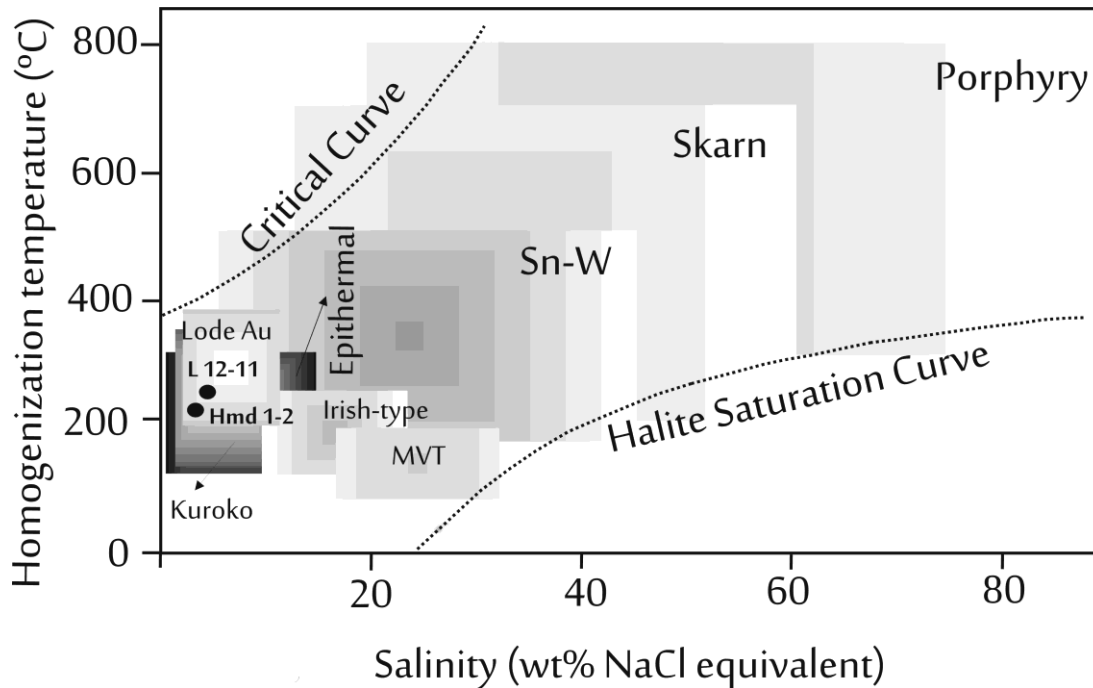


Figure 6.4. Average Th °C and wt. % NaCl values of L 12-11 and Hmd 1-2 are plotted on the homogenizing temperature-salinity diagram (from Wilkinson, 2001) indicating epithermal type of hydrothermal deposits in the study area

6.5. Stable Isotope Geochemistry:

As it was indicated previously in the methodology part, the stable isotope analyses were performed by Cornell Stable Isotope Laboratories. There were 9 rock samples sent to the laboratory which were mainly pure kaolin rock samples (Table 6.5). The reason of conducting the Oxygen/Hydrogen isotope analyses on these kaolin rock samples is to detect the origin of the fluids, whether they were magmatic or meteoric waters, affected these rocks in the study area. Thus, it would be more possible to suggest the type of epithermal system in which Ahırözü kaolin deposits take place; such as low sulphidation or high sulphidation deposits.

Table 6.5. The data derived by Oxygen/Hydrogen stable isotope analyses for 9 kaolin samples acquired from the study area

Sample ID	$\delta^2\text{H}$ vs. VSMOW	$\delta^{18}\text{O}$ vs. VSMOW
L4B	-88.22	5.31
HMD 1-5	-88.81	4.18
HMD 1-4	-86.76	4.96
L-6	-87.65	6.64
HMD-1A	-82.95	5.03
HMD 1-2	-86.77	5.19
HMD 1-1	-87.87	7.51
HMD 2A	-83.70	6.53
L-3	-80.86	8.73
HMD 1-3	-88.05	5.78

According to the isotopic compositions of the rock samples, δD varies between -80.86 and -88.81 whereas $\delta^{18}\text{O}$ values ranges from 5.03 to 8.73. In Figure 6.5, relationship between δD and $\delta^{18}\text{O}$ can be observed. The δD and $\delta^{18}\text{O}$ values forming an area implied as clays and Al-Fe hydroxides represents the climatic conditions in the duration of the time of formations (Faure, 1977). The reason of this sharp difference in the formation is directly related to the isotopic content of the meteoric water due to chemical weathering, as well (Faure, 1977). The δD and $\delta^{18}\text{O}$ values of clay minerals and hydroxides of modern soils directly implies the climatic conditions. For instance, clays occurred in cooler climates have lower δD and $\delta^{18}\text{O}$ values comparing to the clays formed at warmer climates since the isotopic composition of meteoric water is climatically controlled (Faure, 1977; Taylor, 1974).

Moreover, magmatic waters overlap with the isotopic compositions restricted from + 5.5 to 10.0‰ for $\delta^{18}\text{O}$ and -50 to -85 ‰ for δD (Faure, 1977). On the other hand, metamorphic waters are limited for the range of δD from -20 to -65 ‰ whereas it is restricted for the range of $\delta^{18}\text{O}$ beginning from +5 to +25 ‰ (Taylor, 1974).

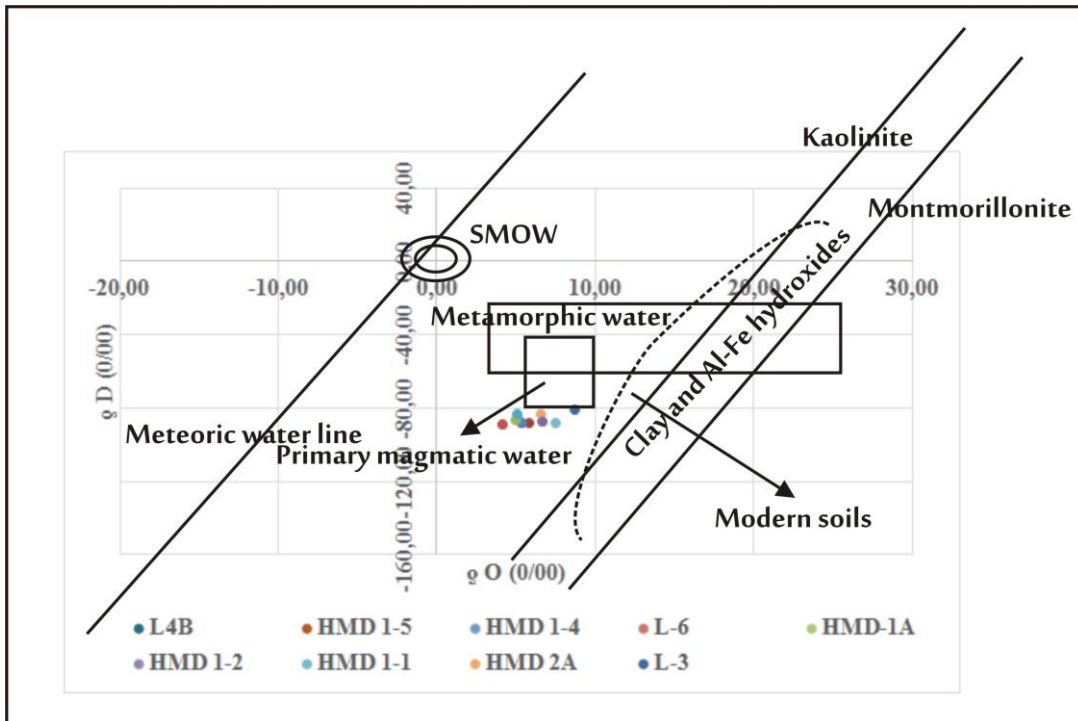


Figure 6.5. Data derived by hydrogen and oxygen stable isotope analyses minerals (after Taylor, 1974)

CHAPTER 7

CO₂–ROCK-WATER INTERACTION: LISTWANITES

AN EXPERIMENTAL STUDY ON SERPENTINE-BASED REACTIONS IN THE STUDY AREA

Listwanite is a secondary rock formation resulted from the carbonization of serpentinitized ultramafic rocks (Ash & Arksey, 1990). In general, in the duration of the formation of listwanites, the primary minerals of the ultramafic or mafic rocks such as; olivine and pyroxene are altered to form serpentine. Afterwards, serpentinites may alter to listwanites. Listwanites do not have to totally consist of carbonate minerals. Rather, they may consist of carbonate veins (Mervine, 2013). These carbonate veins can include magnesite, calcite, dolomite or other carbonate minerals (Matter & Kelemen, 2009). Thus, it was mostly expected to deal with carbonate alteration at the end of each reaction period. Carbonization of an ultramafic serpentinitized rock resulted from the reaction occurred while each Mg and Ca atom combining with CO₂ molecule by forming magnesium and calcite minerals (Mervine, 2013).

7.1. Introduction to the Experimental Procedure:

Ultramafic rock samples (serpentinitized dunite) were acquired from the drill cores at Kavak chromite mine in Eskişehir-Mihalıççık province to study rock-water-CO₂ interactions of listwanites (carbonate-altered serpentinites), experimentally, located at the study area which is Ahırözü, Mihalıççık-Eskişehir, Turkey. In the study area, listwanites were observed mostly within granite-serpentinite contact zone where hydrothermal originated Ahırözü kaolin deposits (Ayının Tepe kaolins and Hamidiye

kaolins) distributed throughout in the study area (Sincan 1978; Ömeroğlu et al. 2013 a, b).

The objective of this experimental research was to discover the alteration processes and mineralogical changes might have occurred while the serpentized ultramafic rocks at the low temperature-low pressure hydrothermal conditions being altered to form listwanites by studying on CO₂-rock-water based reactions in the study area which is Ahırözü, Mihaliççık-Eskişehir. As it was indicated previously in Chapter 1, CO₂-rock-water interaction experiments at low temperature and pressure conditions were performed at the University of Illinois at Chicago, USA under the supervision of Prof. Dr. Steve Guggenheim. These experiments were conducted since I was granted by the scholarship given by TÜBİTAK “The Scientific and Technological Research Council of Turkey” in the scope of the scholarship 2214-A International Research Fellowship Programme in 2014 as a visiting researcher/student intern in USA during the mid period of my PhD studies.

The experiments were mainly aimed to focus on the dissolution of minerals, and then rocks in low-temperature-low pressure aqueous environments (Guggenheim, 2014). Therefore, it was planned to determine and identify any change occurring in the mineral chemistry of the ending product at the end of each reaction period (*run*) by comparing it to the starting material (serpentinite) which was marked as BM 2-1A.

In these experiments, reaction period known as “run” defines the total time that the vessel being rotated in an oven at a stable temperature after it is pressurized with CO₂ gas. In the meanwhile, reaction product describes the run product of a starting material at the end of any reaction period (*run*). Moreover, in order to compare any change occurred in the mineralogy of a rock (starting material) at the end of each run, temperature-pressure-time diagrams were generated.

The CO₂-rock-water interaction experiments were performed with P (CO₂) = 110 to 130 Bar at the temperatures of 25⁰ C and 80⁰ C, by doubling the experimental time periods at each run (Ömeroğlu et al. 2015). On the contrary, it was not planned to do any experiment at higher temperatures than 80⁰C since the purpose of this research was to detect any change observed in the mineralogy of serpentinite without

damaging its chemistry suddenly and, then, to identify the sub-phases occurring in the duration of hydrothermal alteration processes. It was also decided to investigate the reactions taking place at 25⁰ C to reveal the mineral phases arising with respect to the changes formed in pressure and time values at extremely very low temperature conditions. Then, at the end of each run, reaction product (final product) was analyzed by X-ray diffraction (XRD) to determine the newly formed mineral phase.

In the experiments at 80 °C, it was detected that magnesite (MgCO₃) was commonly occurred as the component of the solid final product (Ömeroğlu et al. 2015). However, the co-existing aqueous liquid, upon evaporation, generally included nesquehonite (MgCO₃·3H₂O). On the contrary, in the experiments conducted at 25 °C, it was identified that the solid reaction products comprised nesquehonite instead of magnesite (Ömeroğlu et al. 2015). Starting material used in all experiments performed both at 25 °C and 80 °C temperatures consisted of mostly lizardite mineral, as well.

7.2. Starting Material:

As the starting material, serpentinite rock sample was chosen to study CO₂-water-listwanite (carbonated serpentinite) based reactions took place in the study area. In Figure 7.1, except for Lizardite 1T, there were other minerals suggested by indicating their characteristic peaks might have matched the d-values of the starting material on the given XRD diffractogram; such as Brucite, Pecoraite, Antigorite, Lizardite 1M, Chrysotile and Moissanite-6H-SiC. However, when we compared and tried to match the trend of the XRD diffractogram of our starting material and the strongest peaks of the other suggested minerals, except for Lizardite 1T, there were missing peaks observed not matching the XRD pattern of the starting material (Figure 7.1). Thus, it was identified that the starting material, serpentinitized rock, was composed of mostly Lizardite 1T (Figure 7.1).

7.3. Preparation of the Original Sample for the CO₂-Rock-Water Reactions Experiment:

Onset of the experiment, the starting material (BM 2-1A) which was obtained from the Kavak chromite mine, Mihaliççık, Eskişehir, was crushed and powdered, and then ground to pass 325 to 200 mesh sieves (Figures 7.2.A & 7.2.B). Approximately 2.5 gr to 3.00 gr powdered material of selected rock sample was ground while adding small amount of distilled water on it by using the agate mortar. Thus, after grinding the starting material in the agate mortar, the sample (BM 2-1A) was decided to be x-rayed by using two methods which were backfill and smear (Figures 7.3.A & 7.3.B). The reason of doing this was to compare the results later to reduce the human error.

In smear method, amount of material that you put on the mount was very important since if the material had been plastered on it thicker than it should have been, the X-ray diffraction (XRD) peaks could be shifted which might have afterwards changed the results while determining the mineral content of the original rock sample. By using this method, we plastered few amount of moisturized, and then powdered starting material which was less than 0.5 gr on the x-ray mount and tried to apply the layer of material thinner on the mount by using razors on it.

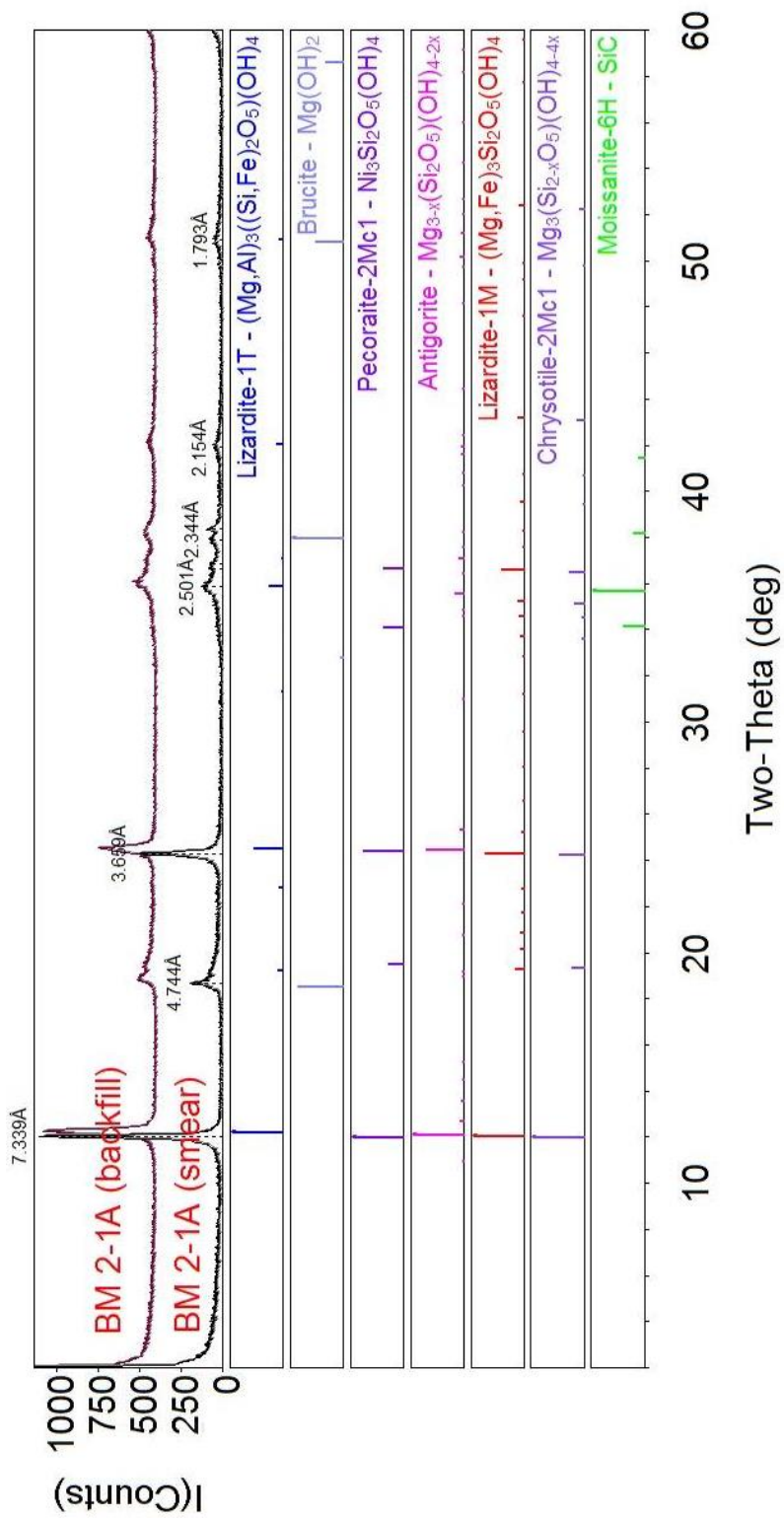


Figure 7.1. XRD pattern of BM 2-1A (starting material) acquired by using both backfill and smear method generated by using JADE software



Figure 7.2. A. Samples are crushed and powdered by using hammer B. Samples ground to pass 325 to 200 mesh sieves

On the other hand, the backfill method is much more accurate if the material is well compressed and flattened. Hence, in the backfill method after the material was ground which was approximately 2.5 gr sample, the starting material had to be dried and then placed into the x-ray mount from the backward direction.

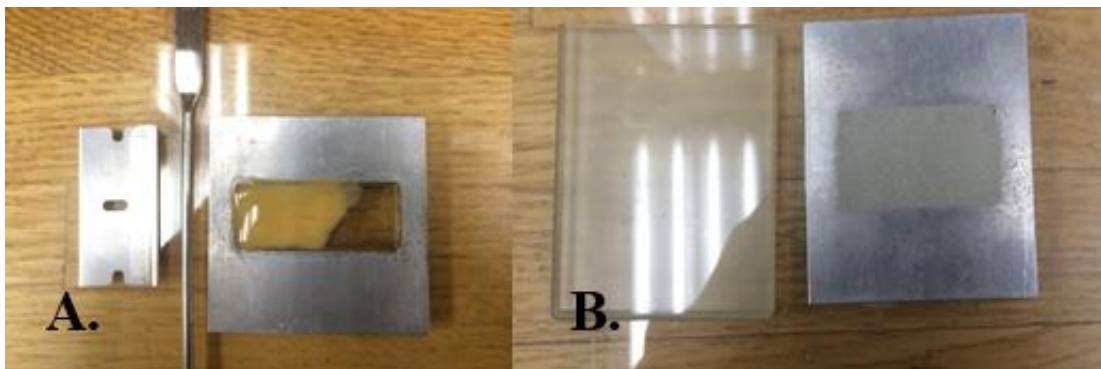


Figure 7.3. A. Powdered sample was grinded B. Front side of the sample flattened by using backfill method to x-ray

7.4. Experimental Procedures:

Lizardite starting material which was previously acquired from drill cores, first crushed and powdered. Then, more than 20 gr of the original sample which was ground to pass 325 to 200 mesh sieves was separated in order to use at the each run of the experiment. However, in each run of the experiment, only 2.5 gr of lizardite starting material was always first weighted and afterwards put into the titanium made vessel with a bore of 2 cm diameter and 20 cm long in total (Figure 7.4). Then, 20 ml water and three 1.3 mm ceramic balls were added into the vessels to prevent the particles being coated with reaction products. The vessels of each experiment were pressurized with CO₂. Then, they were placed in an oven and rotated at one rotation per minute. Experiments were conducted at both 25⁰ C and 80⁰ C with P (CO₂) = 110 to 130 Bar.



Figure 7.4. Titanium made vessel used in the experiments

7.5. Experimental Data:

Experiments were both conducted at 25⁰ C and 80⁰ C with P (CO₂) = 110 to 130 Bar at the different time periods. In these experiments, at both temperatures, the vessels were put into a rotating oven by doubling the time that the previous vessel had completed its reaction cycle.

In the experiment, at each “Run” both while placing in and taking out the vessels from the ovens, the weight of sealed pressurized vessels were noted to compare them to each other to detect if any CO₂ leak occurred at the end of any reaction. The reason of doing this was associated with untightened nut or valve of a vessel might have caused the experiment get failed since the loss of CO₂ might have changed the results at the end of the experiments.

After taking the vessels out from the oven and opening them, first their aqueous liquid content and solid content were separated from each other. In order to do this, the final product was centrifuged at the end of each experiment which were formed due to the reaction conditions in the vessels at 11000 rpm for 5 minutes. Afterwards, we poured the whole aqueous liquid of these products that we obtained at the end of the reaction into a beaker to x-ray it separately, upon evaporation. However, while placing the solid content of the final product, that we had separated from the aqueous liquid content, within the tubes on a quartz glass to let it dry. These solid final reaction materials were also x-rayed after they got totally dried.

Terms describing the data used during the experiments:

Date/hr in: date that the vessel placed in the oven

Date/hr out: date that the vessel taken out from the oven

Temperature: Temperature of the oven that the vessel placed in (in this experiment we have 25⁰ C and 80⁰ C ovens used).

Pressure: Indicating bar unit of CO₂ pressure pumped into the vessels.

Total time in the oven: *The total time in hour and/or day that the mixture in the vessel spent in the oven.*

For each “Run” of the experiments given in the sections of 7.4.1 and 7.4.2 below, the dried solid materials acquired from each final reaction product occurred in the vessels were grinded and powdered in an agate mortar. Then, these products were x-rayed by using smear method. The co-existing aqueous liquid final product was x-rayed, upon evaporation, by using smear method, and evaluated separately, as well.

7.5.1. Experiments Conducted for 80⁰ C:

7.5.1.1. Run 2-2:

Vessel No. 4

Starting material: Lizardite (BM 2-1A)

Date/hr in: Oct 27, 2014/ 2:03 p.m

Date/hr out (date that the vessel taken out from an oven): Oct 28, 2014/ 11:02 a.m

Temperature: 80⁰ C

Pressure: 111.1 Bar

Total time in the oven: 21 hr

At the end of the Run 2-2, when the starting material was compared to the final reaction product, it was observed that magnesite (MgCO₃), which is a carbonate mineral, occurred (Appendix B, Figure B-1). In addition to magnesite, lizardite 1T (Mg₃Si₂O₅(OH)₄) mineral was also acquired as a component of the reaction indicating the entity of the original material in the final product, as well. Except for these, other mineral XRD patterns were suggested if the peaks of the final product material matching with these minerals such as; siderite (FeCO₃) (?), wustite (FeO)

(?), ferropericlase ($\text{Fe}_{0.20}\text{Mg}_{0.80}\text{O}$) (?), chrysotile ($\text{Mg}_3\text{Si}_2\text{O}_5(\text{OH})_4$) (?), moissanite (SiC) (?), antigorite ($\text{Mg}_{3-x}(\text{SiO}_5)(\text{OH})_{4-2x}$) (?) and lizardite 1M ($\text{Mg,Fe}_3\text{Si}_2\text{O}_5(\text{OH})_4$) (?) (Appendix A, Figure A-1). However, different from lizardite 1T and magnesite, further analyses were strongly advised to perform since except for these two minerals, other possible suggested minerals did not introduce the strong matching peaks, as well.

However, the co-existing aqueous liquid content of the final product “Run 2-2” did not give any match with any mineral or chemical component in JADE database.

7.5.1.2. Run 2-3:

Vessel No. 5

Starting material: Lizardite (BM 2-1A)

Date/hr in: Oct 27, 2014/ 2:03 p.m

Date/hr out (date that the vessel taken out from an oven): Oct 28, 2014/ 11:02 a.m

Temperature: 80⁰ C

Pressure: 117.8 Bar

Total time in the oven: 21 hr

As it is given above, this experiment was applied at 80⁰ C for 21 hour with 117.8 bar CO₂ pressure. Different from Run 2-2, in Run 2-3, a new mineral component which was nesquehonite ($\text{MgCO}_3 \cdot 3\text{H}_2\text{O}$) in addition to magnesite (MgCO_3) was detected (Appendix B, Figure B-2). Lizardite 1T ($\text{Mg}_3\text{Si}_2\text{O}_5(\text{OH})_4$) was the other dominant mineral phase found in the reaction product (Appendix A, Figure A-2). Except for these, other mineral XRD patterns were suggested if the peaks of the final product material matching with these minerals such as; ferropericlase ($\text{Fe}_{0.20}\text{Mg}_{0.80}\text{O}$) (?), chrysotile ($\text{Mg}_3\text{Si}_2\text{O}_5(\text{OH})_4$) (?), moissanite (SiC) (?), antigorite ($\text{Mg}_{3-x}(\text{SiO}_5)(\text{OH})_{4-2x}$) (?), periclase (MgO) (?), pecoraite ($\text{Ni}_3\text{Si}_2\text{O}_5(\text{OH})_4$) (?) and lizardite 1M

(Mg,Fe)₃Si₂O₅(OH)₄ (?) (Appendix A, Figure A-2). But as it was indicated in Run 2-2, different from the entities of lizardite 1T, nesquehonite and magnesite minerals, the other minerals given above with a question mark could not be included by the final product since the full matching of the strongest peaks of these minerals were not observed and further analyses, thus was advised to be performed.

The co-existing aqueous liquid, upon evaporation, also consisted of pure nesquehonite in this experiment (Appendix B, Figure B-3).

7.5.1.3. Run 2-4:

Vessel No. 5

Starting material: Lizardite (BM 2-1A)

Date/hr in: Oct 29, 2014/ 2:55 p.m

Date/hr out (date that the vessel taken out from an oven): Oct 31, 2014/ 4.00 p.m

Temperature: 80⁰ C

Pressure: 126.4 Bar

Total time in the oven: ~49 hr

In Run 2-4 which was performed at 80⁰C for approximately 49 hour with 126.4 bar CO₂ pressure, as a newly formed mineral, magnesite (MgCO₃) was detected (Appendix B, Figure B-4). Except for magnesite, lizardite 1T (Mg₃Si₂O₅(OH)₄) was also present (Appendix A, Figure A-4). Except for these, there were other possible mineral phases detected with respect to the XRD pattern of Run 2-4; such as wustite (FeO) (?), ferropericlase (Fe_{0.20}Mg_{0.80}O) (?), chrysotile (Mg₃Si₂O₅(OH)₄) (?), moissanite (SiC) (?), antigorite (Mg_{3-x}(SiO₅)(OH)_{4-2x}) (?), siderite (FeCO₃) (?), pecoraite (Ni₃Si₂O₅(OH)₄) (?) and lizardite 1M (Mg,Fe)₃Si₂O₅(OH)₄ (?) (Appendix A, Figure A-4). However, these suggested minerals given with a question mark indicating a possibility of their presence here, could not be stated that they were

definitely included by the final product in Run 2-4 since the full matching of the strongest XRD peaks of these minerals were not observed and further analyses, thus, was advised to be performed, as well.

In this experiment, in the solid phase of reaction product, no nesquehonite occurrence was detected. On the contrary, in the co-existing aqueous liquid, entity of nesquehonite ($\text{MgCO}_3 \cdot 3\text{H}_2\text{O}$) was identified with respect to x-ray patterns (Appendix B, Figure B-5).

7.5.1.4. Run 2-5 :

Vessel No. 3

Starting material: Lizardite (BM 2-1A)

Date/hr in: Oct 29, 2014/ 2:55 p.m

Date/hr out (date that the vessel taken out from an oven): Nov 3, 2014/ 2:55 p.m

Temperature: 80⁰ C

Pressure: 133 Bar

Total time in the oven: 120 hr

In Run 2-5, experiment was performed with 133 bar CO_2 pressure at 80⁰ C for 120 hour. At the end of the reaction, a new material was observed to form including magnesite (MgCO_3). Lizardite 1T ($(\text{Mg},\text{Al})_3((\text{Si},\text{Fe})_2\text{O}_5)(\text{OH})_4$) was the other mineral phase dominantly found in the reaction product (Appendix B, Figure B-6). Different from these minerals, there were other possible mineral entities could be suggested. Hereby, these minerals were given as chrysotile ($\text{Mg}_3\text{Si}_2\text{O}_5(\text{OH})_4$) (?), moissanite (SiC) (?), antigorite ($\text{Mg}_{3-x}(\text{SiO}_5)(\text{OH})_{4-2x}$) (?), pecoraite ($\text{Ni}_3\text{Si}_2\text{O}_5(\text{OH})_4$) (?) and lizardite 1M ($(\text{Mg},\text{Fe})_3\text{Si}_2\text{O}_5(\text{OH})_4$) (?) (Appendix A, Figure A-6).

Similar to Run 2-3 and 2-4, nesquehonite ($\text{MgCO}_3 \cdot 3\text{H}_2\text{O}$) was also determined in the co-existing aqueous liquid of Run 2-5 (Appendix B, Figure B-7).

7.5.1.5. Run 2-8 :

Vessel No. 6

Starting material: Lizardite (BM 2-1A)

Date/hr in: Oct 31, 2014/ 4:00 p.m

Date/hr out (date that the vessel taken out from an oven): Nov 10, 2014/ 4:00 p.m

Temperature: 80⁰ C

Pressure: 127 Bar

Total time in the oven: 240 hr

Run 2-8 was performed with 127 bar CO₂ pressure at 25⁰ C for 240 hour. In the experiment of Run 2-8, in addition to the entity of lizardite 1T ((Mg,Al)₃((Si,Fe)₂O₅)(OH)₄), magnesite (MgCO₃) was also identified as a newly formed carbonate mineral due to serpentine-CO₂ based reactions (Appendix B, Figure B-8). Different from magnesite and lizardite 1T, as it was indicated before, there could be other possible mineral entities such as; chrysotile (Mg₃Si₂O₅(OH)₄) (?), antigorite (Mg_{3-x}(SiO₅)(OH)_{4-2x}) (?), pecoraite (Ni₃Si₂O₅(OH)₄) (?), lizardite 1M (Mg,Fe)₃Si₂O₅(OH)₄ (?), wustite (FeO) (?) and siderite (FeCO₃) (?) in the reaction product, as well (Appendix A, Figure A-8).

In the co-existing aqueous liquid, upon evaporation, nesquehonite (MgCO₃·3H₂O) as a newly formed mineral was also detected (Appendix B, Figure B-9).

7.5.1.6. Run 2-9:

Vessel No. 6

Starting material: Lizardite (BM 2-1A)

Date/hr in: Nov 11, 2014/ 3:00 p.m

Date/hr out (date that the vessel taken out from an oven): Dec 1, 2014/ 3:00 p.m

Temperature: 80⁰ C

Pressure: 113.7 Bar

Total time in the oven: 480 hr

Run 2-9 put in a reaction at 80⁰ C with 113.7 bar CO₂ pressure for 480 hour. At the end of the experimental period, it was defined that the final product consisted of magnesite as a newly formed carbonate mineral (Appendix B, Figure B-10). Lizardite 1T ((Mg,Al)₃((Si,Fe)₂O₅)(OH)₄) which was comprised by the starting material, still existed after the reaction occurred in the vessel (Appendix B, Figure B-10). However, as a new mineral phase formed for the first time, vermiculite mineral (Mg₃(Si,Al)₄O₁₀(OH)_{2.4}H₂O) was also detected in the reaction product of Run 2-9 (Appendix B, Figure B-10). Except for these minerals, there were other mineral formation possibilities were identified in the following which were chrysotile (Mg₃Si₂O₅(OH)₄) (?), antigorite (Mg_{3-x}(SiO₅)(OH)_{4-2x}) (?), pecoraite (Ni₃Si₂O₅(OH)₄) (?) and lizardite 1M (Mg,Fe)₃Si₂O₅(OH)₄ (?) (Appendix B, Figure B-10).

In the co-existing aqueous liquid, upon evaporation, no peak match found by the JADE software.

7.5.1.7. Run 2-10:

Vessel No. 1

Starting material: Lizardite (BM 2-1A)

Date/hr in: Nov 14, 2014/ 4:00 p.m

Date/hr out (date that the vessel taken out from an oven): Dec 23, 2014/ 3:00 p.m

Temperature: 80⁰ C

Pressure: 129 Bar

Total time in the oven: 960 hr

Run 2-10 was performed based on the reactions with $P(\text{CO}_2) = 129$ bar at 80°C for 960 hour. At the end of the experiment, magnesite mineral (MgCO_3) formed in addition to lizardite 1T ($(\text{Mg,Al})_3((\text{Si,Fe})_2\text{O}_5)(\text{OH})_4$) (Appendix B, Figure B-11).

The co-existing aqueous liquid of this reaction product included nesquehonite ($\text{MgCO}_3 \cdot 3\text{H}_2\text{O}$) (Appendix B, Figure B-12).

7.5.1.8. Run 2-13:

Vessel No. 2

Starting material: Lizardite (BM 2-1A)

Date/hr in: Nov 25, 2014/ 2:20 p.m

Date/hr out (date that the vessel taken out from an oven): Feb 13, 2015/ 2:20 p.m

Temperature: 80°C

Pressure: 121.4 Bar

Total time in the oven: 1920 hr

Run 2-13 was conducted with $P(\text{CO}_2) = 121.4$ bar at 80°C for 1920 hour. At the end of the reaction, magnesite mineral (MgCO_3) was observed in the content of the final product (Appendix B, Figure B-13). Lizardite 1T ($(\text{Mg,Al})_3((\text{Si,Fe})_2\text{O}_5)(\text{OH})_4$) was included by the final product, as well (Appendix B, Figure B-13). Different from these two dominant minerals occurred in the reaction product of Run 2-13, there were other possible mineral phases were suggested as the entities that they could be found in the reaction product which were chrysotile ($\text{Mg}_3\text{Si}_2\text{O}_5(\text{OH})_4$) (?), antigorite ($\text{Mg}_{3-x}(\text{SiO}_5)(\text{OH})_{4-2x}$) (?) and pecoraite ($\text{Ni}_3\text{Si}_2\text{O}_5(\text{OH})_4$) (?) (Appendix B, Figure B-13).

No peak match detected in the co-existing aqueous liquid of this reaction product.

7.5.2. Experiments Conducted For 25⁰ C:

7.5.2.1. Run 3-4:

Vessel No. 3

Starting material: Lizardite (BM 2-1A)

Date/hr in: Nov 7, 2014/ 3:00 p.m

Date/hr out (date that the vessel taken out from an oven): Nov 14, 2014/ 3:00 p.m

Temperature: 25⁰ C

Pressure: 114Bar

Total time in the oven: 168 hr

Run 3-4 was performed at 25⁰ C for 168 hour with 114 bar CO₂ pressure. In Run 3-4, nesquehonite (MgCO₃·3H₂O) formed as a newly occurred carbonate mineral at the end of the reaction (Appendix C, Figure C-1). Except for nesquehonite, lizardite 1T ((Mg,Al)₃((Si,Fe)₂O₅)(OH)₄) was also included (Appendix C, Figure C-1). Except for these two main minerals, as it was indicated before in Run 2 series, there were other minerals might be suggested as the entities found in the final product which were chrysotile (Mg₃Si₂O₅(OH)₄) (?), antigorite (Mg_{3-x}(SiO₅)(OH)_{4-2x}) (?), lizardite 1M (Mg,Fe)₃Si₂O₅(OH)₄ (?), moissanite (SiC) (?) and pecoraite (Ni₃Si₂O₅(OH)₄) (Appendix C, Figure C-1).

In the co-existing aqueous liquid, upon evaporation, the occurrence of nesquehonite was also defined (Appendix C, Figure C-2).

7.5.2.2. Run 3-5:

Vessel No. 12

Starting material: Lizardite (BM 2-1A)

Date/hr in: Nov 7, 2014/ 3:00 p.m

Date/hr out (date that the vessel taken out from an oven): Nov 21, 2014/ 3:00 p.m

Temperature: 25⁰ C

Pressure: 114Bar

Total time in the oven: 336 hr

Run 3-5 was performed with 114 bar CO₂ pressure at 25⁰ C for 336 hour. Run 3-5 comprised two dominant minerals which were nesquehonite and lizardite 1T ((Mg,Al)₃((Si,Fe)₂O₅)(OH)₄) (Appendix C, Figure C-3). In the meanwhile, as it was stated that nesquehonite (MgCO₃·3H₂O) was identified as a newly produced carbonate mineral in this experiment. Different from nesquehonite and lizardite 1T, there were other possible mineral phases could be suggested as the entities found in the reaction product such as; chrysotile (Mg₃Si₂O₅(OH)₄) (?), antigorite (Mg_{3-x}(SiO₅)(OH)_{4-2x}) (?), lizardite 1M (Mg,Fe)₃Si₂O₅(OH)₄ (?) and pecoraite (Ni₃Si₂O₅(OH)₄) (?) (Appendix C, Figure C-3).

In the co-existing aqueous liquid, we also defined the existence of nesquehonite (Appendix C, Figure C-4).

7.5.2.3. Run 3-6:

Vessel No. 7

Starting material: Lizardite (BM 2-1A)

Date/hr in: Nov 7, 2014/ 3:00 p.m

Date/hr out (date that the vessel taken out from an oven): Dec 05, 2014/ 3:00 p.m

Temperature: 25⁰ C

Pressure: 113Bar

Total time in the oven: 672 hr

Run 3-6 was performed at 25⁰ C with 113 bar CO₂ pressure for 672 hour. At the end of the reaction period, lizardite 1T ((Mg,Al)₃((Si,Fe)₂O₅)(OH)₄) was dominantly identified in the solid phase of the reaction product (Appendix C, Figure C-5). Different from lizardite 1T; chrysotile (Mg₃Si₂O₅(OH)₄) (?), antigorite (Mg_{3-x}(SiO₅)(OH)_{4-2x}) (?), lizardite 1M (Mg,Fe)₃Si₂O₅(OH)₄ (?) and pecoraite (Ni₃Si₂O₅(OH)₄) (?) were identified as the other possible mineral phases included by the reaction product, as well (Appendix C, Figure C-5).

In the co-existing aqueous liquid product of Run 3-6, nesquehonite was detected in addition to the weak peaks implying the entity of silicon oxide (SiO₂) inside of it (Appendix C, Figure C-6).

7.5.2.4. Run 3-8:

Vessel No. 8

Starting material: Lizardite (BM 2-1A)

Date/hr in: Nov 25, 2014/ 2:20 p.m

Date/hr out (date that the vessel taken out from an oven): Jan 20, 2015/ 2:20 p.m

Temperature: 25⁰ C

Pressure: 121.7Bar

Total time in the oven: 1344 hr

In this experiment, Run 3-8 was performed at 25⁰ C with P(CO₂) = 121.7 bar for 672 hour. At the end of this reaction, lizardite 1T ((Mg,Al)₃((Si,Fe)₂O₅)(OH)₄) was detected in the solid phase of the final product (Appendix B, Figure B-7). Except for lizardite 1T; chrysotile (Mg₃Si₂O₅(OH)₄) (?), antigorite (Mg_{3-x}(SiO₅)(OH)_{4-2x}) (?), lizardite 1M (Mg,Fe)₃Si₂O₅(OH)₄ (?) and pecoraite (Ni₃Si₂O₅(OH)₄) (?) were determined as the other possible mineral phases included by the reaction product (Appendix C, Figure C-7).

In the co-existing aqueous liquid, upon evaporation, nesquehonite (MgCO₃·3H₂O) was observed in addition to the weak entity of silicon oxide (SiO₂) (Appendix C, Figure C-8).

7.6. Research Results:

In this part, tables (Tables 7.1 & 7.2) and diagrams (Figures 7.5 & 7.6) were generated to demonstrate the change occurred in the mineral chemistry in the rock sample BM 2-1 regarding to pressure-time and temperature values.

Hereby, comparison diagrams were generated by using xrd patterns of final products for each run to observe the mineralogical changes occurred both at 80⁰C and 25⁰C in the solid reaction product at the end of each run (Figures 7.7 & 7.8). Hence, at 80⁰C except for Run 2-3, no nesquehonite mineral peak was detected in the reaction products, however magnesite formation was very common in addition to lizardite 1T (Figure 7.7). In the experiments performed at 25⁰C, in Run 3-4 and Run 3-5, nesquehonite and lizardite 1T was formed whereas there was only lizardite 1T entities were observed at Run 3-6 and Run 3-8 (Figure 7.8).

Table 7.1. The table showing the data derived at 80⁰ C

Run No.	Vessel No.	Pressure (Bar)	Temperature (°C)	Time (hour)	day	date that the vessel put into the oven	date that the vessel taken out from the oven
2-2	4	111.1	80	21	app. 1 day	10/27/14	10/28/14
2-3	5	117.8	80	21	app. 1 day	10/27/14	10/28/14
2-4	5	126.4	80	49	app. 2 days	10/29/14	10/31/14
2-5	3	133	80	120	5 days	10/29/14	11/03/14
2-8	6	127	80	240	10 days	10/31/14	11/10/14
2-9	6	113.7	80	480	20 days	11/11/14	12/01/14
2-10	1	129	80	960	40 days	11/14/14	12/24/14
2-13	2	121.4	80	1920	80 days	11/25/14	02/13/14

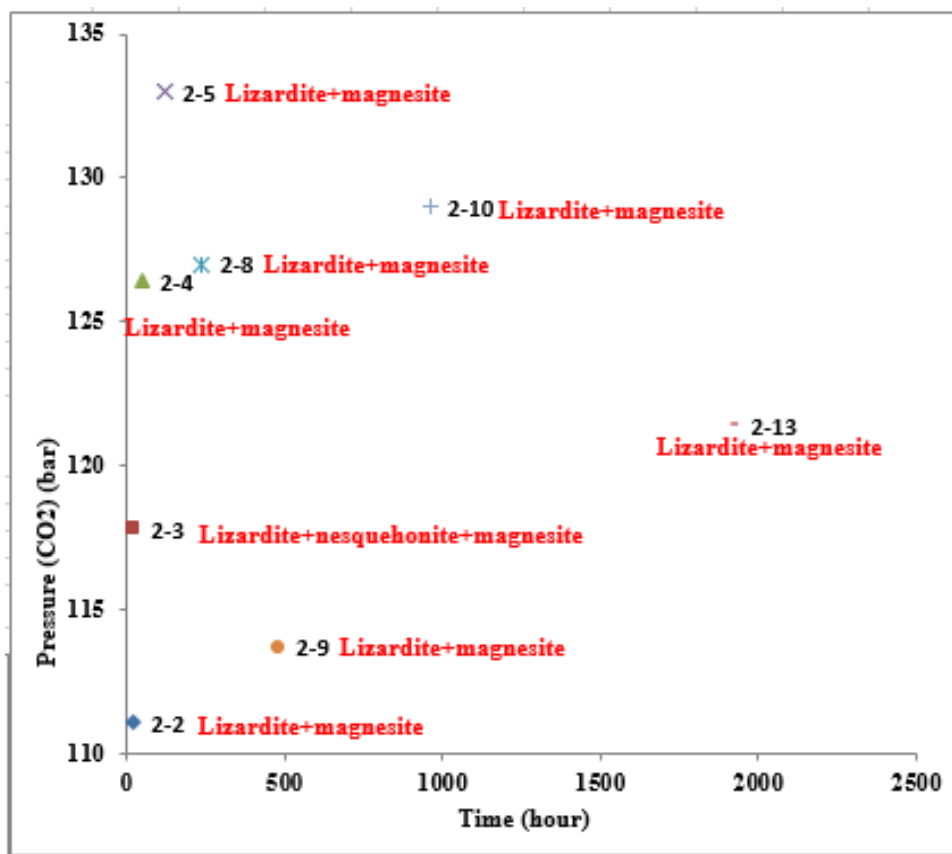


Figure 7.5. Pressure vs. time diagram show the changes observed at 80⁰ C. The minerals showed in red colour are the ones formed after the reaction

Table 7.2. The table showing the data derived at 25⁰ C

Run No.	Vessel No.	Pressure (Bar)	Temperature (°C)	Time (hour)	day	date that the vessel put into the oven	date that the vessel taken out from the oven
3-4	3	114	25	168	7 days	11/07/14	11/14/14
3-5	12	114	25	336	14 days	11/07/14	11/21/14
3-6	7	113	25	672	28 days	11/07/14	12/05/14
3-8	8	121.7	25	1344	56 days	11/25/14	01/20/14

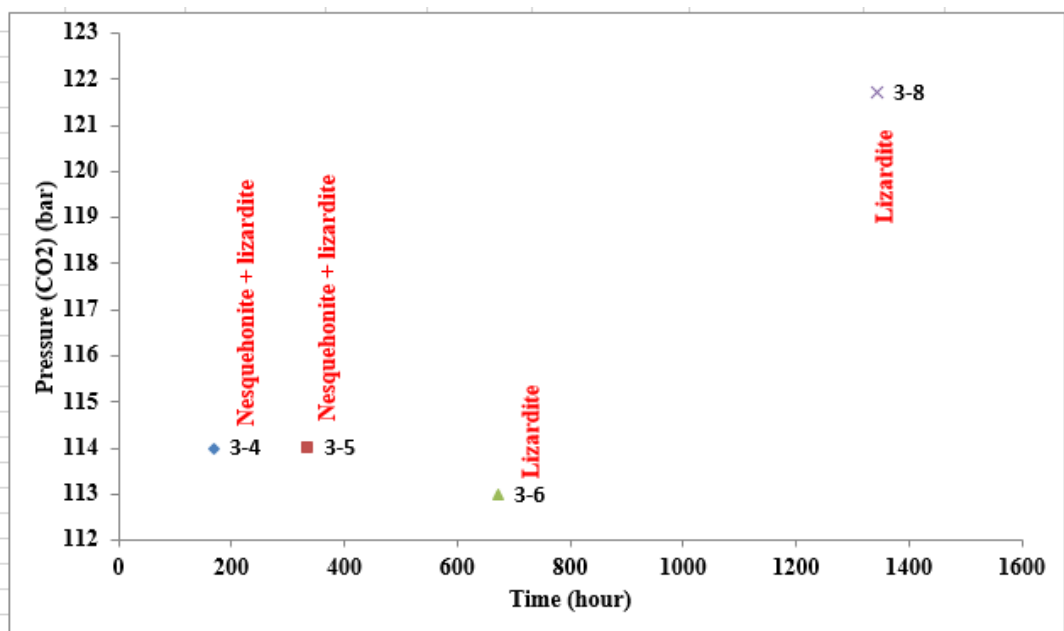


Figure 7.6. Pressure vs. time diagram used to plot each run for 25⁰ C by showing the components of final products. The minerals showed in red colour are the ones formed after the reaction

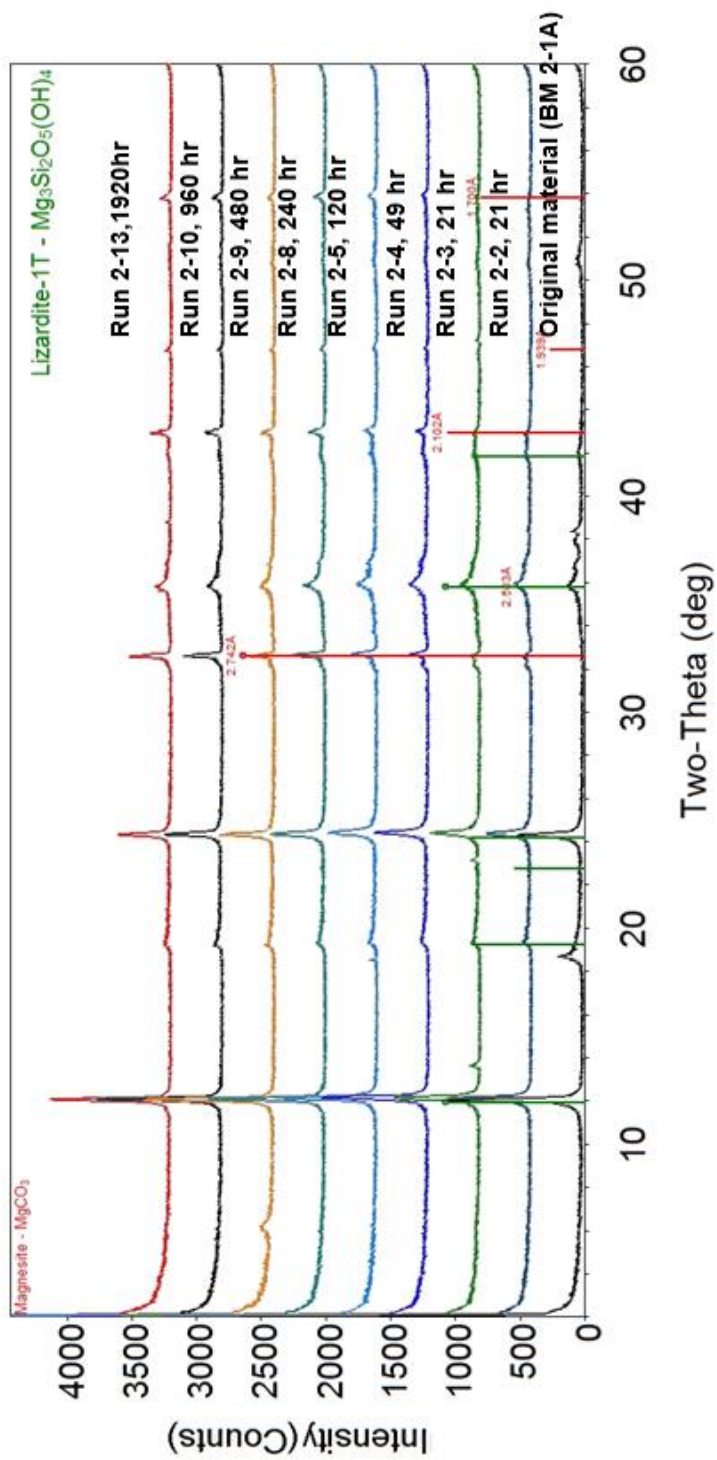


Figure 7.7. Comparison diagrams showing the existence of nesquehonite only in Run 2-3 in the solid phases of reaction products

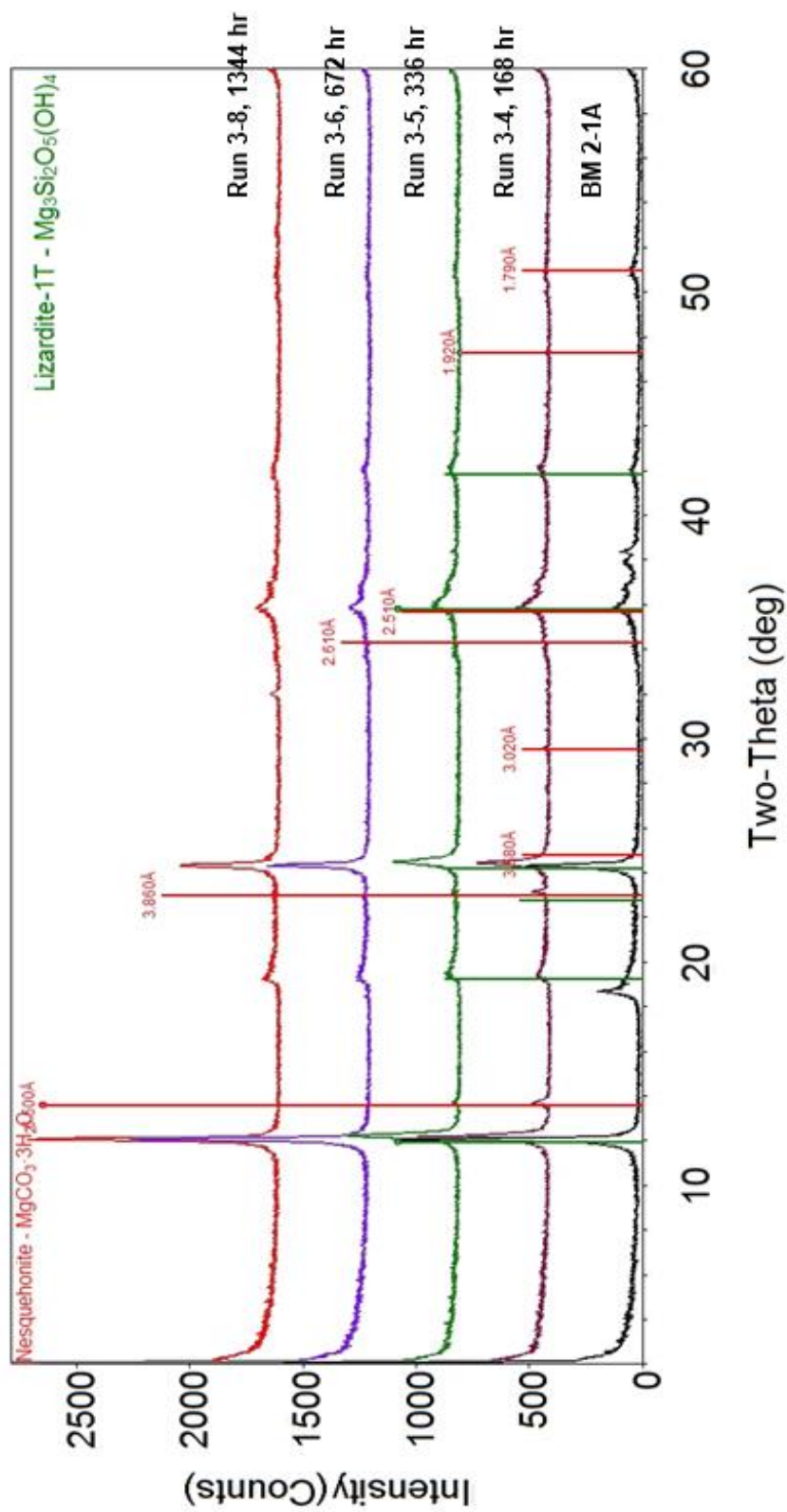


Figure 7.8. Nesquehonite formation took place in Run 3-4 and Run 3-5 is given by comparing each final product with each other at 25^o C

CHAPTER 8

DISCUSSIONS

8.1. Studies on Hydrothermal Alteration and Zoning:

Kaolin deposits are widespread in Turkey. However, they have variable geological characteristic associated with their different geological settings. Most of the Turkish kaolin deposits originated by hydrothermal alteration of andesitic, dacitic rocks and tuffs along the fault zones related with the extensional-compressional tectonic regimes as seen mainly in the Western Anatolia. On the other hand, as in the case of the studied Ahırözü kaolins and the few other locations, hydrothermal alteration occurred along the fault zones where Late Triassic granitic intrusions have fault contacts with the tectonically obducted serpentinite-matrix melange (Şengüler, 2011). In general, the Turkish kaolin deposits exhibit mineralogical and chemical characteristics indicating both supergene and hypogene alteration in an epithermal system.

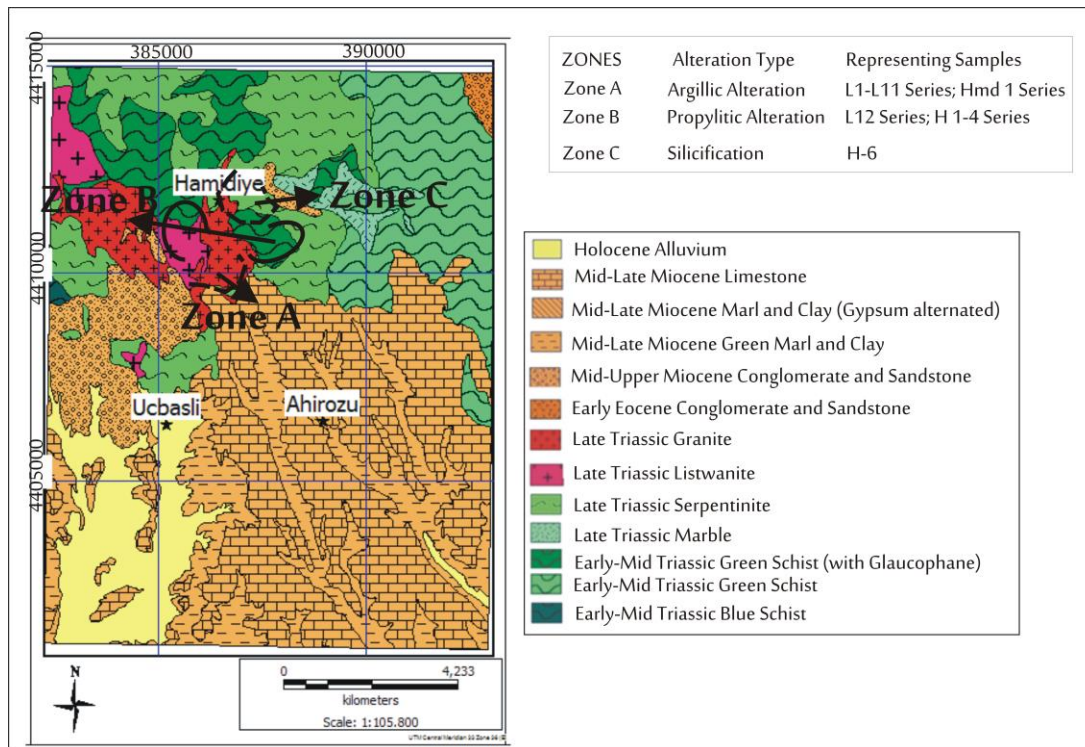


Figure 8.1. Zone map of study area (after Gözler, 1987; Ömeroğlu-Sayit et al., 2018)

Based on the field observations, mineralogical and petrographical investigations which revealed textural characteristics, primary and secondary mineral phases and the occurrence of three lateral alteration mineral zonations (Zone A, B and C) are studied in the area of interest (Figure 8.1):

Zone A is an argillic zone comprising intense argillization (mainly kaolin minerals), pyrite and natroalunite occurrences. The presence of K-feldspar showing the graphic texture indicates that the protolith rock has a granitic origin.

Moreover, the kaolin minerals indicated in Zone A were also detected as kaolinite and halloysite minerals by means of SEM-EDX analyses. Both their morphology and chemical composition were analyzed by using this method. Thus, tubular crystals implied the entity of halloysite mineral whereas stacking structures served an important function as a morphological feature while identifying kaolinite minerals.

Dawsonite mineral found in argillic zone (Zone A) implies the feldspar enriched igneous rock and formed resulted from hydrothermal activities throughout the veins and fractures of the kaolinized altered rocks (Palache et al. 1951b).

In the outward direction, **Zone B** is a propylitic zone, characterized mainly by chloritization associated with carbonatization represented by dolomite. The main alteration products are chlorite-smectite-illite-and epidote in propylitic zone. Stockwork structures with thin quartz veins are common in this zone which were formed in green-schist units.

The rocks in **Zone C** were dominantly silicified and may represent the siliceous sinter formation in the study area.

Occurrence of hematite, both in Zone A and Zone B, detected based on XRD analyses is directly related to the presence of pyrite and magnetite minerals in the samples primarily. Oxidation of pyrite and magnetite minerals resulted in hematite throughout the veins in the rock samples. Hematite is very common accessory mineral observed in igneous rocks formed as a weathering product (Deer et al. 1962). Hematite is a mineral which is very common in hydrothermal systems (Deer et al. 1962).

Goethite represents the occurrences above the vadose zone indicating the low temperature dominated in the study area (Harrison et al. 1975). Goethite is both very common in both argillic and propylitic zones.

8.2. Textural and Mineralogical Aspects in the Interpretation of the Style of Epithermal Systems:

In propylitic alteration zone (Zone B), secondary carbonate minerals formed by replacement throughout the veins were very common. Stockwork structures in the samples were also detected in Zone B. Throughout the stockwork structures, vein filling carbonate and hematite occurrences were identified which is more common in low sulphidation systems (Arribas, 1995; Sillitoe & Hedenquist, 2003; White &

Hedenquist, 1995). However, stockwork structures can be determined in both low sulphidation and high sulphidation systems, as well as not a particular texture to be used while identifying the type of an epithermal system (White and Hedenquist, 1995). Thus, vein-filling carbonate occurrences could be suggested as very important textural feature while identifying the type of deposit instead of stockwork structures which should be taken into consideration. There were natroalunite minerals which were described as sulphate bearing minerals, is an alunite group mineral which is rare in nature (Palache et al. 1951a). According to Arribas, (1995), White & Hedenquist, (1995) and Sillitoe & Hedenquist, (2003), there are hypogene and supergene originated alunites found in epithermal deposits. However, magmatic hydrothermal alunite occurs associated with minerals; such as diaspore, pyrophyllite, kaolinite, dickite, and zunyiteas (Meyer and Hemley 1967). Pyrophyllite was not observed in any of our samples in XRD analyses. Thus, the detected natroalunite in our samples was suggested to be occurred due to supergene conditions. Crustified amorphous quartz occurrences were observed in the samples acquired from Zone B. Generally, carbonate material was observed to surround the crustified silicate material by replacing the primary mineral indicating the low sulphidation supergene alteration (Arribas, 1995; Sillitoe & Hedenquist, 2003; White & Hedenquist, 1995). On the other hand, dickite which is a key alteration mineral in high sulphidation systems (Arribas, 1995; Sillitoe & Hedenquist, 2003; White & Hedenquist, 1995) can not be observed in any of the samples in SEM-EDX analyses while studying the types of kaolin minerals. On the contrary, adularia is a common minerals implying the entity of low sulphidation system (White & Hedenquist, 1995). However, adularia mineral could not be detected in any of the samples acquired from the study area.

The entity of psilomelane in the rock samples can be associated with the presence of pyrolusite or barite minerals which is common in both low sulphidation deposits and high sulphidation deposits (White & Hedenquist, 1995).

8.3. Wall Rock Alteration and Listwanite Occurrences:

AI and CCPI have been proved to be particularly beneficial in mineral exploration by providing a quantitative estimate of the intensity of footwall alteration related to massive sulfide deposits, increasing to maximum values in the hydrothermal vent zone below the massive sulfide ore lenses (Saeki & Date, 1980). However, both CCPI and AI can be very useful while studying intense carbonate and chlorite alteration also observed in epithermal deposits.

The broad pattern of sodium depletion that accompanies the AI increase is very significant since the data displayed a variation from the albite-plagioclase end of the diagram to the chlorite alteration, with an increasing AI and decreasing Na₂O (Large et al. 2001) (Figure 6.3). In Figure 6.3, it is obvious that an increasing AI is also accompanied by increasing K₂O (K-Feldspar indicator) (Large et al. 2001) (Figure 6.3). Moreover, according to Large et al. (2001), detecting chlorite alteration by using CCPI, it has to be considered that the index is also affected positively by Mg-Fe carbonate alteration (dolomite, ankerite, or siderite) in addition to pyrite, magnetite, or hematite enrichments in the system. Because all three of the hydrothermal minerals—Fe-Mg chlorite, Fe-Mg carbonate, and pyrite—are typically developed in the inner alteration zones. However, this index could not be efficiently used while studying the kaolinized rock samples (Hmd-series & L-1 to L-11 series) representing the argillic zone comparing the rock samples reflecting the propylitic zone (H-series and L-12/L-13 series). These indicated rock samples exposed to propylitic alteration were dominantly distributed nearby the chlorite end of the diagram.

Listwanites are situated throughout the contact between granite and serpentinite in the study area and this rock unit was identified as an alteration product as result of the interaction of CO₂-H₂O-serpentinite. Two groups of experiments were conducted to investigate the mineralogical and chemical changes occurred in serpentinite while altering to form listwanites. Listwanites are carbonate altered serpentinites. Therefore, in these experiments, to detect the formation of carbonate minerals served

an important function. From the beginning of the experiment, it was aimed to deal with carbonate altered components identified within each final product. In the experiments performed at 80⁰ C, we ensured the entity of the occurrence of two carbonate group minerals which were nesquehonite and magnesite. Magnesite was, generally, identified in the solid phase of the reaction product whereas nesquehonite produced, upon evaporation, in the co-existing aqueous liquid. Meanwhile, in the experiments conducted at 25⁰ C, only nesquehonite was acquired as a newly formed mineral phase. Magnesite was determined much more abundant component rather than nesquehonite in the solid phase of the experiments performed at 80⁰ C. The reason of this transformation was that nesquehonite tends to dehydrate at the longer time periods and higher pressures by forming magnesite. Nesquehonite is a mineral occurring at extremely low P (CO₂) conditions.

8.4. Origin of the Hydrothermal Fluids:

Homogenization temperatures (Th⁰C) represent the minimum temperature of entrapment of a fluid in a mineral (Yang, 2016). According to the fluid inclusion experimental data, it was obtained that the values varied between 126⁰C and 365⁰C (Ömeroğlu-Sayıt et al. 2018). In the meanwhile, wt. % NaCl varied between 3.9- 6.2 % (Ömeroğlu-Sayıt et al. 2018). Hence, it can be directly discussed that these are the results obtained stating that the Ahırözü kaolin deposits have an epithermal hydrothermal origin regarding to the homogenization temperature versus salinity diagram (Wilkinson, 2001). On the other hand, the results obtained from the stable isotope analyses (oxygen/hydrogen) implied that there was an influence of magmatic waters, which are controlled by the magmas on the alteration of kaolinized rocks. (Faure, 1977). As it was indicated in Chapter 6, the isotopic compositions derived from the kaolinized rock samples collected from the study area, δD varies between - 80.86 and -88.81 whereas δ¹⁸O values ranges from 5.03 to 8.73. Since it is known that volcanic and plutonic rocks have uniform δD and δ¹⁸O values, the magmatic waters introduce isotopic compositions varying from +5.5 to +10 ‰ for δ¹⁸O

whereas ranging over -50 to -85 ‰ for δD comprising the values that we obtained as a result of stable isotope analyses (Taylor, 1974). However, there was no sample detected comprised by magma box, itself (Figure 6.5).

The geochemical imprints of the Ahırözü kaolin deposits in the Mihaliççık-Eskişehir area indicate that these kaolin deposits were formed due to hydrothermal alteration of granitic intrusives emplaced in a volcanic arc related tectonic setting (Pearce et al. 1984). Generally, according to the trace element analyses, the kaolin rock samples were depleted in Rb and Pb while being enriched by Cs and U elements (Ömeroğlu-Sayıt et al. 2018). These enrichments and depletions detected in the chemical component of the kaolinized rock samples may be either related to the parent rock, or the abundances of the large ion lithophile (LILE) elements in major silicate minerals such as feldspar and mica, are mobile in the duration of hydrothermal alteration (Ömeroğlu-Sayıt et al. 2018).

CHAPTER 9

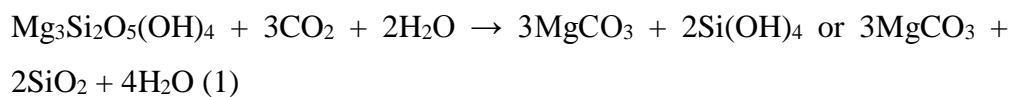
CONCLUSIONS AND RECOMMENDATIONS

Conclusions reached in this study in order to answer the questions arised in the introduction are:

1. Kaolin deposits are widespread in Turkey. However, they have variable geological characteristic associated with their different geological settings. Most of the Turkish kaolin deposits originated by hydrothermal alteration of andesitic, dacitic rocks and tuffs along the fault zones related with the extensional-compressional tectonic regimes as seen mainly in the Western Anatolia. On the other hand, as in the case of the studied Ahırözü kaolins and the few other locations, hydrothermal alteration occurred along the fault zones where Mesozoic granitic intrusions have fault contacts with the tectonically obducted Mesozoic serpentinite-matrix melange. In general, the Turkish kaolin deposits exhibit mineralogical and chemical characteristics indicating both supergene and hypogene alteration in an epithermal system.
2. According to the mineralogical and petrographical analyses it has been detected that the kaolin rock samples were originated from granitic/felsic igneous rocks since they preserve K-feldspar and primary quartz minerals in their content in addition to graphic texture that they still preserved.
3. Based on the field observations, mineralogical and petrographical investigations which revealed textural characteristics, primary and secondary mineral phases and the occurrence of three lateral alteration mineral zonations (Zone A, B and C) are studied in the area of interest. Zone A is an argillic zone comprising intense silicification, argillization (mainly kaolin group clay minerals, and smectite in lesser amounts), pyrite, hematite and natroalunite formation. The presence of K-feldspar with graphic texture

shows that the protolith rock has a granitic composition. In the outward direction, Zone B- is a propylitic zone, characterized mainly by chloritization associated with carbonatization represented by dolomite. The main alteration products are chlorite-smectite-illite-and epidote in propylitic zone. Stockwork structures with thin quartz veins are common in this zone which were formed in green-schist units. The rocks in Zone C were dominantly silicified and represent sinter formation in the study area.

4. Regarding to the mineralogical and petrographical studies, it was determined that the rocks representing propylitic alteration were generated from metamorphic or mafic/ultramafic rocks in the study area. These results were reached depending on the entities of primary minerals found in the rock content and relict textural features. The reason of metamorphic and mafic/ultramafic rocks, found in the study area, dominantly altered to chlorite due to the entity of primary Mg-Fe rich minerals (e.g. amphiboles and biotite) interacting with hydrothermal fluids throughout the fault fractures.
5. AI and CCPI index were both used while verifying the samples exposed to chloritization regarding to mathematical formulas and numeric data. Also, according to the index, it has been also proved that the samples reflecting the mineralogical properties of propylitic alteration consist of carbonate minerals; such as dolomite in addition to chlorite. These carbonate minerals were mainly detected throughout the veins.
6. Except for the three zones identified in the study area, listwanites were also detected as the alteration product in the study area within the contact of granite-serpentinite rocks. These rocks were altered from serpentinized ultramafic rocks. Based on the findings in the dissolution studies of the samples, briefly, it was concluded that aqueous carbonation of serpentine was occurred as in the following reaction equilibrium (Park & Fan, 2004):



Serpentine+3CO₂+2H₂O → Magnesite+2Si(OH)₄ or Magnesite + *amorphous silica* (2)

7. Homogenization temperatures (Th⁰C) vary between 126⁰C and 365⁰C according to the fluid inclusion analyses. Moreover, wt. % NaCl range between 3.9- 6.2 %. These results indicate that the Ahırözü kaolin deposits have an epithermal hydrothermal origin based on the homogenization temperature versus salinity diagram (Wilkinson, 2001).
8. The mineralogical and geochemical investigations of the Ahırözü kaolin deposits in the Mihaliççık-Eskişehir area demonstrate that they are the products of hydrothermal alteration of granitic intrusives emplaced in a volcanic arc related tectonic setting. The kaolin samples are characterized by depleted Rb and Pb in contrast to the enriched Cs and U elements. These variations may either be inherited from the parent rock, or probably the abundances of the trace elements, especially large ion lithophile (LILE) elements in major silicate minerals such as feldspar and mica, are mobile during hydrothermal alteration.
9. In order to detect whether the system is high sulphidation or low sulphidation deposits in the study area, stable isotope analyses (oxygen/hydrogen) were also carried out. As a result of these analyses the rock samples matched with the area indicating the fluids having magmatic origin, which is suggested as high sulphidation system, interacted with the rocks in the study area. But these plotted samples were not directly comprised by the magmatic box, either. Contrarily, the lack of pyrophyllite minerals (Hedenquist *et al.* 2000) and the presence of crustified amorphous silicate in addition to carbonate vein filling identified in the thin-sections may also imply the low sulphidation system in the study area. The entity of goethite states over steam heated alteration implying the interaction of fluids and rocks at low temperature since it forms over vadose zone, as well. Hence, considering that both mineralogical, textural and stable isotope data, it can be suggested that Ahırözü kaolin deposit has been interacted by both supergene and hypogene alteration processes.

10. In future studies, it is advised to study on the relationship between metal-mineralization and listwanized rocks which were not investigated regarding to economic geology, as well, in the scope of this study. Instead, listwanites were studied to understand the mineralogical changes occurred while carbonate altered ultramafic rocks forming listwanized rock units in hydrothermal fields.

REFERENCES

- Abdioğlu E., Arslan M., Kadir S., Temizel İ., (2015), Alteration mineralogy, lithochemistry and stable isotope geochemistry of the Murgul (Artvin, NE Turkey) volcanic hosted massive sulfide deposit: Implications for the alteration age and ore forming fluids, *Ore Geology Reviews*, 66, 219-242.
- Akaryalı E., (2016), Geochemical, fluid inclusion and isotopic (O, H and S) constraints on the origin of Pb–Zn ± Au vein-type mineralizations in the Eastern Pontides Orogenic Belt (NE Turkey), *Ore Geology Reviews*, 74, 1-14.
- Altner D., Koçyiğit A., Farnacci A., Nicosia U., Conti M. A., (1991), Jurassic, Lower Cretaceous stratigraphy and paleogeographic evolution of the southern part of northwestern Anatolia, *Geologica Romana*, 28, 13-80.
- Arribas A. Jr., (1995), Characteristics of high-sulfidation epithermal deposits, and their relation to magmatic fluid. *In* Magmas, Fluids and Ore Deposits. (J.F.H. Thompson, ed.) *Mineralogical Association of Canada Short Course*, 23, 419-454.
- Ash C. H. & Arksey R. L., (1990), The listwanite - lode gold association in british columbia. Geological Fieldwork 1989, Paper 1990, *British Columbia Geological Survey Branch*, 359-364.
- Baioumy H., (2013), Hydrogen and oxygen isotopic compositions of sedimentary kaolin deposits, Egypt: Paleoclimatic implications. *Applied Geochemistry*, 29, 182-188.
- Bethke P. M., (1984), Controls on base and precious metal mineralization in deeper epithermal environments. U.S. Geol. Surv. Open-file Report 84-890.
- Bodnar R.J., (1993), Revised equation and table for determining the freezing point depression of H₂O-NaCl solutions. *Geochimica et Cosmochimica Acta.*, 57, 683-684.

- Bohlke J. K., (1989), Comparison of metasomatic reactions 311-322. wall rocks: Intensive variables, mass transfers., and between a common CO₂-rich vein fluid and diverse Au mineralization at Alleghany, California; *Economic Geology*, 84, 291-327.
- Boskabadi A., Pitcairn I. K., Broman C., Boyce A., Teagle D. A. H., Cooper M. J., Azer M. K., Stern R. J., Mohamed F. H., Majka J., (2016), Carbonate alteration of ophiolitic rocks in the Arabian–Nubian Shield of Egypt: sources and compositions of the carbonating fluid and implications for the formation of Au deposits, *International Geology Review*, 59, 391-419.
- Chen P-Y., Lin M-L., Zheng Z., (1997), On the origin of the name kaolin and the kaolin deposits of the Kauling and Dazhou areas, Kiangsi, China. *Applied Clay Science*, 12, 1-25.
- Chitale D. V. & Guven N., (1987), Natroalunite in a lateritic profile over Deccan Trap basalts at Matanumad, Kutch, India. *Clays and Clay Minerals*, 35, 196–202.
- Corazza E., C. Sabelli, and Vannucci S., (1977), Dawsonite: new mineralogical data and structure refinement. *Neues Jahrbuch für Mineralogie, Monatsh.*, 381–397.
- Cravero F., Gonzalez I., Galan E., Dominguez E., (1997), Geology, mineralogy, origin and possible applications of some Argentinian kaolins in the Neuquen basin. *Applied Clay Science*, 12, 27-42.
- Deer W. A., Howie R. A., Zussman J., (1962) Rock-forming minerals, v. 5, non-silicates, Geological Society, 21–27.
- Delaloye M. & Bingöl E., (2000), Granitoids from western and northwestern Anatolia: Geochemistry and modelling of geodynamic evolution, *International Geology Review* 42, 241-268.

- Dill H. G., Dohrmann R., Kaufhold S., Çiçek G., (2015), Mineralogical, chemical and micromorphological studies of the argillic alteration zone of the epithermal gold deposit Ovacik, Western Turkey: Tools for applied and genetic economic geology. *Journal of Geochemical Exploration*, 148, 105-127.
- Dill H. G., Kus J., Dohrmann R., Tsoy Y., (2008), Supergene and hypogene alteration in the dual-use kaolin-bearing coal deposit Angren, SE Uzbekistan. *International Journal of Coal Geology*, 75, 225-240.
- dos Santos A. E. A. Jr. & Rossetti D. F., (2008), Origin of the Rio Capim Kaolin based on optical (petrographic and SEM) data, *Journal of South American Earth Sciences*, 26, 328-9-341.
- dos Santos A. E. A. Jr., Rossetti D. F., Murray, H., (2007), Origins of the Rio Capim kaolinites (northern Brazil) revealed by $\delta^{18}\text{O}$ and δD analyses, *Applied Clay Science*, 37, 281-294.
- Ece Ö., İ., Ekinçi B., Schroeder P., A., Crowe, D., Esenli, F., (2013), Origin of the Düvertepe kaolin-alunite deposits in Simav Graben, Turkey: timing and styles of hydrothermal mineralization. *Journal of Volcanology and Geothermal Research*, 255, 57–78.
- Ece Ö.I & Schroeder P.A. (2007), Clay mineralogy and chemistry of halloysite and alunite desposits in the Turplu area, Balıkesir, Turkey, *Clays and Clay Minerals*, 55, 18–35.
- Ece Ö. I., Schroeder P. A., Smilley M. J., Wampler J.M. (2008), Acid-sulphate hydrothermal alteration of andesitic tuffs and genesis of halloysite and alunite deposits in the Biga Peninsula, Turkey, *Clay Minerals*, 43, 281–315.
- Ekosse G., (2000), The Makoro kaolin deposit, southeastern Botswana: its genesis and possible industrial applications, *Applied Clay Science*, 16, 301-320.
- Faure G., (1977), Principles of Isotope Geology, *John Wiley & Sons, Inc.*

- Fernandez-Caliani J. C., Galan E., Aparicio P., Miras A., Marquez M. G., (2010), Origin and geochemical evolution of the Nuevo Montecastelo kaolin deposit (Galicia, NW Spain), *Applied Clay Science*, 49, 91-97.
- Fuji, N., Kayabalı İ., Saka A. H., (1995), Data book of ceramic raw materials of selected areas in Turkey. General Directorate of Mineral Research and Exploration (MTA) Turkey, Monograph Series 1, 144.
- Giggenbach W. F., (1992), Magma degassing and mineral deposition in hydrothermal systems along convergent plate boundaries. *Economic Geology*, 87, 1927-1944.
- Goldbery R. & Loughnan F. C., (1970), Dawsonite and nordstrandite in the Permian Berry Formation of the Sydney Basin, New South Wales. *American Mineralogist*, 55, 477-490.
- Gözler Z., (1987), Ankara İ27 Paftasının Jeoloji Haritası, MTA-Ankara.
- Guggenheim S., (2014), Mineral and Rock Digestion Experiments Using the Pressure Vessel sapling System (laboratory notes).
- Hall R. B., (1978), World nonbauxite aluminum resources-Alunite. *U. S. Geological Survey Professional Paper*, 1076-A.
- Hansen L. D., Dipple G. M., Gordon T. M., Kellett D. A., (2005), Carbonated serpentinite (İstwanite) at Atlin, British Columbia: A geological analogue to carbon dioxide sequestration, *The Canadian Mineralogist*, 43, 225-239.
- Harrison R. K., Aitkenhead N., Young B. R., Dagger P. F., (1975), Goethite from Hindlow, Derbyshire. *Bulletin of Geological Survey, Great Britain*, 52, 51-54.
- Hedenquist J.W., (1987), Mineralization associated with volcanic related hydrothermal systems in the Circum-Pasific basin. In Transactions of the Fourth Circum-Pasific Energy Resources and Mineral Resources Conference (M.K. Horn,ed.) August 1986, Singapore, *American Association of Petroleum Geologists*, Tulsa, Oklahoma, 513-524.

- Hedenquist J. W., Arribas A. Jr., Gonzalez-Urien E., (2000). Exploration of Epithermal Gold Deposits, *SEG Reviews*, 13, 245-277.
- Hedenquist J. W., Izawa E., Arribas A., White N. C., (1996), Epithermal gold deposits: Styles, characteristics and exploration, *Resource Geology Special Publication, poster*.
- Hedenquist J.W., Matsuhisa Y., Izawa E., White N.C., Giggenbach W.F., Aoki M. (1994), Geology and geochemistry of high-sulfidation Cu-Au mineralization in the Nansatsu district, Japan. *Econ. Geo.*, 89, 1-30.
- Henley R.W. & Ellis A.J. (1983) Geothermal systems, ancient and modern: A geochemical review. *Earth Science Reviews*, 1–50.
- Ishikawa Y., Sawaguchi T., Iwaya S., Horiuchi M., (1976). Delineation of Prospecting Targets for Kuroko Deposits Based on Modes of Volcanism of Underlying Dacite and Alteration Halos, *Mining Geology*, 26, 105-117.
- Iwao S., (1962), Silica and alunite deposits of the Ugusu mine; a geochemical consideration on an extinct geothermal area in Japan, *Japanese Journal of Geology and Geography*, 33, 131-144.
- Izawa E., Urashima Y., Ibaraki K., Suzuki R., Yokoyama T., Kawasaki K., Koga A., Taguchi S. (1990) The Hishikari gold deposit: high-grade epithermal veins in Quaternary volcanics of southern Kyushu, Japan. *Journal of Geochemical Exploration*, 36, 1–56.
- Jackson M. L. (1975) *Soil Chemical Analysis – Advanced Course*. 2nd edition, published by the author, Madison, Wisconsin, USA.
- Kadir S. & Erkoyun H. (2013) Genesis of the hydrothermal Karaçayır kaolinite deposit in Miocene volcanics and Paleozoic volcanic rocks of the Uşak-Güre basin, western Turkey. *Turkish Journal of Earth Sciences*, 22, 444–468
- Karakaş Ö., (2006), Sivrihisar-biçer civarı Neojen (Üst Miyosen-Pliyosen) basenindeki kil parajenezlerinin ortamsal yorumu, Ankara Üniversitesi Fen Bilimleri Enstitüsü Yüksek Lisans Tezi

- Kerrick R. W., (1989), Geochemical Evidence on the Source of Fluids and Solutes for Shear Zone Hosted Mesothermal Au Deposits; in Mineralization in Shear Zones, J.T. Bursnal, Editor, *Geological Association of Canada, Short Course Notes*, 6, 129-197.
- Large R. R., Gemmell J. B., Paulick H., Huston D. L., (2001), The alteration box plot: a simple approach to understanding the relationship between alteration mineralogy and lithochemistry associated with volcanic-hosted massive sulfide deposits. *Economic Geology*, 957-971.
- Mandarino J. A. & Harris D. C., (1965), New Canadian mineral occurrences: I. Eucryptite, pollucite, rozenite, epsomite, dawsonite, fairchildite and butschliite. *Canadian Mineralogist.*, 8, 377–381.
- Matter, J., M. & Kelemen, P., B. (2009), Permanent storage of carbon dioxide in geological reservoirs by mineral carbonation, *Nature Geoscience*, 2, 837 - 841.
- Mervine E., (2013), Monday Geology Picture: Listwanite Hills in the Sultanate of Oman (web-post).
- Meyer C. & Hemley J.J. (1967), Wall rock alteration. *In Geochemistry of Hydrothermal Ore Deposits* (H.L. Barnes, ed.). Holt, Rinehart & Winston, New York, 166-235.
- Mutlu H., Sariiz K., Kadir S., (2005), Geochemistry and origin of the Şaphane alunite deposit, Western Anatolia, Turkey, *Ore Geology Reviews*, 26, 39-50.
- Okada K., Hirabayashi J., Ossaka J., (1982), Crystal structure of natroalunite and crystal chemistry of the alunite group. *Neues Jahrbuch für Mineralogie, Monatsh.*, 534–540.
- Okay A. I., (2008), Geology of Turkey: A Synopsis, *Anschnitt*, 21, 19-42
- Okay A. I. & Monié P., (1997), Early Mesozoic subduction in the Eastern Mediterranean. Evidence from Triassic eclogite in northwest Turkey. *Geology*, 25, 595-598.

- Okay A. I., Monod O., Momié P., (2002), Triassic blueschists and eclogites from northwest Turkey: vestiges of the Paleo-Tethyan subduction, *Lithos*, 64, 155-178.
- Okay A. I., Satır M., Siebel W., (2006), Pre-Alpide orogenic events in the Eastern Mediterranean region. In: Gee, D.G. & R.A. Stephenson (eds.), *European Lithosphere Dynamics*, Geological Society, London, Memoirs 32, 389-405.
- Okay A.I. and Tüysüz O., (1999), Tethyan sutures of northern Turkey. In *The Mediterranean Basins: Tertiary extension within the Alpine orogen*, Geological Society, London, Special Publication 156, 475-515.
- Ömeroğlu I., Guggenheim S., Günal Türkmenoğlu A., Koster van Groos A., F., Sayın Ş., A., (2015), An experimental study of CO₂-H₂O-listwanite-based reactions using serpentine from the Ahırözü kaolin deposits, Eskişehir-Mihalıççık, Turkey, *EuroClay 2015*, Edinburgh-Scotland, p. 493.
- Ömeroğlu I., Günal-Türkmenoğlu A., Demirci C., (2016), Hydrothermal Alteration Products in the Vicinity of the Ahırözü Kaolin Deposits, Mihalıççık-Eskişehir, Turkey, 5th Mediterranean Clay Meeting, Çeşme-İzmir/Turkey, p. 48.
- Ömeroğlu I., Günal-Türkmenoğlu, A., Sayın Ş. A., (2013), Investigation of the Genesis of Ahırözü Kaolin Deposits (Eskişehir, Turkey) Using Mineralogical, Petrographical And Geochemical Analyses, *50th Anniversary of Clay Mineral Society Annual Meeting*, Urbana-Champaign-USA, p.188.
- Ömeroğlu-Sayıt I., Günal-Türkmenoğlu A., Sayın Ş. A., Demirci C., (2018), Hydrothermal alteration products in the vicinity of the Ahırözü kaolin deposits, Mihalıççık-Eskişehir, Turkey, *Clay Minerals*, 53, 289-303.
- Palache C., Berman H., Frondel C., (1944), Dana's system of mineralogy, (7th edition), Vol. I, 698-707.
- Palache C., Berman H., Frondel C., (1951a), Dana's system of mineralogy, (7th edition), Vol. II, 556-560.

- Palache C., Berman H., Frondel C., (1951b), Dana's system of mineralogy, (7th edition) Vol. II, 276–277.
- Pearce J., A., Harris N. B. W., Tindle A. G., (1984), Trace element discrimination diagrams for the tectonic interpretation of granitic rocks, *Journal of Petrology*, 25, 956-983.
- Park A-H. A., Fan L-S., (2004), CO₂ mineral sequestration: physically activated dissolution of serpentine and pH swing process, *Chemical Engineering Science* 59, 5241 – 5247.
- Reyes A. G., (1990), Petrology of Philippine geothermal systems and the application of alteration mineralogy to their assessment, *Journal of Volcanology and Geothermal Research*, 43, 279–309.
- Rye R. O., (1993), The evolution of magmatic fluids in the epithermal environment: The stable isotope perspective, *Economic Geology*, 88, 733-753.
- Rye R. O., Bethke P. M., Wasserman M. D., (1992), The stable isotope geochemistry of acidsulfate alteration, *Economic Geology*, 87, 225-262.
- Saeki, Y., & Date J., (1980), Computer application to the alteration data of the footwall dacite lava at the Ezuri Kuroko deposits, Akita Prefecture: *Mining Geology*, 30, 241–250.
- Sayın S. A., (1984) *The Geology, Mineralogy, Geochemistry and Origin of the Yeniçağa Kaolin Deposits and Other Similar Deposits in Western Turkey*. PhD thesis, University of London.
- Sayın S. A., (2007), Origin of kaolin deposit: evidence from the Hisarcık (Emet-Kütahya) deposits, Western Turkey, *Turkish Journal of Earth Sciences*, 16, 77-96.
- Sayın S. A., (2016), Quartz-mica schist and gneiss hosted clay deposits within the Yenipazar (Yozgat, Central Anatolia) volcanogenic massive sulphide ore, *Turkish Journal of Earth Sciences*, 25, 81-101.

- Schoch A. E., Beukes G. J., Van der Westhuizen W. A., de Bruijn H., (1989), Natroalunite from Koenabib, Pofadder district, South Africa. *South African Journal of Geology*, 92, 20–28.
- Sei J., Morato F., Kra G., Staunton S., Quiquampoix H., Jumas J. C., Olivier-Fourcade J., (2006), Mineralogical, crystallographic and morphological characteristics of natural kaolins from the Ivory Coast (West Africa), *Journal of African earth Sciences*, 46, 245-252.
- Seyhan İ., (1978) Türkiye kaolin yatakları ile hidrotermal cevherler arasında görülen ilişkiler, *Jeoloji Mühendisliği*, 27-31.
- Siddiqui M. A. & Ahmed Z., (2008), Geochemistry of the kaolin deposits of Swat (Pakistan). *Chemie der Erde*, 68, 207-219.
- Sillitoe R. H. & Hedenquist J. W., (2003), Linkages between Volcanotectonic Settings, Ore-Fluid Compositions, and Epithermal Precious Metal Deposits, Chapter 18, *Society of Economic Geologists, Special Publication 10*.
- Sincan M., (1978) Eskişehir Mihaliççık kaolen etüt raporu Directorate of Mineral Research and Exploration, Ankara.
- Smith J. W. & Milton C., (1966), Dawsonite in the Green River Formation of Colorado. *Economic Geology*, 61, 1029–1042.
- Stoffregen R. E., (1987), Genesis of acid-sulfate alteration and Au-Cu-Ag mineralization at Summitville, Colorado. *Economic Geology*, 82, 1575-1591.
- Şengüler İ., (2011), Eskişehir Sivrihisar havzası neojen Kompilasyonu ve Kömür Potansiyeli, Maden Tetkik Arama, Enerji Hammadde Etüt ve Arama Dairesi, Ankara, *Geologic Report*.
- Taylor H. P. Jr. (1974), The application of oxygen and hydrogen isotope studies to problems of hydrothermal alteration and ore deposition. *Economic Geology*, 69, 843-883

- Topuz G., Altherr R., Satır M., Schwartz W. H., (2004), Low-grade metamorphic rocks from the Pular Complex, NE Turkey: implications for the pre-Liassic evolution of the Eastern Pontides. *International Journal of Earth Sciences* 93, 72-91.
- Topuz G., Altherr R., Schwartz W. H., Dokuz A., Meyer H-P., (2007), Variscan amphibolites-facies rocks from the Kurtoğlu metamorphic complex (Gümüşhane area, Eastern Pontides, Turkey). *International Journal of Earth Sciences*, 96, 861-873.
- Ünal E., (2010), Genetic Investigation and Comparison of Kartaldağ and Madendağ Epithermal Gold Mineralization in Çanakkale-Region, MSc Thesis, Middle East Technical University.
- Ünal-Ercan H., Ece Ö.I., Schroeder P.A., Karacık Z., (2016), Differentiating styles of alteration within kaolin-alunite hydrothermal deposits of Çanakkale, NW Turkey, *Clays and Clay Minerals*, 64, 245–274.
- White N. C., (1991), High sulfidation epithermal gold deposits: Characteristics, and a model for their origin, *Geological Survey of Japan Report*, 227, 9-20
- White N. C., Hedenquist J. W., (1995) Epithermal gold deposits: styles, characteristics and exploration, *SEG Newsletter*, No.23, 1, 9-13.
- White W. M., (2013), Geochemistry, Chp. 7, 259-313, *published by John Wiley & Sons*
- Wilkinson J. J., (2001), Fluid inclusions in hydrothermal ore deposits, *Lithos* 55, 229-272.
- Yang C., (2016), Homogenization Temperatures of All-Liquid Fluid Inclusions in Halite from the Middle Devonian Prairie Evaporite, Southern Saskatchewan, *Saskatchewan Geological Survey, Saskatchewan Ministry of the Economy, Miscellaneous Report 2016-4.1, Paper A*, 1-13.

Yılmaz O. & Boztuğ D., (1986), Kastamonu granitoid belt of northern Turkey: First arc plutonism product related to the subduction of the paleo-Tethys, *Geology*, 14, 179-183.

APPENDIX A

CHEMICAL COMPOSITIONS OF ROCK SAMPLES

Table A-1. Geochemical compositions of 59 rock samples acquired from the study area

Sample	SiO ₂	Al ₂ O ₃	Fe ₂ O ₃	MgO	CaO	Na ₂ O	K ₂ O	TiO ₂	P ₂ O ₅	MnO	Cr ₂ O ₃	Ni	Sc	LOI	Sum
	%	%	%	%	%	%	%	%	%	%	%	PPM	PPM	%	%
L-1	11.80	0.83	0.93	17.93	26.05	0.02	0.02	0.03	<0.01	0.05	0.222	364	13	42.0	99.92
L-4B	60.24	25.80	1.18	0.26	0.22	0.16	0.07	0.73	0.02	<0.01	0.008	61	22	11.2	99.90
L-11	93.71	0.80	2.76	0.10	0.09	0.02	0.04	<0.01	<0.01	0.03	0.118	380	3	2.2	99.94
L-6	30.14	35.96	0.78	0.42	0.22	2.48	0.08	<0.01	0.04	<0.01	0.019	47	73	29.7	99.83
L-3	35.24	36.18	0.13	0.20	0.13	1.89	<0.01	0.09	0.02	<0.01	0.022	76	83	25.9	99.81
L-7	49.15	17.60	22.49	0.06	0.11	0.05	0.02	0.49	0.02	0.02	0.086	<20	11	9.7	99.84
L-9	81.09	2.53	11.85	0.13	0.11	0.04	0.06	0.07	0.06	0.01	0.565	1544	6	3.2	99.86
L-5	61.75	24.44	0.46	0.14	0.12	0.12	0.04	1.27	<0.01	<0.01	0.011	<20	5	11.5	99.89
L-8	57.46	5.25	29.22	0.06	0.11	0.08	0.05	0.78	0.03	0.01	0.024	<20	7	6.8	99.85
L-4A	21.41	30.20	9.42	0.06	0.11	4.08	0.04	0.25	0.11	<0.01	0.014	64	85	34.1	99.78
L-10	60.28	25.86	0.88	0.11	0.18	0.02	0.02	0.14	<0.01	<0.01	0.010	<20	42	12.4	99.91
L1A	26.77	8.32	6.69	16.43	14.71	0.03	0.27	0.43	0.05	0.29	0.057	654	11	25.7	99.87
L1B	45.75	1.07	5.21	10.11	13.76	0.03	0.15	0.11	0.03	0.05	0.936	735	5	22.6	99.91
L12-1	43.67	12.89	13.03	5.57	6.48	3.87	2.67	1.88	0.43	0.13	0.055	159	22	9.2	99.86
L12-2	74.30	15.61	0.56	0.14	0.09	0.11	0.37	0.40	0.05	<0.01	0.012	<20	4	8.3	99.93
L12-3	30.21	36.50	1.14	0.29	0.22	2.38	0.22	0.13	0.08	<0.01	0.093	26	83	28.5	99.81
L12-4	68.31	10.22	2.70	3.65	3.27	0.12	0.18	0.24	0.03	0.06	0.177	200	6	10.9	99.92
L12-5a	42.33	1.47	8.29	15.09	11.19	0.03	0.04	0.02	0.02	0.10	0.405	1659	9	20.7	99.92
L12-5b	57.69	14.28	6.66	7.66	0.96	5.28	0.84	0.38	0.08	0.14	0.002	135	8	5.8	99.78
L12-6	56.67	17.86	9.70	0.55	0.37	0.06	0.05	0.44	0.03	1.65	0.002	43	27	12.5	99.85
L12-7	83.96	5.66	4.29	0.15	0.15	0.17	0.14	0.06	0.04	<0.01	0.474	212	3	4.8	99.90
L12-8	35.20	3.50	6.21	14.06	13.77	0.09	0.72	0.27	0.05	0.16	0.084	503	8	25.8	99.92
L12-9	61.94	19.17	4.03	0.13	0.21	0.41	0.54	0.67	0.20	<0.01	0.027	<20	12	12.6	99.89
L12-10	73.15	13.34	4.48	0.12	0.10	0.09	0.35	0.39	0.06	<0.01	0.008	<20	5	7.9	99.93
L12-11	73.26	17.62	0.76	0.09	0.08	<0.01	0.27	0.50	0.02	<0.01	0.006	<20	9	7.3	99.93
L13	15.44	4.88	5.52	16.25	20.83	0.25	1.11	0.75	0.11	0.04	0.075	469	17	34.3	99.62
Hmd1-1	71.03	18.49	0.48	0.28	0.24	<0.01	0.30	0.41	0.04	<0.01	0.006	<20	54	8.6	99.92

Sample	SiO2	Al2O3	Fe2O3	MgO	CaO	Na2O	K2O	TiO2	P2O5	MnO	Cr2O3	Ni	Sc	LOI	Sum
	%	%	%	%	%	%	%	%	%	%	%	PPM	PPM	%	%
Hmd1a	66.23	12.76	10.73	0.35	0.22	0.02	0.42	0.39	0.11	0.03	0.007	139	14	8.6	99.88
Hmd2a	68.47	20.62	0.50	0.15	0.15	0.02	0.35	0.65	0.11	<0.01	0.005	<20	37	8.9	99.91
Hmd1-2	73.92	17.00	0.39	0.16	0.14	0.02	0.20	0.33	0.02	<0.01	0.002	<20	66	7.7	99.91
Hmd1-3	72.37	17.80	0.93	0.20	0.13	0.01	0.38	0.41	0.04	<0.01	0.003	<20	24	7.6	99.92
Hmd1-4	57.90	27.72	1.64	0.20	0.13	0.01	0.20	0.41	0.03	<0.01	0.003	44	104	11.7	99.93
Hmd1-5	67.67	19.87	0.50	0.16	0.11	0.25	0.41	0.41	0.07	<0.01	0.012	<20	19	10.4	99.91
Hmd1-6	69.48	17.74	2.55	0.07	0.08	0.18	0.28	0.40	0.09	<0.01	0.009	20	10	9.0	99.90
Hmd1-7	77.27	14.34	0.53	0.07	0.07	0.07	0.21	0.30	0.04	<0.01	0.013	<20	7	7.0	99.90
Hmd1-7a	46.77	15.86	10.47	6.26	1.70	3.56	0.13	1.62	0.15	0.13	0.021	93	51	13.2	99.84
Hmd1-7b	51.61	15.45	18.67	0.61	0.21	0.04	0.02	0.84	0.10	0.02	0.007	102	48	12.2	99.85
Hmd1-8	34.41	11.89	10.91	9.55	8.62	1.23	3.57	1.98	0.33	0.14	0.028	186	19	17.2	99.84
Hmd2	60.89	16.55	9.38	1.06	1.48	0.04	0.13	0.27	0.03	0.12	0.243	405	10	9.7	99.88
Hmd3	82.71	0.79	12.25	0.12	0.14	0.02	0.03	0.01	0.04	0.11	0.312	1176	13	3.2	99.90
Hmd3-1	48.42	15.48	8.07	4.12	6.45	0.01	0.02	0.24	0.03	0.16	0.021	73	59	16.9	99.89
Hmd3-2	22.33	3.32	55.48	0.39	4.46	0.02	<0.01	0.10	0.18	0.18	0.043	923	88	13.2	99.83
Hmd4	75.40	10.98	7.01	0.11	0.20	0.01	0.02	0.39	0.02	0.03	0.051	62	11	5.7	99.91
Hmd5	66.87	15.68	7.74	0.11	0.19	<0.01	0.02	0.55	0.05	0.15	0.024	105	43	8.5	99.86
H-1	17.82	4.45	4.14	16.63	20.95	0.64	0.63	0.56	0.03	0.03	0.081	938	11	33.5	99.63
H-2	56.63	13.86	11.43	3.04	2.00	4.67	1.04	1.73	0.44	0.08	0.088	282	26	4.8	99.82
H-3	45.73	15.42	12.48	6.85	7.89	3.78	0.02	1.47	0.14	0.17	0.026	62	40	5.9	99.85
H-4	54.98	15.75	18.64	0.16	0.19	0.03	0.16	1.19	0.23	<0.01	0.053	60	18	8.4	99.77
H-5	80.56	9.27	4.41	0.35	0.09	<0.01	0.86	0.46	0.06	0.03	0.021	158	8	3.7	99.86
H-6	90.31	3.68	2.77	0.46	0.06	<0.01	1.09	0.16	0.07	0.05	0.005	36	5	1.3	99.92
H-7	85.69	7.04	2.37	0.24	0.12	<0.01	0.34	0.28	0.09	<0.01	0.029	76	5	3.7	99.87
H-8	73.23	8.69	9.94	0.08	0.20	0.05	0.07	0.12	0.02	0.03	0.019	<20	16	7.5	99.93
H8-1	81.72	0.71	10.52	0.03	0.08	0.04	<0.01	0.38	0.04	0.01	0.018	<20	4	6.4	99.92
H-9	27.28	37.05	0.85	0.36	0.22	2.99	0.24	0.06	0.08	<0.01	0.092	37	79	30.6	99.79
H-10	71.92	14.69	3.50	0.17	0.25	0.04	<0.01	0.69	0.02	<0.01	0.006	<20	8	8.6	99.94
H-11	56.37	18.10	13.68	0.27	0.27	0.02	0.04	0.56	0.04	0.03	0.019	28	234	10.5	99.87
H-12	1.94	0.04	2.46	21.17	30.07	<0.01	<0.01	<0.01	0.02	0.03	0.007	189	2	44.2	99.93

Continued from Table A-1

Sample	Ba	Be	Co	Cs	Ga	Hf	Nb	Rb	Sn	Sr	Ta	Th	U	V	W	Zr	Y
	PPM																
	1	1	0.2	0.1	0.5	0.1	0.1	0.1	1	0.5	0.1	0.2	0.1	8	0.5	0.1	0.1
L-1	37	<1	6.1	7.0	2.6	<0.1	0.3	1.3	<1	192.5	<0.1	<0.2	0.6	57	0.7	2.3	2.5
L-4B	17	<1	6.5	4.6	21.0	0.3	2.4	0.8	<1	19.7	<0.1	<0.2	0.3	234	2.8	8.3	0.2
L-11	35	2	28.8	2.1	5.4	0.1	3.1	1.4	<1	5.5	<0.1	<0.2	<0.1	40	2.7	11.6	1.1
L-6	20	<1	6.5	1.5	3.8	<0.1	0.3	3.6	<1	324.5	0.1	<0.2	0.7	517	<0.5	1.3	0.1
L-3	8	<1	7.1	1.6	3.5	<0.1	0.4	1.5	<1	328.3	<0.1	<0.2	<0.1	594	0.8	4.7	<0.1
L-7	9	<1	3.1	1.9	19.0	0.4	0.5	<0.1	1	19.2	<0.1	<0.2	<0.1	400	0.6	7.0	0.2
L-9	55	<1	96.6	6.2	2.7	<0.1	1.3	3.9	<1	26.9	<0.1	<0.2	0.1	105	91.1	3.7	0.8
L-5	12	2	1.5	5.7	19.5	0.2	1.2	0.6	<1	14.5	<0.1	<0.2	0.9	349	4.8	5.8	0.4
L-8	15	<1	1.7	2.7	13.2	<0.1	1.0	0.2	<1	21.2	<0.1	<0.2	0.3	268	0.6	1.3	0.4
L-4A	19	<1	12.8	1.4	8.4	<0.1	0.6	4.8	<1	329.3	<0.1	0.5	0.3	764	1.7	3.3	0.6
L-10	8	<1	0.3	1.6	12.2	0.1	0.6	<0.1	<1	10.7	<0.1	<0.2	0.2	179	0.6	2.3	<0.1
L1A	185	<1	30.4	2.1	11.4	2.4	8.8	13.0	<1	164.1	0.5	6.5	1.7	83	2.7	91.4	20.2
L1B	52	2	28.8	4.5	2.2	0.6	4.3	5.0	<1	152.4	0.4	0.4	0.4	52	3.5	28.4	3.0
L12-1	92	4	28.5	22.5	13.1	3.0	24.3	71.2	1	60.9	1.4	2.1	0.4	172	1.0	132.0	21.6
L12-2	23	<1	2.0	6.3	15.4	3.2	3.4	3.4	<1	76.4	0.2	0.6	0.2	21	2.8	106.3	11.1
L12-3	68	<1	0.5	0.5	5.1	<0.1	0.2	2.2	<1	796.0	<0.1	<0.2	0.3	393	0.5	0.7	0.8
L12-4	22	<1	10.8	6.4	9.2	2.0	1.6	2.0	<1	73.0	<0.1	<0.2	<0.1	37	1.6	67.8	7.4
L12-5a	48	<1	78.9	46.4	2.7	<0.1	0.2	2.4	<1	83.8	<0.1	<0.2	<0.1	49	<0.5	0.6	2.3
L12-5b	37	4	16.3	5.1	19.7	15.4	103.4	27.7	5	32.9	5.9	11.3	1.3	32	0.7	650.3	47.4
L12-6	146	<1	218.0	2.9	16.8	0.4	1.6	2.3	<1	93.9	0.2	<0.2	<0.1	329	<0.5	7.7	4.5
L12-7	25	<1	11.0	6.4	3.5	<0.1	0.6	4.8	<1	218.8	<0.1	<0.2	<0.1	63	7.5	3.6	2.1
L12-8	23	2	31.1	12.4	5.4	0.3	3.6	20.0	<1	92.8	0.2	0.3	<0.1	115	<0.5	20.0	7.3
L12-9	73	2	2.2	11.8	17.4	1.7	3.2	5.3	3	331.2	0.2	1.3	1.1	202	14.5	64.3	3.3
L12-10	33	<1	0.5	8.1	13.9	3.1	2.4	3.9	2	42.9	0.2	0.5	0.4	32	5.9	101.8	4.9
L12-11	19	<1	3.8	3.7	18.4	3.7	3.1	3.1	<1	10.0	0.1	1.0	0.5	31	4.1	94.4	25.2
L13	98	2	22.0	9.4	9.9	1.8	14.0	22.9	1	307.1	0.9	1.3	0.4	105	0.5	64.7	12.3
Hmd1-1	26	<1	0.9	7.6	17.2	4.2	2.8	3.7	1	32.2	0.2	1.1	0.3	29	1.3	129.8	23.1
Hmd1a	28	<1	42.6	11.9	13.9	3.1	2.5	7.4	<1	17.2	0.2	0.7	1.8	43	2.3	104.1	119.4
Hmd2a	40	<1	0.5	8.7	17.1	3.1	3.1	3.9	<1	55.4	0.2	1.0	0.6	78	5.3	103.5	6.1
Hmd1-2	15	1	2.3	9.0	15.7	5.8	3.1	2.9	<1	9.1	0.2	0.9	0.5	37	1.4	192.5	27.4
Hmd1-3	44	<1	1.4	8.2	16.7	4.0	2.5	4.2	<1	37.8	<0.1	0.8	0.4	27	0.6	141.4	21.8
Hmd1-4	24	<1	1.1	6.5	26.8	3.6	2.7	3.2	<1	17.6	0.2	0.7	0.3	40	1.7	116.9	25.5
Hmd1-5	32	<1	1.5	4.9	14.3	4.3	2.7	3.9	<1	67.9	0.2	0.8	0.3	44	2.7	126.6	21.9
Hmd1-6	20	<1	12.7	2.6	16.1	3.8	3.3	3.1	<1	88.1	0.2	1.0	1.0	68	7.3	127.6	42.4
Hmd1-7	23	3	1.7	3.4	14.2	7.6	2.4	2.1	<1	61.7	0.2	0.6	0.5	33	5.1	290.5	20.8

	Ba	Be	Co	Cs	Ga	Hf	Nb	Rb	Sn	Sr	Ta	Th	U	V	W	Zr	Y
	PPM																
	1	1	0.2	0.1	0.5	0.1	0.1	0.1	1	0.5	0.1	0.2	0.1	8	0.5	0.1	0.1
Hmd1-7a	14	<1	40.1	2.6	17.0	2.8	7.2	4.1	<1	58.5	0.5	0.7	0.2	354	1.2	91.5	21.2
Hmd1-7b	17	<1	35.3	5.7	19.0	0.2	0.3	0.7	<1	27.6	0.2	<0.2	0.4	435	7.9	7.6	7.1
Hmd1-8	74	<1	37.2	22.0	15.2	4.4	49.6	90.8	2	88.4	2.5	6.1	1.6	150	<0.5	227.0	25.2
Hmd2	73	<1	62.6	1.8	10.5	0.3	1.3	3.9	<1	18.5	<0.1	<0.2	0.2	93	15.3	10.1	2.2
Hmd3	166	<1	66.9	1.9	1.6	<0.1	0.2	1.5	<1	4.1	<0.1	<0.2	0.1	45	9.5	2.9	1.9
Hmd3-1	27	<1	77.1	4.1	12.6	0.2	<0.1	2.9	<1	33.2	<0.1	<0.2	0.1	215	8.0	1.9	4.7
Hmd3-2	278	16	82.1	1.4	5.6	<0.1	0.7	1.2	2	47.6	<0.1	<0.2	3.0	192	4.4	5.7	24.3
Hmd4	24	<1	12.8	1.6	9.1	0.2	0.3	1.2	<1	10.3	<0.1	<0.2	<0.1	113	30.2	5.9	1.9
Hmd5	120	<1	34.4	0.6	13.2	0.3	0.2	1.0	<1	103.3	<0.1	<0.2	0.1	288	32.2	4.6	4.7
H-1	77	6	27.4	16.7	7.3	1.5	11.7	21.8	<1	399.3	0.6	2.2	0.4	50	1.2	55.5	10.0
H-2	145	<1	44.4	2.7	14.8	3.8	42.1	29.3	1	232.6	3.1	4.9	1.0	167	<0.5	151.4	14.4
H-3	67	<1	47.5	0.2	19.0	2.5	5.0	0.7	<1	71.8	0.4	0.4	0.2	322	<0.5	92.9	29.4
H-4	234	<1	18.6	2.0	14.3	2.1	8.8	4.1	<1	692.2	0.6	1.3	1.1	282	3.5	80.4	11.5
H-5	131	<1	22.2	2.0	18.3	2.5	8.7	28.7	3	72.2	0.7	7.4	1.3	176	23.1	99.8	19.4
H-6	104	1	7.4	1.1	5.2	1.0	3.1	31.3	<1	103.9	0.2	3.1	0.6	31	3.1	35.5	8.5
H-7	84	<1	4.5	1.2	10.5	1.4	5.2	11.8	2	411.3	0.2	4.3	1.3	57	10.4	56.4	12.1
H-8	36	<1	12.3	6.2	15.2	0.1	0.3	2.0	<1	27.1	<0.1	<0.2	<0.1	126	<0.5	3.0	0.5
H8-1	7	<1	0.8	4.9	5.1	<0.1	0.2	0.6	<1	14.1	<0.1	<0.2	0.3	232	<0.5	2.5	0.7
H-9	75	<1	0.4	0.4	3.8	<0.1	<0.1	2.8	<1	944.9	<0.1	<0.2	0.7	466	<0.5	0.7	1.1
H-10	6	<1	1.0	4.2	10.9	<0.1	<0.1	0.8	<1	14.9	<0.1	<0.2	0.2	170	<0.5	2.0	0.7
H-11	9	1	15.7	5.3	12.3	<0.1	<0.1	1.4	<1	14.6	<0.1	<0.2	5.2	366	4.2	2.6	10.6
H-12	345	<1	8.3	<0.1	<0.5	0.2	0.3	<0.1	<1	135.0	<0.1	<0.2	<0.1	18	<0.5	9.9	1.2

Continued from Table A-1

Sample	La	Ce	Pr	Nd	Sm	Eu	Gd	Tb	Dy	Ho	Er	Tm	Yb	Lu
	PPM													
	0.1	0.1	0.02	0.3	0.05	0.02	0.05	0.01	0.05	0.02	0.03	0.01	0.05	0.01
L-1	0.4	0.6	0.06	<0.3	0.11	0.06	0.26	0.03	0.34	0.06	0.17	0.02	0.15	0.02
L-4B	0.3	0.3	<0.02	0.7	<0.05	<0.02	<0.05	<0.01	<0.05	<0.02	<0.03	<0.01	<0.05	<0.01
L-11	0.4	0.3	0.05	0.5	<0.05	<0.02	0.10	0.01	0.15	<0.02	0.05	0.01	<0.05	<0.01
L-6	0.6	2.0	0.21	0.7	0.23	0.05	0.05	<0.01	<0.05	<0.02	<0.03	<0.01	<0.05	<0.01
L-3	0.7	2.0	0.14	0.6	<0.05	<0.02	<0.05	<0.01	<0.05	<0.02	<0.03	<0.01	<0.05	<0.01
L-7	0.2	0.6	0.03	<0.3	<0.05	<0.02	<0.05	<0.01	0.10	<0.02	0.05	<0.01	0.12	<0.01
L-9	0.9	1.2	0.11	0.7	<0.05	0.03	0.31	0.02	0.11	0.03	<0.03	0.01	0.16	<0.01
L-5	0.5	0.4	0.03	0.5	<0.05	0.03	0.11	0.01	0.11	<0.02	0.07	<0.01	<0.05	<0.01
L-8	0.4	0.2	<0.02	0.5	<0.05	0.02	<0.05	0.02	<0.05	<0.02	0.07	<0.01	<0.05	<0.01
L-4A	2.5	11.8	2.20	5.1	0.12	0.07	0.21	0.03	0.26	0.04	0.12	<0.01	0.06	0.01
L-10	0.5	0.2	<0.02	<0.3	<0.05	<0.02	0.10	0.01	0.11	<0.02	0.03	<0.01	<0.05	<0.01
L1A	14.7	34.7	3.41	13.0	2.96	0.68	3.35	0.59	2.87	0.69	2.07	0.28	1.89	0.30
L1B	4.5	7.2	0.93	4.0	0.67	0.17	0.65	0.09	0.40	0.09	0.24	0.03	0.21	0.05
L12-1	29.3	55.7	6.52	25.5	5.38	1.85	5.53	0.83	4.33	0.82	2.17	0.33	1.81	0.31
L12-2	4.9	13.8	1.92	7.0	1.25	0.24	0.88	0.17	1.32	0.34	1.20	0.23	1.68	0.26
L12-3	1.9	2.4	0.50	2.5	0.67	0.28	0.43	0.05	0.17	<0.02	0.06	<0.01	0.05	<0.01
L12-4	5.4	12.3	1.59	6.8	1.02	0.23	0.80	0.15	1.18	0.25	0.94	0.17	1.14	0.16
L12-5a	0.7	1.6	0.24	1.3	0.19	0.16	0.27	0.05	0.38	0.06	0.28	0.03	0.21	0.04
L12-5b	30.6	78.5	9.49	36.4	7.53	1.94	8.08	1.63	9.58	2.06	5.53	0.80	4.68	0.71
L12-6	2.1	4.9	0.78	3.8	1.29	0.88	1.45	0.27	1.70	0.33	0.97	0.15	0.91	0.16
L12-7	2.0	3.6	0.55	2.9	0.52	0.14	0.58	0.08	0.43	0.10	0.17	0.02	0.18	0.03
L12-8	6.0	11.0	1.19	5.1	0.82	0.36	1.23	0.19	0.98	0.24	0.63	0.10	0.55	0.08
L12-9	22.9	59.2	8.07	31.2	3.76	0.63	1.57	0.19	0.69	0.12	0.57	0.09	0.63	0.12
L12-10	2.1	5.9	0.67	2.6	0.35	0.12	0.38	0.08	0.60	0.19	0.82	0.14	1.11	0.19
L12-11	3.4	8.8	1.21	5.7	1.41	0.43	2.02	0.49	3.64	0.93	3.36	0.54	3.59	0.58
L13	21.3	32.0	5.54	21.6	4.32	1.35	3.81	0.58	3.07	0.63	1.43	0.20	1.06	0.16
Hmd1-1	6.9	17.0	2.15	11.0	2.82	0.58	2.35	0.43	3.27	0.84	2.81	0.43	3.28	0.53
Hmd1a	7.8	19.9	3.80	20.4	8.47	2.95	19.49	3.63	21.70	4.70	13.43	1.97	12.47	1.88
Hmd2a	12.0	35.9	5.93	34.7	9.44	1.63	4.07	0.41	1.57	0.16	0.72	0.14	1.02	0.17
Hmd1-2	2.0	4.9	0.64	2.9	1.19	0.32	2.15	0.50	3.97	1.08	3.55	0.58	3.96	0.65
Hmd1-3	5.6	14.5	2.21	11.8	4.43	1.01	3.80	0.57	3.48	0.94	3.11	0.52	3.64	0.58
Hmd1-4	2.4	6.0	0.88	4.7	1.57	0.37	1.88	0.41	3.22	0.85	2.66	0.47	3.44	0.59
Hmd1-5	6.3	17.0	2.64	13.0	2.63	0.55	2.26	0.45	2.92	0.86	2.82	0.53	3.57	0.59
Hmd1-6	7.8	21.2	3.02	10.4	1.67	0.32	2.38	0.69	5.78	1.62	5.15	0.81	5.24	0.86
Hmd1-7	2.3	6.3	0.77	3.2	0.59	0.16	1.06	0.30	2.70	0.75	2.72	0.46	3.42	0.61

Hmd1-7a	6.4	13.2	2.26	11.6	2.91	1.08	3.83	0.70	4.35	0.84	2.50	0.37	2.42	0.35
Hmd1-7b	0.5	1.0	0.21	1.5	0.49	0.40	1.15	0.20	1.41	0.30	0.91	0.14	0.93	0.16
Hmd1-8	36.6	74.1	8.08	29.9	6.35	2.10	6.19	0.92	5.02	0.98	2.63	0.32	1.85	0.27
Hmd2	3.5	3.4	0.55	2.2	0.39	0.15	0.49	0.07	0.51	0.08	0.28	0.03	0.22	0.04
Hmd3	0.5	0.5	0.09	0.5	0.06	0.03	0.20	0.04	0.25	0.06	0.15	0.03	0.12	0.02
Hmd3-1	0.2	0.4	0.08	0.7	0.26	0.28	0.59	0.13	0.89	0.20	0.62	0.09	0.59	0.11
Hmd3-2	1.9	3.1	0.48	2.5	1.30	0.47	2.30	0.46	2.97	0.71	2.04	0.27	1.85	0.25
Hmd4	2.3	2.3	0.30	1.0	0.24	0.10	0.30	0.05	0.30	0.07	0.24	0.03	0.19	0.02
Hmd5	1.4	2.1	0.34	1.5	0.50	0.27	0.78	0.13	1.05	0.17	0.53	0.08	0.48	0.09
H-1	14.6	24.7	3.13	12.2	2.27	0.75	2.43	0.32	1.77	0.39	0.99	0.13	0.81	0.12
H-2	30.9	64.3	6.26	23.2	4.26	1.44	4.11	0.58	3.23	0.57	1.43	0.21	1.32	0.22
H-3	5.4	13.6	2.06	9.9	3.32	1.29	4.47	0.79	4.83	1.07	2.94	0.44	2.76	0.41
H-4	8.2	16.6	2.17	9.4	2.31	0.79	2.59	0.42	2.34	0.42	1.32	0.19	1.28	0.20
H-5	19.2	43.3	4.32	16.4	3.18	0.74	2.96	0.45	2.85	0.59	1.99	0.27	1.80	0.28
H-6	9.1	19.4	1.94	7.1	1.53	0.36	1.57	0.23	1.45	0.28	0.70	0.13	0.80	0.11
H-7	13.3	28.6	2.96	11.1	2.27	0.50	2.06	0.30	2.07	0.46	1.24	0.19	1.21	0.18
H-8	0.8	1.1	0.09	0.4	<0.05	<0.02	0.06	<0.01	0.06	<0.02	0.04	<0.01	<0.05	<0.01
H8-1	0.6	0.6	0.08	0.5	0.13	0.04	0.12	0.02	0.11	<0.02	0.06	<0.01	0.07	0.01
H-9	0.7	1.6	0.31	1.6	0.65	0.26	0.41	0.04	0.13	0.03	0.04	<0.01	0.07	<0.01
H-10	0.4	0.3	0.03	<0.3	<0.05	0.03	0.07	0.01	0.10	0.02	0.06	<0.01	0.06	0.01
H-11	0.6	2.4	0.54	3.6	1.93	1.22	2.40	0.49	3.99	0.66	2.30	0.38	3.02	0.43
H-12	1.1	1.6	0.23	1.1	0.20	0.08	0.31	0.04	0.25	0.04	0.14	0.02	0.11	0.02

Continued from Table A-1

	TOT/C	TOT/S	Mo	Cu	Pb	Zn	Ni	As	Cd	Sb	Bi	Ag	Au	Hg	Tl	Se
	%	%	PPM													
	0.02	0.02	0.1	0.1	0.1	1	0.1	0.5	0.1	0.1	0.1	0.1	0.5	0.01	0.1	0.5
Sample																
L-1	11.34	<0.02	<0.1	86.8	0.8	5	358.6	21.0	<0.1	0.2	<0.1	<0.1	0.6	<0.01	0.2	<0.5
L-4B	0.04	<0.02	0.1	32.9	0.3	2	22.6	10.2	<0.1	1.1	<0.1	<0.1	<0.5	0.16	<0.1	1.0
L-11	0.05	<0.02	0.9	16.3	1.8	15	409.6	198.3	<0.1	9.8	<0.1	<0.1	0.6	0.13	0.5	<0.5
L-6	0.03	5.65	<0.1	31.8	0.1	1	5.0	9.2	<0.1	<0.1	<0.1	<0.1	<0.5	0.08	<0.1	<0.5
L-3	0.04	4.23	<0.1	2.3	0.2	3	8.5	30.3	<0.1	<0.1	<0.1	<0.1	<0.5	0.11	<0.1	0.6
L-7	0.05	0.19	0.5	46.8	0.6	11	5.0	46.7	<0.1	<0.1	<0.1	<0.1	<0.5	0.21	<0.1	<0.5
L-9	0.41	0.08	0.4	5.8	0.7	9	1606.7	864.3	<0.1	138.1	<0.1	<0.1	0.9	0.14	0.3	0.5
L-5	0.02	<0.02	<0.1	2.1	0.2	4	0.3	1.1	<0.1	0.3	<0.1	0.1	<0.5	0.38	<0.1	<0.5
L-8	0.10	0.09	0.9	196.6	0.2	16	9.1	57.3	<0.1	0.4	<0.1	<0.1	2.1	0.23	<0.1	1.1
L-4A	0.11	8.54	0.7	59.1	2.0	3	44.8	300.5	<0.1	0.8	<0.1	<0.1	1.7	0.55	<0.1	5.9
L-10	0.04	0.02	<0.1	5.6	0.1	2	1.3	3.0	<0.1	<0.1	<0.1	<0.1	<0.5	0.03	<0.1	0.8
L1A	6.08	<0.02	0.9	86.7	31.1	65	589.0	299.8	0.1	0.3	0.4	<0.1	3.5	<0.01	<0.1	1.0
L1B	5.99	<0.02	0.4	17.7	2.6	14	671.8	140.4	<0.1	0.9	<0.1	<0.1	<0.5	<0.01	<0.1	0.6
L12-1	1.59	<0.02	1.0	23.0	4.0	48	124.0	13.9	<0.1	0.5	<0.1	<0.1	<0.5	0.18	0.2	<0.5
L12-2	<0.02	0.38	0.2	1.3	0.2	3	1.6	4.1	<0.1	0.3	<0.1	<0.1	1.2	0.05	<0.1	1.0
L12-3	0.09	4.95	0.1	14.4	0.1	6	8.6	12.5	<0.1	<0.1	<0.1	<0.1	<0.5	0.76	<0.1	<0.5
L12-4	1.47	0.31	0.2	7.0	0.6	13	106.1	7.1	<0.1	0.2	<0.1	<0.1	<0.5	0.06	<0.1	<0.5
L12-5a	3.89	<0.02	0.1	11.2	2.5	18	678.3	3.5	<0.1	<0.1	<0.1	<0.1	<0.5	0.02	0.1	0.7
L12-5b	<0.02	<0.02	<0.1	10.4	0.6	99	125.5	1.5	<0.1	<0.1	<0.1	<0.1	<0.5	0.32	<0.1	<0.5
L12-6	<0.02	<0.02	0.4	82.7	0.6	45	46.1	1.1	<0.1	<0.1	<0.1	<0.1	1.0	<0.01	<0.1	1.0
L12-7	0.05	0.30	0.3	16.8	0.6	7	183.2	199.6	<0.1	6.4	<0.1	<0.1	<0.5	0.62	<0.1	0.7
L12-8	5.76	<0.02	0.6	17.5	2.1	25	398.9	4.4	<0.1	<0.1	<0.1	<0.1	1.3	0.02	0.1	<0.5
L12-9	0.03	1.30	1.0	39.6	0.4	7	9.0	436.3	<0.1	11.6	<0.1	<0.1	2.5	0.89	<0.1	<0.5
L12-10	<0.02	0.24	0.3	3.5	0.2	3	8.8	145.0	<0.1	5.6	<0.1	<0.1	2.0	0.19	<0.1	0.8
L12-11	<0.02	<0.02	0.2	1.7	0.4	2	9.1	19.2	<0.1	0.6	<0.1	<0.1	<0.5	0.19	<0.1	<0.5
L13	8.69	<0.02	<0.1	42.6	2.2	33	354.7	99.8	<0.1	0.3	<0.1	<0.1	<0.5	<0.01	<0.1	1.3
Hmd1-1	0.03	<0.02	0.2	1.6	0.6	2	2.7	<0.5	<0.1	<0.1	<0.1	<0.1	<0.5	0.18	<0.1	<0.5
Hmd1a	<0.02	<0.02	0.7	2.0	0.4	119	145.8	100.1	0.2	0.5	<0.1	<0.1	3.3	0.04	<0.1	1.9
Hmd2a	<0.02	0.03	<0.1	0.8	0.2	1	2.4	2.3	<0.1	0.4	<0.1	<0.1	<0.5	0.31	<0.1	<0.5
Hmd1-2	<0.02	<0.02	<0.1	1.2	<0.1	1	5.0	1.6	<0.1	0.1	<0.1	<0.1	3.2	0.09	<0.1	1.1
Hmd1-3	<0.02	<0.02	0.1	1.3	0.1	2	2.4	0.7	<0.1	<0.1	<0.1	<0.1	1.7	0.13	<0.1	0.6
Hmd1-4	<0.02	<0.02	<0.1	2.2	0.1	4	3.1	5.7	<0.1	0.8	<0.1	<0.1	<0.5	0.17	<0.1	<0.5
Hmd1-5	<0.02	0.73	0.1	2.6	0.2	2	3.5	2.2	<0.1	0.1	<0.1	<0.1	<0.5	0.10	<0.1	<0.5
Hmd1-6	<0.02	0.55	1.3	1.7	0.5	4	24.5	140.2	<0.1	2.5	<0.1	<0.1	<0.5	0.09	<0.1	0.9
Hmd1-7	<0.02	0.21	0.2	1.8	0.3	3	2.5	41.2	<0.1	0.5	<0.1	<0.1	<0.5	0.08	<0.1	<0.5

	TOT/C	TOT/S	Mo	Cu	Pb	Zn	Ni	As	Cd	Sb	Bi	Ag	Au	Hg	Tl	Se
	%	%	PPM													
	0.02	0.02	0.1	0.1	0.1	1	0.1	0.5	0.1	0.1	0.1	0.1	0.5	0.01	0.1	0.5
Hmd1-7a	0.50	<0.02	<0.1	140.6	0.4	83	80.3	2.0	<0.1	0.2	<0.1	<0.1	<0.5	0.06	<0.1	0.9
Hmd1-7b	0.04	<0.02	0.4	81.2	0.4	153	111.8	65.1	<0.1	1.0	<0.1	<0.1	4.5	0.29	<0.1	2.1
Hmd1-8	3.06	<0.02	0.7	65.0	2.3	77	162.8	9.9	<0.1	0.5	<0.1	<0.1	<0.5	0.16	0.2	0.8
Hmd2	0.59	<0.02	0.5	181.0	0.2	30	353.9	617.7	<0.1	30.3	<0.1	<0.1	<0.5	0.07	0.7	1.0
Hmd3	0.06	<0.02	2.5	26.9	0.1	34	1115.3	725.7	<0.1	7.1	<0.1	<0.1	2.1	0.02	0.2	0.5
Hmd3-1	2.84	<0.02	<0.1	149.4	0.2	53	69.3	138.1	<0.1	5.5	<0.1	<0.1	<0.5	0.29	0.1	3.0
Hmd3-2	0.91	0.05	19.6	189.7	0.2	251	837.4	>10000.0	0.3	6.9	<0.1	<0.1	4.3	0.09	0.2	0.7
Hmd4	0.07	<0.02	0.2	51.7	0.3	14	60.6	216.9	<0.1	12.6	<0.1	<0.1	<0.5	0.08	<0.1	<0.5
Hmd5	0.28	<0.02	0.2	81.9	0.7	28	108.2	45.9	0.2	5.8	<0.1	<0.1	2.5	0.25	<0.1	<0.5
H-1	9.11	<0.02	0.1	17.0	3.6	29	840.1	40.3	<0.1	0.2	<0.1	<0.1	<0.5	<0.01	<0.1	1.8
H-2	0.15	<0.02	<0.1	69.5	3.5	106	248.6	63.6	<0.1	<0.1	<0.1	<0.1	2.1	<0.01	<0.1	<0.5
H-3	<0.02	<0.02	0.5	87.2	0.4	88	43.8	1.1	0.2	<0.1	<0.1	<0.1	<0.5	<0.01	<0.1	<0.5
H-4	0.13	0.06	4.4	80.6	4.4	29	57.0	325.2	0.1	1.6	<0.1	<0.1	2.0	10.03	0.2	0.6
H-5	0.09	<0.02	0.6	29.6	4.2	48	143.2	87.7	<0.1	0.4	0.1	<0.1	407.5	0.99	<0.1	0.9
H-6	0.05	<0.02	0.5	4.9	1.1	14	21.4	12.0	<0.1	0.3	<0.1	<0.1	2.0	0.30	<0.1	<0.5
H-7	0.06	0.04	0.3	24.4	1.0	21	50.8	113.3	<0.1	0.5	<0.1	<0.1	17.4	0.10	<0.1	1.7
H-8	0.03	0.08	0.3	29.0	0.4	11	7.9	122.4	0.1	<0.1	<0.1	<0.1	1.5	0.11	<0.1	<0.5
H8-1	0.04	0.06	0.8	36.6	0.5	15	6.0	119.6	<0.1	<0.1	<0.1	<0.1	<0.5	0.47	<0.1	1.2
H-9	0.05	6.44	0.1	8.1	<0.1	4	7.8	15.7	<0.1	<0.1	<0.1	<0.1	<0.5	0.43	<0.1	<0.5
H-10	0.07	0.03	0.1	26.4	<0.1	7	7.9	5.0	<0.1	<0.1	<0.1	<0.1	<0.5	0.02	<0.1	0.6
H-11	0.04	0.03	0.5	189.4	0.1	95	30.6	18.6	0.1	<0.1	<0.1	<0.1	<0.5	0.11	<0.1	5.6
H-12	12.55	<0.02	<0.1	4.8	0.6	14	180.4	29.5	<0.1	0.1	<0.1	<0.1	<0.5	0.01	<0.1	<0.5

APPENDIX B

DIAGRAMS BASED ON LISTWANITE-CO₂-H₂O REACTIONS USING SERPENTINE FOR 80°C

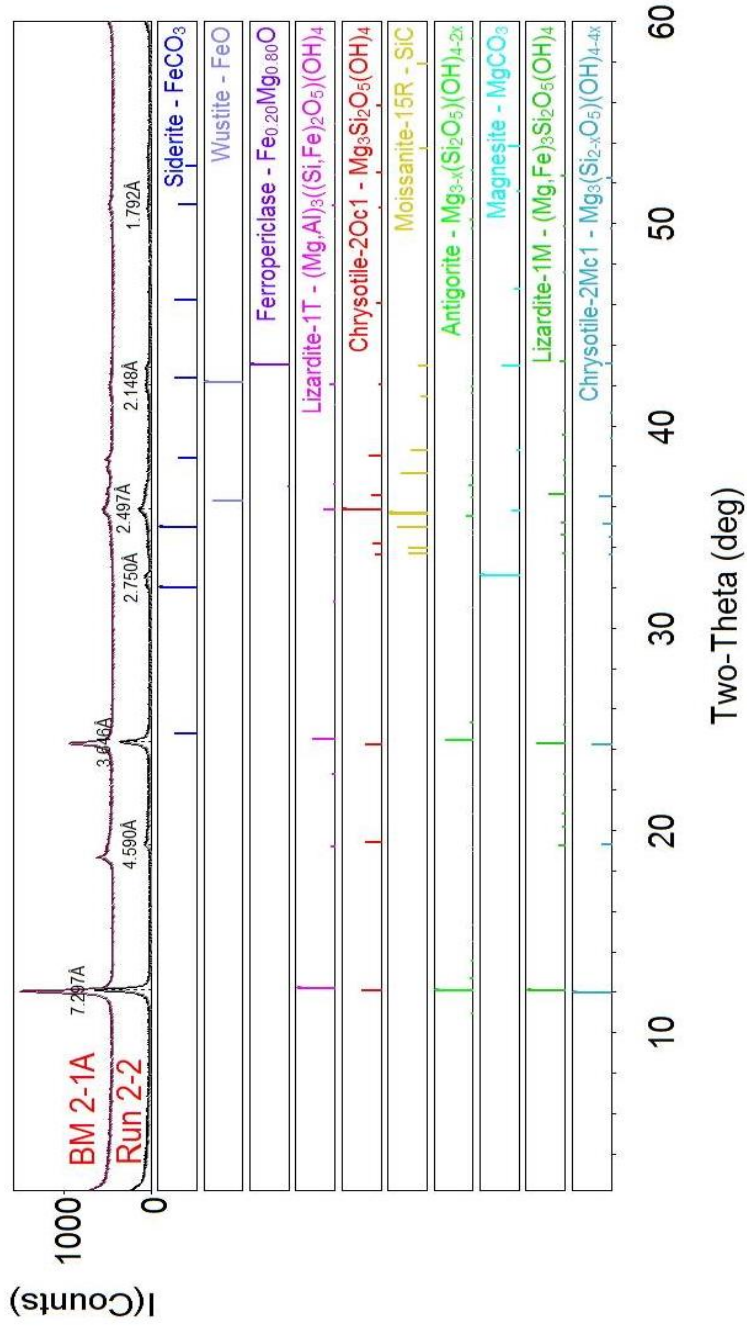


Figure B-1. The final product obtained at the end of Run 2-2

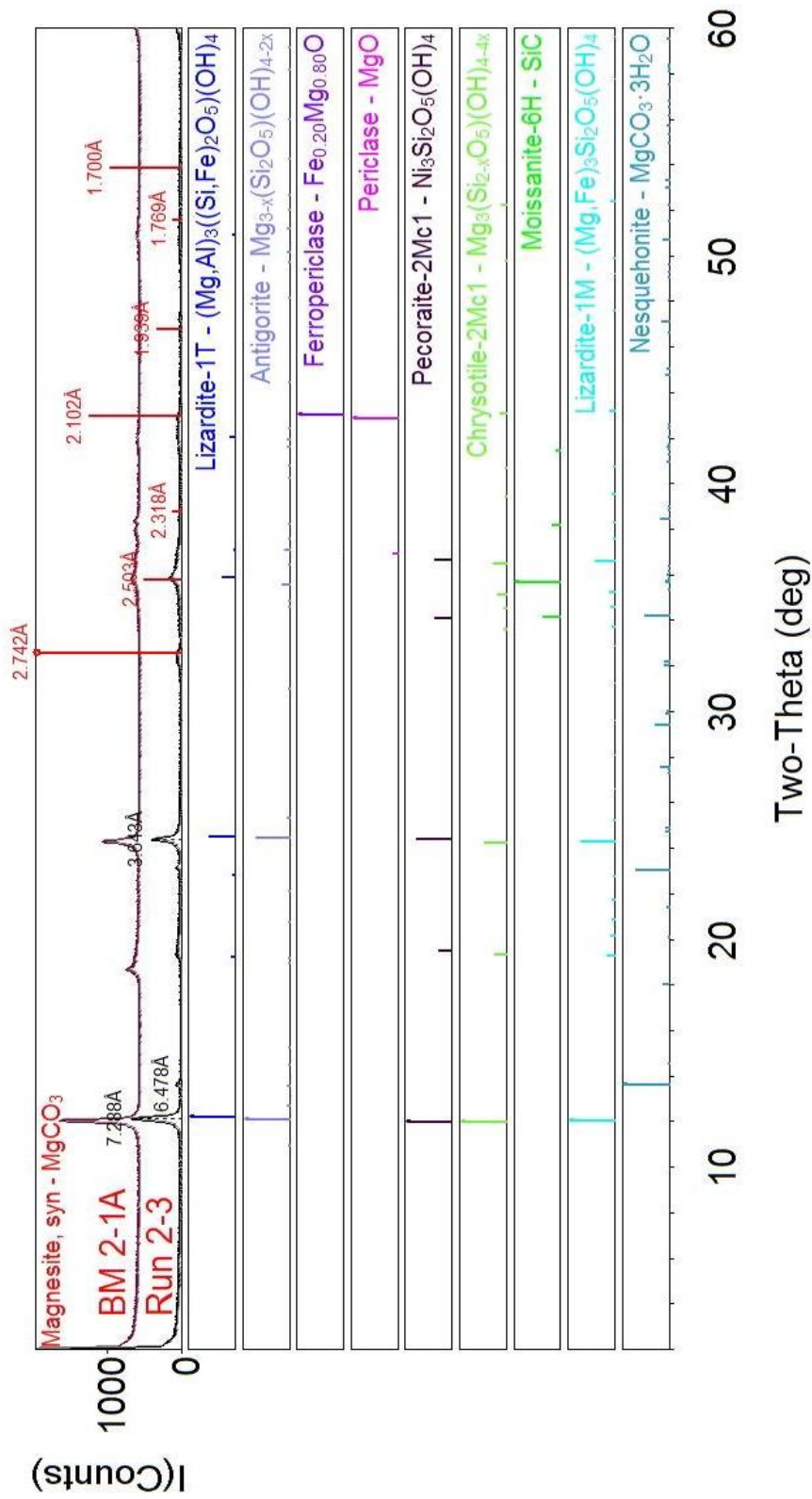


Figure B-2. X-ray reaction pattern of Run 2-3

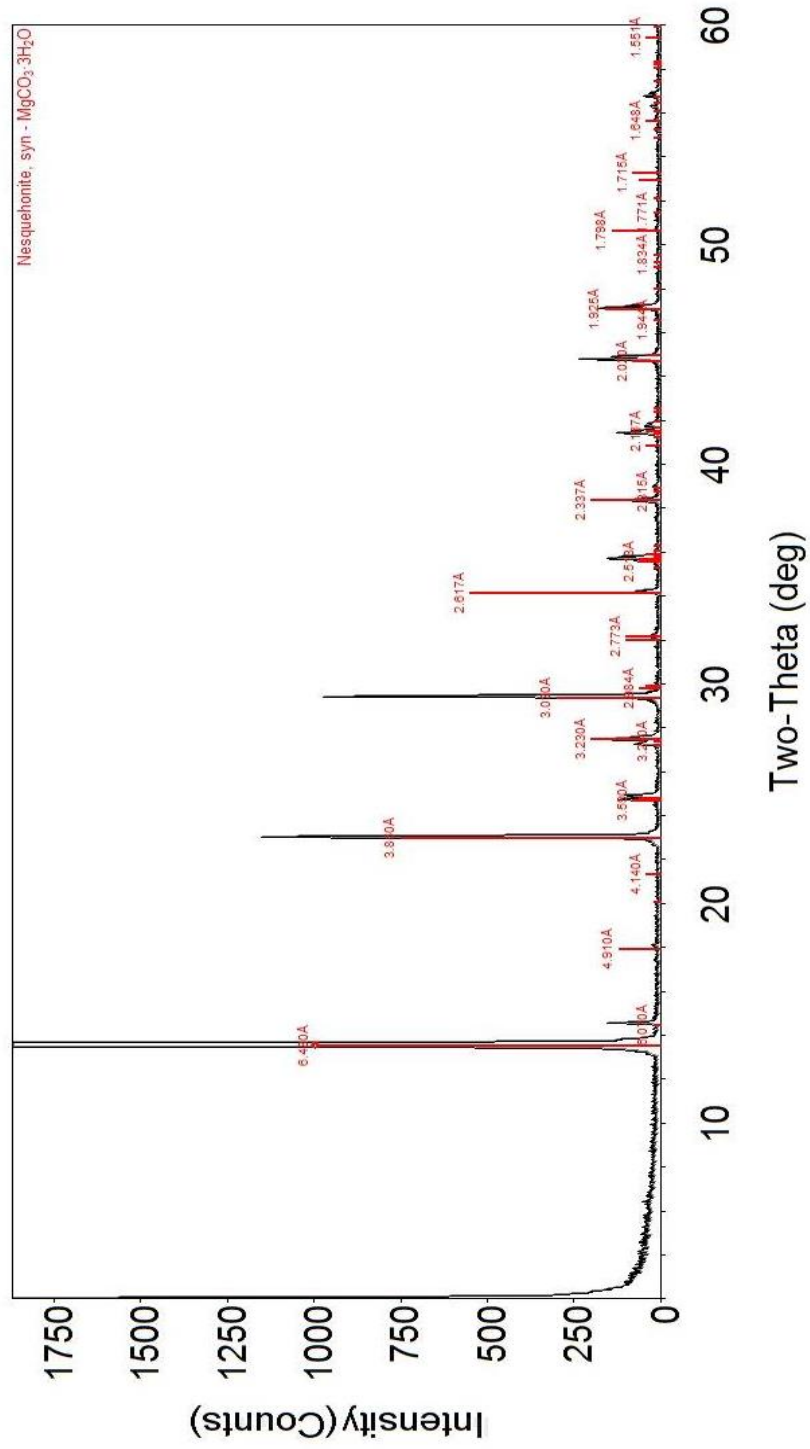


Figure B-3. Aqueous liquid of the final reaction product including nesquehonite in Run 2-3

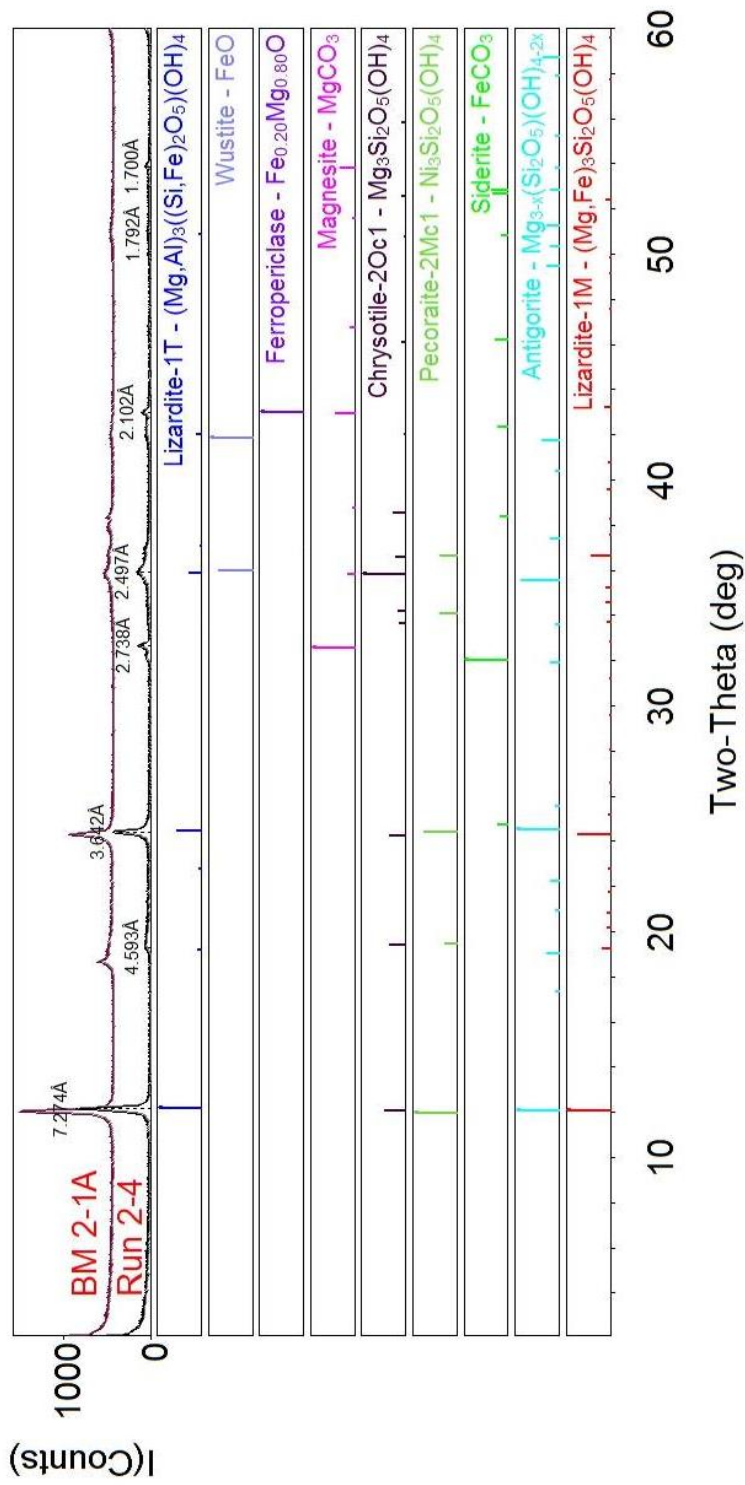


Figure B-4. XRD pattern obtained from the reaction product at the end of Run 2-4

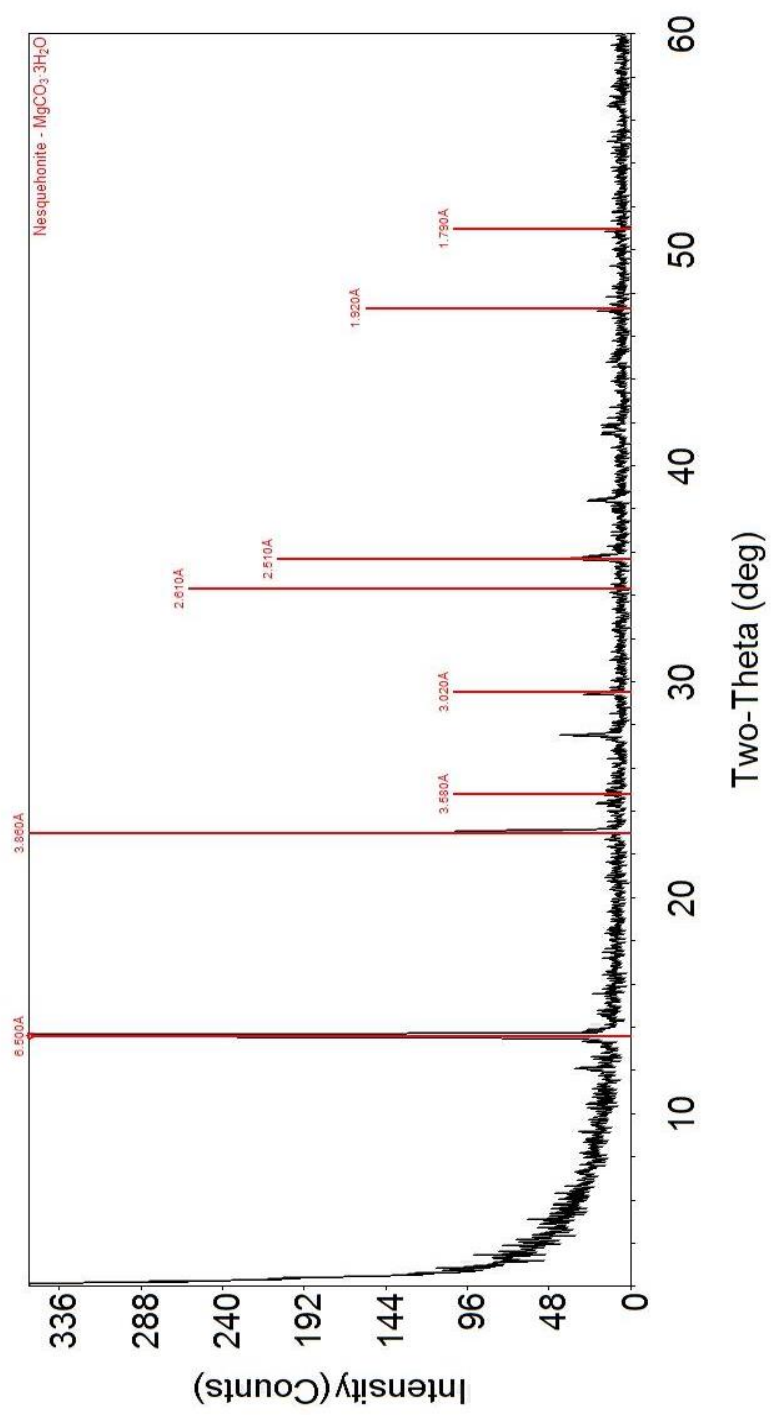


Figure B-5. Aqueous liquid of final reaction product obtained from Run 2-4 consisting of nesquehonite.

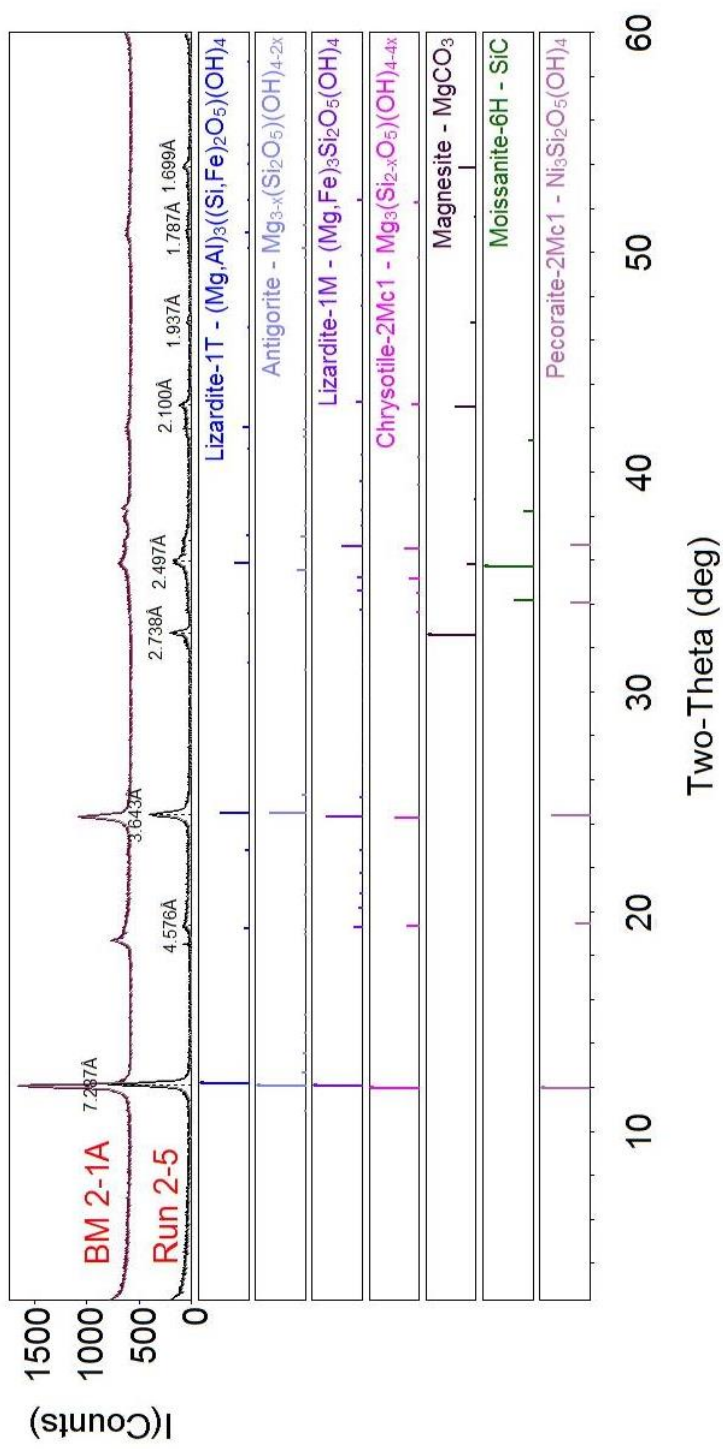


Figure B-6. XRD pattern of reaction product of Run 2-5

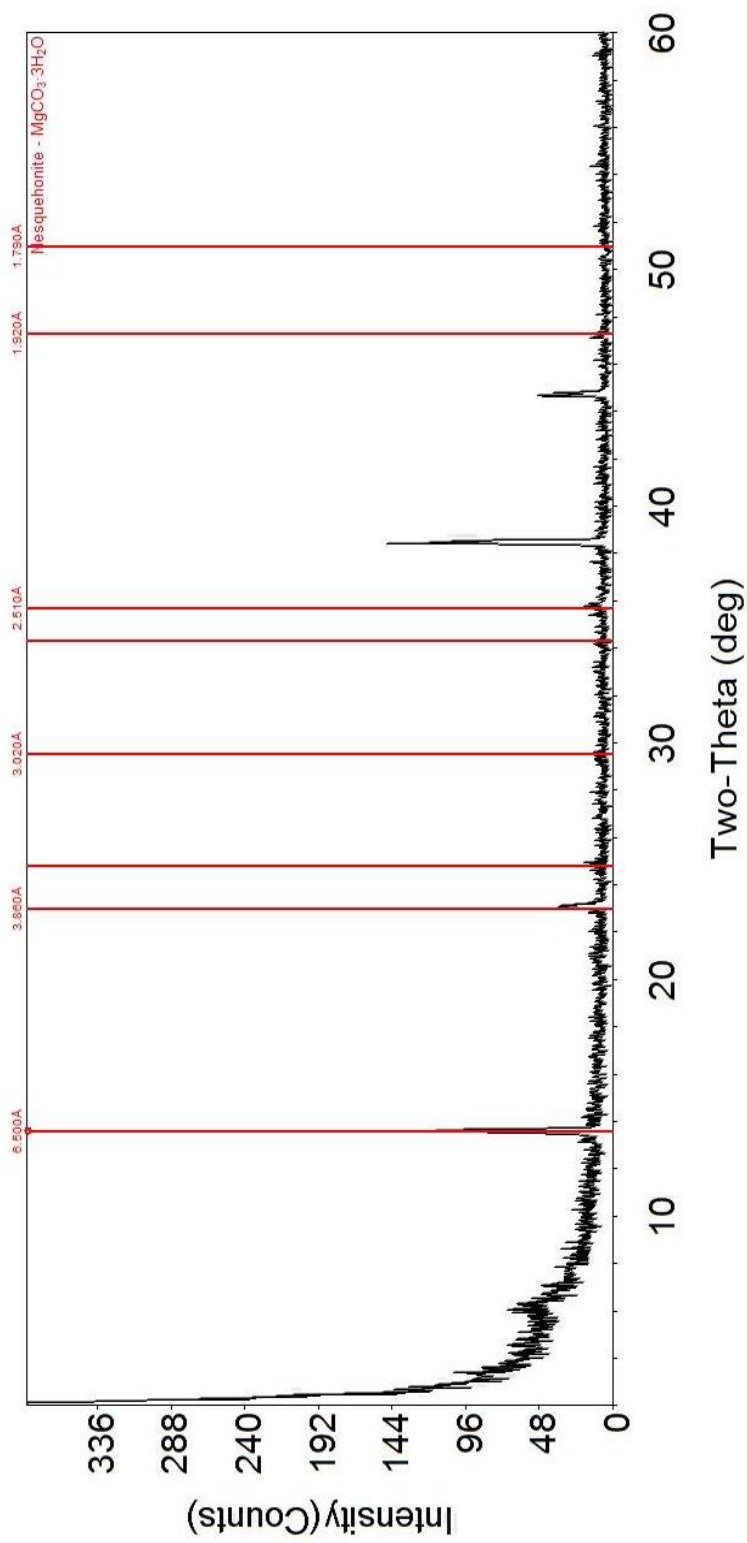


Figure B-7. Aqueous liquid acquired from Run 2-5 including nesquehonite

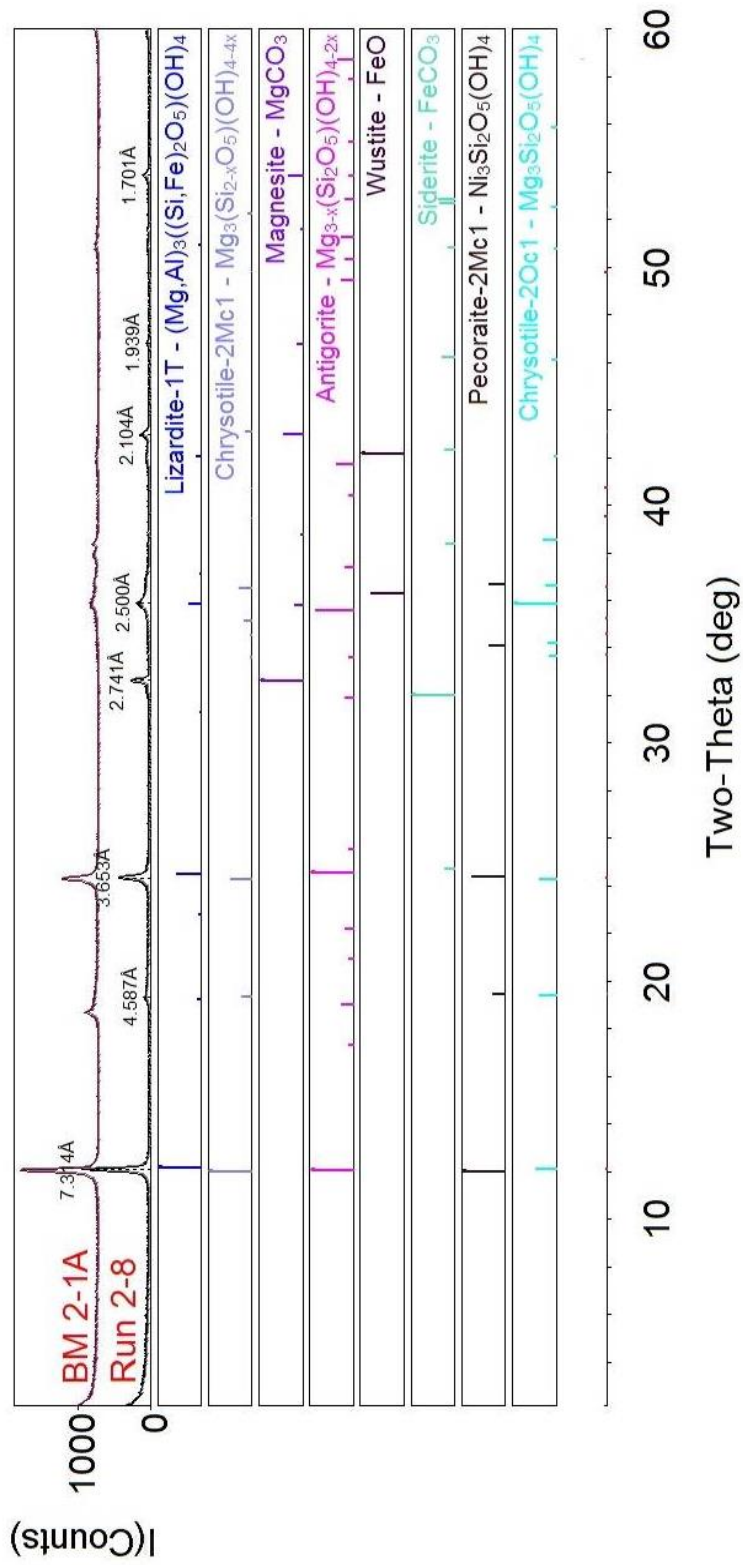


Figure B-8. X-ray pattern of the reaction product of Run 2-8

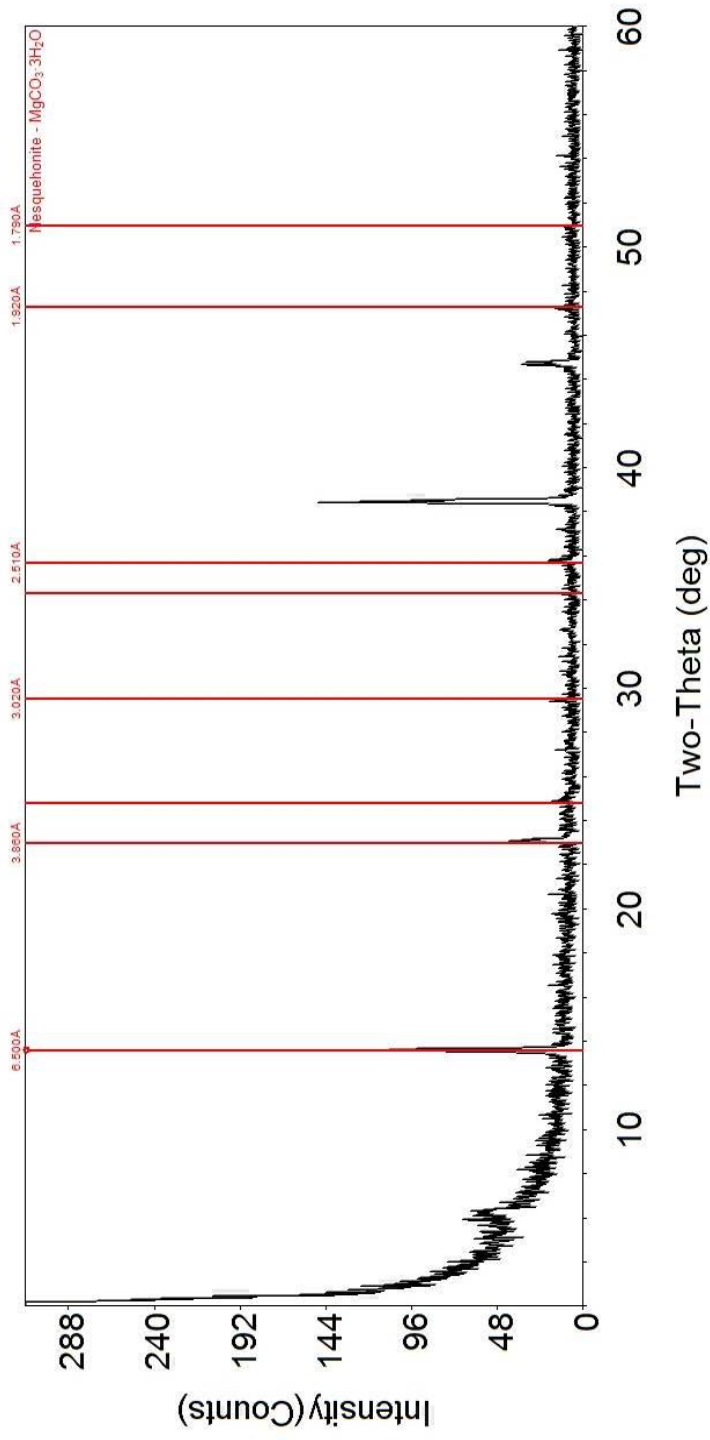


Figure B-9. Nesquehonite observed in the aqueous liquid of Run 2-8

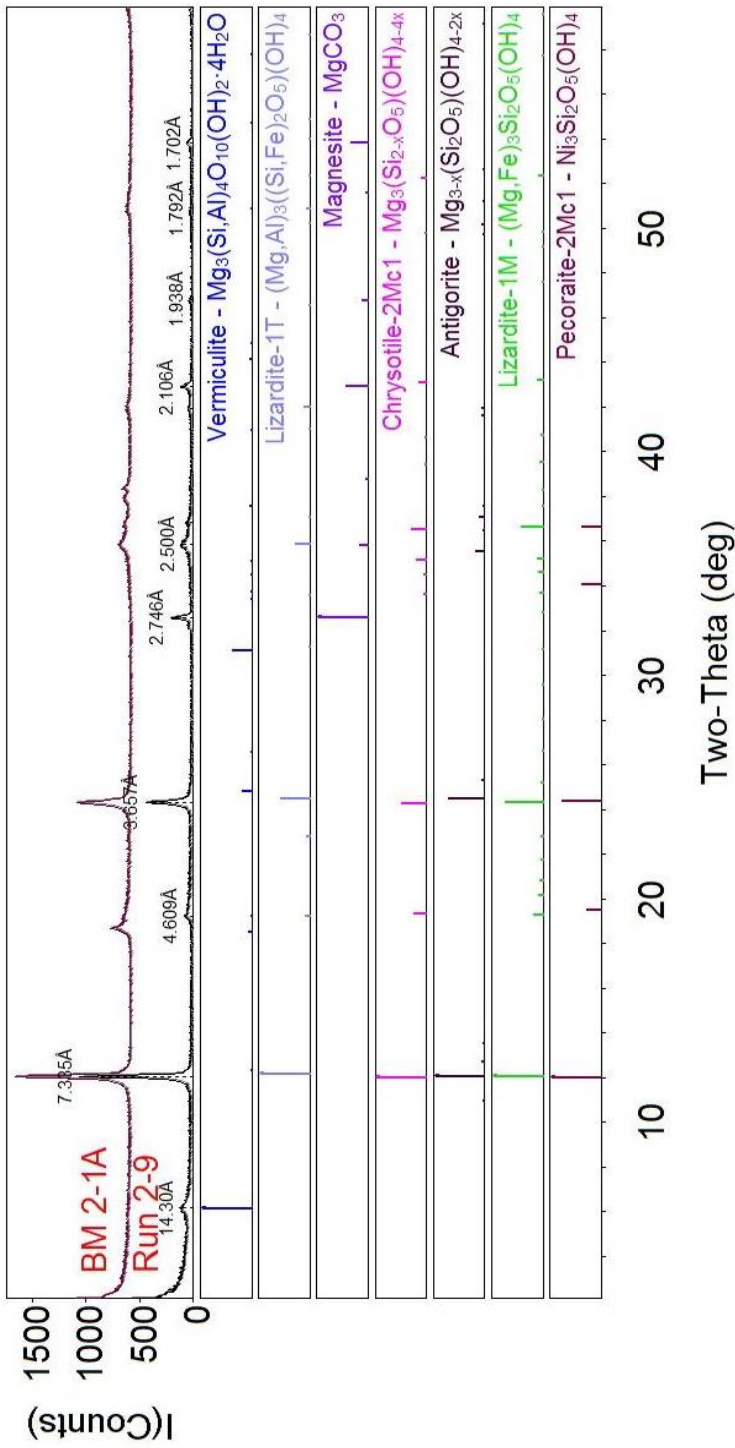


Figure B-10. XRD results acquired from final reaction product at the end of Run 2-9

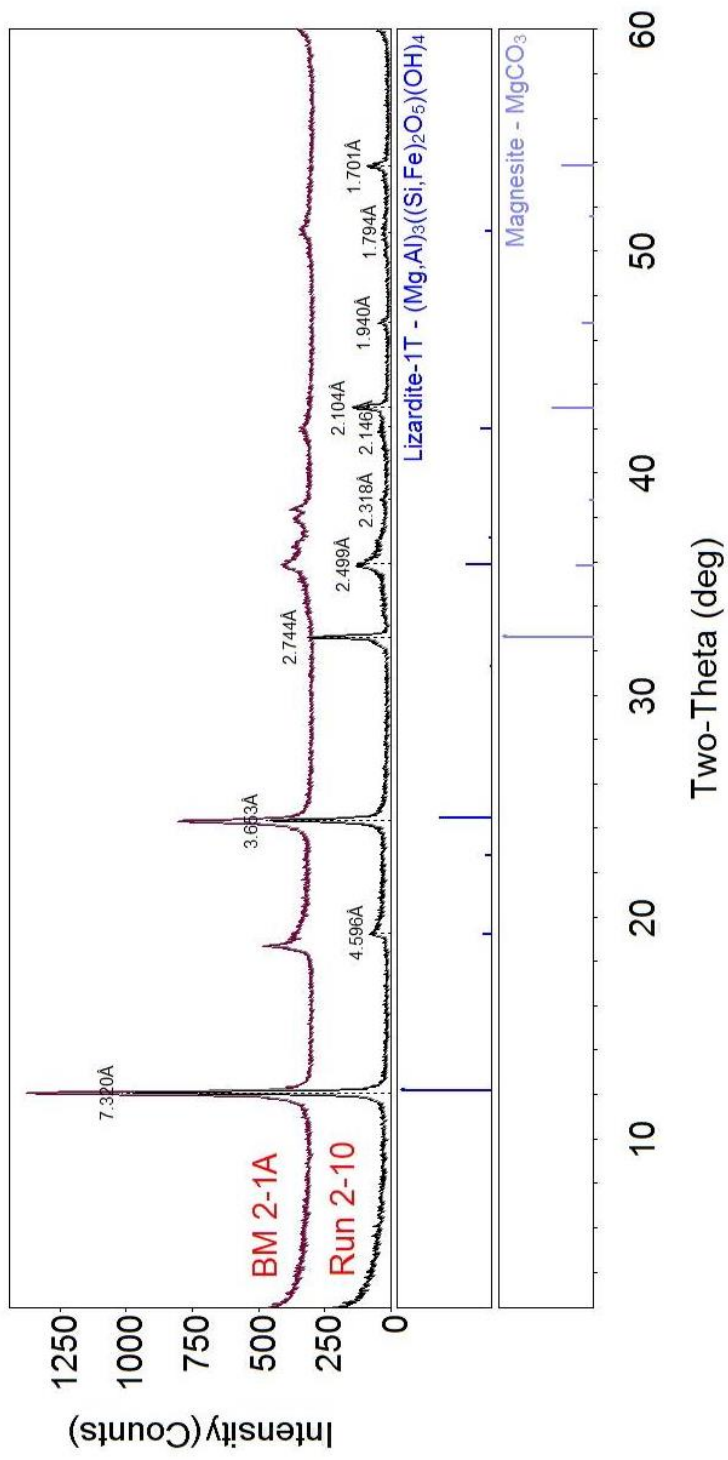


Figure B-11. XRD results acquired from the reaction material of Run 2-10

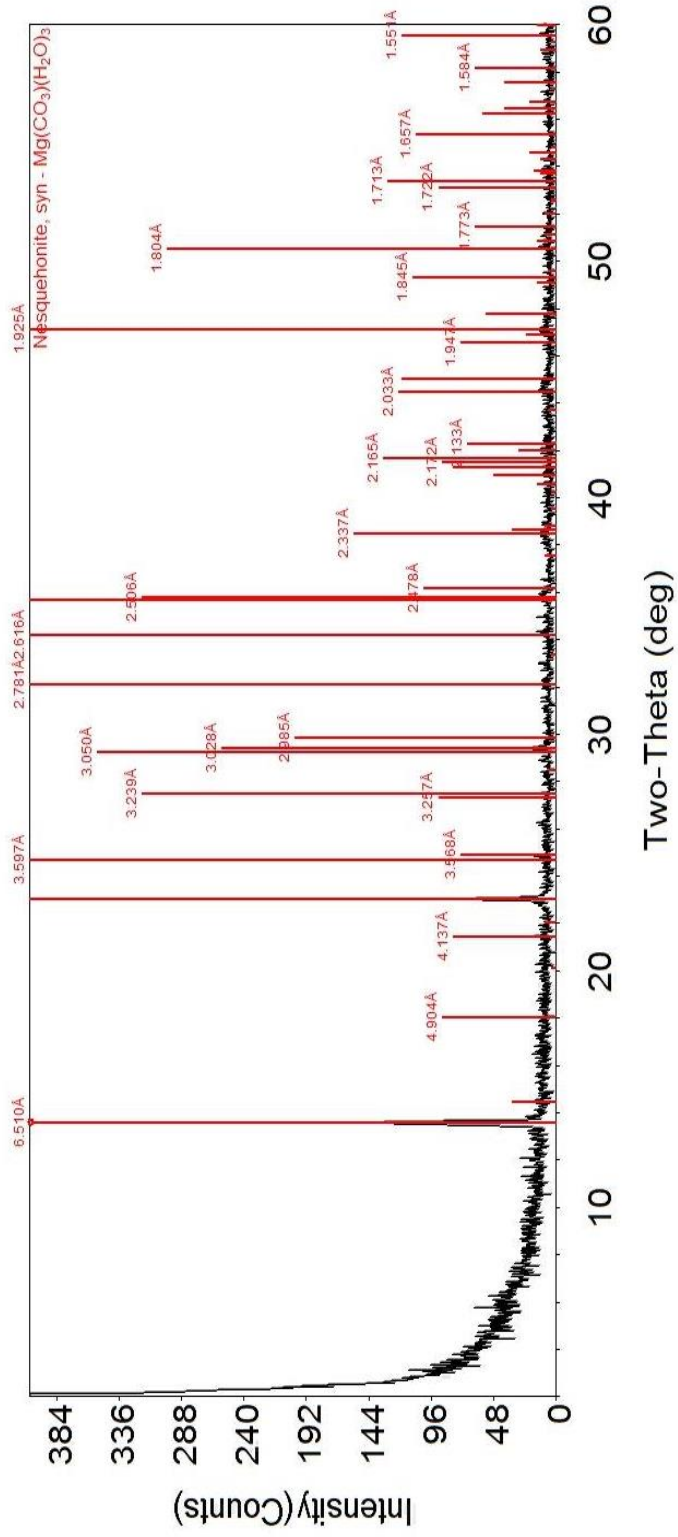


Figure B-12. Nesquehonite produced in the co-existing aqueous liquid

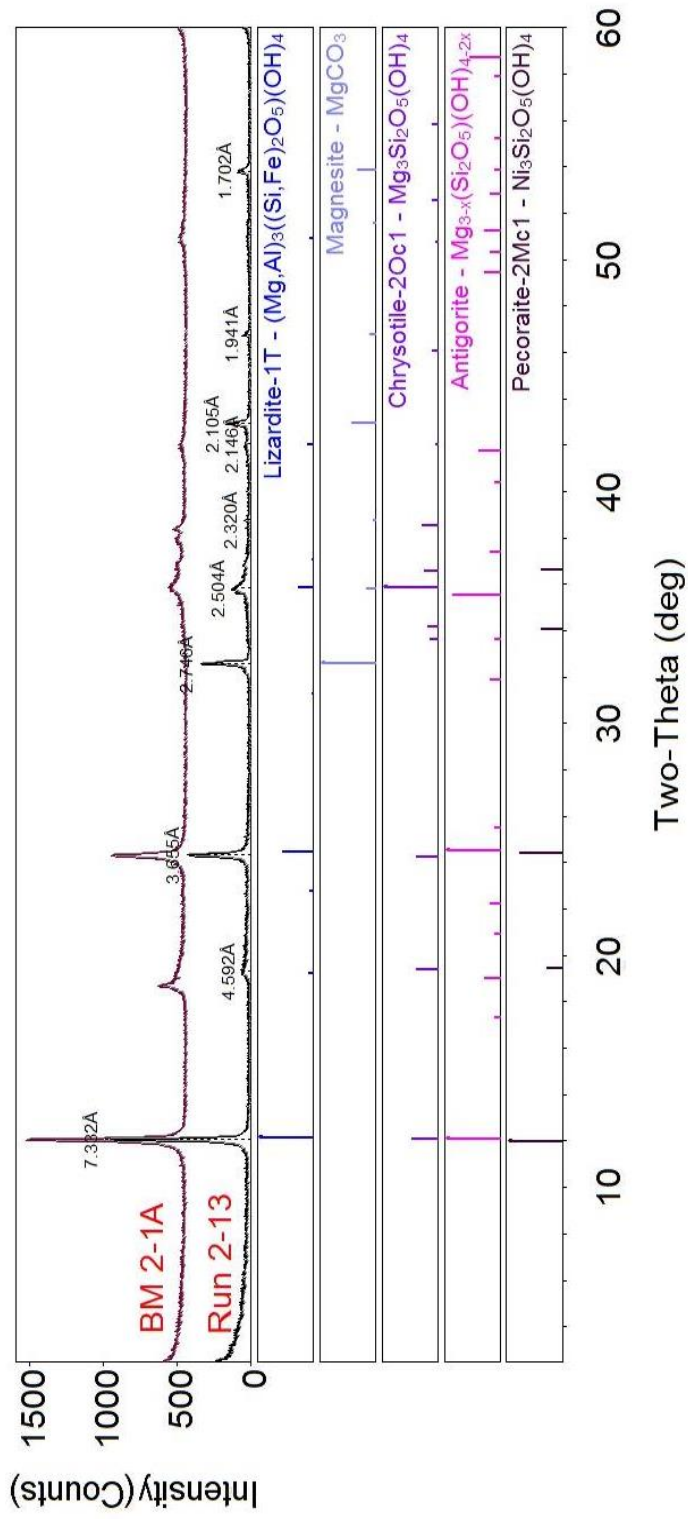


Figure B-13. XRD pattern of final/reaction product of BM 2-1A at the end of Run 2-13

APPENDIX C

DIAGRAMS BASED ON LISTWANITE-CO₂-H₂O REACTIONS USING
SERPENTINE FOR 25°C

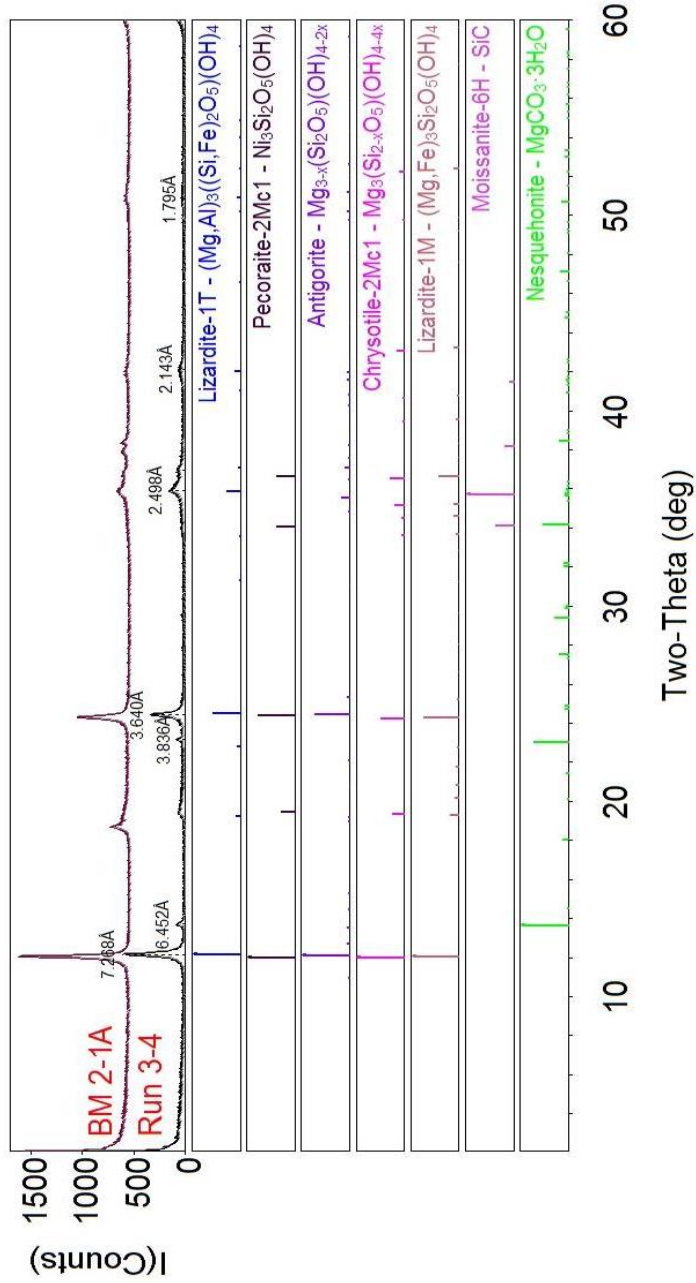


Figure C-1. XRD results obtained from reaction product of Run 3-4

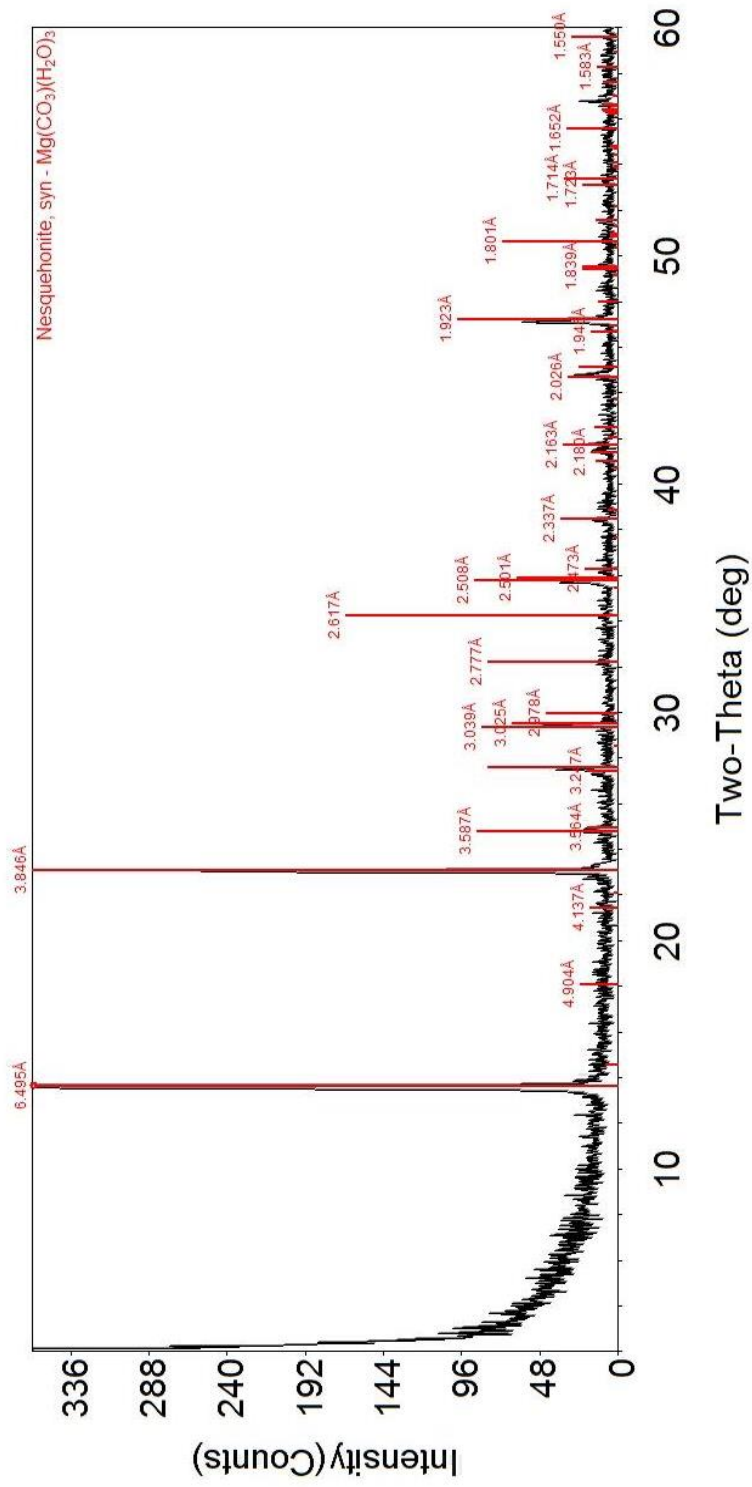


Figure C-2. Nesquehonite obtained from aqueous liquid upon evaporation

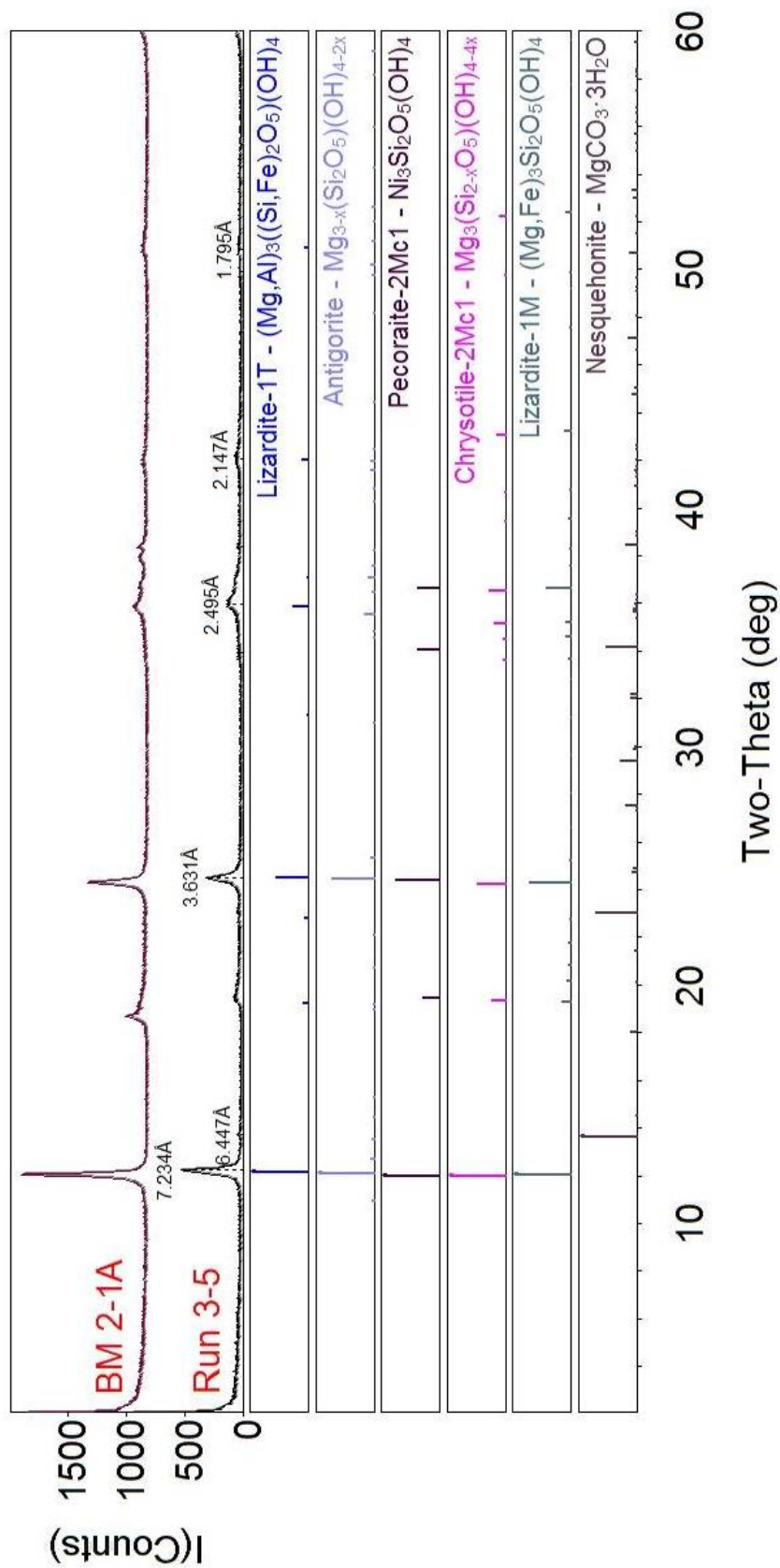


Figure C-3. XRD pattern of reaction product of Run 3-5

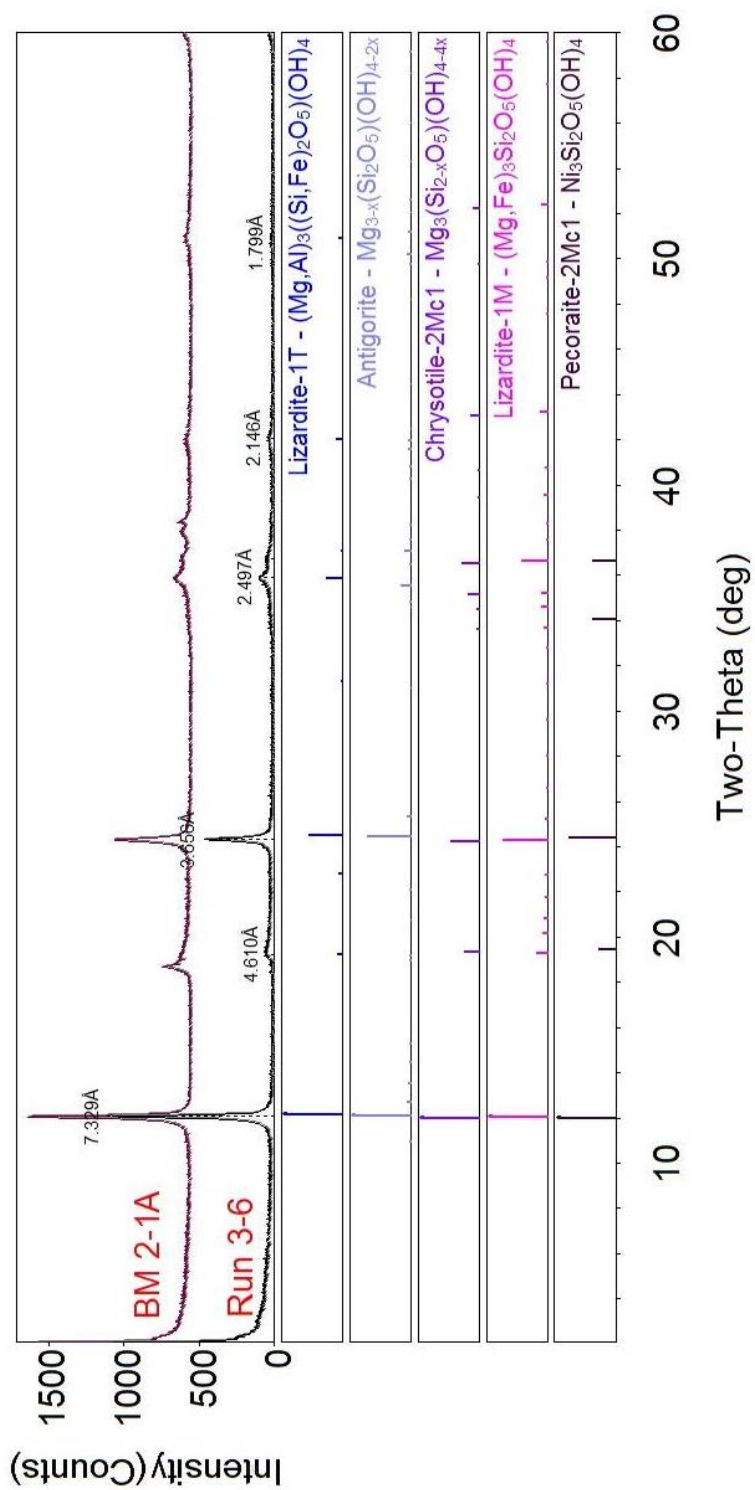


Figure C-5. XRD results of Run 3-6

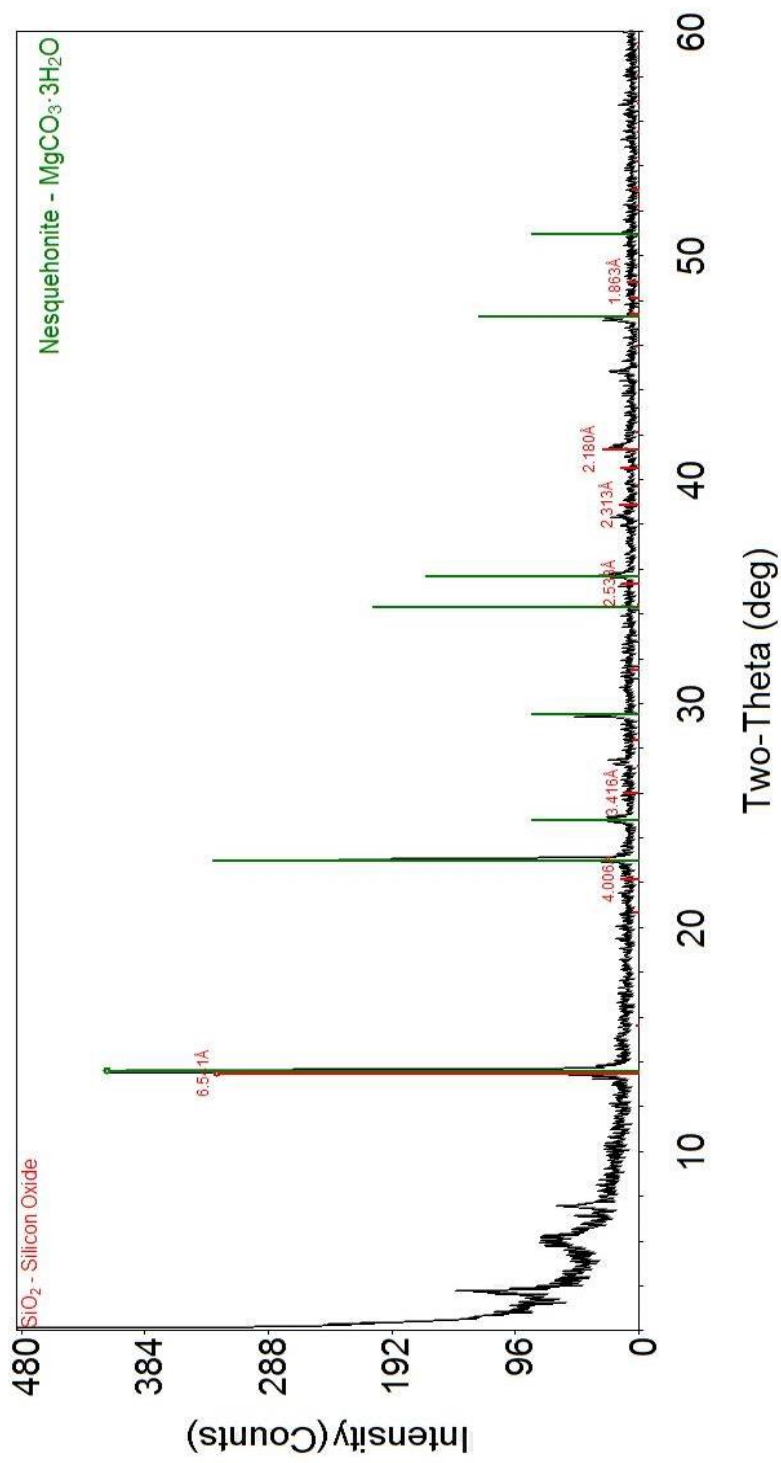


Figure C-6. XRD pattern showing the entity of nesquehonite and silicon oxide peaks in the co-existing aqueous liquid (Red lines represent silicon oxide whereas green lines indicate nesquehonite)

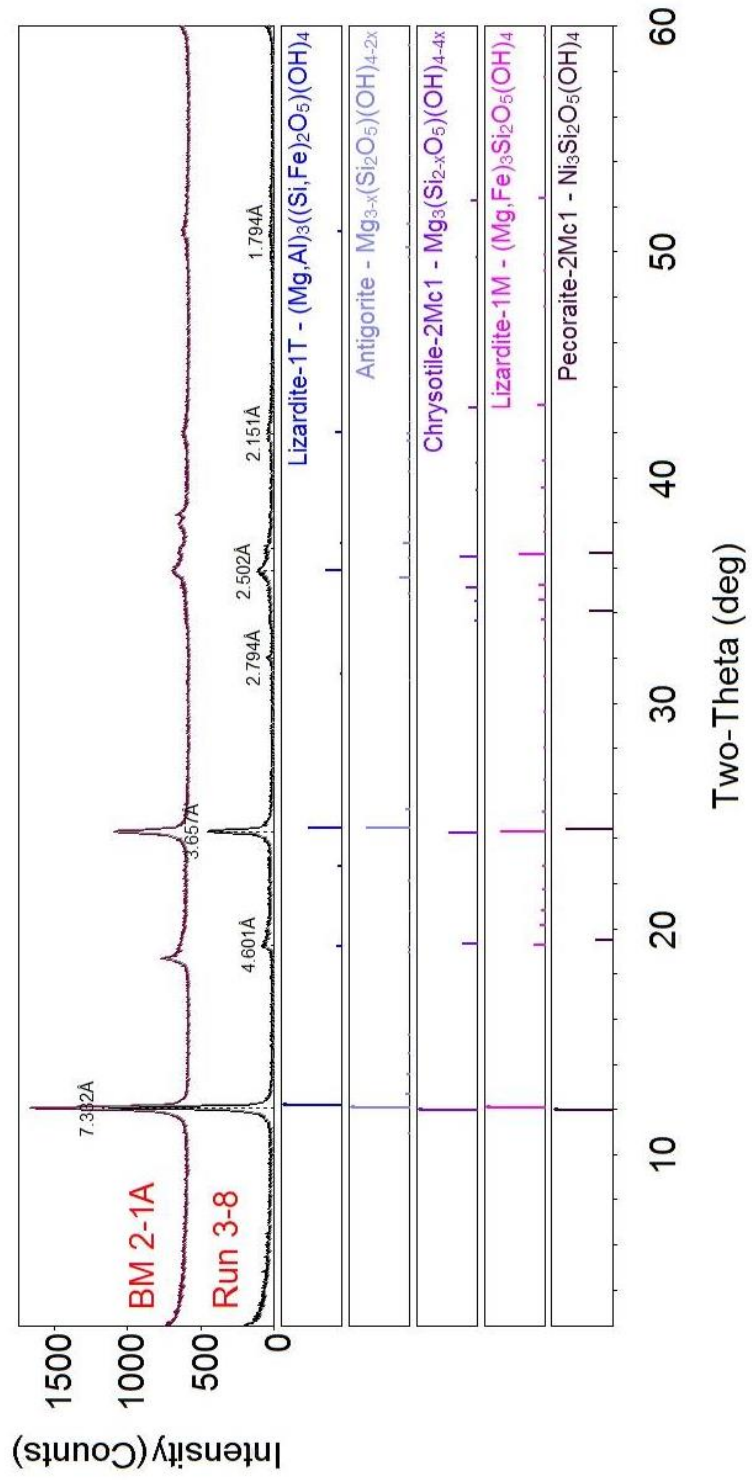


Figure C-7. XRD patterns for Run 3-8

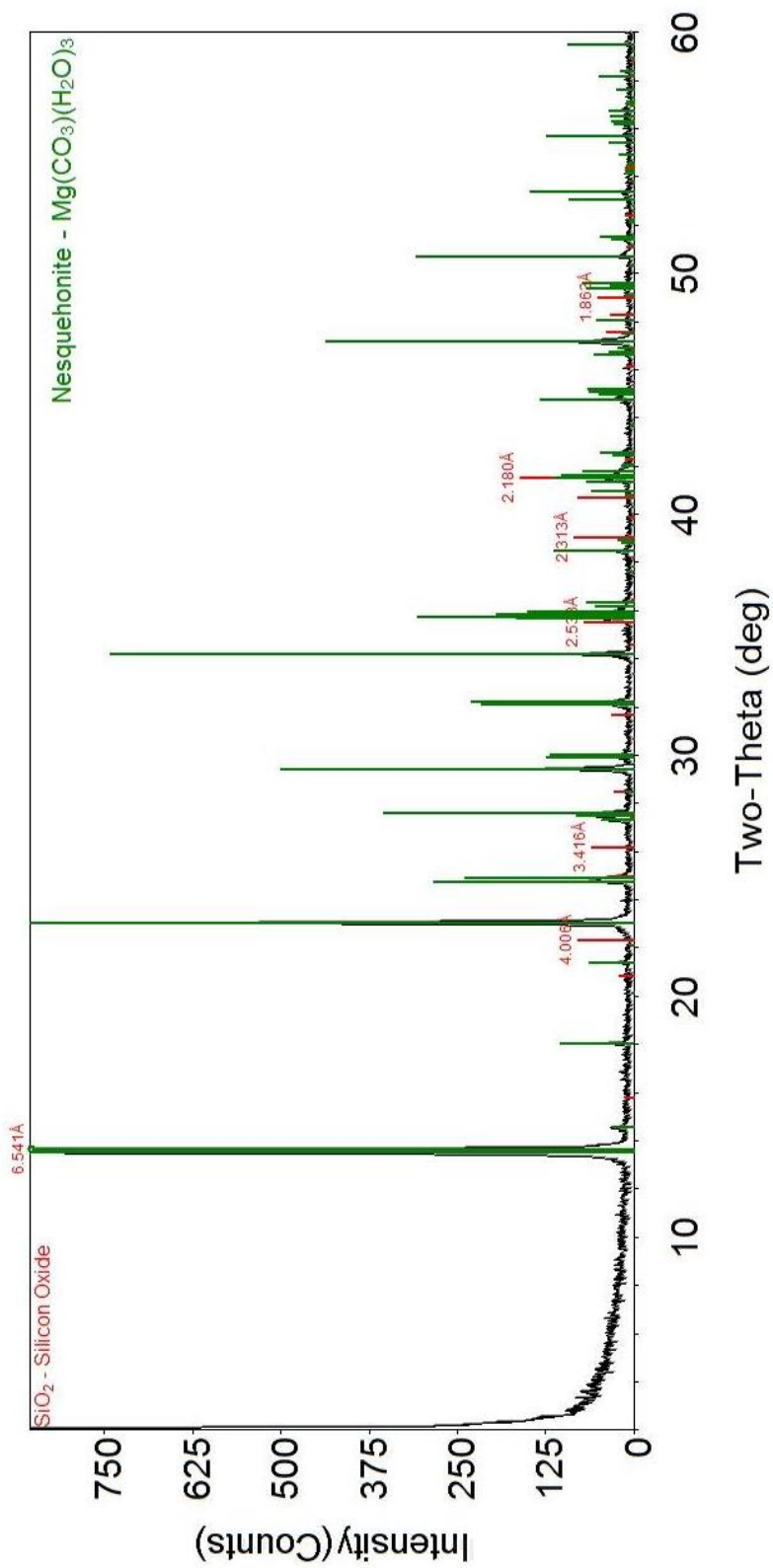


Figure C-8. The co-existing aqueous liquid consisted of silicon oxide and nesquehonite

CURRICULUM VITAE

PERSONAL INFORMATION

Surname, Name: Ömeroğlu-Sayıt, Işıl

Phone: +90 312 210 26 82

email: isilomeroglu@yahoo.com

EDUCATION

Degree	Institution	Year of Graduation
MSc	METU, Geological Engineering	2011
BS	A.U., Geological Engineering	2008

WORK EXPERIENCE

Year	Place	Enrollment
2010-2017	METU Geological Engineering	Research Assistant
2014-2015	UIC-Dept. Of Earth and Env. Sci.	Intern
2008-2011	A.U., Dept of Archaeology, Kültepe Archaeological Excavation Committee	Geologist

FOREIGN LANGUAGES

Advanced English, German beginning

PUBLICATIONS-THESIS

1. Geoarchaeological Investigations Around Kültepe (Kayseri), M.Sc Thesis, September 2011, Advisor: Prof. Dr. G. M. Vedat Toprak, Co-Advisor: Prof. Fikri Kulakoğlu, Middle East Technical University, Department of Geological Engineering.
2. Ömeroğlu, I., Toprak, G. M. V., Kulakoğlu, F., 2012. Kayseri Sarımsaklı Havzası'ndaki Aktif Tektonizma'nın Kültepe Antik Kenti Üzerindeki Etkisi, 16. Aktif Tektonik Araştırma Grubu Çalıştayı (16th Active Tectonism Research Group Workshop), Istanbul, Turkey, p.27
3. Ömeroğlu, I., Günal-Türkmenoğlu, A., Sayın, Ş., A., 2013. Investigation of Kaolin Deposits Around Ahırözü (Mihalıççık-Eskişehir), 66th Geological Congress of Turkey, Ankara, Turkey, p.216-217.
4. Ömeroğlu I., Günal-Türkmenoğlu, A., Sayın, Ş., A., 2013., Investigation of the Genesis of Ahırözü Kaolin Deposits (Eskişehir, Turkey) Using Mineralogical, Petrographical And Geochemical Analyses, 50th Anniversary of Clay Mineral Society Annual Meeting, Urbana-Champaign-USA, p.188.
5. Ömeroğlu, I., Guggenheim, S., Günal Türkmenoğlu, A., Koster van Groos, A., F., Sayın, Ş., A., 2015, An experimental study of CO₂-H₂O-listwanite-based reactions using serpentine from the Ahırözü kaolin deposits, Eskişehir-Mihalıççık, Turkey, EuroClay2015, Edinburgh-Scotland, p. 493.
6. Ömeroğlu, I., Günal-Türkmenoğlu, A., Sayın, Ş., A., 2015. Ahırözü-Mihalıççık (Eskişehir-Türkiye) Kaolen Yatakları Ve Dolaylarında Dağılım Gösteren Bozuşma Ürünlerinin Kökensel Olarak İncelenmesi, 16. Ulusal Kil Sempozyumu (16th National Clay Meeting of Turkey), Çanakkale-Turkey, p.36.
7. Ömeroğlu, I., Günal-Türkmenoğlu, A., Demirci, C., 2016. Hydrothermal Alteration Products in the Vicinity of the Ahırözü Kaolin Deposits, Mihalıççık-Eskişehir, Turkey, 5th Mediterranean Clay Meeting, Çeşme-İzmir/Turkey, p. 48.

8. Ömeroğlu, I., Günal Türkmenoğlu, A., 2017. A Study on Mineral Assemblages, Textures and Zonning Patterns of Hydrothermal Originated Ahırözü Kaolin Deposits, Mihalıççık-Eskişehir, Turkey, 16th International Clay Conference, Granada-Spain.
9. Ömeroğlu-Sayıt, I., Günal-Türkmenoğlu, A., Sayın, Ş., A., Demirci, C., 2018. Hydrothermal alteration products in the vicinity of the Ahırözü kaolin deposits, Mihalıççık-Eskişehir, Turkey, *Clay Minerals*, 53, 289-303.

WORKSHOPS/ SUMMER SCHOOLS /CONFERENCES

The 33rd International Symposium of Excavations, Surveys and Archameometry, Inonu University, 23-27 May, 2011, Malatya-Turkey-*Conference*.

1. Kuvaterner Bilimi Lisansüstü Yaz Okulu (Quaternary Science Summer School for Graduate Students), Ankara University, June 18-23, 2012, Ankara-Turkey-*Summer School*.
2. Attendance of Certificate on Short Course on Geochronology, 26-30 May 2014; Trinity College of Dublin-METU Dept. Of Geological Engineering; Lecturer: Assist. Prof. Dr. Quentin Crowley-*Workshop-Short Course*.
3. Karbonat Kayaları Sedimantolojisi ve Rezervuar Özellikleri, “Sedimentology and Reservoir Properties of Carbonate Rocks”, 5-7 May, 2016; Lecturer: Dr. Erhan Yılmaz (TPAO-Turkish Petroleum Corporation), *Workshop-Short Course*.

SCHOLARSHIPS

1. Awarded with 2214-A *International Research Fellowship Programme* by *The Science and Technological Research Council of Turkey (TUBITAK)*, Oct, 2014- Apr., 2015 at University of Illinois at Chicago (USA)-*Supervisor: Prof. S. Guggenheim*

TITLE OF THE RESEARCH: “*Experimental Study on CO2 Sequestration of Rocks at Hydrothermal Fields*”

PROJECTS

1. AHİRÖZÜ (MİHALIÇCIK-ESKİŞEHİR) DOLAYLARINDAKİ KAOLEN YATAKLARININ JEOLojİSİ MİNERALojİSİ VE OLUŞUMU; Supervisor: **Prof. Dr. Asuman Günal Türkmenoğlu**; Researcher: **Işıl Ömeroğlu, MSc**; METU Research Project No: **BAP-07.02.2012.101**, 2012-2013
2. AHİRÖZÜ (MİHALIÇCIK-ESKİŞEHİR) DOLAYLARINDAKİ KAOLEN YATAKLARININ JEOLojİSİ MİNERALojİSİ VE OLUŞUMU; Supervisor: **Prof. Dr. Asuman Günal Türkmenoğlu**; Researcher: **Işıl Ömeroğlu, MSc**; METU Research Project No: **BAP-03-09-2013-001**, 2013-2014
3. AHİRÖZÜ (MİHALIÇCIK-ESKİŞEHİR) DOLAYLARINDAKİ KAOLEN YATAKLARININ JEOLojİSİ MİNERALojİSİ VE OLUŞUMU; Supervisor: **Prof. M. Cemal Göncüoğlu**; Researcher: **Işıl Ömeroğlu, MSc**; METU Research Project No: **BAP-03-09-2013-001**, 2014-2015
4. AHİRÖZÜ (MİHALIÇCIK-ESKİŞEHİR) DOLAYLARINDAKİ KAOLEN YATAKLARININ JEOLojİSİ MİNERALojİSİ VE OLUŞUMU; Supervisor: **Assoc. Prof. Dr. Kaan Sayıt**; Researcher: **Işıl Ömeroğlu, MSc**; METU Research Project No: **BAP-03-09-2013-001**, 2015-2016

5. ESKİŞEHİR AHİRÖZÜ DOLAYLARINDAKİ KAOLEN YATAKLARI VE CİVARINDAKİ HİDROTERMAL ALTERASYON ÜRÜNLERİNİN KÖKENSEL OLARAK İNCELENMESİ VE EPİTERMAL YATAK GELİŞİMİNE DAİR İLİŞKİLERİNİN ORTAYA ÇIKARILMASI; Supervisor: **Assoc. Prof. Dr. Kaan Sayıt**; Researcher: **Işıl Ömeroğlu, M.Sc.**; METU Research Project No: **BAP-03-09-2017-006, 2017-2018**

AREAS OF INTEREST

- Mineralogy-Petrography
- Clay Mineralogy and Geology
- CO₂ Sequestration-CO₂-H₂O-Rock Interactions
- Hydrothermal Alteration Mineralogy
- Geographic Information Systems
- Geoarchaeology

AWARDS

- Ömeroğlu, I., Toprak, G. M. V., Kulakoğlu, F., Kayseri Sarımsaklı Havzası'ndaki Aktif Tektonizma'nın Kültepe Antik Kenti Üzerindeki Etkisi (Influence of Active Tectonism in Kayseri Sarımsaklı Basin on Kültepe, the ancient site); 16th Active Tectonism Research Group Workshop, Istanbul, Turkey, 18-19 October 2012:

Best Poster Presentation